University of Alberta

Development and Application of Laser-based Ionization Techniques in Time-of-flight Mass Spectrometry

by

David Christopher Schriemer

A thesis submitted to the Faculty of Graduate Studies and Research in partial fulfillment of the requirements for the degree of Doctor of Philosophy

Department of Chemistry

Edmonton, Alberta

Fall, 1997

National Library of Canada
Acquisitions and Bibliographic Services
395 Wellington Street
Ottawa ON K1A 0N4
Canada

Bibliothèque nationale du Canada
Acquisitions et services bibliographiques
395, rue Wellington
Ottawa ON K1A 0N4
Canada

Your file Votre référence

Our file Notre référence

The author has granted a non-exclusive licence allowing the National Library of Canada to reproduce, loan, distribute or sell copies of this thesis in microform, paper or electronic formats.

L'auteur a accordé une licence non exclusive permettant à la Bibliothèque nationale du Canada de reproduire, prêter, distribuer ou vendre des copies de cette thèse sous la forme de microfiche/film, de reproduction sur papier ou sur format électronique.

The author retains ownership of the copyright in this thesis. Neither the thesis nor substantial extracts from it may be printed or otherwise reproduced without the author's permission.

L'auteur conserve la propriété du droit d'auteur qui protège cette thèse. Ni la thèse ni des extraits substantiels de celle-ci ne doivent être imprimés ou autrement reproduits sans son autorisation.

0-612-23066-X

Canada

University of Alberta

Library Release Form

Name of Author: David Christopher Schriemer

Title of Thesis: Development and Application of Laser-based Ionization Techniques in Time-of-flight Mass Spectrometry

Degree: Doctor of Philosophy

Year This Degree Granted: 1997

Permission is hereby granted to the University of Alberta Library to reproduce single copies of this thesis and to lend or sell such copies for private, scholarly, or scientific research purposes only.

The author reserves all other publication and other rights in association with the copyright in the thesis, and except as hereinbefore provided, neither the thesis nor any substantial portion thereof may be printed or otherwise reproduced in any material form whatever without the author's prior written permission.

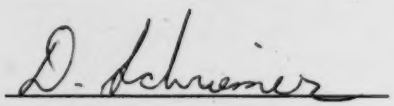

13619 109 Ave.
Edmonton, AB
T5M 2G8

October 2, 1997

University of Alberta

Faculty of Graduate Studies and Research

The undersigned certify that they have read, and recommend to the Faculty of Graduate Studies and Research for acceptance, a thesis entitled "Development and Application of Laser-based Ionization Techniques in Time-of-Flight Mass Spectrometry" submitted by David Christopher Schriemer in partial fulfillment of the requirements for the degree of Doctor of Philosophy.

Dr. L. Li, Associate Professor of Chemistry

Dr. F.F. Cantwell, Professor of Chemistry

Dr. G. Horlick, Professor of Chemistry

Dr. J.C. Vederas, Professor of Chemistry

Dr. M. Williams, Professor of Chemical Engineering

Dr. K.G. Owens, Associate Professor of Chemistry

Oct. 1, 1997

For my wife, Tammy

Abstract

The work presented in this thesis involves the development and expansion of laser-based ionization methods in time-of-flight mass spectrometry for the analysis of a wide range of chemical species. A new method for electron impact ionization based on the generation of photoelectrons is presented and coupled with a gas chromatograph interface and a pulsed laser volatilization interface for the analysis of volatile and non-volatile species, respectively. This photoelectron ionization (PEI) approach is characterized and also compared with alternatives presented in the literature.

A detailed study of matrix-assisted laser desorption/ionization (MALDI) for the analysis of industrially relevant polymers such as polystyrene, polybutadiene, polyisoprene, poly(ethylene glycol) and various copolymers follows the PEI work. Progress in sample preparation for MALDI analysis is presented. It is shown that MALDI can provide reasonably accurate average molecular weight information for polymers of narrow polydispersity, but not for polymers of higher polydispersity (i.e., PD > 1.05). Both instrumental and fundamental reasons for this observation have been identified. The ability of the technique to provide structural and compositional information for a wide range of polymer types is also assessed. The requirements for, and limitations of, structural and compositional investigations of polymers by MALDI are developed and illustrated with examples.

A new technique for the coupling of a biochemical affinity interaction with MALDI is also presented and characterized. Based on the avidin-biotin interaction, it allows for the rapid mass analysis of biotinylated species present in complex solutions. A model study is described that indicates the capability of the technique in mapping a modification site in a protein, using low picomoles of appropriately tagged protein in contaminated solutions. An investigation of an enzyme-inhibitor interaction using this methodology is also presented, in which the biotin was covalently linked to the inhibitor. Finally, an extension

of the method to the analysis of a weak antigen:antibody interaction is presented, representing preliminary work in the development of a high-throughput antigen screening program.

Acknowledgments

I would like to thank Dr. Li for the opportunity to pursue my studies in his laboratory for the past four years. His encouragement, advice and enthusiasm have been greatly appreciated; our many animated discussions are fondly remembered. The knowledge and expertise of Dr. R.M. Whittal were of invaluable assistance. I would also like to thank Dr. T. Yalcin for his assistance in some of the polymer studies. The support of the machine and electronic shops have been instrumental in this work, and is acknowledged with thanks. The many talents of Mr. L. Coulson have aided this work considerably, and I thank him. I especially thank Dr. J. Vederas, Dr. K. O'Callaghan, Dr. M. Andrews and Dr. U. Gulfke for their work on the enzyme inhibition study discussed in this thesis.

I would also like to acknowledge NSERC for providing me with a post-graduate scholarship in my first two years at the University of Alberta. The support of the Killam foundation for my last two years I consider to be a great honour, and I acknowledge it with many thanks. Also, I have appreciated the additional financial support of the Chemistry Department and the University of Alberta throughout the duration of my program.

Table of Contents

Chapter 1 1

Introduction: Laser-Based Volatilization and Ionization in Time-of-Flight Mass Spectrometry 1

1.1 Time-of-Flight as the Mass Analyser 1
1.2 Laser Desorption/Ionization 8
1.2.1 Theory 9
1.2.2 Scope of Applications 10
1.3 Laser Desorption with Post-ionization of Neutrals 11
1.3.1 Multiphoton Ionization 11
1.3.2 Single Photon Ionization 12
1.4 MALDI 13
1.4.1 The Procedure 13
1.4.2 Theory 15
1.4.3 Scope of Applications 17
1.5 Focus of the Current Work 17
1.6 Literature Cited 18

Chapter 2 22

Photoelectron Ionization in a Time-of-Flight Mass Spectrometer 22

2.1 Introduction 22
2.2 Experimental 25
2.3 Results and Discussion 27
2.3.1 Initial Observations 27
2.3.2 The Ionization Process 32
2.3.3 Small Molecule Analysis 35
2.3.4 Polymer Analysis 39
2.3.3.1 Monomer Identification 41
2.3.3.2 Terminal Group Identification 44
2.4 Literature Cited 48

Chapter 3 51

MALDI Analysis of Polymers: Sample Preparation and Average Molecular Weight Determination 51

3.1 Introduction 51
3.2 Experimental 52
3.2.1 Instrumentation 52
3.2.2 Data Collection and Processing 53
3.2.3 Sample Preparation 53
3.2.4 Mass Calibration 54
3.2.5 Samples and Reagents 54
3.3 Results and Discussion 55
3.4 Literature Cited 67

Chapter 4 69

MALDI Analysis of Polymers: Validity of Molecular Weight Determinations 69

4.1 Introduction 69
4.2 Experimental 70
4.2.1 Instrumentation 70
4.2.2 Data Collection and Mass Calibration 71
4.2.3 Sample Preparation 71
4.2.4 Samples and Reagents 72
4.3 Results and Discussion 72
4.3.1 Sample Preparation, Desorption/Ionization 73
4.3.1.1 Multimer Formation 73
4.3.1.2 Overlap of Multiple Distributions 76
4.3.1.3 Matrix/Analyte Dependence 77
4.3.1.4 Cation Concentration Dependence 79
4.3.1.5 Laser Power Dependence 81
4.3.2 Instrumental Issues 83
4.3.2.1 Ion Focussing 83
4.3.2.2 Ion Detection 87
4.3.2.3 Detector Saturation 97

4.3.3 Data Processing and Resolution 100
4.4 Summary 102
4.5 Appendix 104
A) Overlap of Polymer Distributions 104
B) Circuit for the Floated Anode Detector Configuration 105
4.6 Literature Cited 106

Chapter 5 110

MALDI Analysis of Polymers: Structural Information 110

5.1 Introduction 110
5.2 Experimental 110
5.2.1 Instrumentation 110
5.2.2 Data Collection and Mass Calibration 111
5.2.3 Sample Preparation 111
5.2.4 Materials 112
5.3 Results and Discussion 113
5.3.1 Mass Resolution 113
5.3.2 Mass Accuracy 117
5.3.3 Adduction Behaviour 121
5.4 Literature Cited 131

Chapter 6 133

MALDI Analysis of Polymers: Compositional Analysis 133

6.1 Introduction 133
6.2 Experimental 134
6.2.1 Instrumentation 134
6.2.2 Data Collection and Mass Calibration 135
6.2.3 Sample Preparation 135
6.2.4 Materials 136
6.3 Results and Discussion 136
6.3.1 Alternating Copolymers 136
6.3.2 Block/Random Copolymers 148
6.4 Literature Cited 155

Chapter 7 157

Combining Avidin-Biotin Chemistry with Matrix-Assisted Laser Desorption/Ionization 157

7.1 Introduction 157
7.2 Experimental 158
7.2.1 Biotinylation and Isolation of Peptides and Proteins 158
7.2.2 Instrumentation 160
7.2.3 MALDI Sample Preparation 160
7.3 Results and Discussion 162
7.3.1 Biotinylation Reagents 162
7.3.2 Immobilized Avidin/Biotin 166
7.3.3 Method of Analyte Elution 169
7.3.4 Avidin Signal Suppression and the Mechanism of Analyte Elution 170
7.3.5 Assessment 173
7.4 Literature Cited 174

Chapter 8 176

Applications of Avidin-Biotin/MALDI for Rapid Sample Purification and Identification 176

8.1 Introduction 176
8.2 Experimental 177
8.2.1 Biotinylation of Troponin C 177
8.2.2 Inhibition of PAM 178
8.2.3 Enzymatic Digestions 179
8.2.4 Oligosaccharide Analysis 180
8.2.5 Instrumentation 181
8.2.6 MALDI Sample Preparation 182
8.3 Results and Discussion 182
8.3.1 Isolation of Biotinylated Peptides 182
8.3.1.1 Identifying the Location of a Protein Tag. Biotinylated TnC 182

8.3.1.2 Identifying the Location of a Protein Tag. Inhibition of PAM 196
8.3.2 Screening for Antigens 201
8.4 Literature Cited 204

Chapter 9 207

Conclusions and Future Work 207

List of Tables

Table 3.1 Comparison of Molecular Weight Measurements for Polystyrene.....64

Table 3.2 Comparison of GPC and MALDI molecular weight results for polyisoprenes.....66

Table 3.3 Comparison of GPC and MALDI molecular weight results for polybutadienes.....66

Table 4.1 Experiments with their corresponding M_n values and standard deviations for the examination of mass discrimination in MCP saturation.....99

Table 5.1 Mass Measurement Accuracy of Selected Oligomer Peaks of PEG bis(ephedrine) in Figure 5A.....119

Table 5.2 Mass Measurement Accuracy of Selected Oligomer Peaks of PEG bis(acetaminophen) in Figure 5B.....121

Table 6.1 Comparison of experimental mass data and calculated values for several peaks shown in Figure 6.6.....150

Table 6.2 Assignment of peaks detected for a typical repeat unit shown in Figure 6.6.....151

List of Figures

Figure 1.1 Schematic of three different limiting conditions in a simple time-of-flight mass spectrometer: (A) temporal distribution in ion creation, (B) spatial distribution in ion creation and (C) energy (velocity) distribution in ion creation.....3

Figure 1.2 Schematic of the basic Wiley-McLaren ion source geometry.....5

Figure 1.3 Diagram of the time-lag focussing principle. In (A) ions are generated on a surface and allowed expand in a field free region. (B) After a delay time t, the ions are accelerated by applying a voltage pulse to the repeller. (C) With proper choice of delay time t and voltage pulse, ions are temporally focussed at the detector.....7

Figure 1.4 Schematic of a typical time-of-flight instrument used for MALDI, with a diagram of a MALDI sample formulation.....15

Figure 2.1 Photoelectron impact ionization designs according to (A) Boyle,[6] Moritz,[7] and Rohwer[21] (B) Cheng[3] and Colby[22] (C) Moritz.[7] In all designs, voltage $V_1 > V_2$.....24

Figure 2.2 (A) GC/MS design that allowed for both PEI and MPI. Capillary tip was positioned ~1 cm off-centre. (B) Laser volatilization/MS design that allowed for both PEI and MPI. Probe tip was positioned approximately one cm off-centre. In both designs, the UV laser beam passed through the source before impinging on the inner surface of the housing, in PEI mode. 26

Figure 2.3 Mass spectra of (A) Ar, (B) Xe, and (C) CO_2 obtained in PEI mode. The voltage applied to the repeller plate and extraction grid were 4.0 kV and 3.6 kV, respectively. The samples are introduced into the system through the GC interface, at a flow rates such that the system pressure was $< 5 \times 10^{-6}$ torr.....29

Figure 2.4 Mass spectra of pentane obtained by (A) PEI with the GC interface (B) electron impact ionization, from the NIST Mass Spectral Search Program (version 1.5, 07/19/96).....30

Figure 2.5 Log of the Ar^+ ion intensity as a function of the log of the photo detector output for PEI generated from a 266-nm laser beam and a 355-nm laser beam.....31

Figure 2.6 Simulation of photoelectron trajectory using the SIMION program,[30] with source dimensions and applied voltages equivalent to the laser volatilization configuration.....33

Figure 2.7 PEI mass spectra of (A) benzene, molecular ion at m/z 78, and (B) 2,2,5-trimethylhexane, molecular ion at m/z 128 and a fragment ion at m/z 57. Both spectra were obtained from an injection of 100 ng in the GC/MS mode.....36

Figure 2.8 (A) PEI mass spectrum of the dipeptide YG. (B) MPI mass spectrum of YG. Both spectra were obtained from the same sample. Only the position and focus of the laser beam were changed to switch between ionization modes.....38

Figure 2.9 Mass spectra of tetramethylammonium iodide obtained by (A) MPI and (B) PEI. Both spectra were obtained from the same sample. Only the position and focus of the laser beam were changed to switch between ionization modes.....40

Figure 2.10 Laser volatilization/PEI mass spectra of (A) polystyrene (M_n ~95 800), (B) poly(2-vinylpyridine) (M_n ~50 000) (C) poly(2-vinylpyridine) (M_n ~200 000) (D) poly(methyl methacrylate) (M_n ~12 000). 10 µg of polymer was loaded on the probe tip in each case.....42

Figure 2.11 Laser volatilization/PEI mass spectrum of poly(styrene-co-2-vinylpyridine) (M_n ~ 110 000, 30% styrene content), from an analysis of 10 µg.....43

Figure 2.12 Laser volatilization/PEI mass spectra of (A) poly(ethylene glycol) 400 diacrylate (B) and poly(ethylene glycol) 4000 diacrylate, from analyses of 1 µg each.....45

Figure 2.13 Laser volatilization/PEI mass spectra of (A) poly(ethylene glycol) 2000 monomethyl ether (B) poly(ethylene glycol) 1450, from analyses of 1 µg each.....46

Figure 2.14 Determination of preferential dissociation of the terminal group in the laser volatilization process.....47

Figure 3.1 Mass spectra of three polystyrene samples with nominal molecular weights of (A) 330 000, (B) 600 000 and (C) 900 000.....56

Figure 3.2 MALDI spectra of polybutadiene 129 360, representing (A) 0.025 pmol loaded, (B) 0.115 pmol loaded and (C) 3.4 pmol loaded. Ratios represent the number of acceptable shots to total shots fired.....59

Figure 3.3 MALDI mass spectra of (A) polystyrene with a nominal molecular weight of 1.5 million, (B) polyisoprene with a nominal molecular weight of 137 000 and (C) polybutadiene with a nominal molecular weight of 315 200.....61

Figure 3.4 Mass spectrum of polystyrene with a nominal molecular weight of 90 000. 62

Figure 4.1 Spectra of multicomponent blends consisting of (A) polystyrene 3250, 5050, 7000, 9240, 11 600 and (B) polystyrene 3250, 5050, 7000, 9240, 11 600, 20 000, and 22 000. All components were present in equimolar quantities, with 200 pmol total polymer loaded to the probe in both cases. 74

Figure 4.2 An analysis of blends to determine the effect of multimer formation on measured M_n values. (A) polystyrene 5050 and 11 600, 100 pmol of each loaded to probe, expected M_n of 8245; (B) same blend as A, doped with polystyrene 35 000 such that the amount loaded to probe was 75 pmol, with the other two components still present at 100 pmol each.....75

Figure 4.3 Determination of the effect of polymer concentration in the solid sample matrix on the measured M_n of a two-component blend, consisting of polystyrene 5050 and 28 500. For each point, the ratio of the amounts loaded for the two components was maintained. Expected M_n of 16 575. 78

Figure 4.4 (A) Determination of the effect of silver cation concentration, in the solution mixture of polymer matrix and silver salt, on the measured M_n value. 100 pmol of each component (polystyrene 5050 and 28 500) was loaded to the probe, error bars indicate +/- one standard deviation; (B) Same data as in A, with the addition of the corresponding determinations of M_n for the individual components. Expected M_n of 16 575 for the blend.....80

Figure 4.5 Effect of laser fluence on the measured M_n value of a two-component blend consisting of polystyrene 5050 and 28 500. Each component was loaded at 100 pmol. Threshold laser fluence for matrix detection is approximately 4 μJ. Expected M_n of 16 575.....82

Figure 4.6 (A) Investigation of the ion focussing properties of the MALDI TOF instrument used in this work. The sample consisted of polystyrene 5050 and 28 500, 100 pmol of each loaded to the probe. Expected M_n of 16 980. The ion source was operated with 20 kV DC applied, and a 3.6 kV push-out pulse with a 0.3 μs delay, for all detector apertures; (B) As in A, with an additional trace corresponding to a 1.0 μs delay. Error bars in B represent the removal of sample-to-sample error.....85

Figure 4.7 Effect of altering the optical transmissivity of the grounded grid (fronting the first MCP at a distance of 1.85 mm) on the measured M_n value. Post-acceleration of -2 kV was used in all cases. Three equimolar blends were prepared: polystyrene 5050/20 000, 5050/28 500 and 5050/50 000. In each case, 100 pmol of each component was loaded to the probe.....88

Figure 4.8 Effect of changing the applied post-acceleration voltage from -2.0 kV to -4.75 kV across a fixed distance of 1.85 mm. Sample compositions and loadings as in Figure 4.7.....90

Figure 4.9 Determination of the effect of altering detector configuration on the measured M_n value over a range of total acceleration potentials, for a two-component blend consisting of polystyrene 5050 and 28 500 (100 pmol of each loaded to the probe, expected M_n of 16 620): (A) Investigating the effect of changing the post-acceleration potential from zero (and no grounded grid) to -2.0 kV and -4.75 kV; (B) maintaining the applied potential in the post-acceleration region at -4.75 kV, but altering the length of this region to change the field strength from 1090 to 2570 V/mm.....91

Figure 4.10 Approximate form of the detection probability equation as a function of ion energy, for both the high and low mass components of a 5050/28 500 blend. Only ion-to-electron conversion from the primary ions is considered.....94

Figure 4.11 Spectrum of a three-component blend used to investigate the effects of detector saturation on the measured M_n values. Sample consisted of polystyrene 5050, 11 600, and 35 000 (100 pmol of each loaded to probe). The experimental configuration in Table 1 (1B) was used (see discussion in the text).....98

Figure 4.12 Spectrum of a two-component blend consisting of polystyrene 5050 and 11 600 (100 pmol each), (A) with no intensity correction applied and B) with the intensity correction applied.....101

Figure 5.1 MALDI mass spectra of PEG 15 000 obtained by operating the instrument in (A) the continuous extraction mode with HABA as the matrix and sodium cationization; (B), (C), and (D) the time-lag focussing extraction mode with (B) DHB, (C) IAA, and (D) HABA as the matrices and sodium cationization. For (D), M_n = 9380 and D = 1.20. The supplier certifies M_n = 12 500 and PD = 1.20 by gel permeation chromatography.....114

Figure 5.2 MALDI mass spectra of (A) poly(styrene) 32 660 (B) poly(styrene) 45 000, and (C) the expanded spectrum of poly(styrene) 45 000 using retinoic acid as the matrix with silver cationization. For (A) M_n = 29 350 and PD = 1.004. The supplier certifies M_n = 30 000 and PD = 1.025. For (B), M_n =

44 930 and PD = 1.008. The supplier certifies M_n = 45 550 and PD = 1.053. The supplier used gel permeation chromatography for the analyses. 116

Figure 5.3 MALDI spectra of (A) PEG bis(ephedrine) and (B) PEG bis(acetaminophen) using HABA as matrix and sodium cationization. For (A), M_n = 3670 and PD = 1.007. For (B), M_n = 3520 and PD = 1.014. 118

Figure 5.4 MALDI mass spectra of polyisoprene 3280 obtained using tRA with $Cu(NO_3)_2$ as cationization reagent.....123

Figure 5.5 The effect of the addition of $CuCl_2$ on the observed secondary distribution arising from the MALDI analysis of (A) polyisoprene 3280 and (B) polybutadiene 2800.....125

Figure 5.6 The effect of cationization reagent on the appearance of the secondary distribution in polyisoprene 3280, using tRA with (A) $Cu(NO_3)_2$, (B) $Cu(NO_3)_2$ with KCl and (C) $CuCl_2$.....126

Figure 5.7 MALDI mass spectra of (A) polyisoprene 19 300 and (B) polybutadiene 22 430 demonstrating optimum resolution.....128

Figure 5.8 MALDI spectrum of polyisoprene 3280, using dithranol as matrix with $Cu(NO_3)_2$. Spectrum collected from a THF solution containing 0.15 M dithranol, 200 µM polymer and 1% (v/v) of a 0.1 M $Cu(NO_3)_2$ aqueous solution. A 1 µl aliquot was allowed to dry on the probe tip.....129

Figure 6.1 MALDI mass spectrum of an alternating copolymer (A) poly[(o-cresyl glycidyl ether)-co-formaldehyde] with (B) an expansion.....137

Figure 6.2 MALDI mass spectra of glycidyl end-capped poly(bisphenol A-co-epichlorohydrin) with nominal molecular weights of (A) 1750, (B) 4000 and (C) 6100.....141

Figure 6.3 Expansions of the MALDI mass spectra of (A) PBAE 1750 and (B) PBAE 6100.....142

Figure 6.4 End-group compositional analysis of (A) PBAE 1750 and (B) PBAE 6100, for the indicated oligomeric forms. Ratios are calculated from the areas of corresponding peaks.....144

Figure 6.5 Comparison of PBAE 4000 and PBAE 6100 through Q, the ratio of the fraction of diglycidyl species to mono-glycidyl species, over a certain mass range.....147

Figure 6.6 MALDI mass spectrum of (A) poly(propylene glycol-b-ethylene glycol-b-propylene glycol)bis(2-aminopropyl ether) with (B) an expansion.....149

Figure 6.7 MALDI mass spectra of (A) Dow Polyol A and (B) Dow Polyol B.....153

Figure 6.8 Expansions of the MALDI mass spectrum of Dow Polyol B showing (A) the low mass region and (B) the high mass region.....154

Figure 7.1 Schematic of the MALDI procedure for the analysis of biotinylated species complexed to avidin, immobilized on agarose beads.....161

Figure 7.2 MALDI mass spectra of bradykinin (expected MH^+ = 1061.2 u) and (A) biotin-bradykinin (expected MH^+ = 1287.5 u), (B) biotin-LC-bradykinin (expected MH^+ = 1400.7 u) and (C) biotin-SS-bradykinin (expected MH^+ = 1450.8 u) reaction mixtures from HCCA. MALDI mass spectra of (D) biotin-bradykinin, (E) biotin-LC-bradykinin and (F) biotin-SS-bradykinin from HCCA, after purification with immobilized tetrameric avidin.....163

Figure 7.3 An on-probe reduction of the disulphide spacer between biotin and bradykinin. The mass spectrum was obtained from the same solution as used for Figure 7.2F.....165

Figure 7.4 (A) Mass spectrum of biotin-insulin from SA with approximately 0.5 pmol total protein loaded. Expected MH^+ values are 5734.6 u (insulin), 5960.9 u (insulin-biotin), 6187.2 u (insulin-$biotin_2$), and 6413.5 u (insulin-$biotin_3$). Mass spectra demonstrating the purification of biotin-insulin using (B) immobilized tetrameric avidin, (C) immobilized biotin, where the biotin-insulin was complexed with avidin in solution prior to purification with the beads, and (D) immobilized monomeric avidin.....167

Figure 7.5 Mass spectra showing the sensitivity of the immobilized tetrameric avidin-based procedure: (A) spectrum of the reaction mixture, (B) spectrum from the analysis of 50 fmol of biotin-LC-insulin revealing the strong avidin subunit interference and (C) suppression of the avidin subunit peaks with the addition of an aliquot of a biotin solution.....171

Figure 8.1 MALDI mass spectra of (A) unlabelled TnC (expected $[M+H]^+$ = 18 257.4 u) and (B) biotinylated TnC (expected $[M+H]^+$ = 18 685.0 u).....183

Figure 8.2 (A) Mass spectrum from a sample of the tryptic digest of a 100:1 blend of TnC and biotinylated TnC. Inset shows an expansion of the region from m/z 1400 to 1900; (B) purification and analysis of the tryptic digest using the avidin-biotin/MALDI procedure, representing at most 200 fmol of peptide applied to the probe tip.....185

Figure 8.3 Mass spectrum obtained from a tryptic digest of a solution containing BSA, cytochrome c, TnC and a trace amount of biotinylated TnC. Purification and analysis was achieved using the avidin-biotin/MALDI procedure. Spectrum represents at most 20 fmol of peptide applied to the probe tip. 187

Figure 8.4 Mass spectra obtained from 75 minute LAP digestions of an unpurified tryptic digest containing trace amounts of a biotinylated peptide, using (A) 400 pmol and (B) 1.2 nmol of LAP. Biotinylated species were isolated and analysed using the avidin-biotin/MALDI procedure.....189

Figure 8.5 Mass spectra obtained from a CPY digestion of an unpurified tryptic digest containing trace amounts of a biotinylated peptide. The digestion was sampled at (A) 10 minutes, (B) 40 minutes and (C) 120 minutes. Biotinylated species were isolated and analysed using the avidin-biotin/MALDI procedure.....190

Figure 8.6 Nomenclature for the backbone fragmentation of peptide ions. Subscripts refer to the amino acid position in the sequence, determined from the N-terminal (for **a**, **b**, **c** ions) or C-terminal (for **x**, **y**, **z** ions). R refers to the amino acid side-chain.....192

Figure 8.7 MS/MS spectrum of m/z 1625.7 biotinylated peptide, obtained with high energy CID on the ZabSpec oa-TOF. (A) Full spectrum, (B) expansion of the immonium ion region. The biotinylated peptide was isolated and analysed from a tryptic digest using the avidin-biotin/MALDI procedure. 194

Figure 8.8 Expansions of the MS/MS spectrum of Figure 8.7, showing the (A) m/z 165 to 335 region and (B) the m/z 335 to 500 region.....195

Figure 8.9 MALDI spectra of the (A) pure and (B) inhibited PAM (using compound **III**).....198

Figure 8.10 Spectrum arising from the avidin:biotin/MALDI analysis of PAM inhibited with compound **II**. The m/z values indicated represent the mono-isotopic peaks.....199

Figure 8.11 Spectrum of the biotinylated control antibody, using SA as the matrix. Note multiple biotinylation, indicated by the spacing of peaks by 226 u.....202

Figure 8.12 Spectra of the oligosaccharide mixture (A) before and (B) after purification. 203

List of Abbreviations

BSA	bovine serum albumin
CID	collision-induced dissociation
CPY	carboxypeptidase Y
DHB	2,5-dihydroxybenzoic acid
DMF	N,N-dimethylformamide
DMPD	N,N-dimethyl-1,4-phenylenediamine
DNA	deoxyribonucleic acid
DTT	dithiothreitol
EBE	electric sector/magnetic sector/electric sector mass spectrometer
EDTA	ethylenediaminetetraacetic acid
ESI	electrospray ionization
EI	electron-impact ionization
eV	electron volt (=1.602 x 10^{-19} J)
FA	formic acid
fwhm	full width at half maximum
GC/MS	gas chromatography/mass spectrometry
GPC	gel permeation chromatography
HABA	2-(4-hydroxyphenylazo)benzoic acid
HCCA	α-cyano-4-hydroxycinnamic acid
HPDP	N-[6-(biotinamido)hexyl]-3'-(2'-pyridyldithio)propionamide
HPLC	high pressure liquid chromatography
IAA	*trans*-indoleacrylic acid
IR	infrared

K_a	thermodynamic association constant
LAP	leucine aminopeptidase M
LLS	laser light scattering
MALDI	matrix-assisted laser desorption/ionization
MCP	microchannel plate
M_n	number average molecular weight
MO	membrane osmometry
MPI	multiphoton ionization
M_p	most probable molecular weight
MS/MS	mass spectrometry/mass spectrometry
M_w	weight average molecular weight
m/z	mass-to-charge ratio
Nd:YAG	neodynium-doped yttrium aluminum garnet
NHS	N-hydroxysuccinimide
NMR	nuclear magnetic resonance
2P	2-propanol
PAL	peptidylglycine α-hydroxyglycine α-amidating lyase
PAM	peptidylglycine α-amidating mono-oxygenase
PBAE	glycidyl end-capped poly(bisphenol A-co-epichlorohydrin)
PBS	phosphate-buffered saline
PD	polydispersity (M_w/M_n)
PEG	poly(ethylene glycol)
PEI	photoelectron-impact ionization

PGF	poly[(o-cresyl glycidyl ether)-co-formaldehyde]
PHM	peptidyl α-hydroxylating mono-oxygenase
pI	isoelectric point
PPEP	poly(propylene glycol-b-ethylene glycol-b-propylene glycol)bis(2-aminopropyl ether)
ppm	parts per million
RSD	relative standard deviation
SA	sinapinic acid
SALI	Surface Analysis by Laser Ionization
SIMS	secondary ion mass spectrometry
TEA	transverse excitation atmospheric
TFA	trifluoroacetic acid
THF	tetrahydrofuran
TnC	troponin C
TPCK	*tos*-L-phenylalanine chloromethyl ketone
tRA	*all-trans*-retinoic acid
u	unified atomic mass unit (= Da)
UV	ultraviolet
VUV	vacuum ultraviolet
v/v	volume-to-volume ratio

Chapter 1

Introduction: Laser-Based Volatilization and Ionization in Time-of-Flight Mass Spectrometry

There is a long history to the incorporation of lasers in mass spectrometry. Laser pyrolysis of materials, followed by mass spectral analysis, took place almost immediately upon the development of continuous wave lasers in the early 1960's.[1] Many different types of mass analysers were used in this initial work, including time-of-flight mass spectrometric systems. However, it was not until the early 1970's, with the incorporation of Q-switched pulsed laser systems, that the advantages of coupling lasers with time-of-flight mass spectrometers were realized. The rebirth experienced by time-of-flight mass spectrometry particularly in the past 15 years is due in large part to the development of sample volatilization and ionization methods based on pulsed laser systems. The following section outlines the theory and state-of-the-art in time-of-flight, especially as they relate to laser-based systems. Subsequent sections will discuss the implementation and applications of lasers in analytical time-of-flight mass spectrometry.

1.1 Time-of-Flight as the Mass Analyser

Time-of-flight mass analysis involves the separation of ions according to their differences in velocity. In a simplified geometry, ions present in a source region are accelerated by an electric field present in this source. They enter a field free region called the drift tube, where the separation occurs. Ions are detected at the end of this tube. The basic equation governing the process in time-of-flight is

$$zeEs = \frac{1}{2}mv^2, \tag{1}$$

where z represents the charge on the ion, e the fundamental unit of charge, E the electric field in the source and s the location of the ion in the source. The mass and final velocity of the ion are indicated by m and v, respectively. The velocity of the ion can be simply expressed as

$$v = D/t, \tag{2}$$

where D is the length of the drift tube and t is the time required for the ion to travel this length. Combining equations (1) and (2) leads to the familiar expression of m/z as a function of t:

$$\frac{m}{z} = \left[\frac{2eEs}{D^2}\right]t^2. \tag{3}$$

Note that this treatment considers the time spent by the ions in the source to be negligible.

Based on the measurement of an ion's arrival time at the detector, and knowledge of the instrumental quantities represented in the square brackets of equation (3), the m/z value for an ion can be determined. Usually, however, the arrival time of at least two m/z standards are measured in order to generate a calibration equation of the following type:

$$\frac{m}{z} = (\alpha t + \beta)^2. \tag{4}$$

The terms α and β represent values particular to the design and operation of the instrument.

In time-of-flight, peak resolution for a single mass can be determined by the time dispersion in the ion packet at the detector. Taking the derivative of equation (3) and rearranging leads to the resolution expression:

$$\frac{m}{\Delta m} = \frac{t}{2\Delta t}. \tag{5}$$

The value Δt is usually measured as the peak's full width at half maximum (fwhm). Traditionally, poor resolution has been the weakness of time-of-flight mass spectrometry. The first instruments were characterized by values rarely in excess of 100.[2] There are three primary contributions to peak width: temporal distribution in ion formation (Δt_o), the initial spatial distribution of ions in the source (Δs) and the ions' initial energy distribution imparted by the ionization process (ΔU_o). The dominance of any one of these contributions is dependent upon how ionization occurs. Three limiting cases will be considered for instrumental configurations involving sample ionization with lasers. Their development is supported by Figure 1.1A-C.

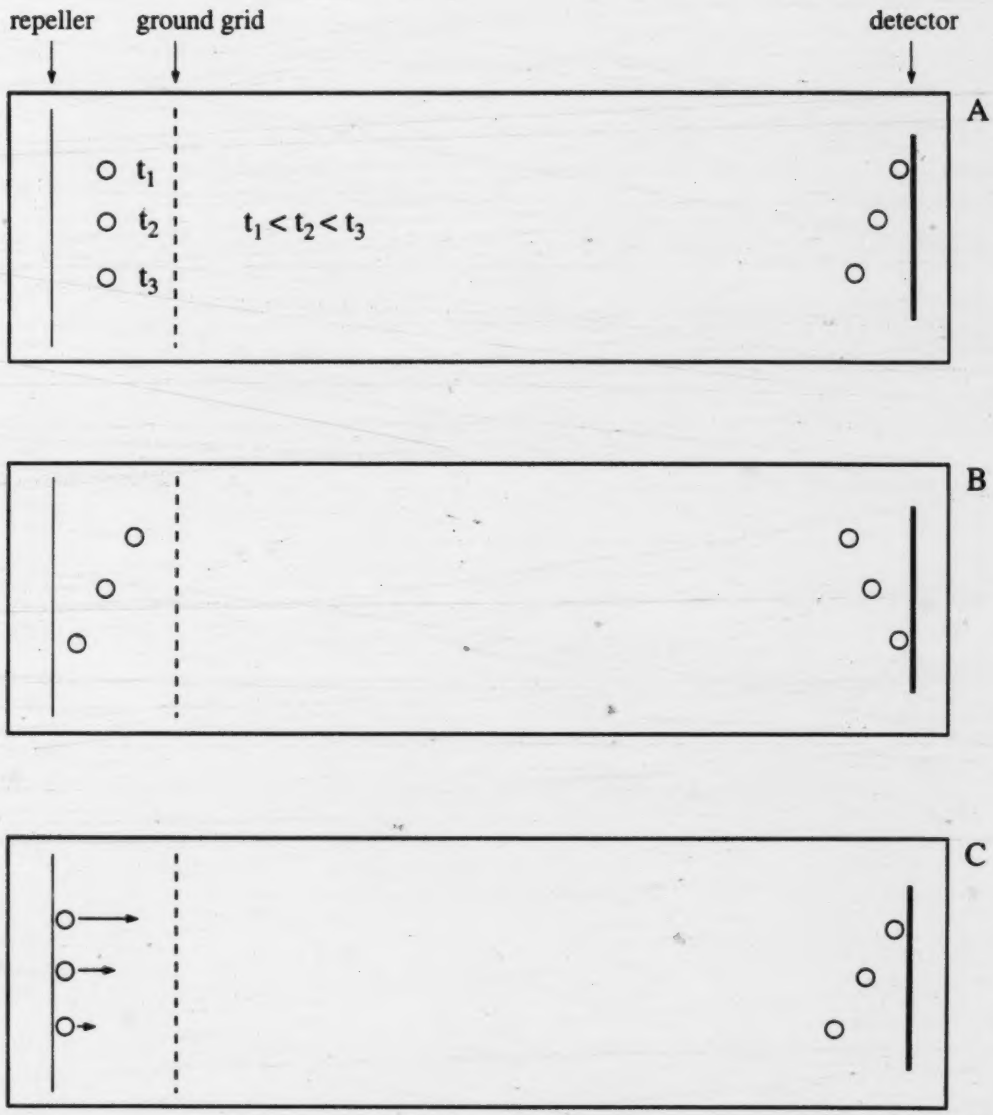

Figure 1.1 Schematic of three different limiting conditions in a simple time-of-flight mass spectrometer: (A) temporal distribution in ion creation, (B) spatial distribution in ion creation and (C) energy (velocity) distribution in ion creation.

i) $\Delta t_0 = \text{constant},\ \Delta s = 0,\ \Delta U_0 = 0$

If ions of a given mass bear no spatial or initial energy distribution in the source, then the only significant determinant of resolution at the detector is the initial temporal distribution (Figure 1.1A). In ionization by pulsed lasers, this represents the amount of time over which ions are generated, and correlates to the pulse width of the laser beam. For such ionization procedures, pulse widths are most often less than 10 ns fwhm. According to equation (5), increasing the resolution is then a simple matter of increasing the flight time. This can be accomplished by increasing the length of the drift tube or by decreasing the accelerating potential of the source.

ii) $\Delta t_0 = 0,\ \Delta s \neq 0,\ \Delta U_0 = 0$

Ions generated by a laser process can be spatially distributed to some degree. The ions experience different accelerating voltages by virtue of their position, which translates into a time-dispersion in the plane of the detector (Figure 1.1B). The solution to this problem involves either minimization or compensation of the spatial distribution. In laser time-of-flight mass spectrometry, this dispersion can be minimized in two ways. In the first place, generating ions by a laser interaction with gas phase species allows for reduction of the ionization volume by tighter focussing of the laser. In the second place, generating ions from a surface oriented parallel to the detector implies that the spatial distribution is governed essentially by surface irregularities.

Ion sources can be designed to compensate for spatial distributions. The single stage source displayed in Figure 1 has only a limited capacity to do so. Wiley and McLaren designed a two-stage source which is capable of providing a space focal plane of variable position.[2] Here, the term "space focal plane" refers to a region in the instrument where the initial spatial distribution has been reduced to zero. The schematic of this source is displayed in Figure 1.2. Briefly, it consists of an additional electrode placed between the repeller electrode and the ground grid illustrated in Figure 1.1. This defines two regions which can be operated with different electric fields. For this geometry, it is necessary to relax the assumption of negligible ion time in the source. Doing so results in the following general expression for the total flight time of an ion originating from anywhere in the first region:

$$t = t_o + \frac{\sqrt{2m}}{zeE_s}\left[\left(U_o + zesE_s\right)^{1/2} \pm U_o^{1/2}\right] + \frac{\sqrt{2m}}{zeE_d}\left[U^{1/2} - \left(U_o + zesE_s\right)^{1/2}\right] + \frac{D(2m)^{1/2}}{2U^{1/2}}, \quad (6)$$

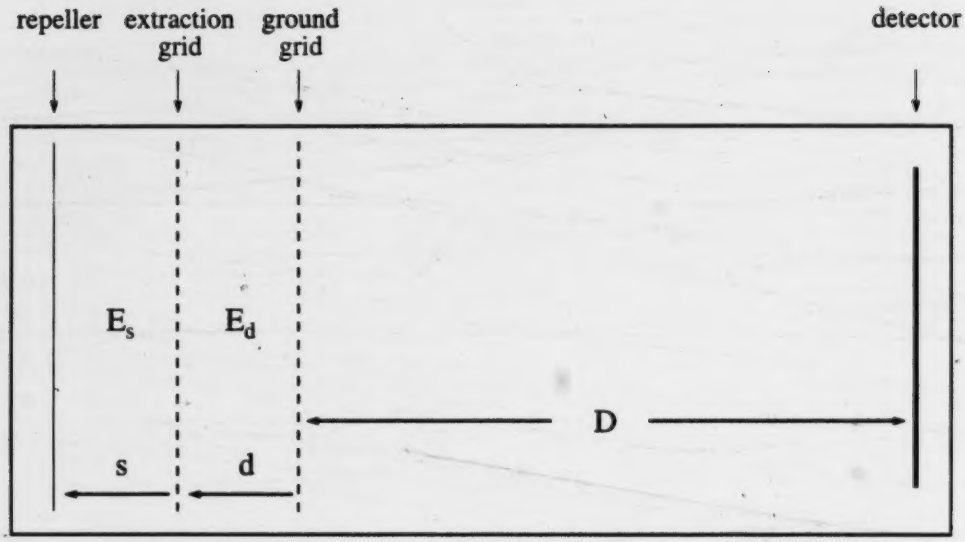

Figure 1.2 Schematic of the basic Wiley-McLaren ion source geometry.

where E_s and E_d refer to the electric fields in the first and second regions, respectively, and U to the total ion energy. Assuming the resolution-limiting factor is the spatial distribution, we can assume the ion's initial energy U_o to be zero. Taking the derivative of this expression with respect to position, *s*, and setting it equal to zero gives rise to the space focussing condition:[3]

$$D = 2s_o k_o^{3/2}\left[1-\left(\frac{1}{k_o + k_o^{1/2}}\right)\left(\frac{d}{s_o}\right)\right], \tag{7}$$

where

$$k_o = \frac{s_o E_s + dE_d}{s_o E_s}. \tag{8}$$

Here, *d* refers to the length of the second acceleration region, and s_o to the average, initial ion position. Therefore, a unique E_s/E_d ratio defines the space focal plane at a distance *D*.

iii) $\Delta t_o = 0,\ \Delta s = 0,\ \Delta U_0 \neq 0$

In laser time-of-flight mass spectrometry, it is likely that a non-zero ΔU term is the limiting factor in the determination of resolution. For example, laser desorption/ionization processes can produce ions with kinetic energy distributions up to tens of electron volts.[4] In the pursuit of improved resolution, this has proven to be the most difficult term to overcome. As shown in Figure 1.1C, an ion with a high initial kinetic energy will arrive at the detector before an ion with a low initial kinetic energy, all other things being equal. Equation (6) indicates that the influence of the ion's initial energy can be minimized by ensuring that the total ion energy is large by comparison. In other words, high total accelerating voltages are required.

A dual stage source provides only a modest improvement in energy focussing over the simple one stage source. Such dual stage sources generally allow resolutions of a few hundred for laser-based ionization systems.[5] Further improvements in energy focussing can be obtained with *time-lag focussing* or *reflectrons*. In time-lag focussing, ions are allowed to separate in the source region, according to their initial kinetic energy differences, for a certain time (Figure 1.3A). This takes place in an initially field-free region, and allows the energy distribution to be converted into a spatial distribution. A voltage pulse is then applied to the repeller for ion acceleration into the drift tube (Figure 1.3B). Ions with a higher initial energy will receive a lower acceleration potential from the source than those

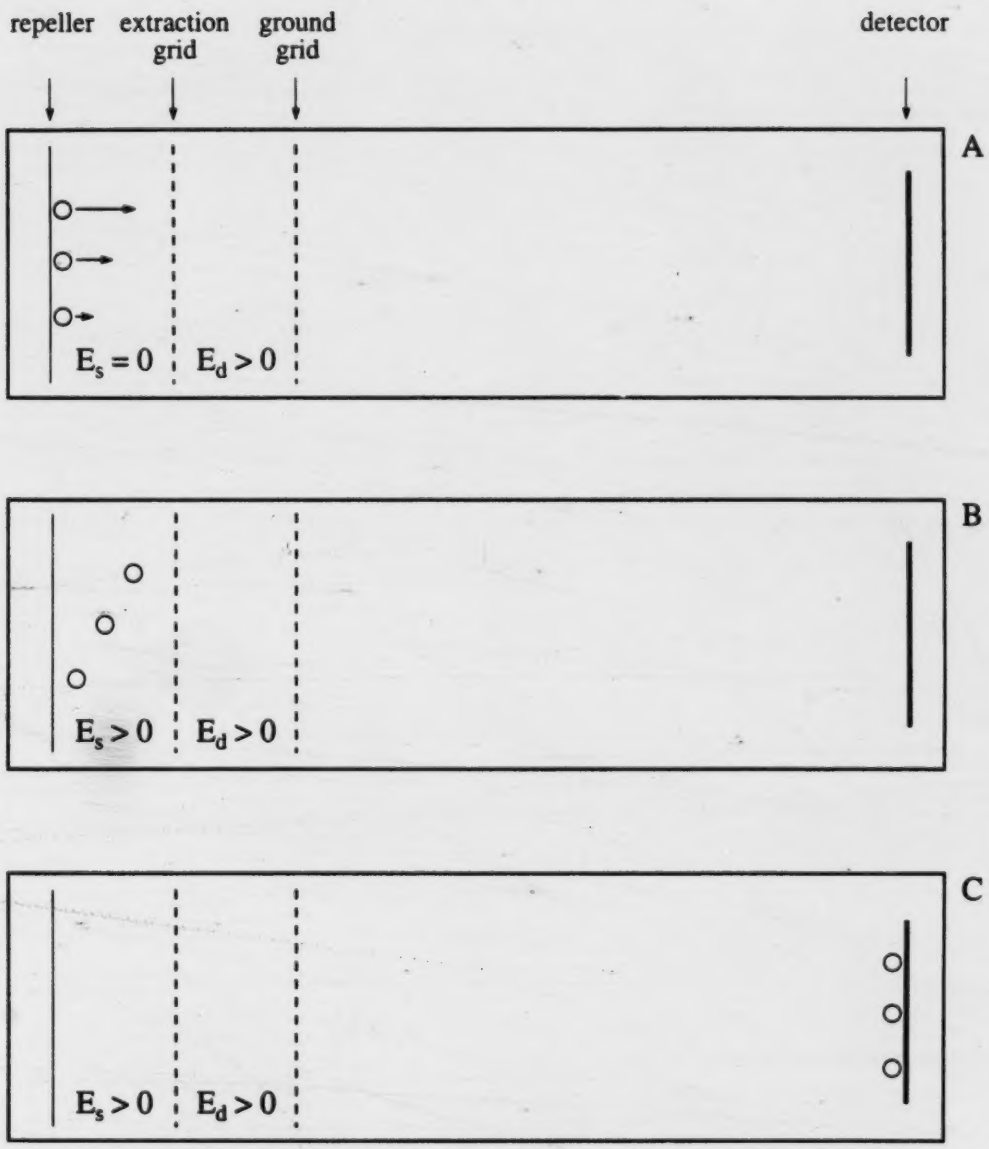

Figure 1.3 Diagram of the time-lag focussing principle. In (A) ions are generated on a surface and allowed expand in a field free region. (B) After a delay time t, the ions are accelerated by applying a voltage pulse to the repeller. (C) With proper choice of delay time t and voltage pulse, ions are temporally focussed at the detector.

ions with a lower initial energy. The time delay and the voltage ratios on the source elements are selected to focus this induced spatial distribution at the detector (Figure 1.3C). However, this voltage ratio is not the same as that required for the focussing of the initial spatial distribution. The usefulness of time-lag focussing will therefore depend upon which contribution is the limiting factor to the resolution. In laser-based ionization processes, spatial distributions can usually be minimized to the extent that kinetic energy distributions are the limiting factor. This is especially true for MALDI, where dramatic improvements in resolution have been realized with this technique.[6-9]

A post-source method also exists for ion energy focussing, leading to improved resolution. It involves the placement of an electrostatic ion mirror at the opposite end of the drift tube.[10,11] Ions of the same mass but different initial kinetic energies enter the mirror and penetrate to depths dependent upon the magnitude of these initial kinetic energies. This creates a spatial distribution of ions in the mirror that is correlated to the ion's initial kinetic energy. The mirror serves to reflect and focus these ions at the detector surface. A resolution of 25 000 has been achieved with such a design for a gas-phase laser ionization method,[12] although routinely resolution of only a few thousand can be obtained.

Commercial time-of-flight systems are configured to operate in linear or reflectron mode, or both. Source designs vary in complexity, but usually involve some variant of the original Wiley-McLaren design. Systems incorporating laser-based gas phase ionization methods typically use a very simple one or two stage source, and rely on a reflectron design for improved resolution. For systems based upon laser desorption and ionization from surfaces, time-lag focussing is currently popular, occasionally configured with an ion mirror for further improvements in resolution. Mass accuracies as good as 5 ppm have been reported on the newer reflectron instruments,[13] although accuracies of 10-100 ppm are more routine. Much of the recent growth in the area of time-of-flight mass spectrometry has been based on laser volatilization of samples from surfaces, and the following sections survey the developments in this area.

1.2 Laser Desorption/Ionization

A review of lasers in mass spectrometry published in 1980 indicates the diverse application of lasers to this point.[1] The characterization of organic species proceeded largely through the analysis of pyrolysis products, quite often involving an indirect pyrolysate transfer (e.g., through a gas chromatograph to the mass spectrometer). Ionization was achieved usually by electron impact, and most often coupled to a mass

spectrometer other than a time-of-flight. A concerted volatilization and ionization of simple organics such as alkyl sulfonates on a time-of-flight instrument was presented in 1970 by Vastola et. al.[14] Their observance of a quasi-molecular ion consisting of the alkali-cationized organic species signaled the birth of this type of mass spectrometry. After a brief lull, Kistemaker and coworkers published a direct laser desorption/ionization analysis of more complex biochemicals in 1978.[15] This work involved the irradiation of samples, deposited in pure form as very thin layers, with a CO_2 laser (10.6 μm radiation, pulse width of 0.15 μs and 1MW/cm^2). Spectra were shown exhibiting quasi-molecular ions of complex species such as digitonin ($[M+Na]^+$ = 1251 u). Although a double-focussing sector instrument was used in this work, subsequent studies were conducted using time-of-flight instruments.[4,16]

1.2.1 Theory

The mechanism of volatilization and ion formation involves many processes, and depends on the temporal pulse width of the laser beam, the power density at the sample surface, the sample substrate and sample preparation method.[17] The bulk of the studies conducted in this area seem to favor thermal mechanisms. In studies undertaken by Cotter using a pulsed CO_2 laser (~100 ns pulse width, 1 MW/cm^2 power density), it was indicated that ions are produced during the pulse, and for several μs after the pulse.[4] The ions formed during the laser pulse can have energies in the tens of electron volts, with wide energy distributions. The energies of the ions produced after the pulse (some tenths of an electron volt) are consistent with a thermal mechanism for volatilization, in which ions are produced during the relaxation of an instantaneously high temperature. However, for this CO_2 laser system and others involving even shorter pulse widths and higher power densities, the existence of the ions formed during the pulse cannot be completely rationalized by equilibrium thermal processes, as the temperatures would be unreasonably high. In this domain, the rate of heating is thought to be important, as thermal evaporation can be seen to compete directly with decomposition mechanisms.[18,19] As long as the heating rate exceeds that of the decomposition rate, emission of intact molecules appears possible. Cotter has also studied thermally sensitive compounds to illustrate these points. In the analysis of some quaternary ammonium salts, ions indicative of decomposition have been noted several μs after, but not during, the laser pulse.[20]

The term "desorption" is used in this regard to indicate the generation of intact gas-phase molecules or ions during the laser pulse, and produced under non-thermal

equilibrium processes.[21] This term should not be used for the longer time-scale thermal processes, as is often the case in the literature. The mechanisms that *do* apply in desorption are broadly classified as collective, non-equilibrium processes that appear to occur in the condensed phase. The general term "volatilization" will be used to refer to the production of gaseous species from a surface, without specifying a mechanism.

However it is rationalized, the laser volatilization phenomenon appears to generate neutral species that are significantly ionized in the gas-phase. This is particularly true for alkali-cationized species. For example, there is coincidence in the appearance temperatures for laser-generated Na^+ and the sodium cation of sucrose.[22] This suggests that volatilization of Na^+ is required to assist the ionization of sucrose. At power densities above approximately 10^7 W/cm^2, there appears to be no wavelength dependence to the success of volatilization and ionization, although at ion detection thresholds, slight wavelength dependencies have been found.[21] For those species that resonantly absorb at the laser wavelength, ionization processes can become more complicated. Under non-resonant desorption conditions, even-electron quasi-molecular ions are typically generated at fluence levels around the detection threshold. Under resonant conditions, photo-ionization processes can give rise to radical cations and ions formed by hydrogen addition or abstraction.[23] Such processes become very important for the technique of matrix-assisted laser desorption/ionization, as discussed in section 1.4.2.

1.2.2 Scope of Applications

Time-of-flight instruments designed around the laser volatilization phenomenon are used in two ways: in bulk analysis for structural information, or in spatial analysis of a sample. The former application typically involves lower power densities ($\leq$ 1MW/cm^2) applied to large spots (~1 mm^2). This usually does not lead to visible damage of the sample. Quasi-molecular ions such as $[M+Na]^+$ are generated, and often with a degree of fragmentation or decomposition. Spectra have been shown for the direct laser desorption/ionization of intact species with masses of several thousand units.[24] The latter application involves focussed high energy lasers, using commercial instruments called LAser Microprobe Mass Analysers (LAMMAs).[25] These were designed as alternatives to ion microprobes and secondary ion mass spectrometry (SIMS) instruments. The power densities used are often much greater than for bulk analysis, and lead to physical damage of the sample. Using lasers such as a Nd:YAG operated at the fourth harmonic (266 nm) allows for very small spot sizes (less than 1 μm^2), and consequently good spatial

resolution. Thermal processes are less important under these conditions. Both elemental and organic compound analyses are possible with such instrumentation.

A weakness of the direct desorption/ionization technique concerns the ionization efficiency. It has been shown that the ratio of ion production to neutrals is roughly 10^{-4}:1 at power densities below 10^8 W/cm^2.[1,26] While the efficiency of ion production is greater at higher power densities, the excessive fragmentation or pyrolysis that often results minimizes the information content. Furthermore, the efficiency is not reproducible from sample to sample due to a significant sample matrix effect on the ion yield.[27] This is similar to what has been observed in SIMS analyses.[28] The efficiency of neutral generation is not nearly as sensitive to the sample matrix. To improve the sensitivity and minimize the influence of the matrix, methods have been designed to ionize the neutrals generated from the laser volatilization process.

1.3 Laser Desorption with Post-ionization of Neutrals

The early days of lasers in mass spectrometry were dominated by electron-impact ionization of the neutrals produced from the volatilization process. While neutrals are generated in greater abundance than ionic species, they are generated over an even greater time window than the ionic species.[4] This had allowed the coupling of laser volatilization techniques with scanning-type instruments such as quadrupoles or magnetic sectors.[1] In time-of-flight, the efficiency of electron-impact post-ionization was not good. Electron impact was therefore abandoned in favor of pulsed laser ionization methods.[3] With the advent of short-pulsed excimer and Nd:YAG lasers, post-ionization could be achieved in under 10 ns. Two post-ionization schemes have been pursued with some vigor: multiphoton ionization and single photon ionization.

1.3.1 Multiphoton Ionization

This ionization mechanism involves the absorption by gas-phase neutrals of two or more photons. The combined absorbance of these photons must give rise to an increase in energy which is beyond that necessary for ionization. The most common form of multiphoton ionization is resonance-enhanced multiphoton ionization.[29] In this process, one photon is absorbed, bringing the molecule into a higher energy, quantum-mechanically allowed electronic state. A second photon of the same energy is then absorbed, raising the combined energy in excess of the molecule's ionization potential. The nature of this

process implies that the method will be selective: only those molecules which possess an electronic state having an energy coincident with that of the incoming photon will be efficiently ionized. Efficiencies of 10-100% have been estimated for several small aromatic molecules.[30] Non-resonant multiphoton processes do occur, however their efficiencies are much lower.

Multiphoton ionization has been coupled to laser volatilization of pure samples.[30] The coupling can involve MPI of directly desorbed neutrals, or these neutrals can be entrained in a supersonic jet of a simple gas such as CO_2. This jet causes collisional cooling of the entrained species, giving rise to a greatly reduced kinetic energy spread of the neutrals in the source. In either form, a second laser beam passes directly through the source region for ionization. The power density of this laser is selected according to the degree of fragmentation required; a higher power density (>1 MW/cm^2) leads to more extensive fragmentation, while a lower power density serves to preserve the molecular ion.

1.3.2 Single Photon Ionization

The principal weakness of an ionization procedure based on resonant photon absorption concerns its inherent selectivity. While such a feature has advantages in the analysis of known compounds in the presence of non-absorbing impurities, the technique cannot be used for surveying unknowns. Non-resonant multiphoton techniques have been applied to address this issue,[31] however the required power densities for universality in the detection of organic and inorganic species is in excess of 10^{10} W/cm^2 for the 193 nm output of a ArF excimer laser.[27] A further difficulty with this approach concerns the excessively high photo-fragmentation that would result for those species that do happen to resonantly absorb at the wavelength used. The approach adopted by Becker and others has involved a single high energy photon for ionization. Substantially lower power densities can be used because it involves a single photon process. To achieve an energy of 10.5 eV necessitates a wavelength of 118 nm. Such radiation is in the vacuum ultraviolet (VUV) range. This requires non-trivial laser configurations, which still do not possess sufficient energy for completely universal ionization.

Similar to concerted laser desorption/ionization, laser post-ionization has been used for bulk analyses in the characterization of a range of nonvolatile organic materials. Multiphoton and single photon ionization have been applied to simple organics,[20,32] peptides,[33,34] nucleosides[35] and synthetic polymers.[31,36,37] The amount of structural information that can be obtained from such configurations is limited by both the

volatilization and ionization processes. Volatilization procedures based upon laser irradiation of pure compounds can lead to decomposition, and they do appear to have mass limits (approximately several thousand u). Therefore, even though the ionization step can be performed in a gentle fashion, the presence of a molecular ion is not guaranteed. Post-ionization by multiphoton techniques also has its mass limit. For example, the sample amount corresponding to the ion detection threshold increases with an increase in peptide mass.[30] The largest peptidic species analysed by a laser desorption/multiphoton ionization process appears to be bovine insulin.[33] It has been postulated that the rate of radiationless processes increases with peptide size. Upon irradiation and excitation, thermalization of the excitation energy through the increasing number of the degrees of freedom begins to compete effectively with the ionization process.[30]

Laser-based post-ionization schemes have also been coupled to other volatilization mechanisms, most notably ion or atom bombardment in SIMS. This configuration in particular has been applied to depth and spatial analysis, allowing for high sensitivity and less complication from matrix effects. Such systems have allowed for detailed surface analyses, providing information on the nature of organic adsorbates, as well as inorganic composition. In the science of surface analysis, this so-called sputtered neutral mass spectrometry has gained a level of prominence, particularly for those applications requiring its high sensitivity.[38]

With the advent of matrix-assisted laser desorption/ionization (MALDI) and electrospray ionization (ESI), bulk analysis by either concerted laser volatilization/ionization or volatilization/post-ionization has become less popular, due to the higher sensitivity and greater mass limits of MALDI and ESI. In MALDI, we return to a concerted desorption/ionization mechanism. This technique is discussed in the following section. ESI is not a focus of this thesis and will not be discussed.

1.4 MALDI

1.4.1 The Procedure

In MALDI, the analyte of interest is embedded in a matrix material, and irradiated with a pulsed laser beam. Conventionally, the matrix material is a small organic compound that absorbs resonantly at the laser wavelength used for desorption, usually in the UV range. An appropriate matrix is characterized by a high molar extinction coefficient at the laser wavelength used, vacuum stability, and miscibility with the analyte in the solid

phase.[39] Some of the more successful matrices include 2,5-dihydroxybenzoic acid,[40] cinnamic acid derivatives[41] and 3-hydroxypicolinic acid,[42] although matrix selection is highly dependent upon the nature and purity of the analyte. The matrix and analyte are applied to a probe tip in some fashion and then inserted into the time-of-flight mass spectrometer (see Figure 1.4). The power density of the laser beam when focussed on the sample surface is on the order of 1 MW/cm^2. This is sufficient for matrix volatilization. The expanding plume of matrix from the surface carries with it molecules of the embedded analyte. The analyte becomes ionized, and is detected in the protonated and/or alkali-cationized form. Usually, the singly charged quasi-molecular ion is the dominant form, with minimal fragmentation observed. Cationization with other species such as silver ions has been known to occur, and more rarely, radical cations have been produced.[43] The gas phase species generated by this desorption/ionization process are characterized by a significant velocity distribution (~400 m/s at fwhm)[44] and an average velocity that is only weakly dependent upon mass. The magnitude of the velocity distribution is the primary contributing factor to the peak width at the detector. As stated previously, the time-lag focussing principle has been successful in minimizing the peak width and improving the resolution of the analysis by compensating for the initial velocity (energy) distribution.

MALDI is tolerant of many common salts at levels of approximately 10 mM in the final matrix/analyte preparation.[45] The procedure can also tolerate various surfactant and buffer systems used in biochemical procedures.[46] Nevertheless, it should be stressed that sensitivity and the quality of the signal obtained benefits greatly from a high degree of purity. Signals can often be obtained in a contaminated environment, but severe adduction behaviour between the analyte and the impurity can erode the information content of the spectrum. Furthermore, it has become clear that desorption/ionization efficiency can vary widely from species to species. For example, MALDI analysis of the peptides resulting from a tryptic digest of a protein does not generate a spectrum that represents all the fragments known to be present. Such representation is highly dependent upon the choice of matrix as well as the method of sample preparation. Developing optimal sample preparation methods remains an active area of research. Often, two or three procedures are required to ensure that a high percentage of the peptides are represented in the spectrum. The experimental observation is that both the presence and concentration of one peptide can severely affect the intensity of the signal arising from a second peptide.[47] This observation explains in part why quantitation by MALDI is difficult. With the proper choice of sample preparation procedure and internal standard, quantitation is currently possible to a 10%

level of accuracy, with a relative precision in the analyte/internal standard ratio of ~10%.[48,49]

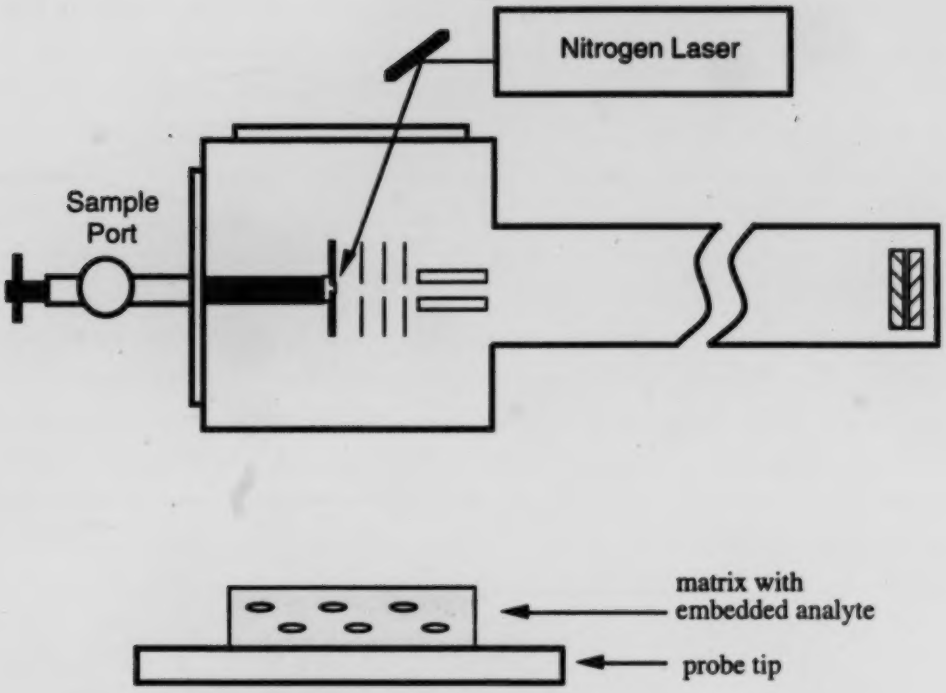

Figure 1.4 Schematic of a typical time-of-flight instrument used for MALDI, with a diagram of a MALDI sample formulation.

1.4.2 Theory

The MALDI process is not fully understood. The desorption step, the ionization step and the extent to which they are inter-related are still a matter of debate. Any proposed desorption mechanism must allow for a number of experimental observations. These include the strong dependence of matrix and analyte ion intensity on the laser fluence and spot size, a very forward-peaked velocity profile of the analyte with its very weak dependence on mass, and of course the generation of intact gas-phase macromolecules. Any proposed ionization mechanism must rationalize the existence of protonated and alkali-

cationized analyte molecules with only minor charging, the phenomenon of matrix-ion suppression, and the wavelength dependence of ionization. Both mechanisms must also allow for the observation of minimal fragmentation of the macromolecules.

The MALDI process involves the extremely fast deposition of energy into the sample by the pulsed laser beam, and it is the absorption and redistribution of this energy that is in question. Briefly, thermal processes or electronic processes are thought to be operative. Proposed thermal models were found to correlate very well with the observed trends of signal intensity as a function of laser fluence.[50,51] Occasionally, such models give rise to disconcertingly high surface temperatures where macromolecular decomposition would be expected to occur. A "cool plume" model has been proposed whereby the phase transition that occurs upon ultra-fast heating is followed by a rapid expansion of the ablated material into the gas phase.[52] Such an expansion results in the cooling of the entrained analyte molecules, and may in part explain why these higher temperatures do not damage the analyte. Furthermore, it seems consistent with the weak dependence of ion velocity on mass. Other thermally-related mechanisms such as mechanical shock and pressure pulses have been invoked although they appear less feasible.[50] A completely non-thermal mechanism proposes that the surface-adsorbate complex is electronically excited to a repulsive, antibonding state. The interesting feature with this model is that it explains the forward-peaked velocity profile.[52] However the applied energy is absorbed, it is clear that extensive ionization and fragmentation of the matrix molecules occurs, while the analyte molecule is somehow shielded from decomposition. Primary energy deposition gives rise to electronic excitation of the matrix molecules and at least some of this energy leads to vibrational excitation sufficient for matrix decomposition. Some of this energy must also be redistributed to the lattice so that the phase transition temperature can be reached. Vertes has proposed that an energy-transfer bottleneck exists between the matrix and the analyte, such that there is very little vibrational excitation of the analyte molecules.[52]

For the ionization process, most of the data seems to support the essential role of the matrix in the process, with only minor support for the desorption of preformed ions.[23,52,53] The debate concerns what determines the success of ionization. For protonation, it appears that proton transfer occurs between the matrix and the analyte through an activated form of the matrix. This activated form could be a photo-ionized species or simply an electronically excited neutral species. There is evidence that cationization also involves such activated matrix molecules.[53]

1.4.3 Scope of Applications

Fortunately, there are sufficient empirical guidelines governing the design of matrix/analyte formulations to allow for an independent development of applications. To this end, most of the research to date has pursued the use of MALDI in the field of biochemistry. MALDI provides fast determination of the molecular weight of biologically relevant species such as peptides, proteins, DNA and oligosaccharides. The technique does not induce much fragmentation, therefore structural information is not easily obtained. However, metastable ion analysis can be achieved with a reflectron time-of-flight instrument to aid in structural analysis.[54-57] Also, new mass spectrometric designs have been applied to enhance fragmentation by means of collision induced dissociation of the quasi-molecular ions generated by the MALDI process.[58-60]

Biochemical processing procedures have also been coupled to the method. For example, endoproteolytic cleavage of a protein by trypsin generates a peptide map that is extremely useful in identifying the protein.[61] By such a coupling, the speed and sensitivity of these biochemical procedures have been improved dramatically. This remains an active research area. The rapid sample throughput in MALDI has also allowed for accelerated drug discovery.[62] MALDI has more recently been applied to the field of industrial polymer analysis.[63,64] The attraction is the fast access to average molecular weight that the technique seems capable of providing. Structural information on the polymer repeat unit and endgroups can also be obtained.

1.5 Focus of the Current Work

The work presented in this thesis concerns the further development and application of laser-based time-of-flight methods. A new universal ionization procedure using lasers is presented, and applied to samples volatilized by lasers. It is shown to have certain advantages over the previously discussed approaches. Further sections concern the implementation of the MALDI technique. One involves the development and critical evaluation of the technique for industrial polymer analysis. Another section pursues the coupling of molecular recognition events to the technique, for the purpose of handling complex biochemically oriented samples.

1.6 Literature Cited

(1) Conzemius, R. J.; Capellen, J. M. *Int. J. Mass Spectrom. Ion Phys.* **1980**, *34*, 197.

(2) Wiley, W. C.; McLaren, I. H. *Rev. Sci. Instrum.* **1955**, *26*, 1150.

(3) Cotter, R. J. *Time-of-Flight Mass Spectrometry: Instrumentation and Applications in Biological Research*; American Chemical Society: Washington, DC, 1997.

(4) Cotter, R. J.; Tabet, J. *Int. J. Mass Spectrom. Ion Phys.* **1983**, *53*, 151.

(5) Opsal, R. B.; Colby, S. M.; Wilkerson Jr., C. W.; Reilly, J. P. In *Lasers and Mass Spectrometry*; D. M. Lubman, Ed.; Oxford University Press: New York, 1990; p 490.

(6) Vestal, M. L.; Juhasz, P.; Martin, S. A. *Rapid Commun. Mass Spectrom.* **1995**, *9*, 1044.

(7) Brown, R. S.; Lennon, J. J. *Anal. Chem.* **1995**, *67*, 1998.

(8) Colby, S. M.; King, T. B.; Reilly, J. P. *Rapid. Commun. Mass Spectrom.* **1994**, *8*, 865.

(9) Whittal, R. M.; Li, L. *Anal. Chem.* **1995**, *67*, 1950.

(10) Mamyrin, B. A.; Karataev, V. I.; Schmikk, D. V.; Zagulin, V. A. *Zh. Eksp. Teor. Fiz.* **1973**, *64*, 82.

(11) Tang, X.; Beavis, R.; Ens, W.; Lafortune, F.; Schueler, B.; Standing, K. G. *Int. J. Mass Spectrom. Ion Processes* **1988**, *85*, 43.

(12) Bergmann, T.; Martin, T. P.; Schaber, H. *Rev. Sci. Instrum.* **1989**, *60*, 792.

(13) Edmondson, R. D.; Russell, D. H. *J. Am. Soc. Mass Spectrom.* **1996**, *7*, 995.

(14) Vastola, F. J.; Mumma, R. O.; Pirone, A. J. *Org. Mass Spectrom.* **1970**, *3*, 101.

(15) Posthumus, M. A.; Kistemaker, P. G.; Meuzelaar, H. L. C.; Ten Noever de brauw, M. C. *Anal. Chem.* **1978**, *50*, 985.

(16) Graham, S. W.; Dowd, P.; Hercules, D. M. *Anal. Chem.* **1982**, *54*, 649.

(17) Nuwaysir, L. M.; Wilkins, C. L. In *Lasers and Mass Spectrometry*Oxford University Press: New York, 1990; p 291.

(18) Macfarlane, R. D.; Torgerson, D. F. *Science* **1976**, 920.

(19) Beuhler, R. J.; Friedman, L. *Int. J. Mass Spectrom. Ion Processes* **1987**, *78*, 1.

(20) Cotter, R. J. *Anal. Chem.* **1984**, *56*, 485A.

(21) Hillenkamp, F.; Karas, M.; Rosmarinowsky, J. In *Desorption Mass Spectrometry: Are SIMS and FAB the Same?*; P. A. Lyon, Ed.; American Chemical Society: Washington, DC, 1985; Vol. 291; pp 71.

(22) van der Peyl, G. J. Q.; Isa, K.; Haverkamp, J.; Kistemaker, P. G. *Nucl. Instrum. Meth.* **1982**, *198*, 125.

(23) Ehring, H.; Karas, M.; Hillenkamp, F. *Org. Mass Spectrom.* **1992**, *27*, 472.

(24) Cody, R. B.; Bjarnason, A.; Weil, D. A. In *Lasers and Mass Spectrometry*; D. M. Lubman, Ed.; Oxford University Press: New York, 1990; p 316.

(25) Hillenkamp, F.; Kaufmann, R.; Nitsche, R.; Unsold, E. *Appl. Phys.* **1975**, *8*, 341.

(26) Cotter, R. J. *Anal. Chim. Acta* **1987**, *195*, 45.

(27) Becker, C. H. In *Lasers and Mass Spectrometry*; D. M. Lubman, Ed.; Oxford University Press: New York, 1990; p 84.

(28) Demirev, P. A. *Mass Spectrom. Rev.* **1995**, *14*, 279.

(29) *Lasers and Mass Spectrometry*; Lubman, D. M., Ed.; Oxford University Press: New York, 1990.

(30) Lubman, D. M.; Li, L. In *Lasers and Mass Spectrometry*; D. M. Lubman, Ed.; Oxford University Press: New York, 1990; p 353.

(31) Pallix, J. B.; Schuhle, U.; Becker, C. H.; Huestis, D. L. *Anal. Chem.* **1989**, *61*, 805.

(32) Voumard, P.; Zhan, Q.; Zenobi, R. *Rev. Sci. Instrum.* **1993**, *64*, 2215.

(33) Grotemeyer, J.; Schlag, E. W. *Org. Mass Spectrom.* **1987**, *22*, 758.

(34) Li, L.; Lubman, D. M. *Anal. Chem.* **1988**, *60*, 1409.

(35) Lubman, D. M.; Li, L. *Int. J. Mass Spectrom. Ion Processes* **1989**, *88*, 197.

(36) Schuhle, U.; Pallix, J. B.; Becker, C. H. *J. Vac. Sci. Technol. A* **1988**, *6*, 936.

(37) Lykke, K. R.; Wurz, P.; Parker, D. H.; Pellin, M. J. *Appl. Opt.* **1993**, *32*, 857.

(38) Wild, R. K. *Adv. Mater. Opt. Elect.* **1995**, *5*, 53.

(39) Juhasz, P.; Costello, C. E.; Biemann, K. *J. Am. Soc. Mass Spectrom.* **1993**, *4*, 399.

(40) Strupat, K.; Karas, M.; Hillenkamp, F. *Int. J. Mass Spectrom. Ion Processes* **1991**, *111*, 89.

(41) Beavis, R. C.; Chait, B. T. *Rapid Commun. Mass Spectrom.* **1989**, *3*, 432.

(42) Wu, K. J.; Steding, A.; Becker, C. H. *Rapid Commun. Mass Spectrom.* **1993**, *7*, 142.

(43) Juhasz, P.; Costello, C. E. *Rapid Commun. Mass Spectrom.* **1993**, *7*, 343.

(44) Beavis, R. C.; Chait, B. T. *Chem. Phys. Lett.* **1991**, *181*, 479.

(45) Shaler, T. A.; Wickham, J. N.; Sannes, K. A.; Wu, K. J.; Becker, C. H. *Anal. Chem.* **1996**, *68*, 576.

(46) Mock, K. K.; Sutton, C. W.; Keane, A.; Cottrell, J. S. In *Techniques In Protein Chemistry IV*; R. H. Angeletti, Ed.; Academic Press, Inc.: San Diego, CA, 1993.

(47) Cohen, S. L.; Chait, B. T. *Anal. Chem.* **1996**, *68*, 31.

(48) Nicola, A. J.; Gusev, A. I.; Proctor, A.; Jackson, E. K.; Hercules, D. M. *Rapid Commun. Mass Spectrom.* **1995**, *9*, 1164.

(49) Gusev, A. I.; Wilkinson, W. R.; Proctor, A.; Hercules, D. M. *Fresenius J. Anal. Chem.* **1996**, *354*, 455.

(50) Dreisewerd, K.; Schurenberg, M.; Karas, M.; Hillenkamp, F. *Int. J. Mass Spectrom. Ion Processes* **1995**, *141*, 127.

(51) Dreisewerd, K.; Schurenberg, M.; Karas, M.; Hillenkamp, F. *Int. J. Mass Spectrom. Ion Processes* **1996**, *154*, 171.

(52) Vertes, A.; Gijbels, R. In *Laser Ionization Mass Analysis*; A. Vertes, R. Gijbels and F. Adams, Ed.; John Wiley & Sons, Inc.: New York, NY, 1993; Vol. 124; p 127.

(53) Knochenmuss, R.; Dubois, F.; Dale, M. J.; Zenobi, R. *Rapid Commun. Mass Spectrom.* **1996**, *10*, 871.

(54) Tang, X.; Ens, W.; Mayer, F.; Standing, K. G.; Westmore, J. B. *Rapid Commun. Mass Spectrom.* **1989**, *3*, 443.

(55) Spengler, B.; Kirsch, D.; Kaufmann, R.; Jaeger, E. *Rapid Commun. Mass Spectrom.* **1992**, *6*, 105.

(56) Cordero, M. M.; Cornish, T. J.; Cotter, R. J.; Lys, I. A. *Rapid Commun. Mass Spectrom.* **1995**, *9*, 1356.

(57) Kaufmann, R.; Chaurand, P.; Kirsch, D.; Spengler, B. *Rapid Commun. Mass Spectrom.* **1996**, *10*, 1199.

(58) Kosaka, T.; Ishikawa, T.; Kinoshita, T. *Rapid Commun. Mass Spectrom.* **1995**, *1995*, 1342.

(59) Bateman, R. H.; Green, M. R.; Scott, G.; Clayton, E. *Rapid Commun. Mass Spectrom.* **1995**, *9*, 1227.

(60) Doroshenko, V. M.; Cotter, R. J. *Anal. Chem.* **1996**, *68*, 463.

(61) Schar, M.; Bornsen, K. O.; Gassmann, E. *Rapid Commun. Mass Spectrom.* **1991**, *5*, 319.

(62) Haskins, N. J.; Hunter, D. J.; Organ, A. J.; Rahman, S. S.; Thom, C. *Rapid Commun. Mass Spectrom.* **1995**, *9*, 1437.

(63) Danis, P. O.; Karr, D. E. *Org. Mass Spectrom.* **1993**, *28*, 923.

(64) Danis, P. O.; Karr, D. E.; Mayer, F.; Holle, A.; Watson, C. H. *Org. Mass Spectrom.* **1992**, *27*, 843.

Chapter 2

Photoelectron Ionization in a Time-of-Flight Mass Spectrometer[a]

2.1 Introduction

Mass spectrometric systems that can alternate between different ionization modes with a minimum of modification are desirable.[1] In this way, one instrument can be used to handle a variety of samples. For mass spectral service laboratories, this represents a cost-effective means of meeting the needs of various clients. There has been interest expressed in the design of such flexible systems for time-of-flight mass spectrometry.[1-8] Ideally, these systems should allow for the ionization of sample molecules by different mechanisms, to obtain maximum structural information. The combination of these techniques should also allow for ionization of all gas-phase species (i.e.: universal ionization). Time-of-flight mass spectrometry excels in the application of selective ionization methods, such as resonant MPI, MALDI and ESI. However, while selectivity can be beneficial, it also restricts the widespread application of the instrument for routine chemical analysis, particularly in the surveying of unknowns. Laser-based ionization schemes with reduced compound selectivity have been developed, most notably non-resonant MPI and single photon ionization using a vacuum UV laser beam.[9-12] Nevertheless, these schemes do retain some selectivity and possess a broad range in ionization efficiency.

The classical universal ionization method is electron-impact (EI). EI has been applied to chemical analysis in the early days of time-of-flight,[13] and in a few instances since [4,5,14-19] Conventional electron sources generate electron beams with densities of approximately 10^7 electrons/cm^3 (i.e., from a 100 eV beam with a flux of 1mA/cm^2). This is a low density beam. The equation governing the intensity of an ion beam generated by the EI process is:[20]

---

[a] This chapter serves as a review of three separate publications: (A) Schriemer, D.C.; Li, L. "A Dual Ionization Source with Laser Desorption Sample introduction in a TOF mass Spectrometer" *Instrum. Sci. Technol.*, **1995**, 23, 317-328. (B) Schriemer, D.C.; Li, L. "Laser-Induced Surface Ionization in a Time-of-Flight Mass Spectrometer" *Rev. Sci. Instrum.*, **1996**, 66, 55-62. (C) Schriemer, D.C.; Li, L. "Surface Analysis of Bulk Polymers Using Laser-Induced Photoelectron Ionization with Laser Desorption in a Time-of-flight Mass Spectrometer" *Anal. Chem.*, **1996**, 68, 250-256.

$$i_i = i_e N E_t l \quad (1)$$

where i_i represents the ion current, i_e the electron current, N the concentration of the analyte in cm^3, E_t the total ionization cross section and l the ionization path length in cm. In the analysis of simple organic species with a conventional electron source, ionization efficiencies are on the order of 10^{-4}.[8] For an EI experiment in time-of-flight, the necessary pulsed ion beam can be generated using a pulsed electron beam. This is usually done in a field-free region, where ion extraction is achieved by a pulsing of the acceleration plate(s). The ions generated tend to have a significant spatial distribution in the source, leading to poor resolution.[3,4] Recently, the photoelectric effect has been used in time-of-flight to produce electron beams capable of intercepting molecular beams.[3,6,7,21,22] In three of these experiments,[6,7,21] a tantalum metal wire was inserted between the repeller plate and the extraction grid in the ionization region of a time-of-flight mass spectrometer (Figure 2.1A). A laser beam with a photon energy exceeding the work function of the metal was used to produce photoelectrons from the wire. Since a higher positive voltage was applied to the repeller than the extraction grid, these electrons were accelerated from the wire to the repeller plate by the electric field. The electrons could then ionize the chemical species in the region between the wire and the repeller plate. The mass resolution was very limited with this design, mainly due to the large spatial distribution of the generated ions.[6,7,21] Simpler versions of this setup have involved the illumination of extraction grids to produce the electrons, and do not require the presence of the wire (Figure 2.1B).[3,22] Although the design was simpler, resolution was still poor due to broad spatial distributions. A third design generated photo and thermal electrons external to the source region, which were then accelerated in a weak electric field established between two copper plates (Figure 2.1C).[7] The ions were formed and then extracted with a voltage pulse applied to the repeller. Better resolution was achieved with this design.

In this chapter, an alternative design for the incorporation of photoelectrons in EI time-of-flight mass spectrometry is presented. The ionization mechanism was investigated and the technique applied to samples introduced from a gas chromatograph, and by laser volatilization. It is shown that photoelectron-impact ionization (PEI) and multiphoton ionization (MPI) can implemented in one instrument without reconfiguration.

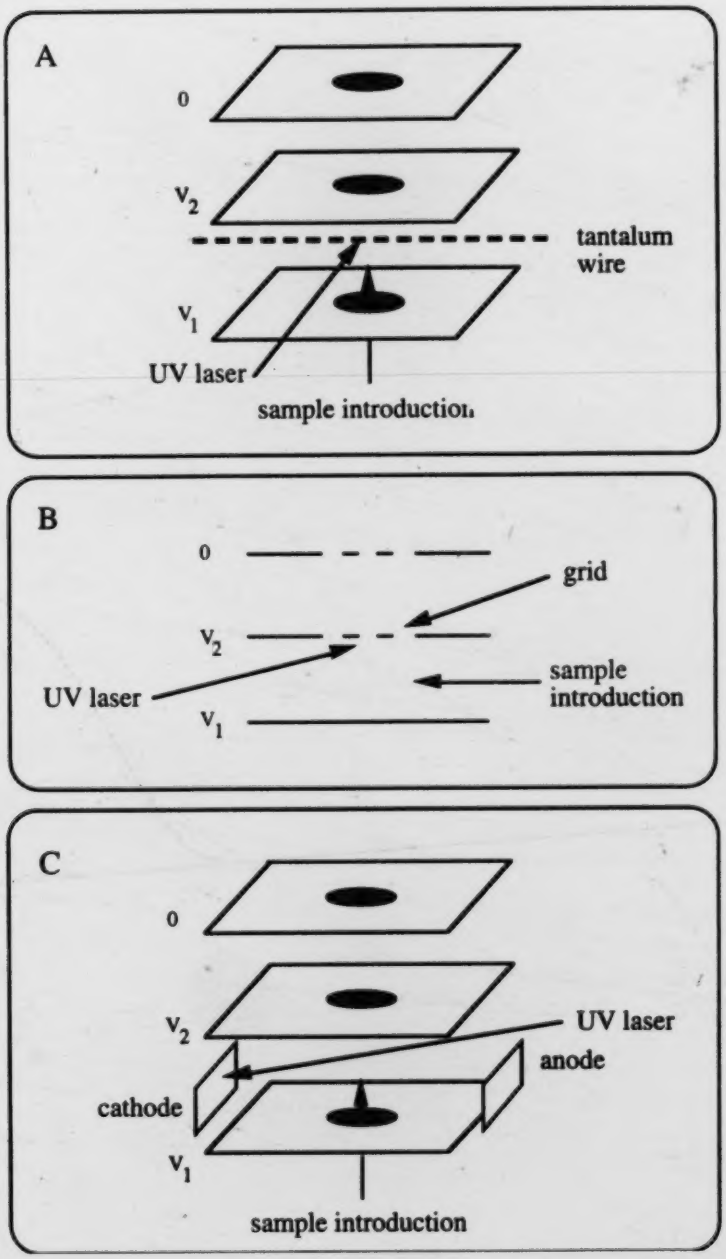

Figure 2.1 Photoelectron impact ionization designs according to (A) Boyle,[6] Moritz,[7] and Rohwer[21] (B) Cheng[3] and Colby[22] (C) Moritz.[7] In all designs, voltage $V_1 > V_2$.

2.2 Experimental

A linear time-of-flight mass spectrometer was used for ion detection. The instrument consisted of a four-port cross pumped by a 6 inch diffusion pump (Varian Associates, Inc., Lexington, MA). This cross was also fitted with four quartz window viewing ports. A 1 m long flight tube was mounted vertically and differentially pumped using a 4 inch diffusion pump (Varian). Ion detection was achieved using conventional microchannel plates (MCPs, R.M. Jordan Co., Grass Valley, CA). The output of the detector was digitized at a sampling rate of 100 MHz using a LeCroy 9400 digital oscilloscope (Chestnut Ridge, NY) and downloaded to a personal computer through a general-purpose interface bus (GPIB). This was controlled by software written in house.[23]

The source region of the spectrometer was patterned after the basic Wiley-McLaren design.[24] It consisted of three plate electrodes spaced 1.2 cm apart and suspended inside a cylindrical enclosure made of gold-plated stainless steel. In one design, an interface connected a capillary column gas chromatograph (Hewlett Packard model 5840A) to the time-of-flight mass spectrometer. Figure 2.2A shows a diagram of the interface and the position of the capillary column in the source region. A 0.25 mm i.d., 15 m long fused silica capillary (DB-5 phase, J & W Scientific, Folsom, CA) was threaded through a 1m heated transfer line. The transfer line was inserted into the mass spectrometer through a vacuum lock. The capillary was positioned between the repeller plate and the extraction grid of the source region. Volatile samples and various gases were introduced into the mass spectrometer system through the gas chromatograph, at flow rates of the helium carrier gas so as to maintain a measured operating pressure $< 5 \times 10^{-6}$ torr. Liquid samples were injected as 1 µl dilute solutions in decane, while gases such as argon, xenon and carbon dioxide were introduced into the carrier gas stream by way of a pre-column two-way junction.

In the second design, the instrument was configured to allow for laser volatilization experiments. A 0.7 cm long, 0.5 cm diameter stainless steel tip was attached to a probe by way of an insulating rod of machinable glass. This served as the sample holder. It was inserted through a vacuum lock into the ionization region to a fixed distance (Figure 2.2B). An Allmark transverse excitation atmospheric (TEA) CO_2 laser (10.6-µm output, A-B Lasers, Acton, MA) was used for sample volatilization, with the beam introduced on axis with the probe. This beam was focussed to a 1-2 mm^2 spot using a 25 cm focal length germanium lens, and applied at a repetition rate of 3 Hz. The typical power density used

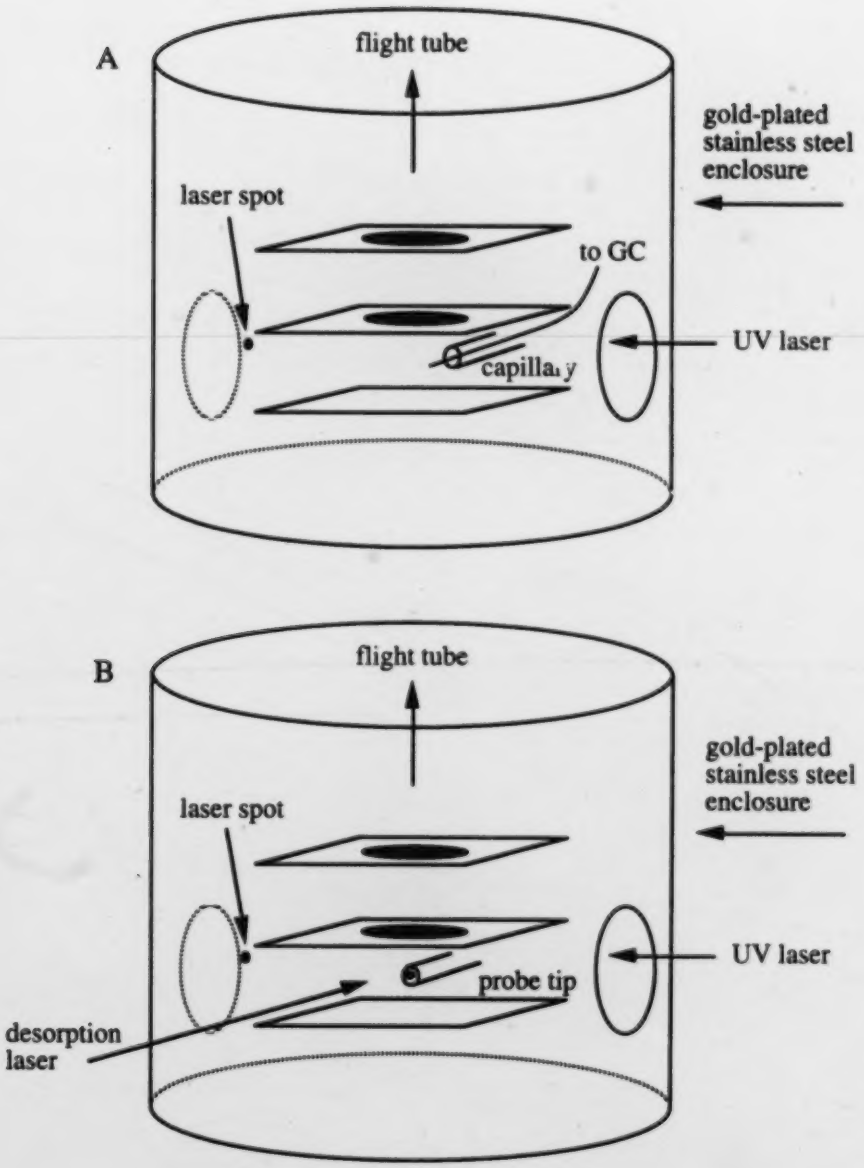

Figure 2.2 (A) GC/MS design that allowed for both PEI and MPI. Capillary tip was positioned ~1 cm off-centre. (B) Laser volatilization/MS design that allowed for both PEI and MPI. Probe tip was positioned approximately one cm off-centre. In both designs, the UV laser beam passed through the source before impinging on the inner surface of the housing, in PEI mode.

was ~1 MW/cm^2. Operating pressures with this configuration were < 1x10^{-7} torr. Typically, 0.1 to 10 µg of a non-volatile sample was loaded on the probe tip as a thin film. This was achieved by dissolving the sample in an appropriate solvent, and then delivering it in µl amounts to the tip.

In either design, a Nd:YAG laser (GCR-3, Spectra-Physics, Mountain View, CA) was used for photoelectron ionization and multiphoton ionization. It was operated in frequency-tripled and quadrupled mode, providing UV radiation of 355 nm and 266 nm, respectively. Pulse widths for this laser are approximately 7 ns fwhm. Variable repetition rates were used. The laser beam was focused by means of a 30-cm focal length cylindrical quartz lens, and directed orthogonally to the GC capillary in the one design (Figure 2.2A). It was also directed orthogonally to the CO_2 laser beam in the other design, and delayed by ~20 µs (Figure 2.2B). Details regarding the ionization processes will be discussed in section 2.3.2. Note that ions were formed in continuous fields, and extracted promptly upon formation. For the GC interface, the repeller voltage was set to 4.0 kV and the extraction grid voltage to 3.6 kV. The field-free region was set to ground. For the laser volatilization interface, the repeller was set to 9.2 kV and the extraction grid to 8.4 kV, with the field-free region also set to ground.

For the investigation of power dependence in PEI, laser energy was altered with a set of neutral density filters (Reynard Enterprises Inc., Laguna Niguel, CA) and monitored with an ultra-fast photo detector (Motorola, product MRD721).

All chemicals investigated were reagent grade and used without further purification. The polymers studied in this work were purchased from Aldrich (Milwaukee, WI) and Polysciences Inc. (Warrington, PA). All biochemicals were purchased from Sigma (Milwaukee, WI). The solvents used in this study were reagent grade, and used without purification.

2.3 Results and Discussion

2.3.1 Initial Observations

The phenomenon giving rise to this work was first noted in an MPI experiment, in which samples were introduced using a supersonic jet of CO_2. The 266 nm laser beam from the Nd:YAG laser was focussed in the middle space of the source region, to ionize the analyte entrained in the jet. This was achieved, however exceedingly intense ions from the CO_2 were observed as well. Ionization and fragmentation of this gas is impossible by a

multiphoton process at the wavelength and power densities used (~10^7 W/cm^2). The instrument was then reconfigured according to the GC/MS design discussed above. Various volatile samples were analysed, also with the laser beam focussed in the middle space of the source region. Figures 2.3A-C display the spectra collected from three gases introduced separately through the GC (argon, xenon and carbon dioxide). The spectra of the noble gases are characterized by significant multiple charging (Ar^{6+}, Xe^{9+}), indicative of a high energy ionization process.[25,26] This conclusion is supported by the significant fragmentation of carbon dioxide. A spectrum was also taken from a one µl injection of pentane (Figure 2.4A). The fragmentation pattern is very similar to that of a library EI spectrum of pentane, obtained with an electron energy of 70 eV (Figure 2.4B). The resolution for species introduced through the GC/MS ranged from 300 to 400.

The fragmentation patterns and degree of ionization observed were independent of whether 266 nm or 355 nm radiation was used. However, there was a considerably different response to changes in the laser power at these two wavelengths. The area of the Ar^+ signal was monitored as a function of energy, at each wavelength. In each case, the energy was adjusted with filters in the path of the beam, while keeping the focussing of the beam constant. The data from this investigation are displayed in Figure 2.5 as a log-log plot. The abscissa of this graph represents the output from the fast-response photo detector. Assuming that the ionization volume does not change with a change in laser energy, this output is proportional to the laser power. The equation governing the signal intensity arising from a radiant process is:[27]

$$I \propto P^n, \tag{2}$$

where I represents the intensity of the measured signal, P the power of the applied radiation, and n the number of photons required for the process. The slope of a log-log plot would ideally indicate the number of photons involved. For the data collected, the slope of the linear fit in Figure 2.5 for 266 nm radiation is 1.09 (RSD of 4.5%), while the slope of the linear fit for 355 nm radiation is 1.84 (RSD of 3.4%). For 266 nm, a slope 1.09 suggests that the process requires a single photon. At 355 nm, the slope is somewhat less than two, suggesting a two photon process. Given the non-integer values of these slopes and their standard deviations, it is difficult to conclude that pure one and two photon processes were occurring. For irradiation with 355 nm light, it is conceivable that thermal emission also contributed to the total number of electrons, as the power density at the surface was high.

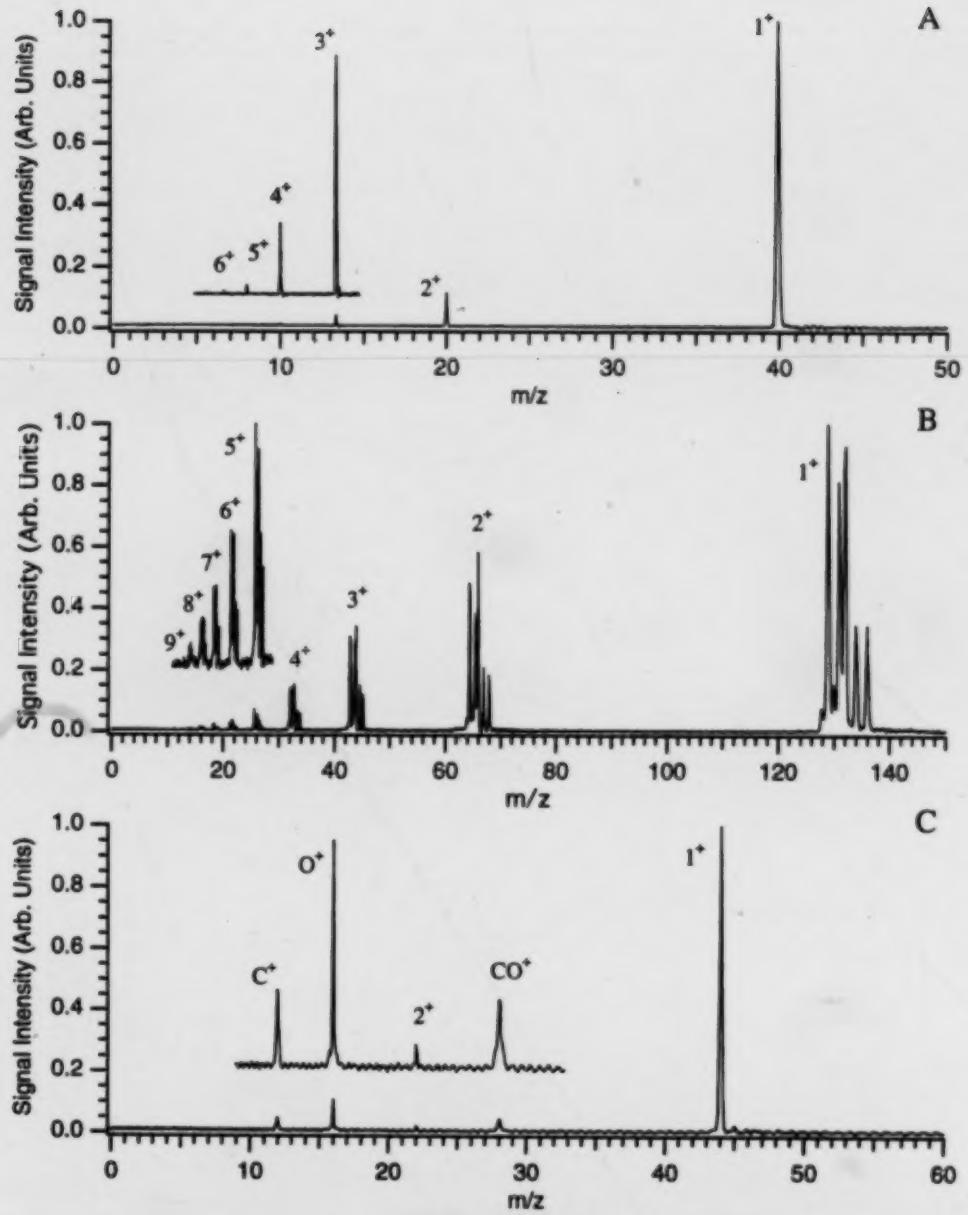

Figure 2.3 Mass spectra of (A) Ar, (B) Xe, and (C) CO_2 obtained in PEI mode. The voltage applied to the repeller plate and extraction grid were 4.0 kV and 3.6 kV, respectively. The samples are introduced into the system through the GC interface, at a flow rates such that the system pressure was $< 5 \times 10^{-6}$ torr.

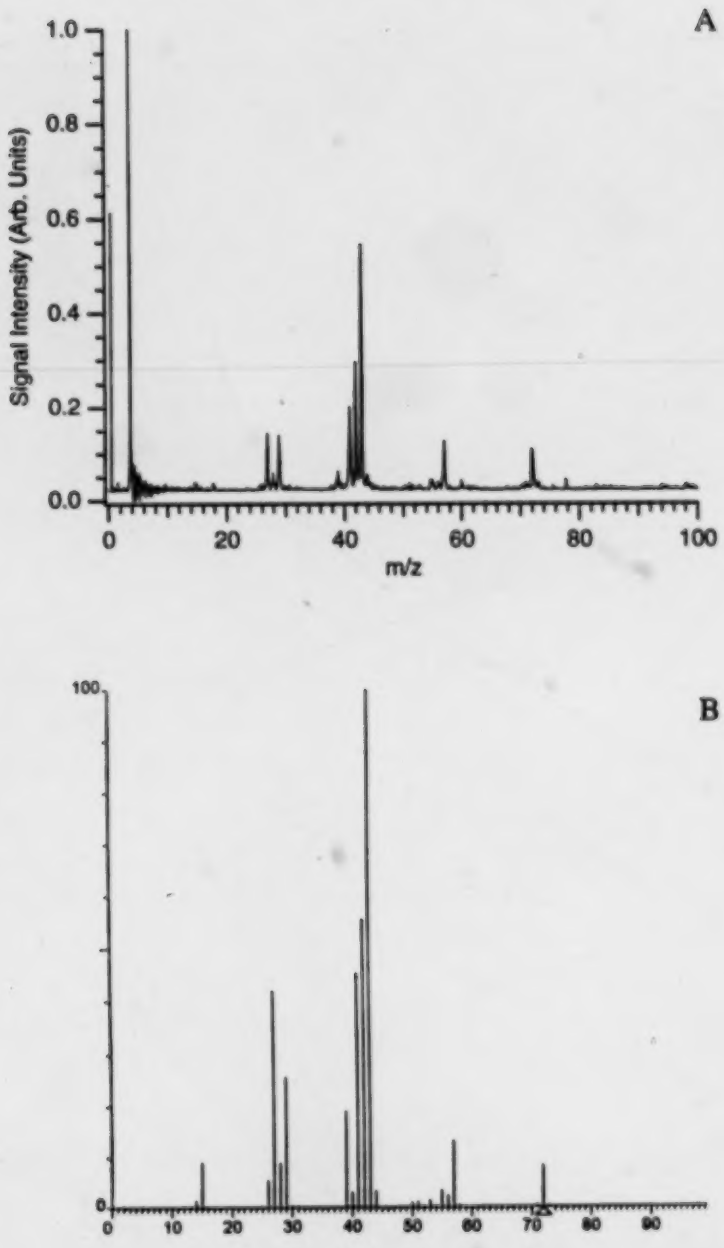

Figure 2.4 Mass spectra of pentane obtained by (A) PEI with the GC interface (B) electron impact ionization, from the NIST Mass Spectral Search Program (version 1.5, 07/19/96).

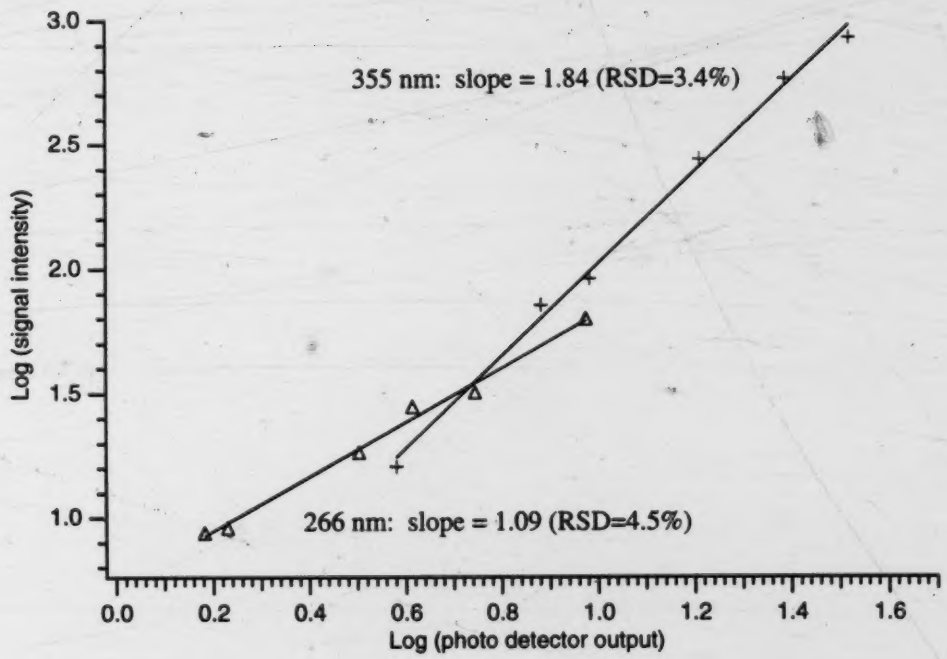

Figure 2.5 Log of the Ar^+ ion intensity as a function of the log of the photo detector output for PEI generated from a 266-nm laser beam and a 355-nm laser beam.

2.3.2 The Ionization Process

It was noted that intense ions would only be produced when radiation from the ionizing laser was incident upon the grounded cylinder housing the source region (see Figure 2.2B). This cylinder was constructed of stainless steel coated with a thin layer of gold, and contained four circular holes to allow transmission of the sample and laser beam through the source. Careful examination of the inner surface revealed tiny pockmarks on the edge of one of these holes, where the stainless steel was exposed. These marks were approximately 200 μm in diameter, and arose during operation of the instrument in MPI mode. In this mode, adjusting the position and focus of the laser beam is necessary to obtain the desired signal. These adjustments occasionally led to the intense irradiation of the metal cylinder, and the ablation of the gold layer at that particular spot.

Once formed, these small spots of exposed steel became efficient sources for defined photoelectron generation. Gold has a work function of 5.1 eV for photoelectron generation,[25] which is greater than the energy of a single 266 nm photon (4.66 eV). Therefore, striking the gold surface with a low power-density 266 nm beam cannot produce photoelectrons. Photoelectrons can be produced from gold at this wavelength, but require two photons for the process, and therefore a much higher power density.[28] On the other hand, efficient photoelectron generation could be induced by the 266 nm beam on the stainless steel surface, for its work function of 4.5 eV is less than the 266 nm laser energy.[25] Thus, with the use of low laser power, the photoelectrons were mainly produced from the 200 μm diameter spot not covered by the gold film, and independent of the 266 nm laser spot size. The low power density was supplied by the unfocussed output of the laser at this wavelength (approximate peak power of 1.5×10^5 W). These electrons were produced with an average initial energy of 0.16 eV, as determined by the following equation:[29]

$$KE_e = h\nu - W_e, \qquad (3)$$

where KE_e refers to the kinetic energy of the ejected electron, $h\nu$ to the energy of a laser photon and W_e to the work function of the metal surface. Electrons with this energy cannot induce EI mass spectra. However, the fate of electrons produced in such a source region could be simulated with the SIMION program.[30] Figure 2.6 shows the results of the simulation. The electric field in the source region was defined by the voltages used in a typical laser volatilization experiment. The photoelectrons produced from the small

stainless steel spot could be accelerated by the fringing fields near the electrodes to a very high maximum energy (approximately 8.8 KeV). As the simulation indicates, the electrons could be transmitted through the source without discharging on the electrodes.

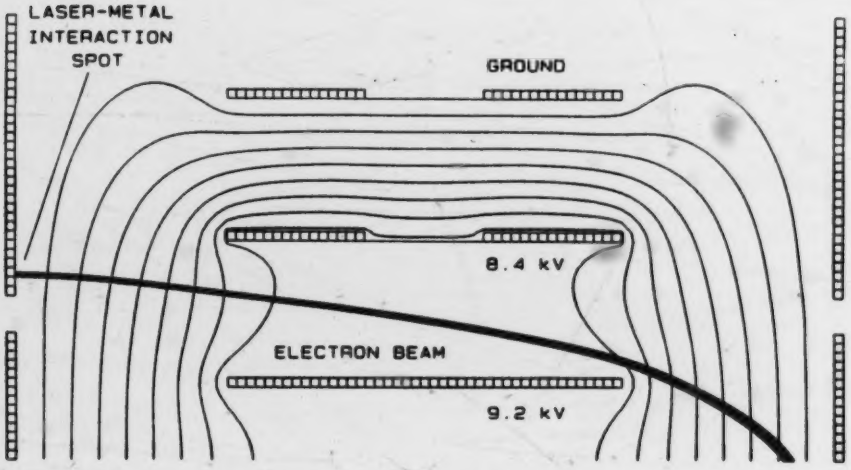

Figure 2.6 Simulation of photoelectron trajectory using the SIMION program,[30] with source dimensions and applied voltages equivalent to the laser volatilization configuration.

Several additional features are apparent from this simulation. First, there would be little spread in the photoelectron beam as it traverses the source. Second, the electron beam would not be perfectly parallel to the plate electrodes. This implies that the ions generated by this electron beam in the source would bear a spatial distribution. As discussed in section 1.1, the effect of such a distribution on the resolution can be minimized by the proper choice of E_s/E_d. The voltages used in the simulation correspond to the empirically-determined point of maximum resolution. When converted into E_s/E_d, it was found that this ratio agrees with the theoretical ratio for space focussing at the detector. Third, the size of the laser-metal interaction spot for photoelectron generation determines the width of the electron pulse; a larger spot implies a larger spatial distribution. A larger spot would

ultimately reduce the mass resolution, due to an inefficient compensation of the spatial distribution. Fourth, the duration of the photoelectron beam is equivalent to that of the UV laser pulse (i.e., ~ 7 ns fwhm), indicating that the time-spread of ion formation is equally short.

Based on the approximations of the spot size and the laser power, it is estimated that the stainless steel surface was irradiated with 3.5×10^{-7} J. For a unit quantum yield, this translates into a pulse of 4.7×10^{11} electrons generated over ~7 ns, for a transient current of 11 A. Such a short, intense beam of ionizing electrons is ideally suited to time-of-flight applications, as discussed in section 1.1.

Note that electron generation using 355 nm radiation would be less efficient, as it would require a two-photon process and higher irradiance. In the current design, this implies that the spot size of electron generation would be determined by the spot size of the laser on the cylindrical housing. This is because the work function of the gold will also be exceeded in a two-photon process. The graph in Figure 2.5 was generated from a focussed beam of 355 nm radiation, in order to produce electrons from a small region as in the 266 nm experiment. The power densities in this case were on the order of a MW. At these levels, thermal emission of electrons becomes possible.[7,22] This can cause a reduction in the slope of the power dependence,[7] and may explain why the slope of the graph in Figure 2.5 is somewhat less than two. However, it is significant that photoelectrons can be produced at this wavelength. Laser technology exists that is capable of delivering radiation in this UV region at costs comparable to that of a conventional pulsed electron gun (e.g.: N_2 laser delivering 337 nm radiation).

The picture that has emerged from this investigation is that a short, intense pulse of electrons can be generated from a surface external to the electrodes, and accelerated to high energy. These electrons are transmitted through the source and give rise to extensive multiple charging of atomic species, and fragmentation patterns for larger organic species that compare well with classical EI spectra. The multiple charges observed in the spectra of the atomic species is consistent with the ejection of a single electron from an inner shell. This singly charged atom would then undergo a series of radiationless transitions to generate multiply charged ions, according to the Auger process.[20] The fragmentation of organic species under EI conditions has a complex dependence upon electron energy. It has been observed that fragmentation patterns are very dependent on electron energy below 50 eV. At higher electron energies, the patterns remain essentially unchanged, at least from 50 to ~200 eV.[20] It has been established that the number of allowed electronic states is determined by the Frank-Condon principle, and the kinetics of dissociation from these

states dictate the observed fragmentation pattern.[31] The electron energy will determine the internal energy of the molecule and thus the population of these states. At the higher electron energies used in this work, the relative changes in electronic state population do not appear to vary significantly, thus generating spectra very similar to those arising from lower electron energies.

The design used in this work is simpler than those addressed in section 2.1. No additional electrode needed to be placed in the source region. Better resolution was obtained by injecting the electrons in a tight beam roughly parallel to the electrodes, rather than in a diffuse beam on axis with the spectrometer.[3,6,21,22] Conceptually, it is similar to the design where the electrons were generated between copper plates,[7] although much easier to implement. The following sections describe the implementation of this new design, using both the PEI and MPI modes.

2.3.3 Small Molecule Analysis

The EI mass spectra generated by photoelectron impact are useful for structural analysis and for molecular identification based on library-searchable spectra, but an additional feature associated with this technique is its good ionization efficiency. Figures 2.7A and 2.7B show the mass spectra of benzene and 2,2,5-trimethylhexane obtained by PEI from an injection of 100 ng each. Significant chemical noise arises from the low-grade diffusion pump oil, limiting the sensitivity of the design. This is particularly true for the 0 to 200 u range. For these two compounds, the limits of detection are estimated to be about 5 ng. Note that with an injection of 100 ng of sample, the signal duration was approximately 3 seconds for both compounds. With the laser operating at 10 Hz, 30 spectra were obtained during the elution time. Each laser pulse intersected the sample stream for ~7 ns, therefore with this continuous sample introduction source, the ionization duty cycle was only 7×10^{-8}. The spectra in Figures 2.7A and 2.7B represent an average of 10 shots. Therefore, the amount of sample consumed in the production of the spectra in Figure 2.7 was:

$$(7\times10^{-8})\times(10/30)\times100ng = 2.3fg.$$

Considerable sample waste arises from the fundamental mismatch between a continuous separations technique (GC) and a pulsed detector (time-of-flight). Nevertheless, since complete spectra are collected with every pulsed event, time-of-flight is appropriate for

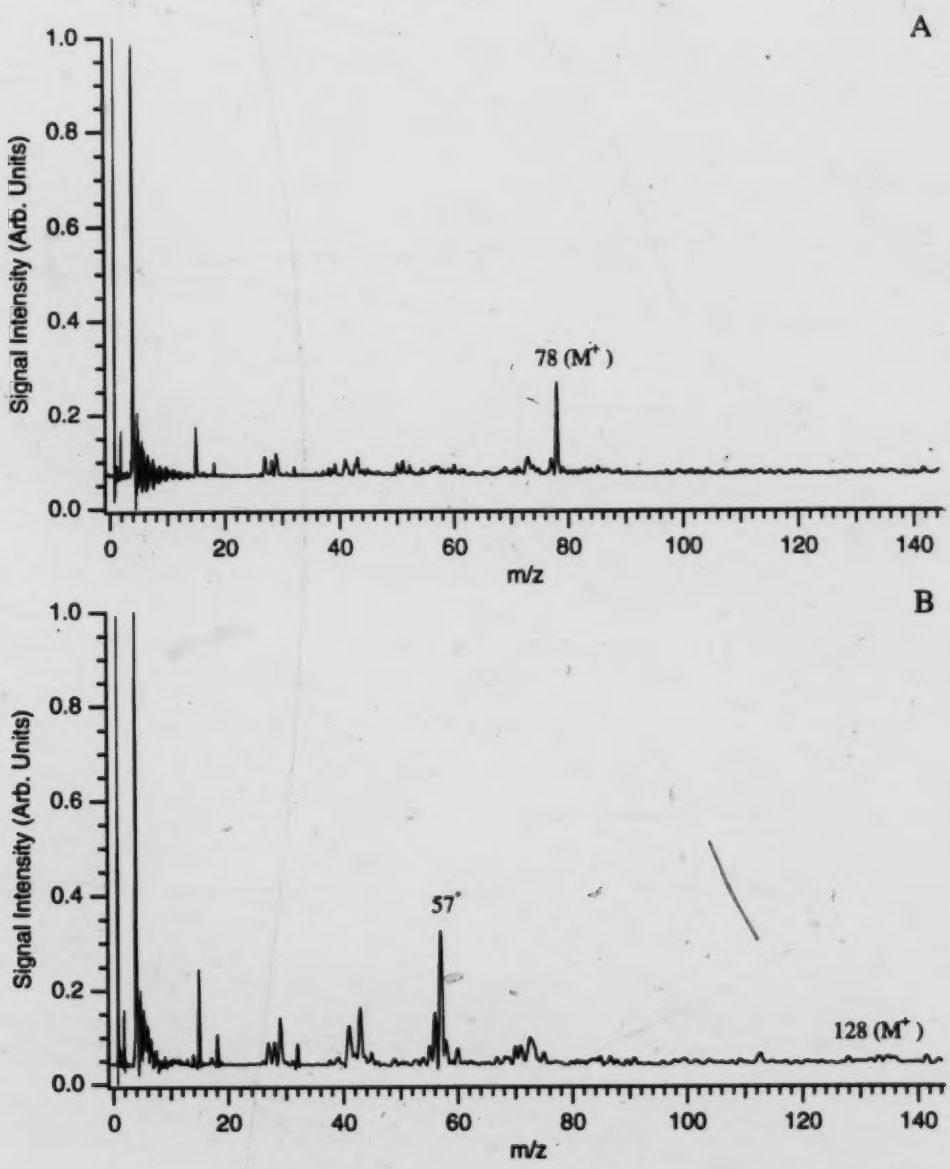

Figure 2.7 PEI mass spectra of (A) benzene, molecular ion at m/z 78, and (B) 2,2,5-trimethylhexane, molecular ion at m/z 128 and a fragment ion at m/z 57. Both spectra were obtained from an injection of 100 ng in the GC/MS mode.

coupling with fast chromatographic techniques. Certain forms of capillary gas chromatographic separations can be accomplished in mere seconds, with peak widths much less than a second. Therefore scanning-type mass spectrometers such as magnetic sectors, quadrupoles and ion traps are not fast enough to function as detectors.[32] GC/MS systems based on EI/time-of-flight technology have recently been marketed that allow for up to 500 spectral collections per second and applied to fast separations.[19] In such an instrument, electron generation is not based on lasers but rather electron gun technology, partly because the less expensive lasers have limited repetition rates.

If the analyte could be introduced in pulsed form, a greater sampling efficiency should be possible. The instrument was reconfigured tc the laser volatilization design, to allow for the pulsed introduction of non-volatile species. In PEI mode, the detection limits for many organic solids studied were found to be in the high picogram to low nanogram region. For example, with a sample loading of 10 ng of indole-3-acetic acid, a spectrum could be generated in which the base peak (m/z 130, a fragment ion) has a S/N of approximately 25. This is not a large improvement over the sensitivities typical for the GC/MS geometry. The volatilization of these organic species with the laser can take place for many tens of μs after the initial pulse.[14] Drawing out sample volatilization would reduce the sampling efficiency, and may be sufficient to explain the higher-than-expected detection limits. It was also noticed that the chemical background was more intense in the spectra arising from the laser volatilization mode, as compared to the GC/MS mode. This was probably because less neutrals are produced during laser irradiation. More background vapours would be present in the ionization volume of the laser volatilization experiment, whereas in GC mode, they would be swept away by the carrier gas. Note that neither mode of operation was designed for maximum sensitivity. However, sensitivity gains are on the order of 1000-fold compared to a similar laser volatilization/EI system that has incorporated an electron gun.[4]

The instrument could be modified to allow for MPI experiments. Simply by adjusting the position of the laser beam to avoid irradiation of the stainless steel spot ensured suppression of photoelectron generation. Increasing the power density by tighter focussing of the laser beam allowed for efficient MPI. For compounds that can be ionized by both MPI and PEI, the dual ionization source design provided a convenient means of recording both spectra alternately. For example, the peptide YG (amino acid single letter code) was volatilized with the CO_2 laser, and analysed by both PEI and MPI. The spectra are displayed in Figures 2.8A and 2.8B, respectively. In Figure 2.8A, a molecular ion

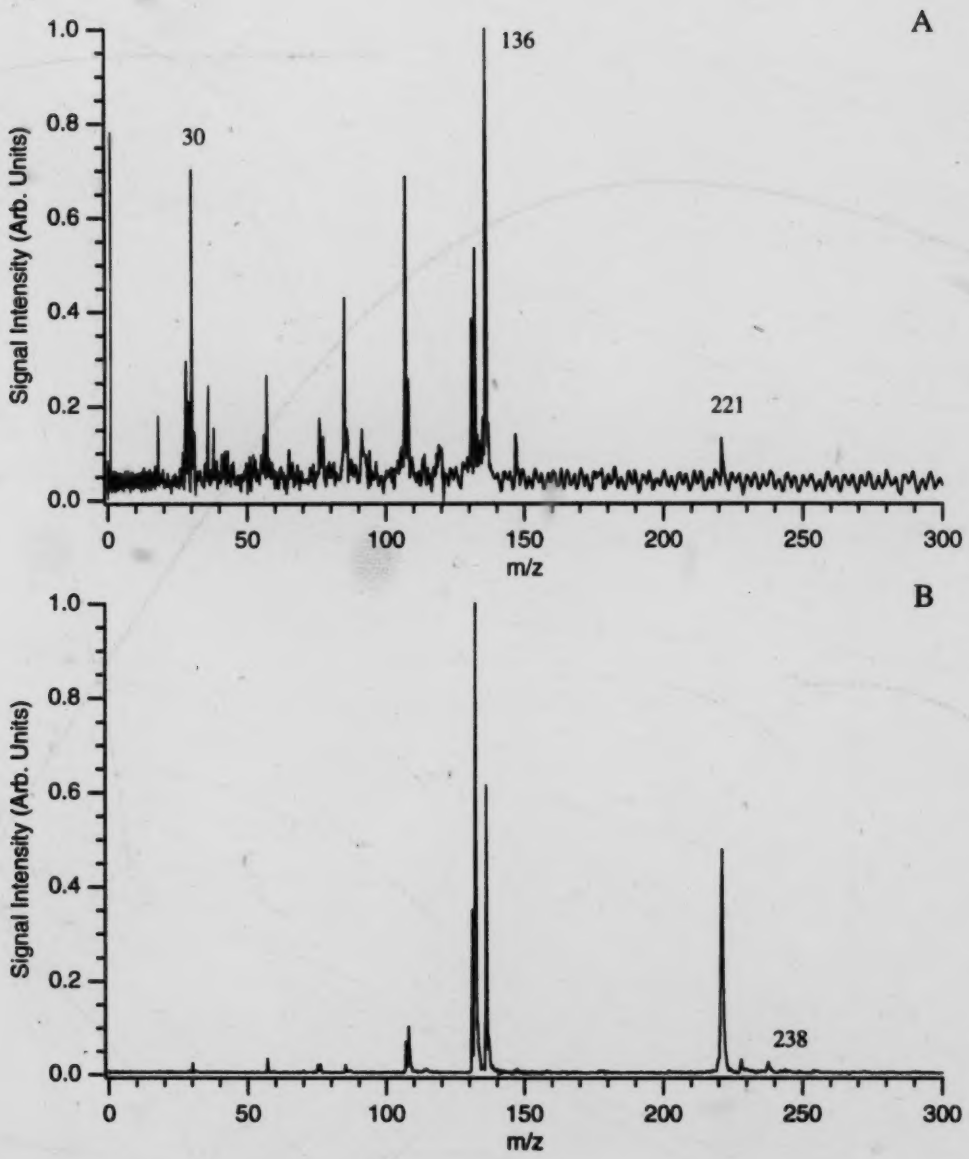

Figure 2.8 (A) PEI mass spectrum of the dipeptide YG. (B) MPI mass spectrum of YG. Both spectra were obtained from the same sample. Only the position and focus of the laser beam were changed to switch between ionization modes.

peak was not observed due to the high energy fragmentation process of PEI. A peak at m/z 221 was obtained, which corresponds to a fragment ion generated by the loss of ammonia from the parent ion (M-17). The M-17 fragment ion is commonly observed for dipeptides with an N-terminal aromatic amino acid, under conditions of rapid heating.[33] The base peak at m/z 136 arose from the cleavage of a C-C bond in the peptide chain and the peak at 30 from the ionization of a glycine fragment (both immonium ions). A weak molecular ion peak at m/z 238 was obtained in the MPI analysis (Figure 2.8B). This was obtained under "softer" ionization conditions (i.e., low power density), capable of preserving the molecular ion. Therefore, between the two techniques, extensive structural information could be obtained.

The benefits of a dual ionization source are particularly evident in the analysis of thermally labile species, where not all of the decomposition products can be analysed by MPI. These species receive enough internal energy under laser desorption conditions to decompose. For example, tetraalkylammonium salts (NR_4X) decompose into NR_3 and RX.[14,34] Both NR_4X and NR_3 resonantly absorb 266 nm radiation, while RX does not. Spectra of tetramethylammonium iodide (Me_4NI) were obtained, and shown in Figures 2.9A (MPI) and 2.9B (PEI). The peak at m/z 74 peak in the MPI spectrum corresponds to Me_4N^+, and indicates that neutral salt clusters can indeed be desorbed. Note also the peak at m/z 58, arising from $N(Me)_3$. The peaks at m/z 127 and 142 in the PEI spectrum correspond to I^+ and MeI^+, respectively. The ionization conditions were too harsh to see Me_4N^+ in the PEI spectrum, but the combination of the two ionization mechanisms allows for a full identification.

2.3.4 Polymer Analysis

Pyrolysis mass spectrometry has been extensively used for the analysis of synthetic polymers.[35] It involves the thermal decomposition of a polymer followed by some method of ionization. Many techniques for thermal decomposition have been developed, and can generally be classified as pulsed mode or continuous mode pyrolysis. Numerous methods for the ionization of the pyrolysate have been investigated, including low and high energy electron impact ionization, chemical ionization and field ionization.[36] Laser pyrolysis and rapid heating techniques have also been developed which bear similarities to the laser volatilization/PEI technique.[36] Using a pulsed laser beam for polymer pyrolysis has the advantage of generating reproducible spectra, something which can be difficult with slower heating techniques. Furthermore, a laser-based method requires minimal sample

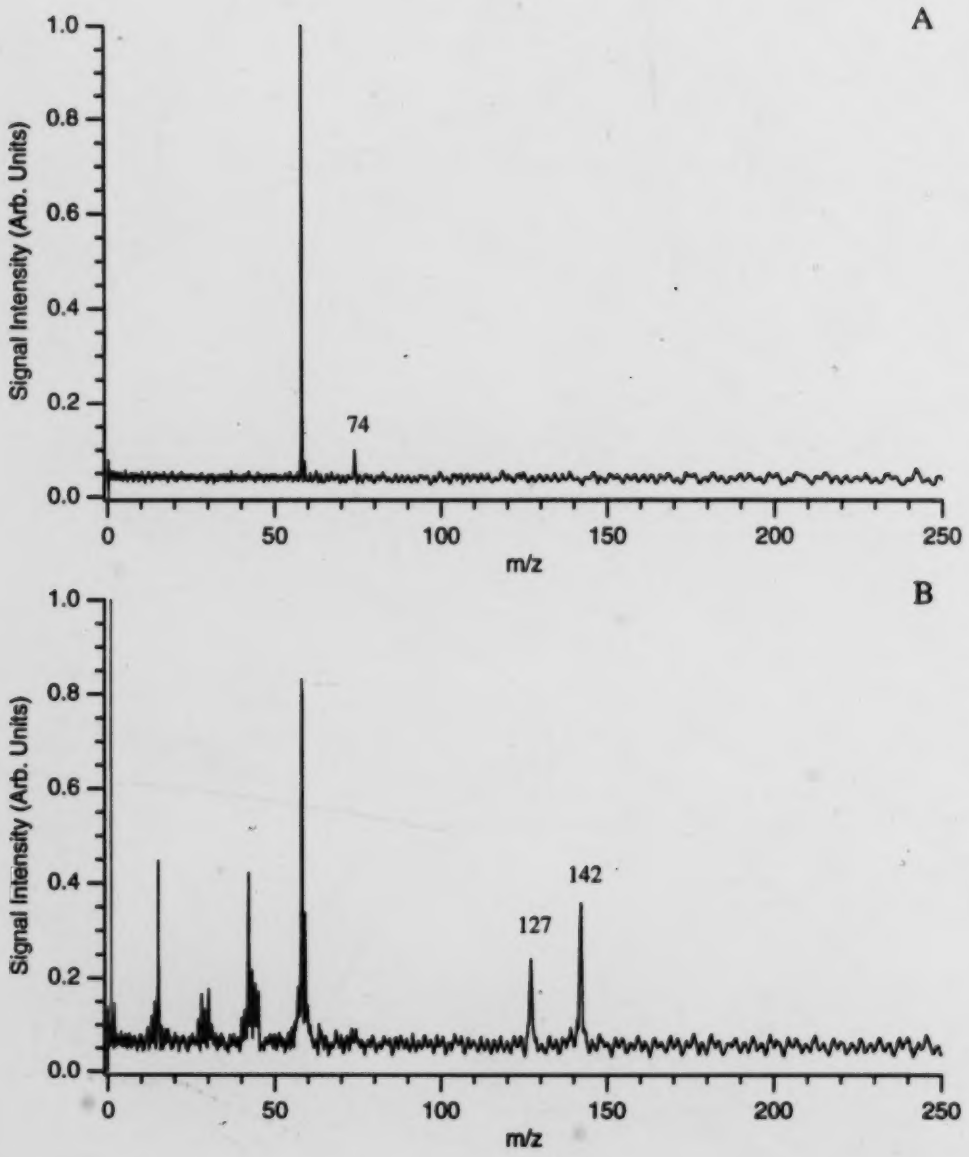

Figure 2.9 Mass spectra of tetramethylammonium iodide obtained by (A) MPI and (B) PEI. Both spectra were obtained from the same sample. Only the position and focus of the laser beam were changed to switch between ionization modes.

pretreatment and allows for a spatial analysis of the sample. The laser volatilization/PEI configuration could be used as a high energy pyrolysis/electron-impact technique capable of generating reproducible spectra. It was applied as a probe for both monomer and terminal group identification.

2.3.3.1 Monomer Identification

A variety of polymers with different molecular weights and monomer structures have been investigated with laser volatilization for neutral generation, followed by photoelectron ionization (using the configuration of Figure 2.2B). Figures 2.10A-D show mass spectra of four polymers: polystyrene (number average molecular weight, M_n, ~ 95 800), two poly(2-vinylpyridine) polymers (M_n ~ 50 000 and M_n ~ 200 000) and poly(methyl methacrylate) (M_n ~12 000). In the spectrum of polystyrene (Figure 2.10A), the peak at m/z 104 corresponds to the styrene monomer. For the spectra of the low molecular weight poly(2-vinylpyridine) (Figure 2.10B) and the high molecular weight poly(2-vinylpyridine) (Figure 2.10C), the peak at m/z 105 corresponds to the mass of the 2-vinylpyridine monomer. In the spectrum of poly(methyl methacrylate), the peak at m/z 100 is indicative of the methyl methacrylate monomer (Figure 2.10C). Note that the presence of an ion peak representing the monomeric unit is conditional upon the mechanism for polymer decomposition.[35,36] For these polymers, depolymerization is the main mechanism of degradation, which gives rise to high monomer populations.[35] The PEI process maintains the dominance of the monomeric unit, and thereby facilitates the assignment of monomer mass.

The ability to identify the basic polymer type with this technique is further illustrated in Figure 2.11, where the mass spectrum of the random copolymer poly(styrene-co-2-vinylpyridine) is shown (M_n ~ 110,000, 30% styrene monomer content). From the mass spectra of the homopolymers (Figures 2.10A and 2.10B), the basic composition of this polymer can be determined. The peaks at m/z 78 and 104 are characteristic of styrene. The peaks at m/z 79 and 105 are representative of 2-vinylpyridine. Figure 2.11 reveals the presence of both of these monomers. For this copolymer, no peaks from styrene-vinylpyridine are observed. This can be attributed to the disintegration of such units under CO_2 laser irradiation.

The intensity pattern in the PEI spectra of a given polymer was found to be dependent on its mass. For example, in the spectra of poly(2-vinylpyridine) (Figures 2.10B and 2.10C), the intensity of the m/z 79 peak decreases relative to the intensity of the m/z 105 peak, with an increase in mass. The peak at m/z 79 in the spectrum of

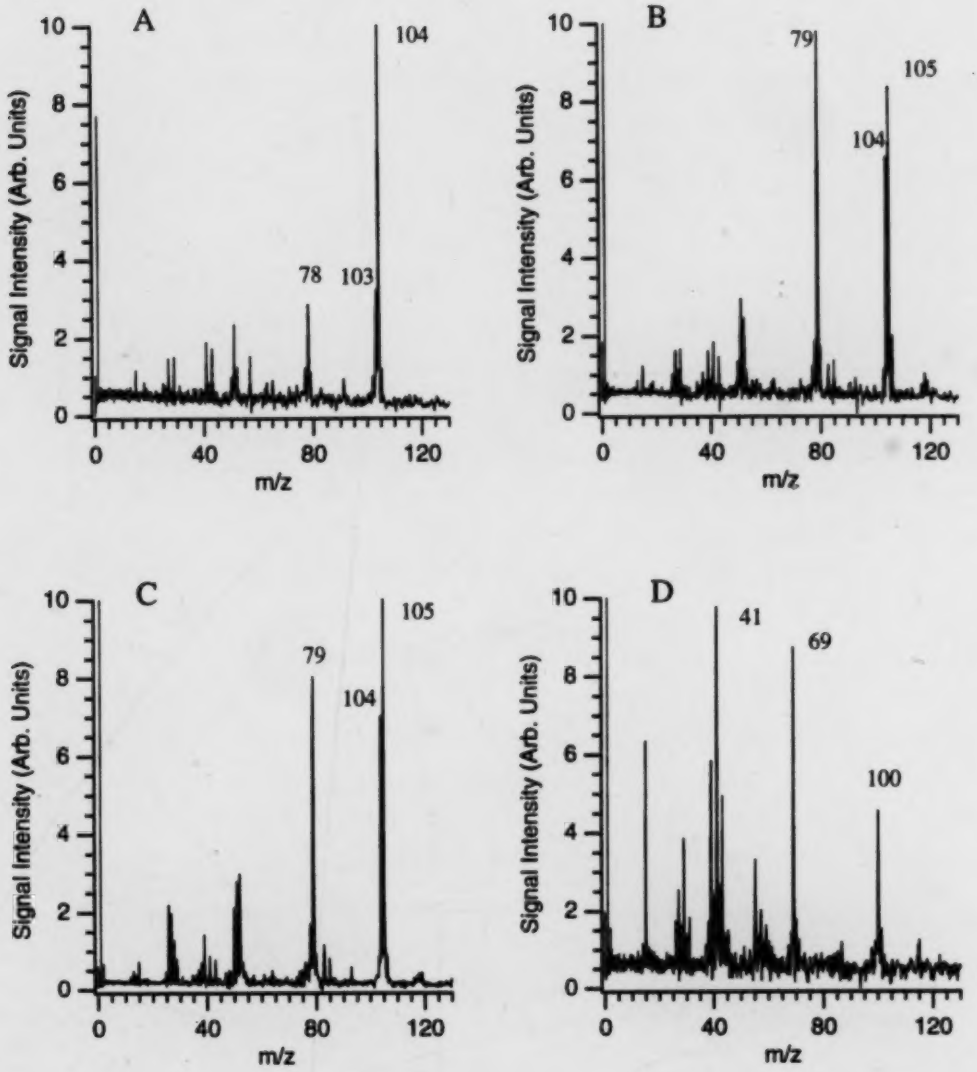

Figure 2.10 Laser volatilization/PEI mass spectra of (A) polystyrene (M_n ~95 800), (B) poly(2-vinylpyridine) (M_n ~50 000) (C) poly(2-vinylpyridine) (M_n ~200 000) (D) poly(methyl methacrylate) (M_n ~12 000). 10 µg of polymer was loaded on the probe tip in each case.

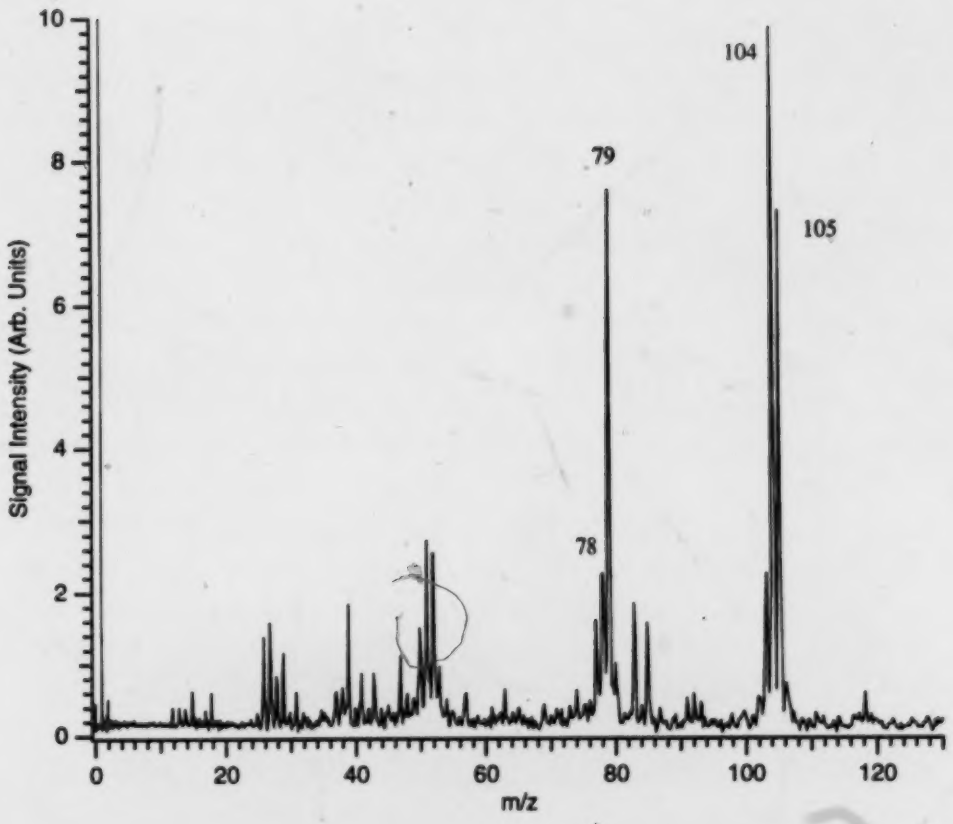

Figure 2.11 Laser volatilization/PEI mass spectrum of poly(styrene-co-2-vinylpyridine) (M_n ~ 110 000, 30% styrene content), from an analysis of 10 μg.

poly(2-vinylpyridine) could have arisen from the fragmentation of the monomer ion at m/z 105, as well as from the ionization of neutral pyridine molecules generated in the volatilization step. The ionization step would not be expected to depend on the polymer mass. Therefore, this observation indicates that the relative amounts of the pyrolysed species changes with mass. This conclusion has a basis in the literature.[37-39]

It should be noted that other laser-induced post-ionization methods have been developed for bulk polymer analysis, in combination with laser volatilization or particle beam sputtering. The use of laser desorption/MPI in supersonic beam mass spectrometry has been reported for the studies of aromatic polymers.[40] However, because of its selectivity in ionization, MPI can only be applied to certain types of polymers. Becker and

co-workers have developed a technique called Surface Analysis by Laser Ionization (SALI), in which a particle beam is used to desorb or sputter neutral species from the polymer surface, followed by ionization with the use of a laser beam at 118 nm (10.5 eV).[41,42] This technique can be used to study both aromatic and nonaromatic polymers. It has been shown that SALI can provide informative mass spectra from polymers.[41,42] The laser volatilization/PEI process provides comparable information, and seems easier to implement.

2.3.3.2 Terminal Group Identification

Laser volatilization/PEI can provide structural information for identification or confirmation of terminal (or end) groups in polymers. As an example, Figures 2.12A and 2.12B show the mass spectra of poly(ethylene glycol) (PEG) 400 diacrylate and PEG 4000 diacrylate, respectively. The peak at m/z 99.0 in both spectra corresponds to CH_2=CHCOOCH$_2$CH$_2^+$, while the peak at m/z 55.0 is likely from CH_2=CHCO$^+$. These two peaks serve to confirm the identity of the terminal group. Note that both peaks are quite intense in the mass spectrum of the low molecular weight PEG 400 diacrylate (Figure 2.12A). The intensities of the peaks at m/z 55.0 and m/z 99.0 are reduced in the spectrum of the higher molecular weight PEG 4000 diacrylate (Figure 2.12B). In this case, the peak at m/z 45.0 arising from the PEG monomer is the base peak in the spectrum. Since both terminals possess a diacrylate group in these two compounds, the peak at m/z 45.0 must be from a protonated monomer species generated in the dissociation of internal repeating units. As the chain length increases from PEG 400 diacrylate to PEG 4000 diacrylate, the population of these species (or their precursors) in the laser-generated neutral plume increases, resulting in the enhancement of the m/z 45.0 peak. Figure 2.12 also indicates that as the molecular weight of the polymer increases, the representation of the terminal groups in the spectrum decreases.

For PEG polymers, the terminal group representation is over-emphasized relative to the monomer. This can be illustrated from the studies of PEGs terminated with monomethyl ether, each having a different M_n value. Figure 2.13A shows a mass spectrum of poly(ethylene glycol) terminated on one end with a methoxy group (MeO-PEG, M_n ~ 2000). Figure 2.13B shows a spectrum of unmodified PEG (M_n ~ 1500) . In both spectra, the base peak at m/z 45.0 arises from the monomer. The major difference between the two spectra is the intensity of the peak at m/z 59.0. It is stronger in the MeO-PEG spectrum of Figure 2.13A. This peak could arise from the ionization of a neutral terminal fragment, leading to $CH_3OCH_2CH_2^+$, as well as from an internal fragment,

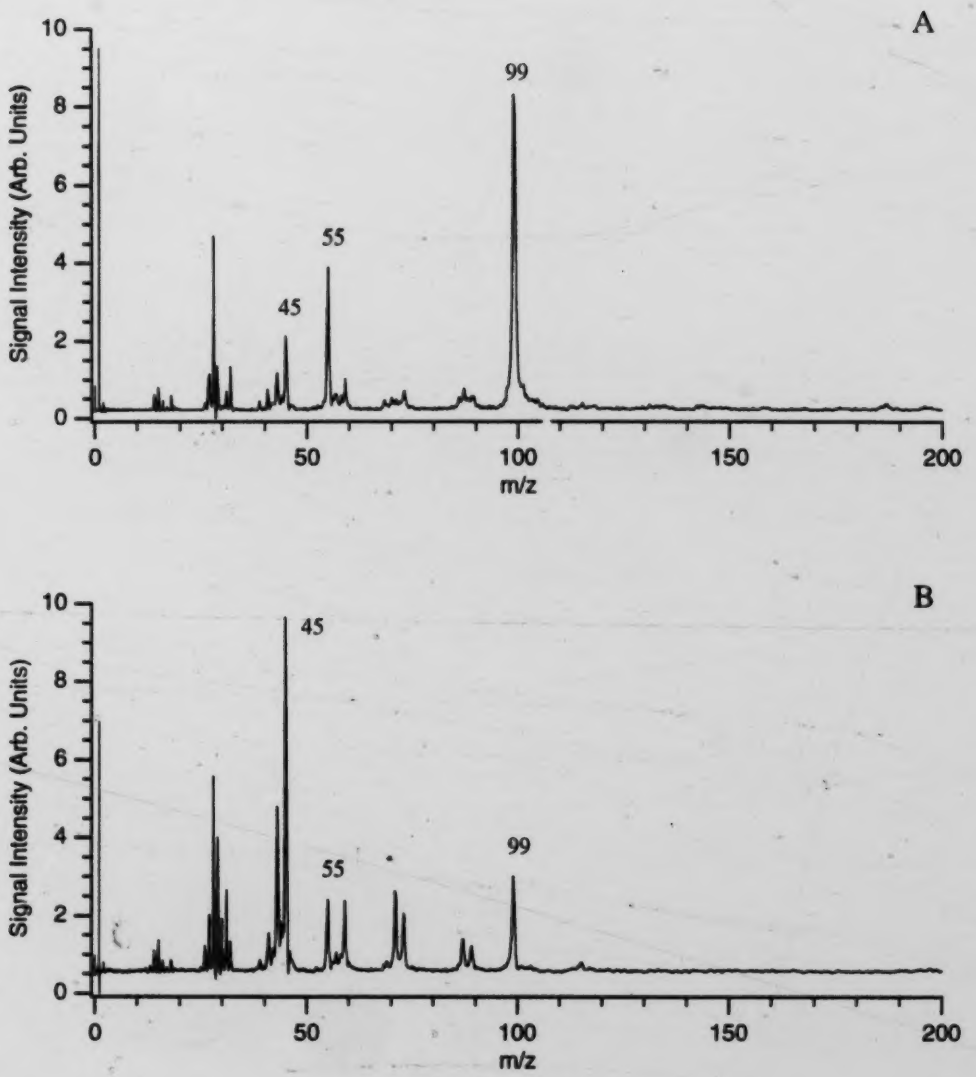

Figure 2.12 Laser volatilization/PEI mass spectra of (A) poly(ethylene glycol) 400 diacrylate (B) and poly(ethylene glycol) 4000 diacrylate, from analyses of 1 μg each.

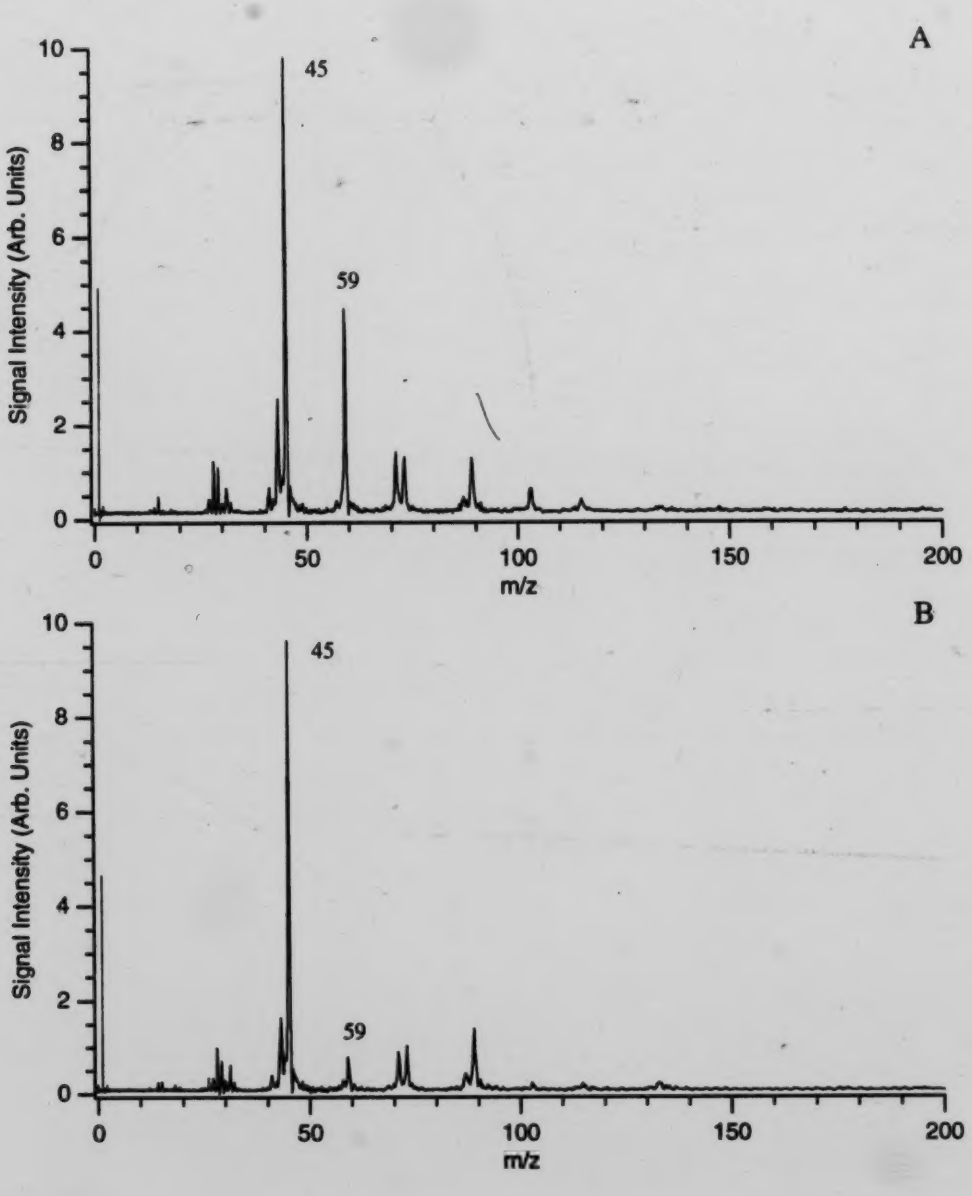

Figure 2.13 Laser volatilization/PEI mass spectra of (A) poly(ethylene glycol) 2000 monomethyl ether (B) poly(ethylene glycol) 1450, from analyses of 1 μg each.

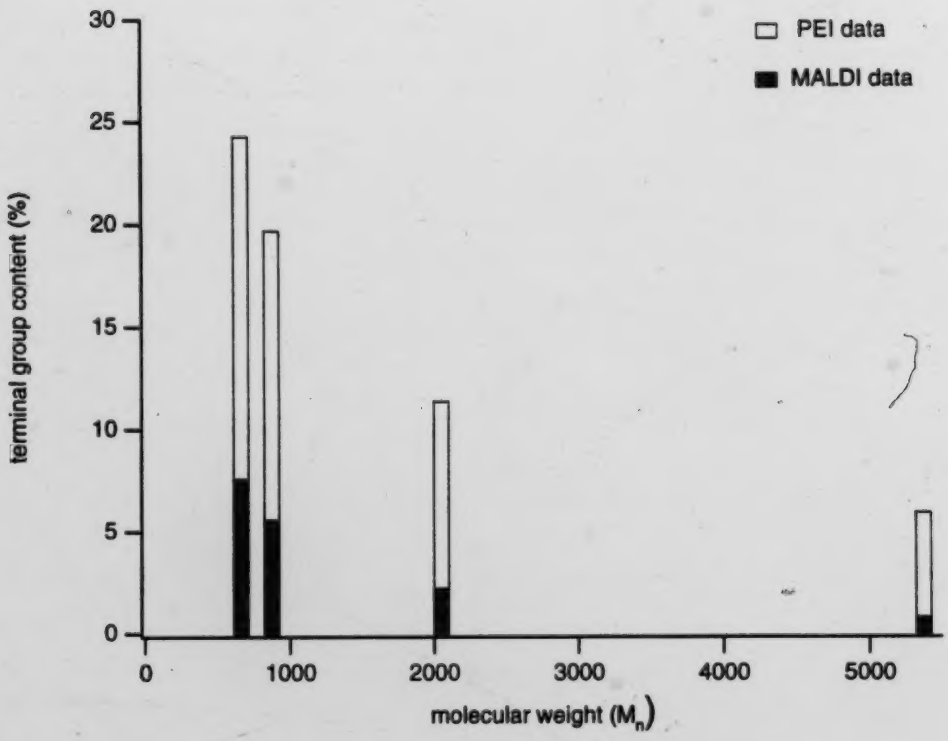

Figure 2.14 Determination of preferential dissociation of the terminal group in the laser volatilization process.

leading to $O{=}CHCH_2O^+$. The presence of this internal fragment would also be expected in the spectrum of unmodified PEG, and indeed, a small peak at m/z 59.0 is observed. Figure 2.14 shows the terminal group content of four monomethyl ether terminated PEGs, having different M_n values. This terminal group content represents the ratio of methoxy units to monomer units in the polymer. The terminal group content as determined by the laser volatilization/PEI process was calculated in the following way: the area of the peak at m/z 59.0 was ratioed against the total area of all peaks in the spectrum corresponding to polymer fragments. These data were corrected for the small contribution of the internal fragments to the m/z 59.0 peak. The calculated terminal group content for each polymer is also included in Figure 2.14. These data were obtained by determining the M_n for each polymer with the use of matrix-assisted laser desorption ionization (MALDI) in a time-lag

focussing time-of-flight mass spectrometer.[43] From the M_n value, the average number of monomers per polymer chain could be determined. The calculated terminal group content is simply the inverse of this number.

The terminal group content decreases with increasing molecular weight in both sets of data, however a strong preference for terminal group representation is reflected in the higher percentages of the laser volatilization/PEI data. For example, in the case of MeO-PEG with an M_n value of 5320, the terminal group content was calculated from the MALDI data to be 0.83%, but the laser volatilization/PEI mass spectrum of this MeO-PEG provided a significantly higher value of 6%. This result suggests that laser volatilization of these polymers does not lead to a complete decomposition of the whole chain, even for the smaller examples (at this power density). There is a preferential dissociation of the terminal group via a single bond breakage, resulting in an enhanced population of terminal group fragments in the neutral plume.

In summary, an new method for coupling electron impact ionization with time-of-flight mass spectrometry was developed, based on photoelectron generation external to the source region. It was shown to provide reasonable sensitivity and resolution, and applicability to a wide range of compounds and sample introduction systems. This method represents an attractive means of incorporating electron impact, as it requires minimal instrumental modification and relies on the very laser apparatus used in other common time-of-flight configurations.

2.4 Literature Cited

(1) Harrison, A. G.; Cotter, R. J. In *Methods in Enzymology*; J. A. McCloskey, Ed.; Academic Press: San Diego, 1990; Vol. 193; p 3.

(2) Wang, A. P. L.; Li, L. *Anal. Chem.* **1992**, *64*, 769.

(3) Cheng, P. Y.; Dai, H. L. *Rev. Sci. Instrum.* **1993**, *64*, 2211.

(4) Fountain, S. T.; Lubman, D. M. **1993**, *65*, 1257.

(5) Pollard, J. E.; Cohen, R. B. *Rev. Sci. Instrum.* **1987**, *58*, 32.

(6) Boyle, J. G.; Pfefferle, L. D.; Gulcicek, E. E.; Colson, S. D. *Rev. Sci. Instrum.* **1991**, *62*, 323.

(7) Moritz, F.; Dey, M.; Zipperer, K.; Prinke, S.; Grotemeyer, J. *Org. Mass Spectrom.* **1993**, *28*, 1467.

(8) Becker, C. H. In *Lasers and Mass Spectrometry*; D. M. Lubman, Ed.; Oxford University Press: New York, 1990; p 84.

(9) Rademann, K.; Kaiser, B.; Even, U.; Hensel, F. *Phys. Rev. Lett.* **1987**, *59*, 2319.

(10) Schuhle, U.; Pallix, J. B.; Becker, C. H. *J. Am. Chem. Soc.* **1988**, *110*, 2323.

(11) Van Bramer, S. E.; Johnston, M. V. *Anal. Chem.* **1990**, *62*, 2639.

(12) Boyle, J.; Pfefferle, L.; LoBue, J.; Colson, S. D. *Combust. Sci. Technol.* **1990**, *70*, 187.

(13) Conzemius, R. J.; Capellen, J. M. *Int. J. Mass Spectrom. Ion Phys.* **1980**, *34*, 197.

(14) Van Breemen, R. B.; Snow, M.; Cotter, R. J. *Int. J. Mass Spectrom. Ion Phys.* **1983**, *49*, 35.

(15) Wolff, M. M.; Stephens, W. E. *Rev. Sci. Instrum.* **1953**, *24*, 616.

(16) *Time-of-Flight Mass Spectrometry*; Price, D.; Williams, J. E., Ed.; Pergamon Press: Oxford, England, 1969.

(17) Eldridge, B. N. *Rev. Sci. Instrum.* **1989**, *60*, 3160.

(18) Holle, A.; Frey, R.; Weib, G. In *Proceedings of the 39th ASMS Conference on Mass Spectrometry and Allied Topics*; Nashville, 1991; p 206.

(19) LECO website: http://www.leco.com/pegasus.htm.

(20) Mark, T. D. In *Gaseous Ion Chemistry and Mass Spectrometry*; J. H. Futrell, Ed.; John Wiley & Sons, Inc.: Toronto, 1986; p 61.

(21) Rohwer, E. R.; Beavis, R. C.; Koster, C.; Lindner, J.; Grotemeyer, J.; Schlag, E. W. *Z. Naturforsch.* **1988**, *43a*, 1151.

(22) Colby, S. M.; Reilly, J. P. *Int. J. Mass Spectrom. Ion Processes* **1994**, *131*, 125.

(23) Coulson, L. D.; Nagra, D. S.; Guo, X.; Whittal, R. M.; Li, L. *Appl. Spectrosc.* **1994**, *48*, 1125.

(24) Wiley, W. C.; McLaren, I. H. *Rev. Sci. Instrum.* **1955**, *26*, 1150.

(25) *CRC Handbook of Chemistry and Physics*; 77th ed.; Lide, D. R., Ed.; CRC Press: New York, 1996, p 12_122.

(26) Lomre, L. A.; Mainfray, G. In *Fundamentals of Laser Interactions*; F. Ehlotzky, Ed.; Springer-Verlag: New York, 1985; p 125.

(27) Lin, S. H.; Fujimura, Y.; Neusser, H. J.; Schlag, E. W. *Multiphoton Spectroscopy of Molecules*; Academic Press: New York, 1984.

(28) Logothetis, E. M.; Hartman, P. L. *Phys. Rev.* **1969**, *187*, 460.

(29) Chang, R. *Chemistry;* 4th ed.; McGraw-Hill, Inc.: Toronto, 1991, p 267.

(30) Dahl, D. A.; Delmore, J. E. *Simion, Version 6.0* Idaho National Engineering Laboratory: Idaho Falls, ID.

(31) McLafferty, F. W. *Interpretation of Mass Spectra;* 3rd ed.; University Science Books: Mill Valley, CA, 1980.

(32) Gardner, B. D.; Holland, J. F. In *Proceedings of the 44th ASMS Conference on Mass Spectrometry and Allied Topics*; Portland, OR, 1996; p 1119.

(33) Nagra, D. S.; Zhang, J. Y.; Wang, A. P. L.; Li, L. *Int. J. Mass Spectrom. Ion Processes* **1992**, *116*, 127.

(34) Lee, T. D.; W.R. Anderson, J.; G.D. Daves, J. *Anal. Chem.* **1981**, *53*, 304.

(35) Irwin, W. J. *Analytical Pyrolysis: A Comprehensive Guide*; Marcel-Dekker: New York, 1982.

(36) Schulten, H.-R.; Lattimer, R. P. *Mass Spectrom. Rev.* **1984**, *3*, 231.

(37) Brannon, J. H.; Lankard, J. R. *Appl. Phys. Lett.* **1986**, *48*, 1226.

(38) Dyer, P. E.; Oldershaw, G. A.; Sidhu, J. *Appl. Phys. B* **1989**, *51*, 489.

(39) Oldershaw, G. A. In *Photochemistry and Polymeric Species*; J. M. Kelly, C. B. McArdle and M. J. Maunder, Ed.; Royal Society of Chemistry: Cambridge, England, 1993; p 54.

(40) Lustig, D. A.; Lubman, D. M. *Int. J. Mass Spectrom. Ion Processes* **1991**, *107*, 265.

(41) Schuhle, U.; Pallix, J. B.; Becker, C. H. *J. Vac. Sci. Technol. A* **1988**, *6*, 936.

(42) Pallix, J. B.; Schuhle, U.; Becker, C. H.; Huestis, D. L. *Anal. Chem.* **1989**, *61*, 805.

(43) Whittal, R. M.; Li, L. *Anal. Chem.* **1995**, *67*, 1950.

Chapter 3

MALDI Analysis of Polymers: Sample Preparation and Average Molecular Weight Determination[a]

3.1 Introduction

Matrix-assisted laser desorption ionization (MALDI) mass spectrometry is being developed as a tool for the analysis of industrial synthetic polymers. MALDI has the potential to offer rapid access to average molecular weight[1,2] and detailed structural information.[3,4] A number of papers have been published on new matrices, polymer/matrix preparations, oligomer characterizations, as well as comparative studies between MALDI and the more traditional molecular weight determination techniques.[5-10] However, most of the effort in polymer analysis has focussed on expanding the list of successful matrix/polymer combinations, and the mass range of their applicability. At present, MALDI cannot be applied to all polymer types. Unlike protein analysis by MALDI, each different polymer type requires a different matrix and/or sample preparation procedure. This is because of their diversity in chemical structure.

Few examples of the detection of high molecular weight polymers by MALDI have been reported. Danis et al. reported the detection of water soluble poly(styrene sulfonic acid) with a molecular weight just under 400 000 u.[11] In addition, they have also indicated the detection of a non-polar polystyrene with a molecular weight of approximately 120 000,[12] and the detection of a poly(methyl methacrylate) sample with a molecular weight of approximately 256 000.[2] Multiply charged ions from a Starburst polyamidoamine dendrimer with a molecular weight as high as 1.2 million has been reported by Savickas.[13] Electrospray ionization and detection of a similar dendrimer (~1 million u) has also been achieved.[14] Electrospray ionization has proved capable of generating mass spectra of poly(ethylene glycol)s with molecular weights up to 7 million; the lack of resolution between charged states prohibits its usefulness however.[15,16]

The difficulty in analysing even higher mass polymers by MALDI could be attributed to instrumental limitations, fundamental limitations of the MALDI process, or

---

[a] This chapter represents the combination of two publications. (A) An accelerated article: Schriemer, D.C.; Li, L. "Detection of High Molecular Weight Narrow Polydisperse Polymers up to 1.5 Million Daltons by MALDI Mass Spectrometry" *Anal. Chem.*, **1996**, 68, 2721-2725. (B) Yalcin, T.; Schriemer, D.C.; Li, L. "MALDI Time-of-Flight Mass Spectrometry for the Analysis of Polydienes" *J. Am. Soc. Mass Spectrom.*, **1997**, in press. T. Yalcin collected the spectra for Figures 3.2 and 3.3B.

both. With currently available detector designs (e.g., microchannel plate detectors, electron multipliers, or a combination of these two types), there can be a reduced detection sensitivity for high mass ions.[17] Furthermore, the MALDI process itself may have an upper mass limit conditional upon the nature of the analyte. This limit could be affected by the chemistry/photochemistry of the analyte, the availability of suitable matrices and ionization reagents, as well as suitable solvents. For example, a matrix that performs very well for a certain class of polymers might not be applicable to other types of polymers due to unfavorable chemical or photochemically induced reactions between the matrix and the analyte (during preparation or ionization). It is also possible that, for a particular analyte, no matrix is available with which it can cocrystallize. This could be due to a mismatch between the chemical nature of the analyte and the proposed matrix, or simply that a common solvent does not exist. In addition, an ionization reagent must be introduced that can effectively ionize the analyte but not disturb favorable crystallization behaviour. It is the combination of these factors that determines the overall efficiency of a preparation,[2] and hence the upper mass limit.

In this chapter, a new matrix/analyte preparation is presented for the average molecular weight analysis of non-polar polymers of narrow polydispersity. This class of polymers has proven to be one of the most difficult to analyse by MALDI.[10] The preparation was successfully applied to the analysis of very high molecular weight polystyrene, polybutadiene and polyisoprene. The results obtained by MALDI are compared with those obtained by traditional molecular weight determination methods such as gel permeation chromatography (GPC), viscosity (V), membrane osmometry (MO) and laser light scattering (LLS).

3.2 Experimental

3.2.1 Instrumentation

Mass spectral data were collected on a model G2025A MALDI time-of-flight system (Hewlett Packard, Palo Alto, CA), equipped with a pulsed nitrogen laser (337 nm radiation, 3 ns pulse width). This instrument was operated in positive ion mode at high voltage (28 kV). A dual microchannel plate (MCP) design was used for ion detection. This was equipped with a secondary ion generator that provided high sensitivity in the detection of high mass ions.[18] In general, laser pulse energies of 2.5-6 μJ were used, corresponding to just above analyte detection thresholds.

3.2.2 Data Collection and Processing

Roughly 50-100 spectra were averaged to produce a mass spectrum for samples yielding strong signals. For high molecular weight samples that tended to yield weaker signals, the maximum number of shots for a given sample were collected. Spectra were acquired and processed with Hewlett Packard supporting software, and reprocessed with the Igor Pro software package (WaveMetrics, Inc., Lake Oswego, Oregon), for presentation and data manipulation. Macros were written for this software platform that allowed for the calculation of the number average molecular weight (M_n) and the weight average molecular weight (M_w). The equations used for molecular weight determination were:

$$M_n = \frac{\sum_i^n (N_i M_i)}{\sum_i^n N_i} \qquad (1)$$

$$M_w = \frac{\sum_i^n (N_i M_i^2)}{\sum_i^n (N_i M_i)} \qquad (2)$$

where N_i and M_i represent signal intensity and mass at point i. The polydispersity (PD) was determined from a ratio of M_w to M_n. The displayed spectra were uncorrected for the intensity distortions arising from calibration (see Chapter 4). The relative standard deviations (RSDs) presented in this chapter were determined from five separate analyses.

3.2.3 Sample Preparation

Polymer samples for MALDI analysis were prepared by mixing the analyte, matrix and cationizing agent. The polymer samples were dissolved in distilled tetrahydrofuran (THF) to prepare stock solutions. *all-trans*-Retinoic acid (tRA) was used as the matrix, which was prepared to a 0.15 M concentration in THF. An aliquot of the polymer solution was then added to the matrix. The concentration of analyte in the final solution ranged from 50 μM (lower mass samples) to 15 nM (higher mass samples). The concentration of

matrix in the final solution remained essentially unchanged at 0.15 M. A small amount of a solution of the cationization reagent was then added. For polystyrene analysis, a saturated ethanolic solution of $AgNO_3$ was used. For polybutadiene and polyisoprene analysis, a 0.1 M aqueous solution of $Cu(NO_3)_2$ was used. In both cases, 1 µl of the salt solution was added to 100 µl of matrix/polymer solution. After brief mixing, 0.3-0.5 µl of the mixture was added to the MALDI probe tip and allowed to air-dry. Note that thin-layer depositions on the probe tip favored the analysis of high mass polymers.

3.2.4 Mass Calibration

Mass calibrations were performed externally. Proteins were used in the calibration of the lower mass polymers. A solution of bovine carbonic anhydrase II, bovine serum albumin and bovine lactase was analysed by MALDI using sinapinic acid (SA) as the matrix. An aliquot of a solution of SA in acetone (20 mg/ml) was first applied to the probe tip and air-dried, followed by an aliquot of the protein sample dissolved in a saturated SA solution (33% acetonitrile in water). This was allowed to air-dry as well. For the calibration of the higher mass polymers, a well-characterized polystyrene 90 000 was used.

3.2.5 Samples and Reagents

All polymers were of narrow polydispersity (PD<1.1). The polystyrene standards used in this study were purchased from Showa Denko KK (Tokyo, Japan), Polymer Laboratories (Amherst, MA), and Aldrich (Milwaukee, WI), ranging from ~90 000 to 1.5 million u. The molecular weights of these samples were provided by the suppliers, and are summarized in Table 3.1 (section 3.3). The polybutadiene and polyisoprene standards used were purchased from Polymer Source, Inc. (Dorval, Quebec, Canada) and Polysciences, Inc. (Warrington, PA). The molecular weights of these samples were provided by the suppliers, and are summarized in Tables 3.2 and 3.3 (section 3.3). tRA was purchased from Aldrich, $AgNO_3$ from Terochem Laboratories Ltd. (Edmonton, Alberta, Canada), and $Cu(NO_3)_2$ from J.T. Baker Chemical Co. (Phillipsburg, NJ). The proteins used in the calibration procedure were purchased from Sigma (Milwaukee, WI). Reagent grade tetrahydrofuran (THF) was purchased from VWR (Toronto, Canada), treated with potassium hydroxide, then distilled over sodium metal in the presence of benzophenone.

3.3 Results and Discussion

Figure 3.1 shows the mass spectra of three different polystyrenes with nominal masses of 330 000 (PS 330, Figure 3.1A), 600 000 (PS 600, Figure 3.1B), and 900 000 u (PS 900, Figure 3.1C). At these masses, the adjacent oligomer peaks are unresolved, and consequently the entire oligomer distribution appears as a broad peak. The salient features in these spectra are the appearance of the singly charged molecular ion peaks as well as peaks from multiply charged ions. In Figure 3.1B, the peak at m/z ~ 400 000 is from the triply charged dimer of PS 600. Likewise, the peak at m/z ~ 620 000 in Figure 3.1C is from the triply charged dimer of PS 900. As the mass increases, it becomes clear that the multiply charged distributions begin to dominate the spectra. The relative decrease in the intensity of the principal distribution is due in part to a drop in detector efficiency. Nevertheless, it is remarkable that ions with a m/z of greater than 900 000 (Figure 3.1C) can be detected with a microchannel plate (MCP) detector. Only one other study demonstrating the ability of MALDI for the direct analysis of species approaching 1 million u has been published.[19] This involved the analysis of human IgM.

In the analysis of polystyrene, tRA was used as the matrix. This matrix was previously reported by Wilkins and his co-workers for the analysis of dendrimers,[20] however it was claimed that the all-trans form provided only weak signals. After irradiation with fluorescent light for 72 hours, presumably to isomerise the all-trans form to the 13-cis form, much stronger signals could be obtained. Nevertheless, the all-trans form appears to be extremely efficient in the analysis of both polar and non-polar polymers, with the selection of the proper cationization reagent. Wilkins' initial investigation of this organic compound as a matrix relied on the generation of protonated analytes. Strong signals can be obtained using sodium cationization in the analysis of polar polymers, while silver and copper cationization are effective means of generating strong signals from non-polar polymers. In the analysis of polystyrene, a small aliquot of a saturated ethanolic solution of $AgNO_3$ was added to the matrix/analyte mixture immediately prior to analysis, and proved to be an easy and effective means of introducing this cationization agent. It is felt that this procedure is more practical than preparing a silver salt of the matrix, as has been done with other matrices.[12] A carboxylate salt of this matrix would be very difficult to prepare in the pure form, since such preparations would always contain Ag^+ ions complexed to the polyalkenyl chain of the matrix.[21] As the matrix slowly oxidizes in the presence of Ag^+, it is preferable to introduce the cationizing agent immediately prior to analysis. When using this matrix, it is important that the solvent remain free of impurities

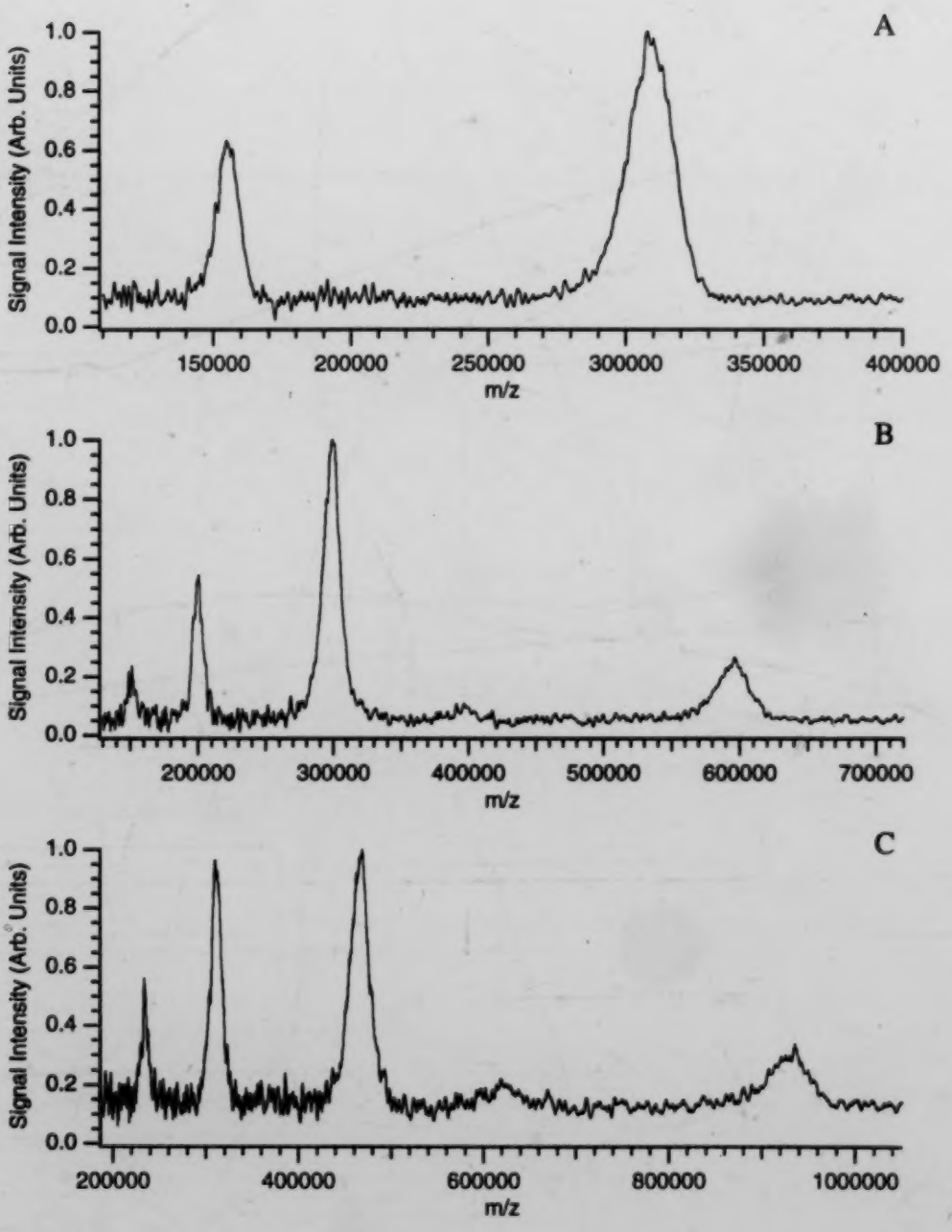

Figure 3.1 Mass spectra of three polystyrene samples with nominal molecular weights of (A) 330 000, (B) 600 000 and (C) 900 000.

such as excess water, peroxides and/or acids and anti-oxidants. For example, using reagent grade THF without further purification resulted in the complete suppression of even low mass polystyrene signals, although it is unclear which contaminant(s) caused this suppression. In this work, the THF was purified prior to use as described in the experimental section. When prepared in this fashion, the matrix solution can be stored for over one week without loss in efficacy.

In the preparation of samples for MALDI, a rule of thumb is to use a matrix-to-analyte molar ratio ranging between 500:1 and 10 000:1. For the MALDI analysis of high mass polymers this does not hold. When the experimenter experiences poor detection sensitivity, it is intuitively sensible that an increase in the amount of analyte would increase the signal strength. However, just the opposite is the case for the analysis of high molecular weight polymers. It was observed that increasing molecular weight required progressively lower molar amounts of sample in order to achieve highest sensitivity. For example, signals were obtained for PS 900 from 10 fmol loaded on the probe tip, or a matrix to analyte ratio of ~8 million:1. With these high molecular weight species, using molar matrix-to-analyte ratios between 500:1 and 10 000:1 yielded no analyte ion signals at all. Optimum ratios for the range of polystyrenes investigated varied between 3000:1 (lower molecular weight) and 10 million:1 (higher molecular weight). The "optimum ratio" is defined as the composition at which a further increase in the polymer concentration does not lead to an increase in signal strength. This range represents a 3300-fold molar increase in the amount of matrix required. The amount of matrix needs to be high enough to minimize polymer entanglement and/or the formation of regions of microcrystallinity.[10] Such behaviour would reduce desorption efficiency and explain why signals were not observed for the lower matrix-to-analyte ratios.

The success of an analysis is dependent upon the molecular weight of the analyte, yet the molecular weight is the variable to be determined by the experiment. From a practical point of view, it is more helpful to consider the ratio of moles of matrix to total moles of monomer. The total moles of monomer is proportional to the weight of the sample, which is a known quantity. When approached in this manner, the polystyrene analyses reported have optimum matrix to monomer ratios ranging between 200:1 (lower masses) and 700:1 (higher masses). Since this range represents only a 3.5-fold increase, this ratio serves as a better guide for the analysis of samples with unknown molecular weights. Such a approach bears similarities to Flory's treatment of polymer solutions.[22]

A similar study of polybutadiene confirms the trends observed for polystyrene, leading to the conclusion that significantly higher matrix-to-analyte ratios are generally

required for the analysis of very high molecular weight species. Polybutadiene was analysed using tRA, and $Cu(NO_3)_2$ as the cationization reagent. Figures 3.2A-C demonstrates the significance of selecting the proper matrix-to-analyte ratio. The spectra in these figures correspond to the MALDI analysis of polybutadiene 129 360, obtained using decreasing matrix-to-analyte ratios. Using a fixed amount of matrix in all cases, this corresponds to a molar polymer loading of 0.025 (Figure 3.2A), 0.115 (Figure 3.2B) and 3.4 pmol (Figure 3.2C). The numbers indicated in each spectrum represent the percentage of shots accepted versus the total number of shots. In each case, the goal of the data collection was to generate a summed spectrum with the highest signal-to-baseline noise (S/N) possible. An individual shot was deemed acceptable when it generated a S/N greater than 3. The more sensitive formulations can generate observable signal for 50 shots or more. However, at each laser position, shots were fired until a consistent reduction in S/N was observed, at which point the laser was advanced to a fresh spot. For the more sensitive preparations, the point of advancement was arbitrarily set to a S/N one third of the maximum obtained for that particular spot. For the poorer formulations, such a criterion meant that the signal became unobservable. In this situation, the point of advancement occurred ~10 shots after the signal became unobservable. In Figure 3.2, the S/N of the summed spectra increased with the amount loaded up to 0.115 pmol (3.2B), whereupon it leveled off and began to decrease with a further increase in the amount loaded. On the Hewlett-Packard MALDI system, the spectrum of Figure 3.2B could be obtained from three sample loading, whereas the spectra arising from the two other preparations required six (3.2A) and seven (3.2C) sample loadings.

A further implication of this experiment concerns the measurement of average molecular weight. An investigation of the M_n values arising from the three polybutadiene spectra reveals a discrepancy. The largest value is found at the highest S/N (Figure 3.2B). An M_n value of 109 300 and a PD of 1.0038 was calculated from this spectrum, whereas an M_n of 105 800 and a PD of 1.0009 was obtained from the spectrum of Figure 3.2C. As the RSDs for both M_n determinations were approximately 0.6%, there is a significant discrepancy between these values by the t-test for the comparison of means (at the 99% confidence limit). This arises from the low S/N of the high mass tail. Thus, selecting the proper matrix-to-analyte ratio is important for the detection of the low abundance oligomers in the distribution.

Since it is necessary to decrease the molar loading of polymer as the molecular weight increases, a limit to the mass range of polymer analysis by MALDI exists. As

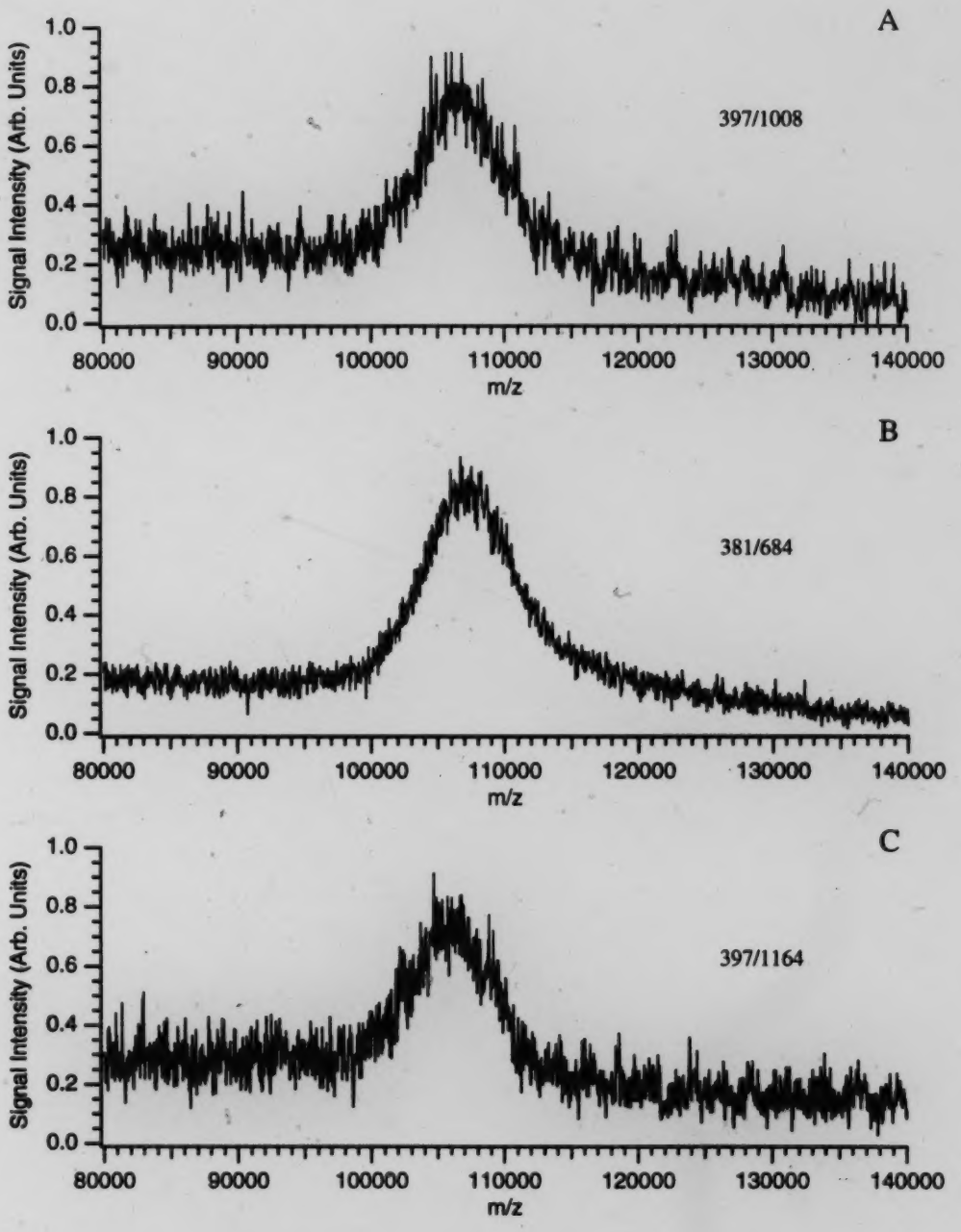

Figure 3.2 MALDI spectra of polybutadiene 129 360, representing (A) 0.025 pmol loaded, (B) 0.115 pmol loaded and (C) 3.4 pmol loaded. Ratios represent the number of acceptable shots to total shots fired.

molecular weight increases, the sensitivity of the instrument is challenged on two fronts: decreased sensitivity due to loss in detector efficiency, as well as decreased sensitivity from the requirement of lower molar sample loading. In the analysis of polystyrene with the current procedure, this limit was reached at approximately 1.5 million u. Figure 3.3A shows the mass spectrum of polystyrene with a nominal mass of 1.5 million u. This spectrum was obtained from 5 fmol of polymer loaded on the probe tip, and represents the average of seven such collections. Even a slight increase in the amount loaded to 15 fmol resulted in signal suppression, and loading less than 5 fmol proved to be beyond the sensitivity of the instrument. The spectrum does not display any signal from the principal distribution, suggesting an insufficient detector sensitivity at this mass. Figure 3.3 shows a peak at m/z 700 000 corresponding to the doubly charged ion distribution and a peak at m/z 476 000 corresponding to the triply charged ion distribution. The molecular weight limits were also determined for polyisoprene and polybutadiene. These were determined to be approximately 150 ku for polyisoprene (Figure 3.3B) and slightly higher than 300 ku for polybutadiene (Figure 3.3C). Both were analysed with tRA using $Cu(NO_3)_2$ as the cationization reagent. Note that the molecular weight limits are significantly different for the three polymers studied. There appears to be a strong influence of polymer type on desorption efficiency, ionization efficiency and/or cocrystallization with the matrix. Note that the limits discussed in this chapter are dependent upon the polydispersity of the samples. Higher polydispersities reduce these limits drastically, and will be discussed in the next chapter.

A challenge in determining the molecular weight of any species in the high mass range is mass calibration. In the mass range of 100 000 u and above, protein standards are rare, and ambiguity can exist as to their exact mass. The goal of obtaining extremely high mass accuracy (<0.01%) must be relaxed in the present application. However, a 1% relative mass accuracy would be sufficient in many cases, for simple average molecular weight determination. This allows for a novel calibration procedure, where the high mass spectra are calibrated with a lower mass polystyrene sample that demonstrates significant multimer formation. The term "multimer" is used to indicated the aggregation of two or more polymeric distributions, bearing a single charge. Figure 3.4 contains a spectrum of one such polystyrene sample (PS 90), showing significant multimer formation. By calibrating even lower mass polystyrenes with protein standards, it was observed that the peak values of the multimers are integer multiples of the peak value for the principal distribution. The peak value of the principal distribution, in this case approximately

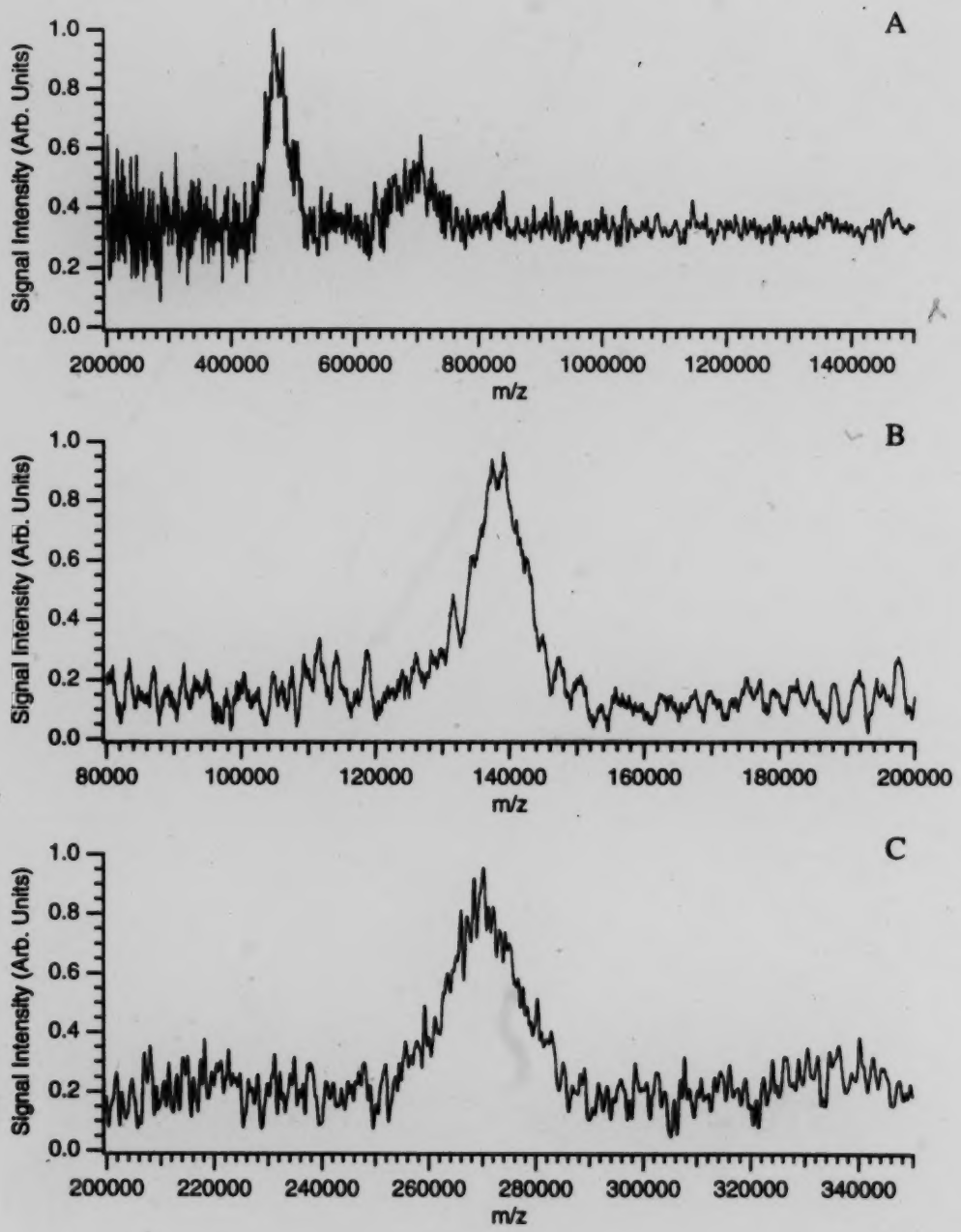

Figure 3.3 MALDI mass spectra of (A) polystyrene with a nominal molecular weight of 1.5 million, (B) polyisoprene with a nominal molecular weight of 137 000 and (C) polybutadiene with a nominal molecular weight of 315 200.

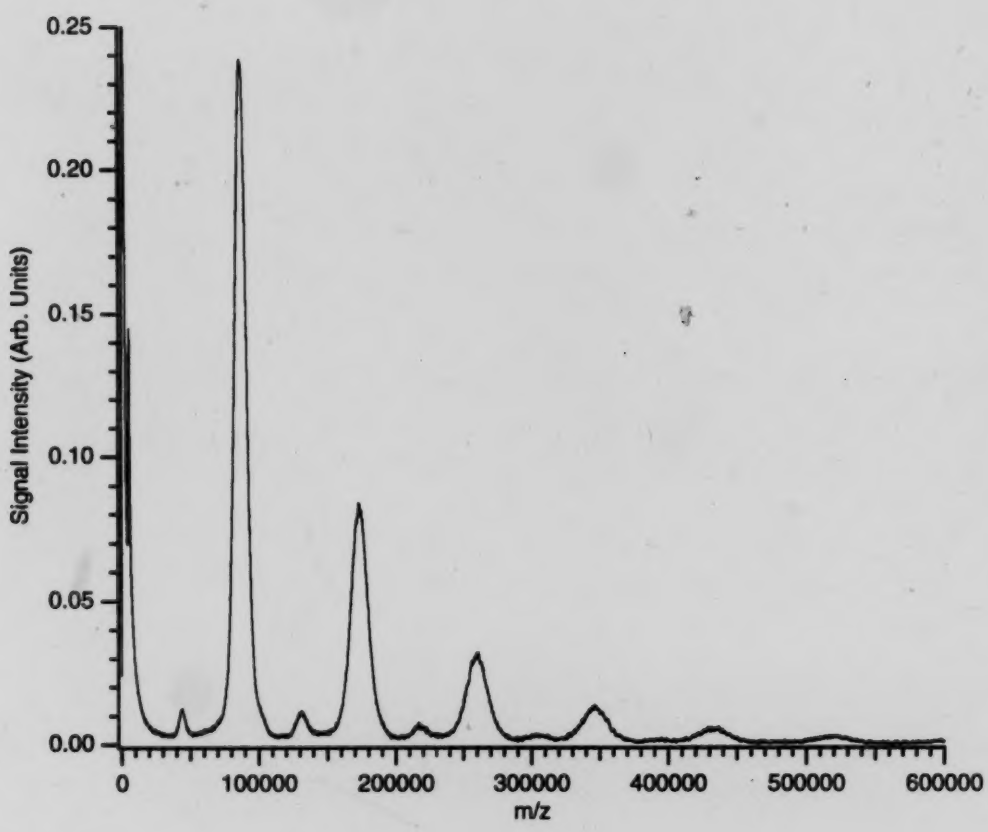

Figure 3.4 Mass spectrum of polystyrene with a nominal molecular weight of 90 000.

86 000 u, could be determined through the normal method of calibration by protein standards. The peak values of the multimer peaks were then simply taken as integer multiples of this value and used as calibration points. This allowed calibration of the instrument up to m/z ~ 600,000.

This indirect calibration procedure does have a higher degree of error associated with it, compared to a direct procedure. Replicate experiments have shown that an RSD of 0.23% for mass determination can be expected. A more direct mass calibration procedure would be ideal, but at present accurate mass calibrants are not available. A possible critique of this calibration procedure involves the issue of mass discrimination in the ion detection

system. However, for narrowly distributed polystyrenes, the peaks span a limited mass range and retain their expected Gaussian symmetry. For such samples, the mass discrimination factor can be ignored.

All the high mass polymers examined in this work display multiply charged ion distributions. The presence of these distributions can be analytically useful, as inferred from the mass spectra of polystyrenes. It is found that doubly charged distributions appear to be consistently overestimated by 0.9%, and triply charged distributions by 2.2%. Applying these correction factors to the 2^+ (m/z 700 000) and 3^+ (m/z 476 000) distributions in the spectrum of Figure 3.3A generates values for the principal distribution of 1 386 000 u and 1 396 000 u respectively. A reasonably accurate estimate of the number average molecular weight would then be 1 391 000 u. Replicate determinations and factoring in the error from the calibration procedure would suggest an average RSD of 0.43% for this molecular weight determination. It should be noted that the accuracy of this MALDI technique and the precision of the m/z determinations for the two peaks in the spectrum are sufficient to identify them as the 2^+ and 3^+ charge states. Also note that this correction procedure was applied to the determination of the principal distributions of PS 600, PS 770 and PS 900, rather than reporting the value of these distributions directly. This procedure was followed in these cases, as the principal distributions lay outside of the calibrated mass range.

Table 3.1 summarizes the data collected for a range of polystyrene standards. The molecular weights determined by classical methods were provided by the suppliers. It is evident that MALDI is capable of generating data for high mass polystyrene standards that follow the trend of the classical techniques of GPC, LLS, IV, and MO. Tables 3.2 and 3.3 list the data for several polyisoprenes and polybutadienes, respectively. While there is a reasonably good correlation between the GPC results and the MALDI results, discrepancies in the M_n values are noted for some samples. Differences as high as 18% in M_n are observed. Similar observations have been made for a number of other polymer/matrix systems.[6,7] The discrepancy may arise from two sources: calibration of GPC chromatograms and sampling in MALDI. Since the GPC calibration of these samples relied on a set of polymer standards of the same type, the average molecular weight values of the standards must be accurately known. As this is not often the case, such a calibration can introduce a large error. The error could be as high as ±10% for the polydienes used in this study, according to one supplier (Polymer Source Inc.). Errors can also be introduced in the MALDI measurement. The MALDI molecular weight distribution may correspond to a truncation of the true polymer distribution, in which only the most abundant oligomers

Table 3.1 Comparison of Molecular Weight Measurements for Polystyrenes

POLYMER STANDARD	MOLECULAR WEIGHT by Classical Methods*	MOLECULAR WEIGHT by MALDI
PS 90 (A)	M_v=96 000 (IV)	M_n=86 800
		M_w=87 000
PS 156 (SD)	M_n=154 000 (MO)	M_n=153 700
	M_v=159 000 (IV)	M_w=153 900
	M_w=162 000 (LLS)	
	M_n=152 000 (GPC)	
	M_w=156 000 (GPC)	
	M_p=156 000 (GPC)	
PS 200 (A)	M_w=216 000 (LLS)	M_n=202 500
	M_v=184 000 (IV)	M_w=202 800
	M_w=208 000 (GPC)	
	M_n=198 000 (GPC)	
	M_p=198 000 (GPC)	
PS 330 (PL)	M_n=302 000 (MO)	M_n=308 900
	M_v=306 000 (V)	M_w=309 100
	M_w=322 000 (LLS)	
	M_n=316 000 (GPC)	
	M_w=327 000 (GPC)	
	M_p=330 000 (GPC)	
PS 400 (A)	M_w=382 000 (LLS)	M_n=402 400
	M_n=335 000 (MO)	M_w=402 900
	M_w=393 000 (GPC)	
	M_n=340 000 (GPC)	
	M_p=357 000 (GPC)	

PS 514 (SD)	M_n=502 000 (MO)	M_n=469 800
	M_v=498 000 (IV)	M_w=470 500
	M_w=505 000 (LLS)	
	M_n=481 000 (GPC)	
	M_w=505 000 (GPC)	
	M_p=514 000 (GPC)	
PS 600 (A)	M_w=670 000 (LLS)	M_n=589 100
	M_n=663 000 (LLS)	M_w=589 400
	M_w=649 000 (GPC)	
	M_n=618 000 (GPC)	
	M_p=649 000 (GPC)	
PS 770 (PL)	M_v=735 000 (IV)	M_n=738 400
	M_n=765 000 (LLS)	M_w=741 100
	M_n=728 000 (GPC)	
	M_w=756 000 (GPC)	
	M_p=771 000 (GPC)	
PS 900 (A)	M_w=929 000 (LLS)	M_n=916 200
	M_w=942 000 (MO)	M_w=917 000
	M_n=892 000 (MO)	
	M_p=949 000 (MO)	
	M_v=932 000 (IV)	
PS 1460 (PL)	M_v=1 507 000 (IV)	M_n=1 391 300
	M_w=1 420 000 (LLS)	M_w=1 393 400
	M_n=1 378 000 (GPC)	
	M_w=1 460 000 (GPC)	
	M_p=1 459 000 (GPC)	

*These results are provided by the suppliers. Note that M_p refers to the most probable mass, and M_v to the average mass as determined by viscometry.

A: Aldrich Chemical Co., SD: Showa Denko K.K., PL: Polymer Laboratories

IV: intrinsic viscosity, LLS: laser light scattering, GPC: gel permeation chromatography, MO: membrane osmometry

Table 3.2 Comparison of GPC and MALDI molecular weight results for polyisoprenes

Sample	GPC (M_n/PD)	MALDI (M_n/PD)
PI 10 (P)	10 500/1.03	10 600/1.009
PI 19 (P)	19 300/1.04	18 480/1.005
PI 38 (PS)	38 500/1.03	36 790/1.005
PI 58 (P)	57 700/1.04	53 120/1.005
PI 84 (PS)	84 200/1.03	74 990/1.007
PI 137 (PS)	137 000/1.06	140 400/1.003

P: Polysciences, PS: Polymer Source

Table 3.3 Comparison of GPC and MALDI molecular weight results for polybutadienes

Sample	GPC (M_n/PD)	MALDI (M_n/PD)
PB 6 (PS)	6200/1.03	5600/1.013
PB 13 (PS)	13 400/1.03	11 780/1.006
PB 22 (P)	22 430/1.07	22 510/1.003
PB 129 (PS)	129 360/1.03	109 220/1.004
PB 315 (PS)	315 200/1.04	271 500/1.001

P: Polysciences, PS: Polymer Source

are represented. If this is the case, the measured M_n for a symmetrical distribution is accurate, but the M_w value would be too low. For a non-symmetrical distribution, both values would be in error. While not explicitly shown in the tables, note that the polydispersity as determined by MALDI is consistently lower than that reported by the other techniques. This has been observed by others,[6,8] and supports the idea of truncation.

In conclusion, a MALDI sample preparation based on *all-trans*-retinoic acid has been developed for the analysis of a class of polymers that previously had been difficult to analyse. It was shown to be applicable to an extremely wide mass range, although this mass range is dependent upon the polymer type. On a very basic level, this work shows that current technology allows for the detection of very massive species. Average molecular weights determined for the narrow polydisperse polymers of this study generally agree with the values obtained from classical molecular weight determination methods. A problem has been identified in the observation of consistently low *PD* values, however. Truncation of the polymer distribution would introduce some error in the average molecular weight determination, particularly for non-symmetric distributions, and particularly at higher m/z where the signal strength is low.

3.4 Literature Cited

(1) Bahr, U.; Deppe, A.; Karas, M.; Hillenkamp, F. *Anal. Chem.* **1992**, *64*, 2866.

(2) Danis, P. O.; Karr, D. E. *Org. Mass Spectrom.* **1993**, *28*, 923.

(3) Whittal, R. M.; Li, L.; Lee, S.; Winnik, M. A. *Macromol. Rapid Commun.* **1996**, *17*, 59.

(4) Lee, S.; Winnik, M. A.; Whittal, R. M.; Li, L. *Macromolecules* **1996**, *29*, 3060.

(5) Montaudo, G.; Montaudo, M. S.; Puglisi, C.; Samperi, F. *Rapid Commun. Mass Spectrom.* **1994**, *8*, 1011.

(6) Montaudo, G.; Montaudo, M. S.; Puglisi, C.; Samperi, F. *Rapid Commun. Mass Spectrom.* **1995**, *9*, 453.

(7) Lloyd, P. M.; Suddaby, K. G.; Varney, J. E.; Scrivener, E.; Derrick, P. J.; Haddleton, D. M. *Eur. Mass. Spectrom.* **1995**, *1*, 293.

(8) Belu, A. M.; DeSimone, J. M.; Linton, R. W.; Lange, G. W.; Friedman, R. M. *J. Am. Soc. Mass Spectrom.* **1996**, *7*, 11.

(9) Jackson, C.; Larsen, B.; McEwen, C. *Anal. Chem.* **1996**, *68*, 1303.

(10) Danis, P. O.; Karr, D. E.; Xiong, Y.; Owens, K. G. *Rapid Commun. Mass Spectrom.* **1996**, *10*, 862.

(11) Danis, P. O.; Karr, D. E.; Holle, A.; Mayer-Posner, F.; Watson, C. In *Proceedings of the 41st ASMS Conference on Mass Spectrometry and Allied Topics*; San Francisco, CA, 1993; p 1093.

(12) Xiong, Y.; Owens, K. G.; Danis, P. O.; Karr, D. E. In *Proceedings of the 42st ASMS Conference on Mass Spectrometry and Allied Topics*; Chicago, IL, 1994; p 980.

(13) Savickas, P. J. Poster presentation at the Sanibel Conference on Mass Spectrometry, Chicago, IL, 1994.

(14) Schwartz, B. L.; Rockwood, A. L.; Smith, R. D.; Tomalia, D. A.; Spindler, R. *Rapid Commun. Mass Spectrom.* **1995**, *9*, 1552.

(15) Fenn, J. B.; Mann, M.; Meng, C. K.; Wong, S. F. *Mass Spectrom. Rev.* **1990**, *9*, 37.

(16) Fuerstenau, S. D.; Benner, W. H. *Rapid. Commun. Mass Spectrom.* **1995**, *9*, 1528.

(17) McCloskey, J. A. In *Methods in Enzymology*; J. A. McCloskey, Ed.; Academic Press: San Diego, 1990; Vol. 193; p 61.

(18) Chakel, L. *Am. Lab.* **1994**, *Sept.*, 32C.

(19) Nelson, R. W.; Dogruel, D.; Williams, P. *Rapid Commun. Mass Spectrom.* **1995**, *9*, 625.

(20) Walker, K. L.; Kahr, M. S.; Wilkins, C. L.; Xu, Z.; Moore, J. S. *J. Am. Soc. Mass Spectrom.* **1994**, *5*, 731.

(21) Cotton, F. A.; Wilkinson, G. *Advanced Inorganic Chemistry;* fifth ed.; John Wiley & Sons: Toronto, 1988, p 757.

(22) Yamakawa, H. Modern Theory of Polymer Solutions, S. A. Rice, Ed.; Harper & Row: New York, 1971, p69.

Chapter 4

MALDI Analysis of Polymers: Validity of Molecular Weight Determinations[a]

4.1 Introduction

The previous chapter suggests that MALDI is capable of providing accurate average molecular weight information for polymers of narrow polydispersity. This conclusion is supported by the work of others.[1-10] Nevertheless, within this subset of narrow polydisperse polymers, there has arisen some question as to the accuracy of the method. Investigations have shown a dependence of the average molecular weight on the adduct-forming cation type,[11-13] the sample preparation method,[14,15,16] laser irradiance,[17] and even the type of mass analyser.[3,18] In many of these cases, the variability imparted to the average molecular weight is minor and has an identifiable source. For example, average molecular weight differences arising from changing the type of adduct-forming cation can be attributed to a minimum size requirement for the polymer chain, to stabilize the cation in the gas phase.[19]

However, MALDI has not been successful in the analysis of polymeric systems of high polydispersity, if success can be defined as achieving both the correct average molecular weight and molecular weight distribution data.[7,20] Here, a "polydisperse" polymer is arbitrarily defined as one having a polydispersity value (*PD*) greater than 1.1. As most benchtop and industrial polymerization procedures result in polydisperse materials, this presents a serious challenge for the procedure. Most studies indicate that MALDI data underestimate the high mass components, resulting in significantly lower average molecular weight values. It has been suggested that factors such as mass discrimination in ion detection and sample preparation could be the cause of this underestimation,[21-23] as well as sensitivity to laser power,[24] and issues involving the proper evaluation of MALDI polymer data.[25-27] However, there is some indication that MALDI can also overestimate the average molecular weight.[28] To date, no systematic study of all the issues relevant to the analysis of polydisperse polymers by MALDI time-of-flight mass spectrometry has been reported. The modest amount of literature on the analysis of polydisperse polymers has focussed primarily on developing experimental

[a] This chapter represents two manuscripts accepted by *Analytical Chemistry* for back-to-back publication (D.C. Schriemer and L. Li.).

procedures to overcome the limitations of direct analysis. Success has been demonstrated in the fractionation of polydisperse polymers by gel permeation chromatography (GPC), whereupon MALDI analysis of the collected fractions provides a self-calibration of the chromatogram.[29,30] While this mitigates some of the desirable features of the MALDI technique (e.g., speed), it does serve as a useful absolute molecular weight determination method to supplement the detection system for GPC.

The study presented in this chapter is an attempt to systematically address where the difficulties lie in the MALDI time-of-flight analysis of polydisperse polymers. Essentially, it involves an investigation of the parameters of the technique that give rise to mass discrimination in the recorded signal. Consideration will be given to the effect of sample preparation in conjunction with the desorption/ionization phenomenon, ion transmission, ion detection as well as data processing. The experimental work for this study has been developed around polystyrene analysis by the procedure discussed in the previous chapter. For this study, all experiments were conducted on a linear MALDI time-of-flight instrument, under time-lag focussing conditions.

4.2 Experimental

4.2.1 Instrumentation

Mass spectral data were collected on a linear time-lag focussing MALDI TOF mass spectrometer,[31] modified for operation up to 30 kV. The first extraction plate was redesigned and a grid was placed on the repeller side. A single DC power supply was used to set the potential on the repeller and first extraction plate and the potential on the second extraction plate through a voltage divider. Under normal operation, the power supply was set to 20 kV DC. In conjunction, a high voltage pulser built in-house and a Hewlett-Packard pulser (Palo Alto, CA) were used to generate the delayed extraction pulse. The extraction pulse and time lag were varied as required to focus the mass range of interest. A nitrogen laser (VSL-337ND, Laser Science, Inc.; Newton, MA) with a 3-ns pulse width was used for desorption at 67.5° to the probe surface normal. A neutral-density filter was used to attenuate the laser energy that reached the sample surface. A mass filter was added to the system. The mass filter prevented saturation of the microchannel plate detector by deflecting matrix ions out of the usual ion trajectory, reducing the ion current from low mass ions. Laser energy was measured with a laser energy meter (Molectron, Portland OR), capable of delivering a precision of better than

2%. A microchannel plate (MCP) detector was used for ion detection. Unless otherwise specified in the text, experiments were conducted with 20 kV DC, a 3.6 kV pulse applied to the repeller, and a pulse delay of 0.65 μs. A -4.75 kV post-acceleration field was established between a grounded grid and the first MCP (1.85 mm apart), and the detector was operated at its full active surface (diameter of 40 mm).

4.2.2 Data Collection and Mass Calibration

The mass spectra were recorded using a LeCroy 9350M digital oscilloscope at a sampling rate of 500 MHz to 1 GHz in conjunction with Hewlett-Packard MALDI software. Peak centroids were determined with the software, and mass calibration of the instrument was achieved using a two-point linear calibration. Calibrated spectra were transferred to a PowerMac and processed using Igor Pro data analysis software (WaveMetrics, Inc., Lake Oswego, OR.). All spectra were baseline corrected, unless otherwise specified, to remove the matrix contribution. Number average molecular weights (M_n) were determined from the mass domain after a correction factor of 1/(dm/dt) was applied to the data. This involved the multiplication of the intensity data by the correction factor, to account for the non-linear correlation between the time and mass domains.[27] This correction will be discussed in section 4.3.3. In general, mass spectra from 100 laser shots were summed to produce a final spectrum in this study. Five such sets were collected, each from a fresh preparation, for the purpose of determining percent relative standard deviations (RSDs) for the measured M_n values.

Mass calibrations were performed externally, using well characterized peptides spanning the mass range of interest. The proteins and peptides used were bovine insulin chain b (oxidized), bovine ubiquitin, equine cytochrome c and bovine carbonic anhydrase II.

4.2.3 Sample Preparation

Polymer samples for MALDI analysis were prepared by combining the analyte, matrix and cationizing agent in tetrahydrofuran (THF). *all-trans* Retinoic acid (tRA) was used as the matrix, according to the procedure described in the previous chapter. Variations in the preparative procedure are cited in the text. In the analysis, 1 μl of the appropriate mixture was added to the MALDI probe tip (surface area of 0.13 cm^2) and

allowed to dry. Peptide analysis for calibration purposes also followed the procedure described in the previous chapter.

4.2.4 Samples and Reagents

The peptide standards listed above were purchased from Sigma (St. Louis, MO). The matrix used in their analyses (sinapinic acid) was purchased from Aldrich (Milwaukee, WI). Polystyrene standards with the following nominal molecular weights were used in this study: 3250, 5050, 7000, 9240, 11 600, 22 000, 28 500 (Shoko Co., Tokyo, Japan); 20 000, 35 000, 50 000 (Aldrich). The matrix tRA was also purchased from Aldrich. The cationizing reagent ($AgNO_3$, Terochem Laboratories Ltd., Edmonton, Canada) was reagent grade and used without further purification. THF (VWR Scientific, Toronto, Canada) was pretreated with potassium hydroxide, filtered, then distilled over sodium metal in the presence of benzophenone as an indicator of dryness.

4.3 Results and Discussion

One of the difficulties in determining the accuracy of the MALDI method for polymer molecular weight determination arises from a dearth of adequate standard materials. With the exception of polymers of very narrow polydispersity, few polymeric systems are characterized to a degree of accuracy that allows a fair assessment of the accuracy of the MALDI experiment. This is particularly true for polydisperse polymers. Therefore, the approach of this work was not to analyse polydisperse polymers directly, but to prepare blends of narrow polydispersity polystyrene in such a fashion as to mimic a polydisperse polymer. The utility of such an approach has been demonstrated.[13,18,28,32] Most of the data presented in this work have been collected from two-component blends. The M_n value of each individual component was determined in a separate MALDI experiment. Blends were then prepared in which each component was present in an equimolar ratio. Obtaining a MALDI mass spectrum from such a blend and determining the combined M_n allowed comparison with an expected M_n. While the data generated from such preparations are only strictly applicable to bimodal distributions, the trends exhibited by these preparations can be extended to more continuous polydisperse distributions. In the following discussion, issues related to the MALDI process itself (sample preparation, desorption/ionization) are addressed, as well as issues involved in the detection of MALDI-generated ions (instrumental considerations).

4.3.1 Sample Preparation, Desorption/Ionization

4.3.1.1 Multimer Formation

Multicomponent blends of polystyrene from 3000 u to 15 000 u provide spectra demonstrating excellent agreement between experimental and expected M_n values (Figure 4.1A). The experimentally determined M_n value for this blend was determined to be 7390 (1.6% RSD). The expected value is 7416. This is well within the precision of the measurement, indicating that molecular weight measurements of polystyrene are accurate at least in this mass range. Attempting to extend the range by the addition of high mass components resulted in a large drop in the experimental M_n value versus the expected value (Figure 4.1B). Notice also that the molecular weight distribution of the original blend is skewed by the addition of these high mass components.

It can be difficult to distinguish sample preparation problems from desorption/ionization issues; indeed, they are often intimately related.[33] One of the most obvious problems can, however, be identified as a sample concern. Polymeric species give rise to multimer formation in much the same way as proteins do.[34] Recall from the previous chapter that a multimer can be defined as the aggregation of two or more polymer distributions. The implication of multimers for the analysis of polydisperse polymeric systems is demonstrated by Figure 4.2. A two-component polystyrene blend was prepared, spanning a mass range where one can expect good agreement between the experimental and expected M_n values (Figure 4.2A). The expected M_n value of this blend is 8245; MALDI analysis generated an M_n value of 8309 (% RSD = 0.35). A high mass component was then added to the preparation (Figure 4.2B). This resulted in a significant reduction of the M_n value for the initial two components to 7762 (7% drop), and parallels the skewing of the molecular weight distribution observed in Figure 4.1B.

A close investigation of the spectrum in Figure 4.2B (insert) provides insight as to why this drop occurred. No multimer formation for the two low mass components is in evidence. However, multimer formation occurs between the high mass component and itself (distribution at ~60 000 u) but also between the mid and high mass components (distribution at ~40 000 u). Higher order multimer formation is in evidence above 60 000 u as well. The addition of polystyrene 28 500 serves to demonstrate both the mass dependent nature of this multimer formation, and its effect on M_n values. In the first place, there is progressively less multimer formation between this high mass component and the lower mass components, to the point where multimer formation between

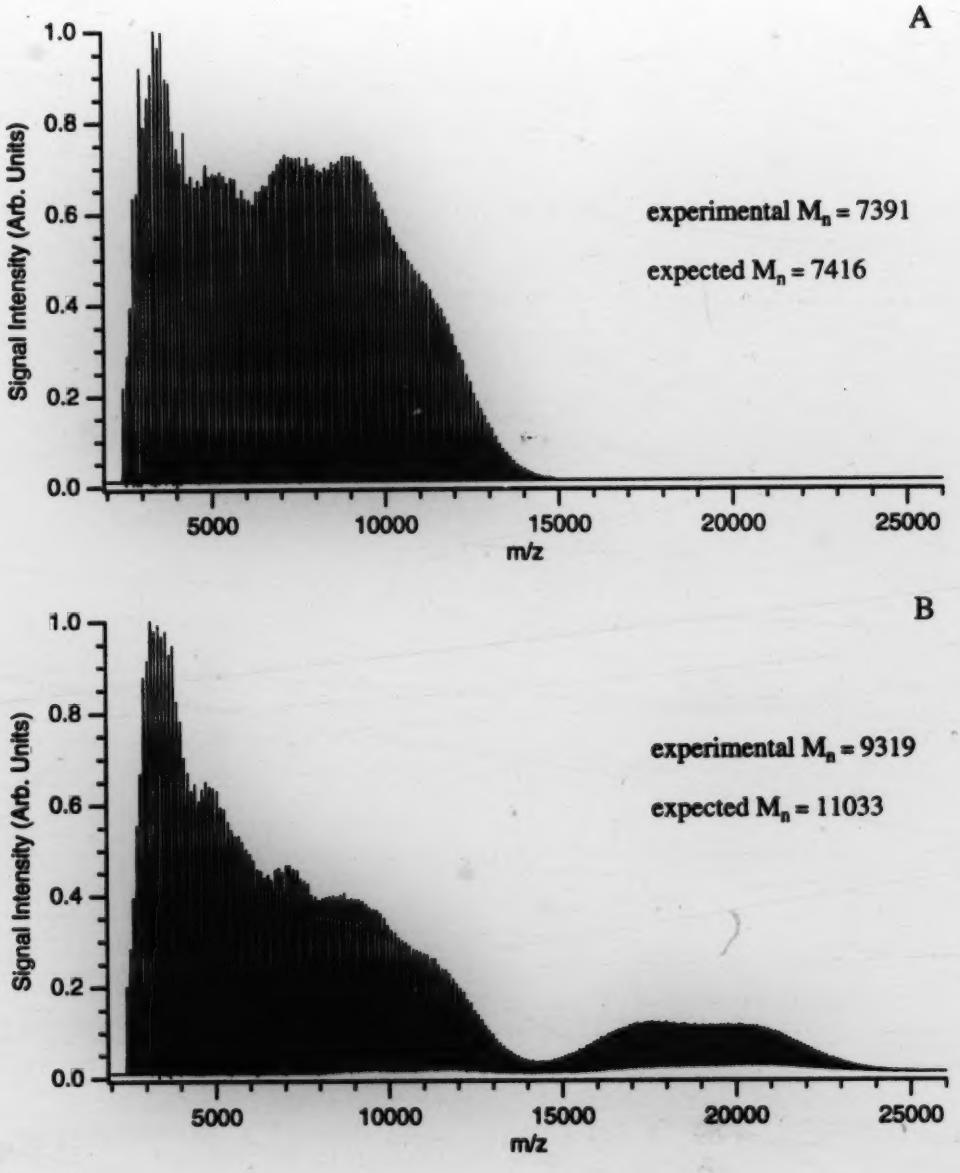

Figure 4.1 Spectra of multicomponent blends consisting of (A) polystyrene 3250, 5050, 7000, 9240, 11 600 and (B) polystyrene 3250, 5050, 7000, 9240, 11 600, 20 000, and 22 000. All components were present in equimolar quantities, with 200 pmol total polymer loaded to the probe in both cases.

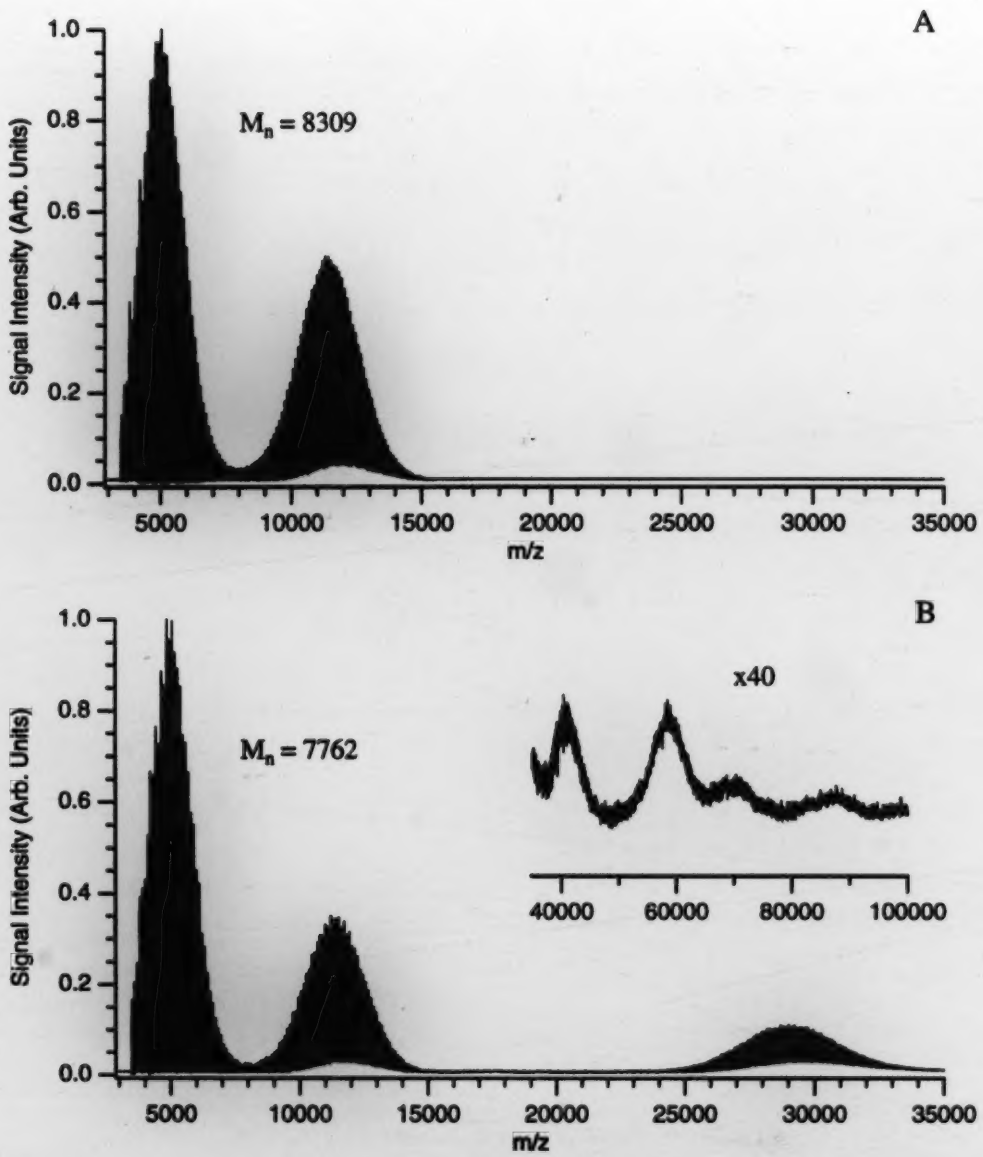

Figure 4.2 An analysis of blends to determine the effect of multimer formation on measured M_n values. (A) polystyrene 5050 and 11 600, 100 pmol of each loaded to probe, expected M_n of 8245; (B) same blend as A, doped with polystyrene 35 000 such that the amount loaded to probe was 75 pmol, with the other two components still present at 100 pmol each.

polystyrene 5050 and 28 500 is negligible. Obviously, multimer formation has the effect of diminishing the intensity of the principal distributions, with the higher mass components affected more than the lower mass components. This skews the M_n values low. In the second place, if the polymer becomes too polydisperse, it will begin overlapping with its own dimer, skewing the M_n values high. It is probable that this multimer formation arises due to prior clustering in the solid matrix preparation,[3] since the on-probe concentration of polymer is quite high. While this is a reasonable conclusion, the involvement of gas phase collisions in the clustering process cannot be ruled out. The type of matrix used appears to effect the extent of multimer formation as well.[3] Nevertheless, in the published spectra of high mass polymers where the displayed mass range is sufficiently broad, all polymer types studied display multimer formation. This is likely a result of the high analyte concentrations typically incorporated into the MALDI analysis of polymers.

4.3.1.2 Overlap of Multiple Distributions

In the above experiment it was easy to discern the multimers from the principal distributions. However if the mass range in Figure 4.2B were completely filled with oligomers (as would be the case in a more continuously polydisperse system), multimers would be indistinguishable from baseline, due to the many possible combinations that could arise. The implications of these observations are numerous, and dependent on which mass range is being investigated. For the 5000 to 50 000 u mass range, both multimer formation and its mass discrimination are important. Overlapping of the principal distribution with the multimer is clearly an unfavorable situation and should be avoided. When multimer formation occurs, there exists an upper limit to the polydispersity of a polymer that can be analysed by MALDI. For a Gaussian distribution, this was calculated to be PD=1.043 (Appendix, section 4.5). If a polymer has a polydispersity above this value, overlap with the dimer would affect the calculated M_n value. However, this mass range is prone to mass discrimination in multimer formation, as Figure 4.2B indicates. Therefore, even when operating under non-overlap conditions, multimer formation can still affect the M_n value of the principal distribution.

In the upper mass range (>50 000 u), the issue of overlap with the dimer is still present. However, this mass range becomes plagued with an addition problem, namely overlap between the principal distribution and the doubly charged principal distribution. The multiple charging is usually not present below ~50 000 u for this analytical procedure. When it does occur, it becomes the limiting factor, rather than overlap with

the dimer, allowing only for a PD=1.028 for polymeric systems displaying a Gaussian distribution (Appendix, section 4.5). Beyond this polydispersity, one would expect the doubly charged distribution to contribute to the principal distribution, resulting in a falsely low M_n value.

4.3.1.3 Matrix/Analyte Dependence

It is not surprising that a mass discrimination in the extent of multimer formation was observed, as entanglement is also a function of polymer chain length.[3] One method for the minimization of multimer formation involves decreasing the concentration of the polymer in the matrix, or in MALDI terms, simply increasing the matrix-to-analyte ratio. This requires a sensitive sample preparation method, not something generally considered when polymers are analyzed by MALDI, as a large quantity of sample is almost always available. Figure 4.3 demonstrates the effect of polymer concentration in the solid sample on the measured M_n value for a two-component blend, which has an expected M_n of 16 575. This blend was prepared from equimolar amounts of polystyrene 5050 and 28500, chosen because negligible cross multimer formation occurs between these two components. The measured M_n value increased with an increase in the matrix-to-analyte ratio. An investigation of the spectra giving rise to these graphs showed a modest decrease in relative multimer intensity, with an increase in the matrix-to-analyte ratio. However, at the highest ratio investigated, multimers were still present. Even tetramers were still in evidence (spectra not shown).

Note two additional features of the plot in Figure 4.3: the expected M_n value is considerably overestimated at the higher matrix-to-analyte ratios, and there appears to be no constant value approached over the range examined. As only the principal distributions are considered in the calculation of M_n, the decrease in multimer formation would contribute at least partially to the increase in M_n with the matrix-to-analyte ratio, as more matrix per polymer chain would serve to better isolate individual chains. Since the expected M_n is overestimated and multimers are still present at the highest matrix to analyte ratio, this in itself is not a sufficient explanation of the data in Figure 4.3. Apparently, a fundamental difference exists between the low and high mass components with respect to their desorption/ionization efficiency. Under progressively more dilute conditions, desorption/ionization begins to favor the high mass component over the low mass component. This implies that an optimum matrix-to-analyte ratio exists for each component in the blend, and that this ratio increases with mass. The implication of such

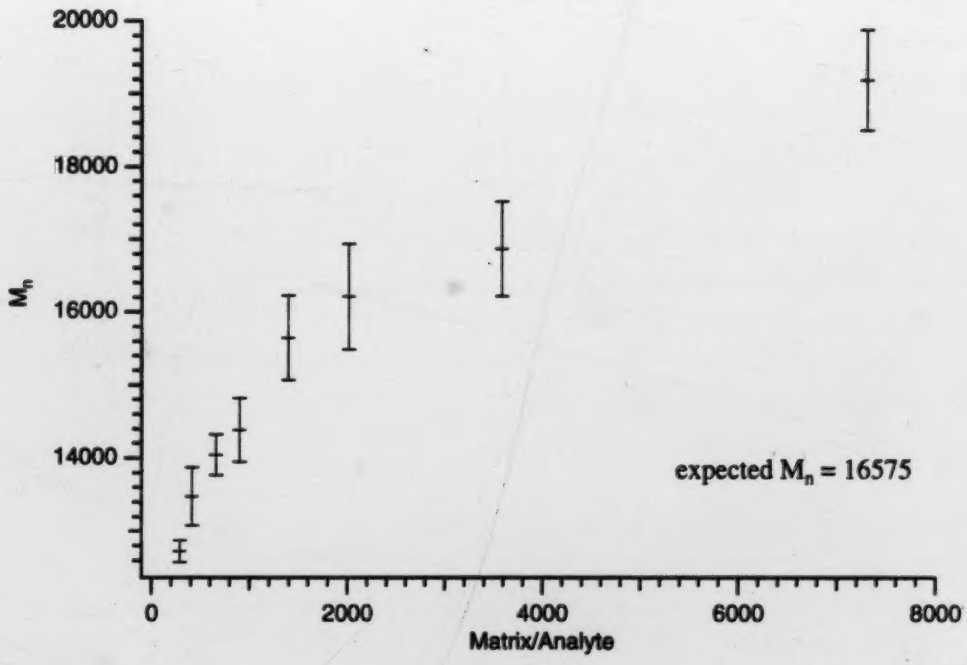

Figure 4.3 Determination of the effect of polymer concentration in the solid sample matrix on the measured M_n of a two-component blend, consisting of polystyrene 5050 and 28 500. For each point, the ratio of the amounts loaded for the two components was maintained. Expected M_n of 16 575.

a conclusion is that one sample preparation *cannot* provide uniform desorption/ionization efficiency across a broad mass range.

A question could be raised regarding the possibility of a molecular weight gradient existing across the thickness of the sample, a gradient that changes depending on the polymer concentration. Such a situation could arise when, during the crystallization/drying step, the high mass component reaches its precipitation point before the lower mass component and is therefore not included in the matrix as efficiently. Reducing the overall concentration could have the effect of minimizing this gradient,[35] thereby causing higher experimentally determined M_n values. While this is consistent

with the trend as seen in Figure 4.3, there are at least two reasons why it is an insufficient explanation. First, this argument cannot be used to explain why the expected M_n value is overestimated at the lower polymer concentrations. Second, given the conditions for the sample preparation (i.e., excellent solvent for polymer and matrix over a broad mass and concentration range, and very fast drying times) one cannot reasonably expect molecular weight dependent fractionation to occur. For optimum mass discrimination, fractionation should occur slowly. Furthermore, a single step batch fractionation would not show a mass discrimination of this selectivity over such a limited mass range.[35] This does not suggest that on-probe fractionation will never be a factor. With higher polydispersities, poorer solvents and longer deposition times, fractionation could occur.

4.3.1.4 Cation Concentration Dependence

A variation in the concentration of cationizing reagent also influenced the measured M_n value. Figures 4.4A and 4.4B demonstrate the effect of varying the concentration of the silver ion over a narrow range (0-1.5 mmolar in the final solution). Figure 4.4A shows that when the concentration of the silver ion in the matrix/analyte mixture was lowered, the measured M_n value of a two-component blend increased, whereas Figure 4.4B demonstrates that the measured molecular weight of the individual components themselves remained unchanged. Therefore, over a broad mass range, the cation concentration has an effect on M_n that does not show up in the analysis of polymers of narrow polydispersity.

At a zero silver ion concentration, a spectrum of the blend could still be obtained. An inspection of the individual oligomers indicated masses consistent with sodium cationization. This sodium ion likely arose from impurities in the matrix/polymer solutions. This point in the graph, as it represents an M_n significantly higher than the silver cationized species, suggests that there is a mass discrimination arising from the nature of the cationizing reagent. This is in line with previous studies of polymers of narrow polydispersity.[11,13] Nevertheless, mass discrimination exists in silver cationization as well, and is a function of silver ion concentration. While the steep-sloped part of the graph in Figure 4.4A represents spectra that contain contributions from both sodium and silver cationized oligomers, the signal strength of sodium cationized oligomers is considerably lower than silver cationized oligomers. Therefore, the M_n values represented by the points on the steep-sloped part of the curve are not simply due to the dilution of the result at a zero silver ion concentration with a constant M_n value

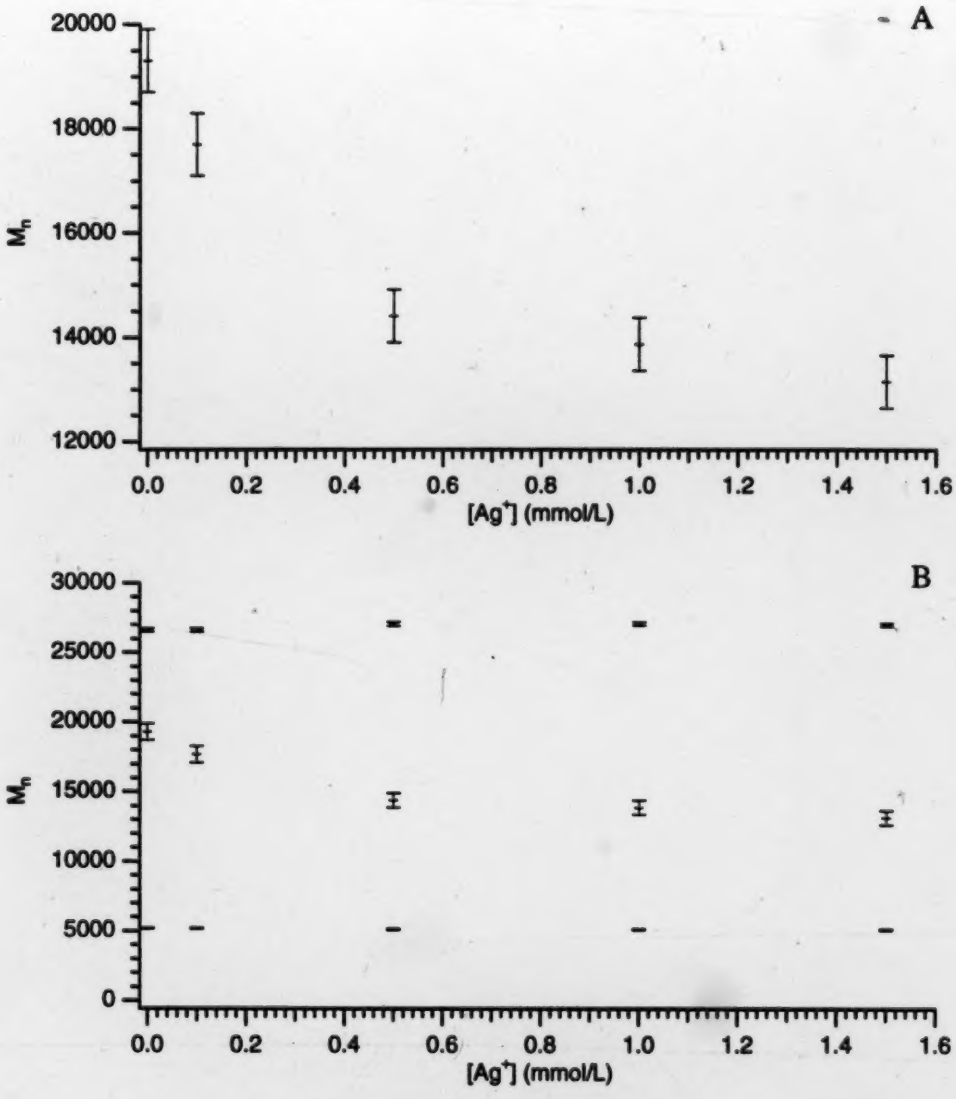

Figure 4.4 (A) Determination of the effect of silver cation concentration, in the solution mixture of polymer, matrix and silver salt, on the measured M_n value. 100 pmol of each component (polystyrene 5050 and 28 500) was loaded to the probe, error bars indicate +/- one standard deviation; (B) Same data as in A, with the addition of the corresponding determinations of M_n for the individual components. Expected M_n of 16 575 for the blend.

arising from silver cationization. These points themselves suggest a mass discrimination in ionization, based on the availability of silver ion .

Note that the molar amount of silver ion present in all the formulations was in excess of the molar amount of polymer, but not the matrix. A three-way competition existed between matrix, low mass, and high mass analyte for the limited amount of silver ion. Above moderate silver ion concentrations (~0.5 mM), the effects of this competition were not evident. This study suggests that cation concentration should be high, but not to the extent that the optimum sample preparation is adversely affected. This is a difficult parameter to extend to other polymer analyses, as it cannot be undertaken on the basis of cation concentration alone. Similar studies should be done on other matrix/polymer/cation model systems, to establish the constant domain of the graph of M_n vs. cation concentration.

Figure 4.4B reveals an interesting trend in the determination of M_n values as polydispersity increases. The precision of M_n determination diminishes with an increasing mass range of analysis. Whereas the precision in the determination of M_n for the individual components remains excellent (%RSD of 0.4 for polystyrene 28 500 and 0.5 for polystyrene 5050), it is worse for the blend (%RSD of 3.5). This represents the worst possible case for a polymer in this mass range. As the sample is bimodal in nature, slight variation in the intensity of one component can significantly affect the measured M_n. A Gaussian distribution over the same mass range, for example, should exhibit a precision characterized by a %RSD less than 3.5.

4.3.1.5 Laser Power Dependence

Recent work by Martin et al. suggested that laser power can also play an important role in measuring the M_n of polydisperse polymers.[24] They suggested that the measured average molecular weight of polydisperse polymers is dependent on the laser power used, with higher laser power giving rise to higher average molecular weights. The implication of this study is that higher mass components in a polydisperse sample always require a higher laser power for comparable desorption/ionization efficiency, with the severity of this discrimination being a function of matrix type. Such a laser power dependence has not been observed for polystyrene analysis using tRA as the matrix. This is demonstrated in Figure 4.5.

In this figure, the M_n value of a two-component blend is displayed as a function of laser energy. Laser energies from just above the matrix detection threshold (~4 μJ) to six times this threshold value were investigated for a blend consisting of polystyrene 5050

and 28 500. In this application, "threshold" is loosely defined as the lowest laser energy giving rise to a measurable signal. The highest laser energy used generated analyte signals close to the maximum signal strengths measurable for the experimental setup. With the possible exception of the M_n value measured at 5.2 μJ, there was no change in M_n values with laser energy, either for the blend or the individual components.

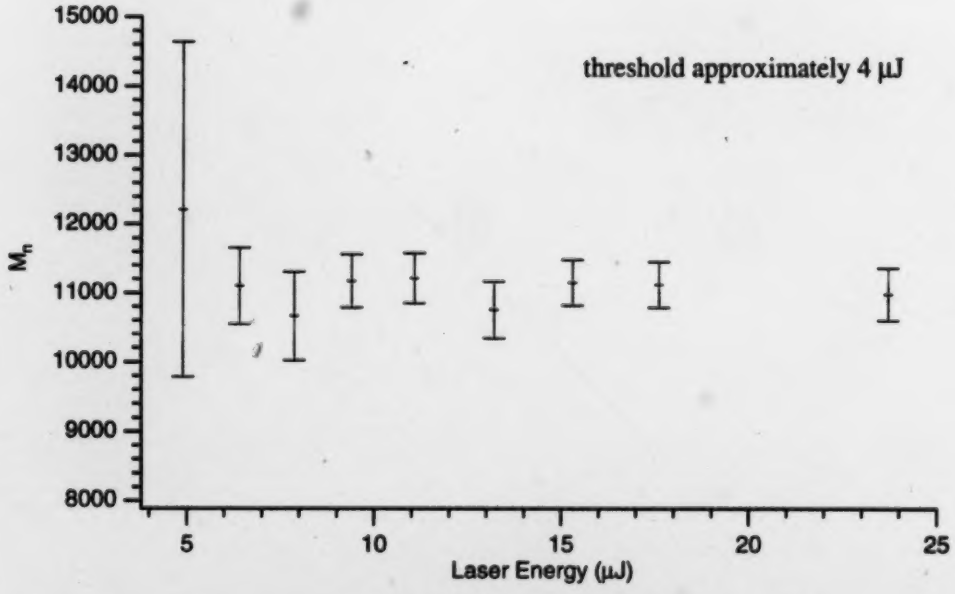

Figure 4.5 Effect of laser fluence on the measured M_n value of a two-component blend consisting of polystyrene 5050 and 28 500. Each component was loaded at 100 pmol. Threshold laser fluence for matrix detection is approximately 4 μJ. Expected M_n of 16575.

The data presented in this figure is an indicator of matrix quality with respect to the targeted analyte. The laser threshold for the analyte is the same for both the high and low mass species (~5.2 μJ). This is true for all polystyrene blends from 5000 u up to at least 50 000 u. The spectra giving rise to Figure 4.5 indicate no evidence of any laser-energy dependent fragmentation (spectra not shown). The matrix therefore provides a good "shield" for the analyte from the affects of UV irradiation. An increase in laser energy results in an increase in the amount of ablated material. Therefore, no dependence of M_n on laser energy implies that the preparation is effective in providing a random

distribution of analyte throughout the matrix. Of course, for this to be true requires there to be no relative change in ionization behaviour for the components of the blend. This is a reasonable assumption, as it was previously shown that if the cation concentration is maintained above a certain level, there is no evidence of mass-dependent competition between the high and low mass components.

4.3.2 Instrumental Issues

The differences among the available time-of-flight instruments are essentially defined according to their approaches to ion source/extraction geometry and detector design. To provide an accurate assessment of all available instruments for the MALDI analysis of polydisperse polymers is difficult; however, key features in the ion source and detector can be addressed for their effect on polymer mass spectra. As many linear time-of-flight instruments use MCP-based detectors, and are now developed around the time-lag focussing principle, this system was chosen for investigation.

4.3.2.1 Ion Focussing

The MALDI process generates gas phase ions containing appreciable axial and radial velocity components.[36,37] The velocity of the ions produced in this event are broadly distributed, but largely independent of mass (except perhaps below ~5000 u [38,39]). The ion optics used in the time-of-flight system must provide focussing of this ion packet on a detector surface oriented perpendicular to the axis of the spectrometer. In a source defined by simple parallel plate electrodes, if one assumes a uniform electric field with no field penetration between regions in the source (a planar equipotential field), the source does not provide axial lensing of the ions produced. This would have the effect of producing a distribution of ions in a plane parallel to the detector surface that bears a mass distribution: the higher mass ions would display a greater radius of impact on the detector surface than the lower mass ions, in the case where the ions have the same initial velocity and velocity distribution. The extent to which this is true, and the effective aperture of the detector, will determine the effect this mass dependent radial dispersion has on the collected mass spectrum.

There are complicating factors. Coulombic repulsion could impart relatively higher velocities and wider velocity distributions to ions of lower mass, and thereby change the radial distribution of masses at the detector. Collisional scattering could also affect the lower masses more. Furthermore, most ion sources impart a certain amount of

lensing action, either intentionally built in (focussing repellers, einzel lenses, xy deflectors, wire ion guides, etc.) or due to field penetration between source elements. Lensing action can alter the mass discrimination in the radial distribution of ions at the detector surface. Theoretically, the trajectories of equal-energy ions bearing different mass-to-charge ratios are the same in electrostatic fields, giving rise to a common focal point.[40] The ion source and the potentials applied to the source elements should be tailored to establishing this focal point near the detector surface. In a time-lag focussing MALDI instrument, this focal point can change since the voltage applied to the source is a variable for achieving good resolution. Therefore, the "quality" of the lens with respect to axial ion focussing is variable, and a poor focus will translate into a wide distribution of ions in the plane of the detector. The extent to which the ion optics are defocussed will also determine the severity of the mass discrimination in this distribution.

The mass discrimination in ion detection arising from these focussing considerations needs to be investigated when considering the MALDI analysis of polydisperse polymers. To illuminate some of the above points, an experiment was conducted with a source characterized by a focussing repeller and a measure of field penetration between source electrodes. In this experiment, a two-component blend was prepared consisting of polystyrene 5050 and 28 500 (expected M_n value of 16 980). MALDI spectra of this blend were collected, in which the detector's ion acceptance window was varied in 0.5 cm intervals from a diameter of 1.0 to 4.0 cm. The M_n value of the blend was measured at each aperture. Figures 4.6A and 4.6B display the results of this experiment, determined as a function of push-out pulse delay. Each point represents the average of five M_n values determined from separate sample preparations. As in previous figures, the error bars in Figures 4.6A and 4.6B represent +/- one standard deviation. In Figure 4.6B, however, the contribution of sample-to-sample error has been removed. This is valid since for any given aperture, M_n values for both pulse delays were determined from the same sample preparation. Expressed in this fashion, the error bars of Figure 4.6B are only meaningful for the comparison between push-out pulse delays.

As indicated in Figure 4.6A, mass discrimination occurred at an aperture of ~1.5 cm and below, for this source geometry and applied voltage. At apertures greater than 1.5 cm, there was little variation in the measured M_n value of the blend. These data are consistent with the idea that each mass transmitted by the source bears a radial distribution at the detector, and that the width of this distribution decreases with increasing mass. Below 1.5 cm, some of the low mass ions were prevented from reaching the detector, giving rise to higher M_n values. Under the cited experimental

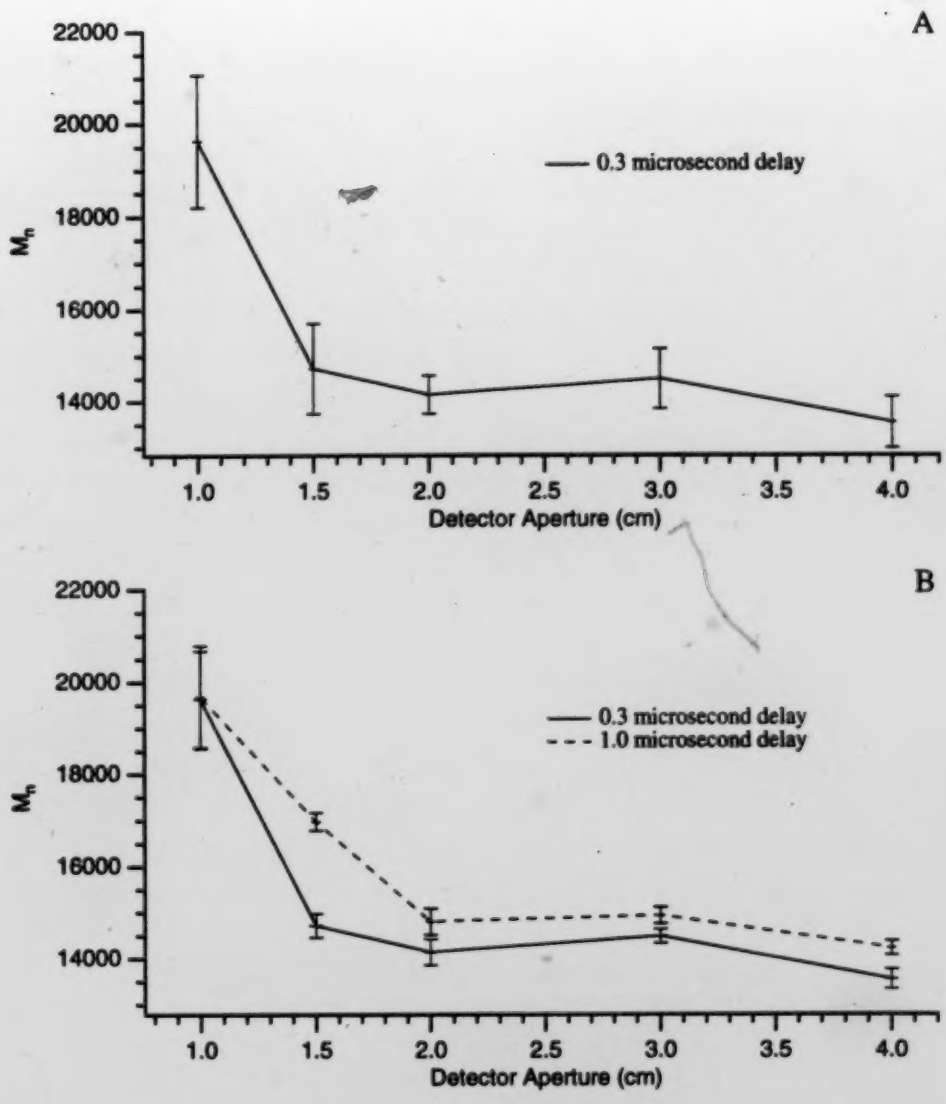

Figure 4.6 (A) Investigation of the ion focussing properties of the MALDI TOF instrument used in this work. The sample consisted of polystyrene 5050 and 28 500, 100 pmol of each loaded to the probe. Expected M_n of 16 980. The ion source was operated with 20 kV DC applied, and a 3.6 kV push-out pulse with a 0.3 μs delay, for all detector apertures; (B) As in A, with an additional trace corresponding to a 1.0 μs delay. Error bars in B represent the removal of sample-to-sample error.

conditions, this source geometry is suitable for the analysis of polymers with a broad polydispersity, as long as the low mass end is >3000 u, and the detector aperture is greater than 1.5 cm.

As demonstrated by Figure 4.6B, the mass discrimination in the spread of the ion packet at the detector was also affected by the push-out pulse delay. At all apertures greater than 1 cm, an increase in the pulse delay caused an increase in the measured M_n value. This conclusion is statistically significant according to the t-test for the comparison of means, at the 95% confidence limit. The largest difference was found at the 1.5 cm aperture, where a relatively greater amount of the low mass ions were prevented from reaching the detector in the long pulse delay mode. This observation is consistent with the widening of the radial distribution for the low mass ions relative to the high mass ions. An increase in the pulse delay allowed an increase in the axial and radial spread of ions in the source, prior to extraction. Dispersion would be more significant for the low mass ions. Upon extraction, the increased spatial distribution in the source translated into a further defocussing of the ions, with the lower masses affected more severely. This led to an increase in the measured M_n value for the blend. One would expect the effects of defocussing to diminish with increasing aperture. This did occur, however a region of constant difference was reached at apertures greater than 2 cm. This could indicate a mass-dependent transmission loss in the source region, where a fraction of the low mass ions were lost due to collisions with source elements. Increasing the pulse delay would increase the loss of the low mass ions. This effect would be constant with changing aperture and manifest itself as an offset in the graph of M_n versus detector aperture. Therefore, Figure 4.6B seems to reflect the contribution of both defocussing and transmission loss.

The operator has control over the severity of the above-described mass discrimination by adjusting the lensing properties of the source, and selecting the appropriate push-out pulse delay. In a time-lag focussing instrument, lensing properties can be altered simply by adjusting the amplitude of the push-out pulse. The required lensing properties should be determined by the mass range to be investigated. Through the analysis of blends, focussing conditions can be established to conform to reasonable detector apertures. The one drawback to this approach relates to the dependence of mass resolution on the amplitude and delay of the push-out pulse. The optimum pulse conditions for axial focussing could place constraints upon the optimization of mass resolution. For the instrument used in this work, this study suggests that a detector with a

minimum 2 cm diameter of active detection area is required, coupled with pulse delays less than 1 μs, to fully intercept all the ions of a broad mass range.

4.3.2.2 Ion Detection

Reports that MALDI fails in the analysis of polydisperse polymers identify the ion detection system as the main area where mass dependent signal detection occurs. For MCP, electron multiplier, or hybrid detection systems, this is attributed to an erosion in the efficiency of ion-to-electron conversion at the detector surface as the mass of the incident ion increases, due to a decrease in impact velocity. Based on this argument, the conversion efficiency for an ion of a given mass could improve with an increase in its velocity. Many designs contain a post-acceleration region, where the primary ion receives additional velocity for the purpose of improving ion-to-electron conversion efficiency of the primary ions. A grounded, high optically transmissive grid (~90%) is often used to isolate the post-acceleration region from the field free drift region of the spectrometer. Nevertheless, post-acceleration does not remove the mass discrimination.

Recent developments in detector design indicate that the conversion of primary ions to electrons at the detector conversion surface is not the only means of signal generation. The phenomenon of secondary ion formation at surfaces has been noted,[41,42] and has been incorporated into detector design for improved high mass sensitivity.[43-45] Thus, aside from the consideration of mass discrimination in ion-to-electron conversion, ion transmission through the grid and secondary ion generation at the grid surface may also give rise to mass discrimination.

An experiment was conducted where a number of polystyrene blends were analysed, using a detector with grids of different transmissivity for delimiting the post-acceleration region. The results are displayed in Figure 4.7 (see insert for detector configuration). The M_n values of three two-component blends were measured with detector configurations incorporating a nickel grid, with either 50% or 90% optical transmissivities. As Figure 4.7 shows, the grid with the lower transmissivity resulted in consistently *higher* M_n values than the higher transmissivity grid. Based on considerations of collisional probability, this is the opposite of what is expected.[46] Decreasing the transmissivity should have the effect of restricting passage of the high mass ions more than the low mass ions, resulting in a lowering of the measured M_n values. Therefore, an additional detection mechanism must have contributed to the signal. This could be identified as arising from secondary ions generated at the grid surface, in keeping with previous studies that have noticed the contribution of secondary

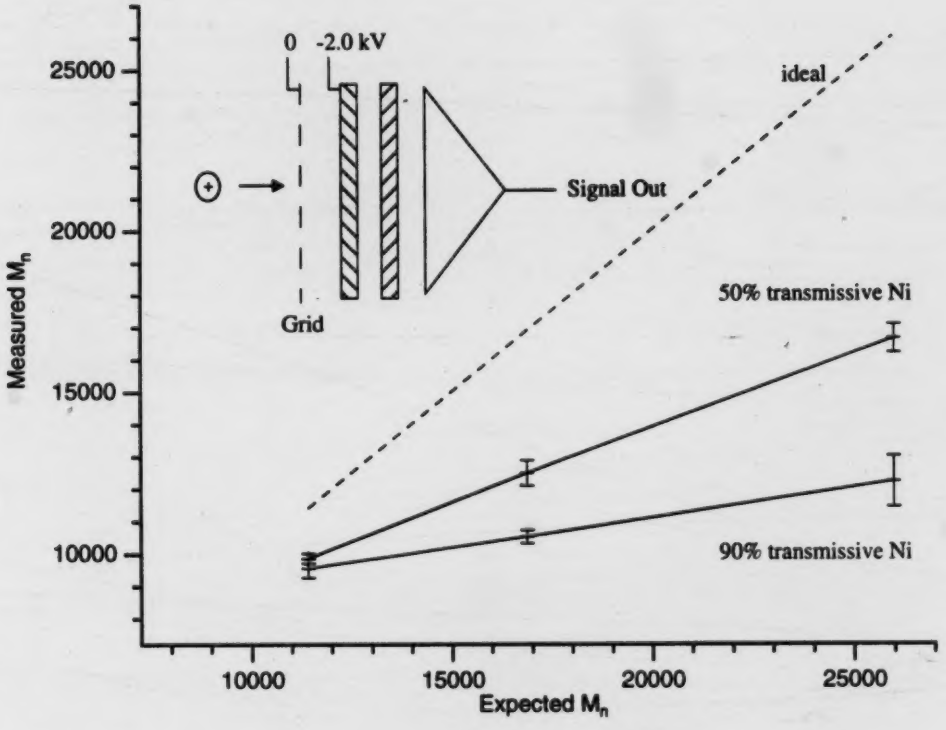

Figure 4.7 Effect of altering the optical transmissivity of the grounded grid (fronting the first MCP at a distance of 1.85 mm) on the measured M_n value. Post-acceleration of -2 kV was used in all cases. Three equimolar blends were prepared: polystyrene 5050/20 000, 5050/28 500 and 5050/50 000. In each case, 100 pmol of each component was loaded to the probe.

ions in primary ion detection.[22,42] These probably arose from the sputtering of nickel ions from the grid,[47] however the contribution of fragment ions (produced from the primary ion during the collision event) cannot be ruled out. Once formed, a certain fraction of these ions entered the post-acceleration region and accelerated to the conversion surface of the detector, contributing to the ion current for the corresponding primary ions. The data presented in Figure 4.7 also shows that the 50% transmissive grid produced a greater slope than the 90% transmissive grid. This indicates that the high mass components of the blends were more efficient in the ion-secondary ion conversion event than the low mass components.

For polymer analysis by MALDI, this implies that detectors with post-acceleration regions can impart mass discrimination by virtue of the ground grid alone: primary ion transmission would decrease with mass, while the contribution of secondary ion generation to the measured signal would increase with mass. A polymer spanning a mass range greater than that described by the 5050/20 000 polystyrene blend would appear to be sensitive to the above described phenomenon. Further complications arise when considering the potential dropped across the post-acceleration region. Figure 4.8 represents measurements of M_n values for three two-component blends similar to the ones described in Figure 4.7, using a 90% optically transmissive Ni grid. Adjusting the applied voltage from -2 kV to -4.75 kV in the post-acceleration region led to an increase in the M_n of all three blends. In this experiment, three variables changed: the impact velocity of the primary ions on the ion-to-electron conversion surface of the MCP, the velocity of the secondary ions generated at the grid after acceleration to the detector surface, and the field strength in the post-acceleration region.

A number of experiments were undertaken to determine the relative contribution of these variables to the measured M_n value. A single two-component blend was prepared, consisting of polystyrene 5050/28 500 (expected M_n of 16 620). The M_n value of this blend was measured under four different detector configurations:

1) no post-acceleration region, by removing the grid and operating the detector with a grounded first MCP and a positively biased anode (Appendix B, section 4.5).
2) a post-acceleration region defined by -4.75 kV applied across 1.85 mm.
3) a post-acceleration region defined by -2 kV applied across 1.85 mm.

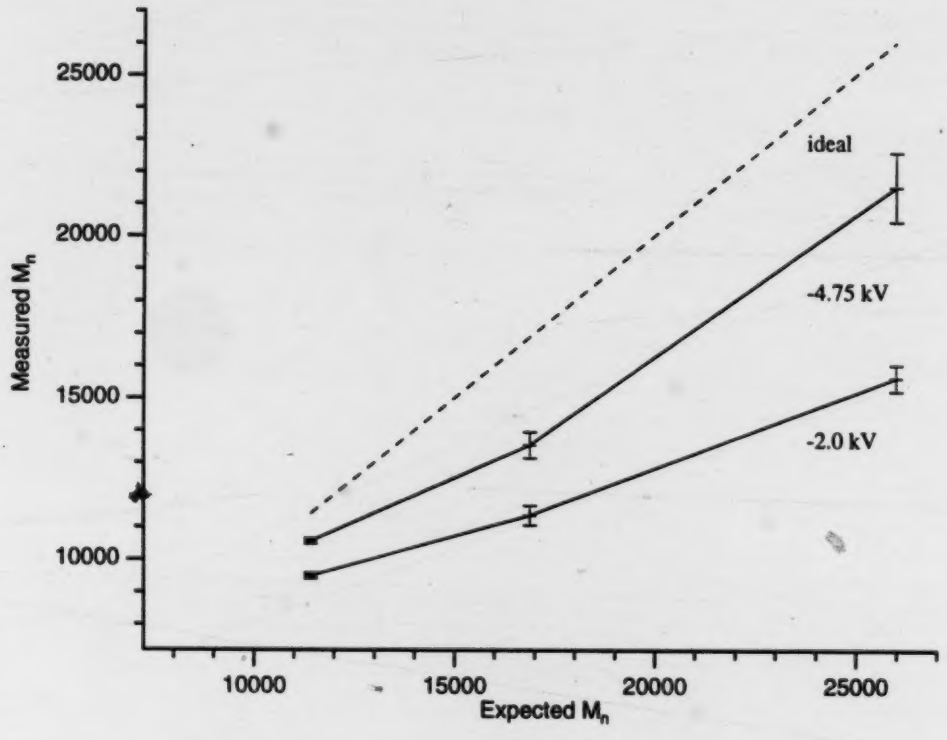

Figure 4.8 Effect of changing the applied post-acceleration voltage from -2.0 kV to -4.75 kV across a fixed distance of 1:85 mm. Sample compositions and loadings as in Figure 4.7.

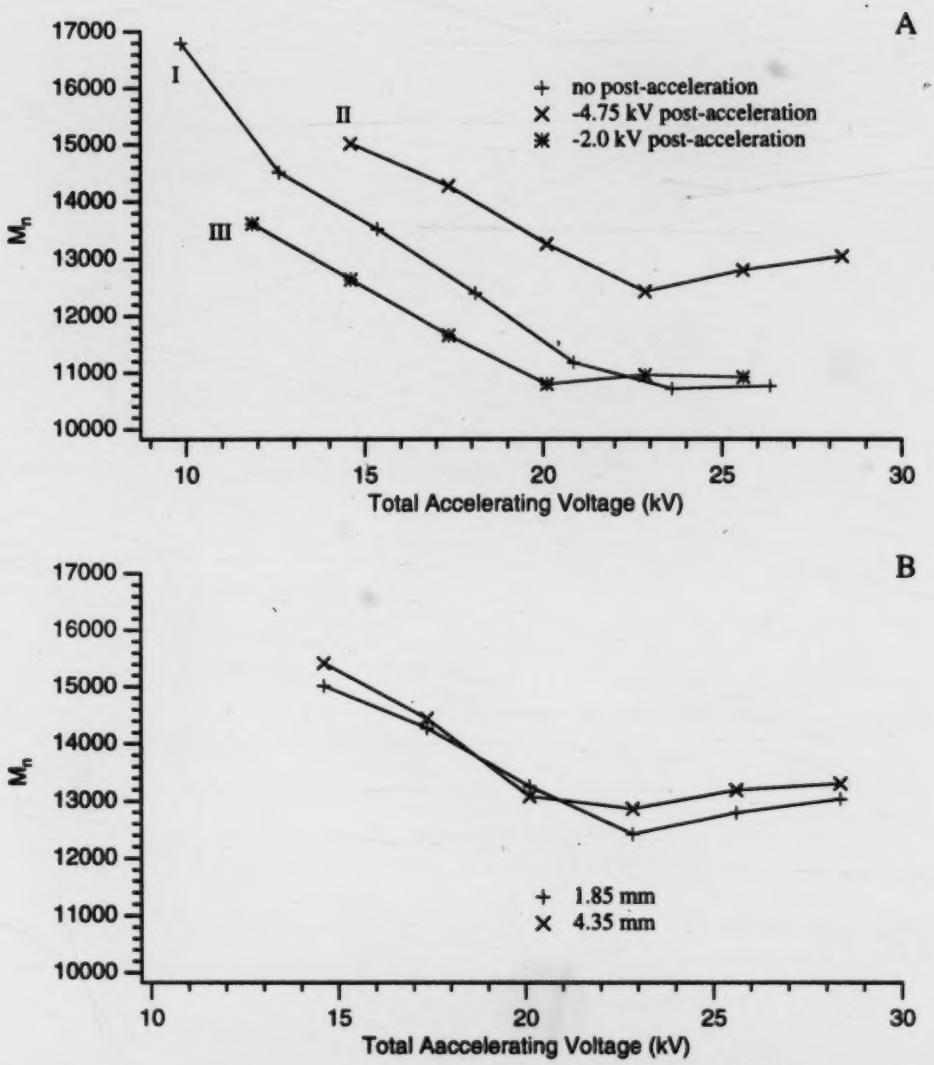

Figure 4.9 Determination of the effect of altering detector configuration on the measured M_n value over a range of total acceleration potentials, for a two-component blend consisting of polystyrene 5050 and 28 500 (100 pmol of each loaded to the probe, expected M_n of 16 620): (A) Investigating the effect of changing the post-acceleration potential from zero (and no grounded grid) to -2.0 kV and -4.75 kV; (B) maintaining the applied potential in the post-acceleration region at -4.75 kV, but altering the length of this region to change the field strength from 1090 to 2570 V/mm.

4) a post-acceleration region defined by -4.75 kV applied across 4.35 mm. The post-acceleration field strength is therefore the same as in configuration 3.

In each configuration, the voltage drops across the MCP's were kept constant such that the gain of the detector was the same for each configuration. The detector was operated at full 4 cm aperture, and a push-out pulse delay of 0.65 μs was used in all cases. The grid used to define the post-acceleration region was constructed of stainless steel, with a 90% optical transmissivity. This grid generates a response similar to the 90% optically transmissive Ni grid. For each configuration, the M_n value of the blend was measured over a range of source acceleration potentials. The results of these experiments are displayed in Figures 4.9A and 4.9B.

In detector configuration 1, the post-acceleration region was removed and the blend measured over a range of acceleration potentials (Figure 4.9A, trace I). This changed the initial velocity of the primary ions, and possibly the ion focussing of the source. Regarding the latter point, the lensing behaviour of the source was maintained at all acceleration potentials by maintaining the voltage ratios on all the source electrodes.[40] However, the radial spread of the ion packet might have increased at the detector with a decrease in acceleration potential. This could intensify the mass discrimination at the detector. Nevertheless, Figure 4.6B indicates no noticeable mass discrimination beyond a detector aperture of 2 cm. At the extremes of source acceleration potential (8.35 to 23.6 kV) a 4 cm detector aperture was sufficient for accommodating any increased radial dispersion that may have arisen from the radial component of the initial velocity. The push-out pulse delay was varied for select acceleration voltages for confirmation, and no statistically significant changes in the measured M_n value of the blend were found. Therefore, maintaining the focussing characteristics of the source and using a wide aperture detector implies that ion transmission to the detector was constant over the acceleration potentials investigated.

Figure 4.9A, trace I, reveals that the measured M_n value decreased smoothly with increasing acceleration potential. Trace I is an indicator of a greater *percent increase* in signal strength for the low mass component than the high mass component, with increasing acceleration potential. In a rigorous treatment of secondary electron generation in an MCP detector, Geno and Macfarlane have indicated the quasi-exponential nature of detection probability as a function of energy, for species with similar chemical compositions.[48] A model was proposed and validated that expressed

detection probability, P, as a function of the secondary electron coefficient, γ, in the following manner:

$$P = 1 - e^{-\gamma} \tag{1}$$

where

$$\gamma = Am\exp\left(B\sqrt{U/m}\right), \tag{2}$$

with m indicating the ion mass and U the ion energy. A and B are constants. The secondary electron coefficient, γ, is indicative of the ion-to-electron conversion efficiency at the MCP surface. Figure 4.10 expresses the approximate form of the detection probability equation, as a function of ion energy, for the low and high mass components of the blend. It should be stressed that it is the relation of these detection probability curves for the individual masses that determines the effect of acceleration potential on measured M_n values. For a given ion energy in the range investigated, the low mass component was in a steeply increasing domain of its detection probability curve, whereas the high mass component was in a very shallow domain. The mass difference was sufficiently great such that an increment in acceleration potential led to a greater percent increase in the secondary electron generation for the low mass component, relative to the high mass component. This resulted in a decrease in M_n. At the highest acceleration potentials investigated, trace I in Figure 4.9A begins to flatten. This would indicate that the high mass component was approaching the steeply rising portion of its detection probability curve. Clearly, in the analysis of polydisperse polymers including a low mass component, no single practical acceleration voltage exists such that uniform detection efficiency for the whole mass range could be expected in an MCP system.

When a post-acceleration region was added to the detection system (configurations 2 and 3), the behaviour of the M_n value as a function of acceleration potential changed. This is shown in Figure 4.9A (traces II and III). These traces display a decidedly bilinear nature. The measured M_n value decreased with increasing acceleration potential, but began to level out at a lower potential than was observed for trace I. Each of these bi-linear traces includes the contribution of post-acceleration to the total acceleration potential. The post-acceleration voltages generating traces II and III were -4.75 kV and -2.0 kV, respectively. When this contribution is subtracted from the total accelerating voltage, it can be seen that the onset of bilinearity occurred at a

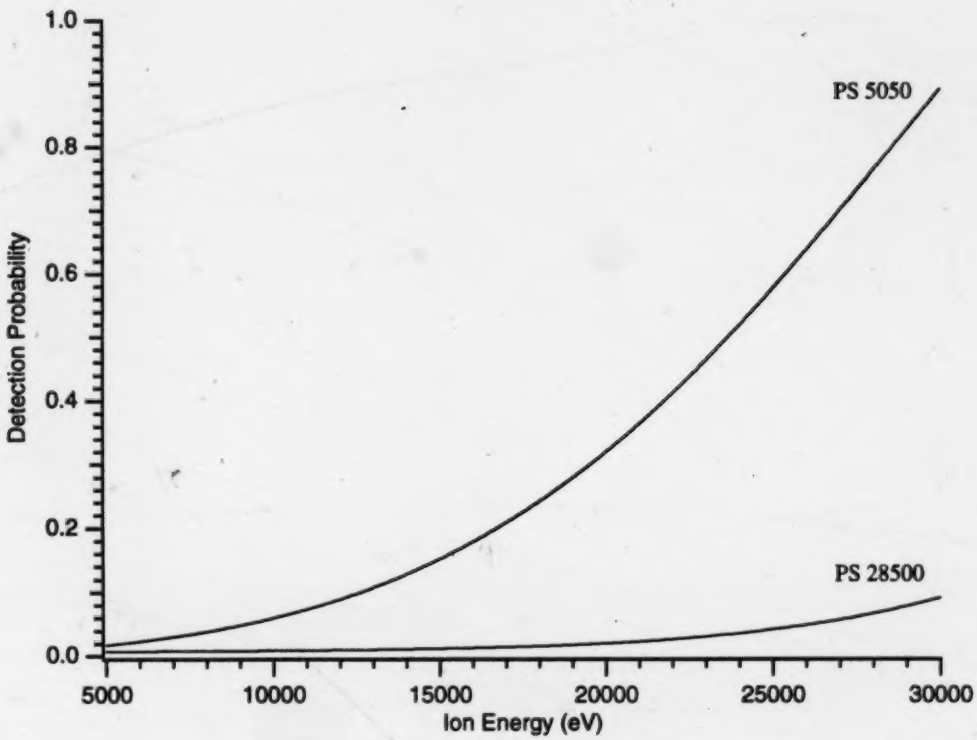

Figure 4.10 Approximate form of the detection probability equation as a function of ion energy, for both the high and low mass components of a 5050/28 500 blend. Only ion-to-electron conversion from the primary ions is considered.

common *source* acceleration potential (~18 kV). This suggests an additional mechanism for signal generation was operative, and is consistent with the onset of appreciable secondary ion formation at the grid. As was stated previously, secondary ion formation will occur to a greater extent for the higher masses. With an increase in source acceleration potential, the percent increase in secondary ion formation for the high mass component was greater than for the low mass component. Clearly, since the negative slopes of the traces change to slightly positive, the increase in secondary ion formation and detection was sufficiently great to overcome the downward trend in M_n observed in trace I, where this secondary ion formation was absent.

Note that the field strength in the post-acceleration region was different for detector configurations 2 and 3. To determine the effect of field strength variation on the detection of secondary ions, a fixed potential was applied to the first MCP (-4.75 kV), and the length of the post-acceleration region adjusted from 1.85 to 4.35 mm (configurations 2 and 4). This corresponded to field strengths of 2570 and 1090 V/mm, respectively. As grids do not provide perfect field boundaries, a certain amount of field penetration from the post-acceleration region into the field-free region was expected to occur.[40] This field penetration could have influenced the amount of secondary ions drawn into the post-acceleration region. Such a phenomenon would be a function of post-acceleration field strength. However, there appeared to be no significant difference between the two field strengths, as evidenced by the similarity of the two traces in Figure 4.9B.

Since field strength does not seem to play a significant role in mass discrimination, a direct comparison of traces II and III in Figure 4.9A provides additional insight into the phenomenon of secondary ion generation. These two traces exhibit similar features, although trace II demonstrates consistently higher M_n values. At a given total acceleration potential, corresponding points in traces II and III reflect the same contribution to secondary electron formation from the impact of primary ions on the MCP surface. However, trace III represents a *source* potential that was 2.75 kV higher than trace II. Therefore, the impact velocity of *primary* ions on the grid surface and the impact velocity of *secondary* ions on the MCP surface were both different for corresponding points in the traces. Regarding the former, this might suggest that more secondary ions were being formed under the experimental conditions of trace III (higher impact velocity on the grid). A consideration of the slopes of all three traces in Figure 4.9A would suggest otherwise. Below ~20 kV, traces II and III demonstrate equivalent slopes, implying no appreciable change in secondary ion formation occurs in this region. The

fact that trace I (no grid) exhibits much the same slope in this region provides confirmation of this point, and indicates that primary ion-to-electron conversion at the MCP surface dominated the rate of change. Regarding the latter variable of secondary ion velocity, a fixed amount of secondary ions formed at the grid would be detected more efficiently in the higher post-acceleration cases. This is supported by equation (2), where the energy term (U) for the secondary ions increases with post-acceleration potential, leading to an increase in detection probability.[48] Therefore, since it was established that the higher mass ions generated more secondary ions, the enhanced detection of secondary ions with a higher post-acceleration voltage would result in higher M_n values, even though the total acceleration potential was the same.

The conclusion to be reached from the above investigations of primary ion conversion is that each process (ion-to-electron conversion, and ion-to-secondary ion conversion) could be rationalized by the model of Geno and Macfarlane. A different set of constants for equations (1) and (2) would apply for the grid surface as opposed to the MCP surface, since they were constructed of different materials.[48] It is the combination of the detection probability curves for the two processes that gave rise to the bilinear features of traces II and III (Figure 4.9A). The departure of traces II and III from the trend reflected by trace I simply indicates that the "threshold" for efficient secondary ion generation at the grid is reached before the "threshold" for efficiency of primary ion conversion at the detector surface (for high mass ions).

One further observation can be made from Figure 4.9A regarding ion transmission efficiency through the grid. At all points below ~20 kV, the M_n values of trace I are greater than the M_n values of trace III. The enhancement in M_n from secondary ion formation at the grid was not great enough to overcome the lowering of M_n from a decreased transmission of the high mass primary ions. This is true up to ~20 kV, whereupon the increase in secondary ion formation at the grid overcame the transmission losses. Whenever grids are inserted in the path of the ions, one can expect a mass dependent loss of ion intensity. This would occur with grids placed in the source region as well.

To remove these detection constraints from the analysis of polydisperse polymers, it would seem a different detection mechanism is required. An ideal detector for this application would be one based on charge detection, rather than primary or secondary ion impact. Fundamentally, such detectors would be insensitive to the velocity of the primary ion. A number of designs based on charge detection have been introduced.[49-51]

These detectors have not been sufficiently developed for time-of-flight, mainly because detector response times do not allow for high resolution analysis.

4.3.2.3 Detector Saturation

In an MCP detector, ions are converted to electrons at the surface of the first MCP, and these electrons are amplified by passage through the channels of the first and second MCPs. This amplification, or gain, is a function of the voltage drops across the MCPs. Detectors based on MCP technology are prone to loss of gain at high signal strengths. This is called saturation. When saturated, the individual channels of an MCP require a finite time for "recovery" before the benefits of their maximum gain can be reestablished.[52] A MALDI experiment is particularly sensitive to the effects of saturation, as a typical experiment generates a large number of matrix ions for the first species detected.

A three-component blend of polystyrene (5050, 11 600 and 35 000) was analyzed to determine the possible effects of detector saturation on the determination of M_n for polydisperse polymers. Figure 4.11 shows a spectrum of the blend. This spectrum was collected under normal conditions, where the matrix ions were deflected up to ~1000 u. A number of analyses were performed on this blend, with the goal of determining the effect of the matrix and the MCP voltages on the measured M_n value. The results of this study are summarized in Table 4.1. In the first experiment (1A), all ions were allowed to reach the detector. In the second part of this experiment (1B), a deflection pulse was applied immediately post-source for the removal of matrix ions. This configuration gave rise to the spectrum of Figure 4.11. Two M_n values were calculated in each experiment: one for the first and second polymer distributions, and the other for the second and third polymer distributions. The data obtained from each spectrum indicates that deflecting the matrix leads to lower M_n values than when the matrix is retained. With retention of the matrix, the detector was at least partially saturated and began a slow recovery after all the transmitted matrix species reached the detector. This recovery was obviously occurring during the time-frame of the experiment (~100 μs), as the lower masses were suppressed more than the higher masses. Appreciable matrix signal was still detected even when the matrix ions were deflected, suggesting that the full influence of detector saturation by matrix ions might not have been removed with deflection.

In the first experiment, the detector was operated in the standard configuration, where the voltage drop across the first MCP was 0.7 kV and the voltage drop across the second MCP was 1 kV. With the voltage drop across the second MCP fixed at

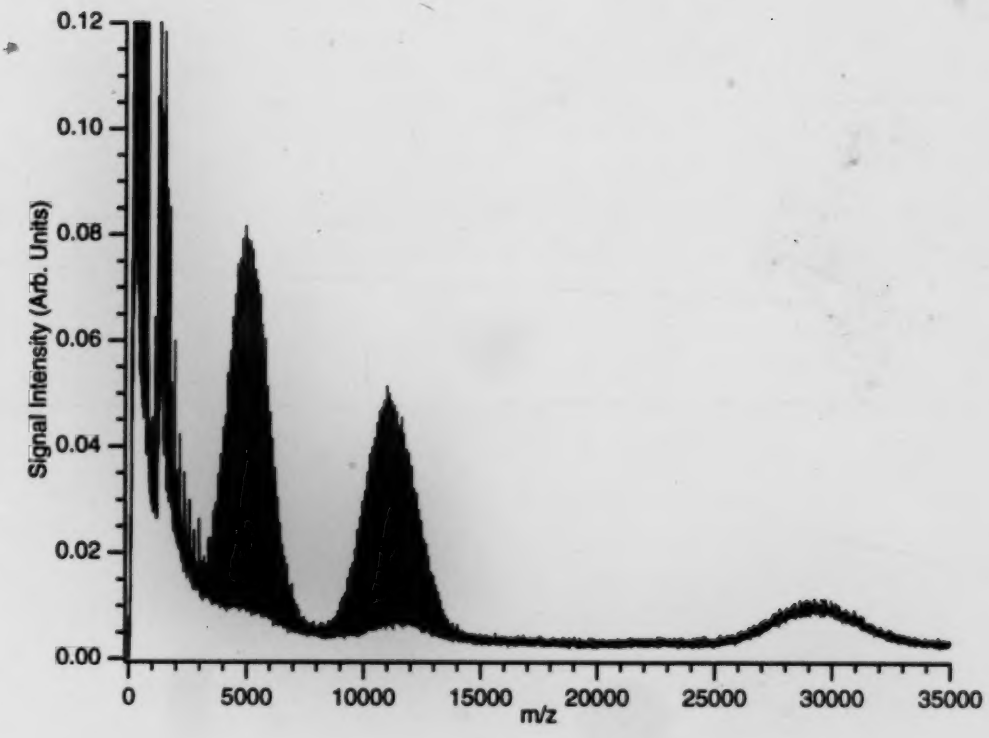

Figure 4.11 Spectrum of a three-component blend used to investigate the effects of detector saturation on the measured M_n values. Sample consisted of polystyrene 5050, 11 600, and 35 000 (100 pmol of each loaded to probe). The experimental configuration in Table 1 (1B) was used (see discussion in the text).

approximately 1 kV, a second experiment was performed in which the voltage drop across the first MCP was changed to 1 kV (experiment 2A) and 0.33 kV (experiment 2B). Matrix ions were deflected in both cases. Two M_n values were measured, as in experiment 1. Matched voltage drops across the MCP's implied operation under saturating conditions, as the M_n values obtained in 2A were significantly higher than those obtained in 1B. With a 0.33 kV voltage drop across the first MCP, there was a considerable weakening of signal intensity, including that of the matrix. In this configuration, the detector was not operating under saturating conditions. In fact, the sensitivity was too poor for reliable detection of the polystyrene 35 000 component. Calculation of M_n for the first two polymer distributions resulted in a value very similar to that obtained from 1B, implying that the detector configuration of 1B was also non-saturating. Therefore, the amount of matrix that made its way to the detector in configuration 1B was not sufficient to saturate the detector.

Table 4.1 Experiments with their corresponding M_n values and standard deviations for the examination of mass discrimination in MCP saturation

	M_n/s	
Experiment	PS 5050 and 11 600	PS 11 600 and 35 000
1A (matrix retained)	8408/103	18 686/371
1B (matrix deflected)	7982/94	17 900/64
2A (1 kV/1 kV)	8381/47	18 967/280
2B (0.33 kV/1 kV)	7946/118	—

Clearly, the extent of detector saturation can affect the M_n determination for polydisperse polymers. MCP detector designs are different for different MALDI systems, therefore it is suggested that tests for saturation be performed for each unique design in order to determine the conditions under which saturation occurs. As electron multiplier-based detector designs or hybrid MCP/electron multiplier detectors are less prone to saturation, this suggests that the above considerations are not as important.

4.3.3 Data Processing and Resolution

Average molecular weights and molecular weight distribution functions generated by a MALDI analysis of polymers are often compared with the results obtained by gel permeation chromatography (GPC). In developing appropriate methods for the comparison of MALDI and GPC data, it has been found that the molecular weight distribution functions are not equivalent when displayed as a function of mass.[14,25,27] This is because intensity data in GPC reflects the weight of molecules as a function of elution time, whereas in MALDI it reflects the number of molecules as a function of time.[27] Since the collected data in GPC represents weight fraction as a function of elution time, the calibration procedure will distort the weight average molecular weight distribution. This is because in a GPC experiment, elution time is a *logarithmic* function of mass.

The approach polymer chemists have taken to preserve the measured molecular weight distribution function in the mass domain is to apply a correction to the intensity data of the calibrated chromatogram.[27,53] This takes the following form:

$$p(m) \propto D(t)/m, \tag{3}$$

where $D(t)$ is the detector response as a function of time, t, and $p(m)$ is the corrected weight molecular weight distribution as a function of mass, m. In time-of-flight, mass is proportional to t^2. Therefore, calibrating the collected data and displaying it according to a mass scale also distorts the molecular weight distribution function, as determined by MALDI. While it has been recognized that the calculation of average molecular weights should not be attempted in such a distorted mass domain, there is no indication that the calibrated mass spectra displayed in the literature are corrected for this distortion. The necessary correction factor has been determined by us and others,[27] and can be expressed as follows:

$$q(m) \propto \frac{D(t)}{dm/dt}, \tag{4}$$

where $D(t)$ is the MALDI detector response as a function of time, t, and $q(m)$ is the corrected number molecular weight distribution as a function of mass, m. The dm/dt term is simply the derivative of the calibration equation. Correction of the data in this fashion

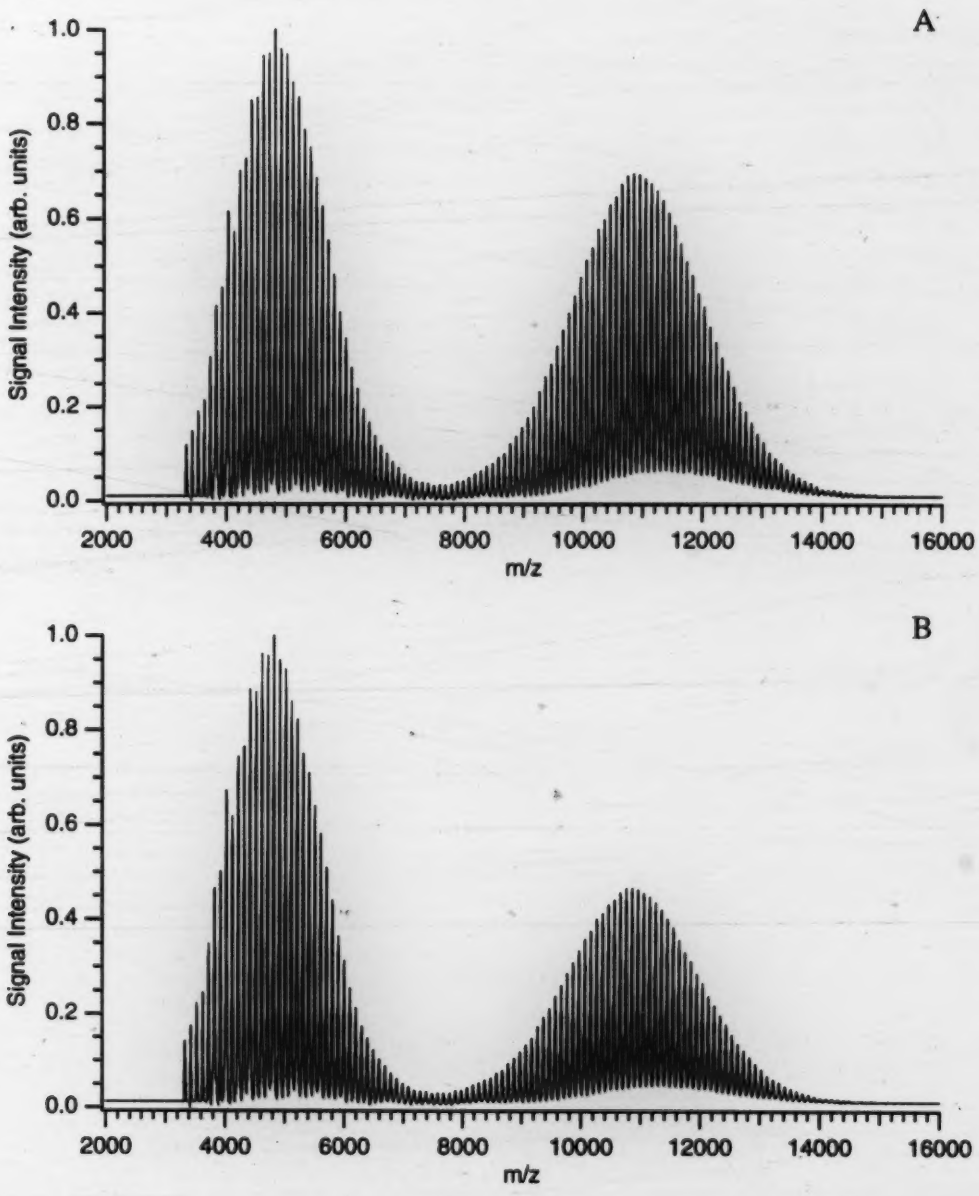

Figure 4.12 Spectrum of a two-component blend consisting of polystyrene 5050 and 11 600 (100 pmol each), (A) with no intensity correction applied and (B) with the intensity correction applied.

allows one to determine the average molecular weight values directly from the mass domain, and preserves the molecular weight distribution function as determined by MALDI. The effects of such a correction are most readily noticeable at lower masses and broad mass ranges, as shown in Figures 4.12A and 4.12B. These figures represent the molecular weight distribution of a two-component blend. Figure 4.12A displays the spectrum without the above correction, while Figure 4.12B shows the same spectrum with the correction applied. The difference between the two is marked, even over this relatively small mass range.

The preservation of the distribution as determined by MALDI does not imply that it is an accurate reflection of the true molecular weight distribution, even in the absence of the previously discussed mass discrimination. MALDI spectra of polymeric species typically display a mass-dependent resolution. Figure 4.11, for example, provides a good illustration of the effects of mass dependent resolution on the molecular weight distribution. In a figure such as this, the spectrum contains both high and low resolution components. Determining the molecular weight distribution function directly from the *intensity* data, without considering the resolution differences, will weight the low mass portion too greatly.

4.4 Summary

The analysis of polymeric species by MALDI TOF mass spectrometry imposes the requirement of uniformity of response over the mass range to be analysed. This requirement is not being met on a number of levels, as this study shows. The most serious impediments to the accuracy of a MALDI analysis relate to the sample preparation and the MALDI process itself. The effects of multimer formation and multiple charging of the principal polymer distribution on the measured M_n are complex, and can lead to either falsely low or high values. This is a serious problem, as the appearance of these features (particularly the multimers) seem to be common to all sensitive sample preparation procedures. The formation of these multimers should be suppressed, as their contribution to the spectrum cannot be removed without *a priori* knowledge of the molecular weight distribution function. While multimer formation can be reduced by decreasing the concentration of the polymer in the solid sample matrix, one runs the risk of reducing the signal strength of the principal distribution, with a possible loss in detection of the low abundance oligomers. The polymer concentration study undertaken in this work suggests an additional and possibly fundamental problem. The

M_n value measured for polydisperse polymers appears sensitive to the polymer concentration in the solid sample matrix. The sample/matrix system studied does provide stable results over a broad range of silver ion concentration and laser fluence, however if each oligomer in a distribution requires a unique amount of matrix to achieve the same desorption/ionization efficiency, then the MALDI process itself does not uniformly represent the polymer distribution. It could be argued that the system studied is not representative of all polymer analyses by MALDI. However, no other system has demonstrated as broad a mass range of analysis. Indeed, it is felt that polystyrene analysis using tRA represents a best-case scenario.

This study also shows that several instrumental variables can affect the M_n value measured for polydisperse polymers. In particular, ion focussing elements in the MALDI TOF instrument can give rise to mass discrimination, as can the detector design and operation. The contribution of these instrumental factors to the overall mass discrimination can be reduced by optimizing the source and detector configurations. However, it is clear that a detection system based on ion impact with an ion-to-electron or ion-to-ion conversion surface leads to mass discrimination. The extent of this discrimination is affected by the introduction of grids anywhere in the flight path of the primary ions.

4.5 Appendix

A) Overlap of Polymer Distributions

Consider a polymer demonstrating a Gaussian molar distribution. The equation relating the standard deviation of the distribution to the number and weight average molecular weights is:[53]

$$\sigma = \left(M_w M_n - M_n^2\right)^{0.5}, \tag{1}$$

The polydispersity, *PD*, is expressed as:

$$PD = \frac{M_w}{M_n}. \tag{2}$$

Combining the two results in the following:

$$\sigma = M_n(PD-1)^{0.5}. \tag{3}$$

An overlap condition between the principal distribution and the dimer needs to be established. Specifying the onset of overlap to occur at two standard deviations, and noting that the standard deviation of the dimer is $\sqrt{2}$ times that of the principal Gaussian distribution[54] leads to the following:

$$M_n + 2\sigma = 2M_n - 2\sqrt{2}\sigma. \tag{4}$$

Combining equations (3) and (4) specifies a unique value for the polydispersity index, namely, *PD*=1.043.

For the situation in which the doubly charged distribution can overlap with the principal distribution, an overlap condition can be specified as follows (again, where the onset of overlap occurs at two standard deviations and where the standard deviation of the doubly charged distribution is one half that of the principal distribution):

$$M_n - 2\sigma = \tfrac{1}{2}M_n + \sigma. \tag{5}$$

Combining equations (3) and (5) leads to a unique value for the polydispersity index, namely, PD=1.028.

B) Circuit for the Floated Anode Detector Configuration

To remove the post-acceleration region between the detector and the field-free drift tube required the anode of the detector to be floated to a high positive potential. For the experiment described in section 4.3.2.2, the anode was floated to 2.0 kV DC. A capacitor was used to decouple the analytical signal from this high DC voltage, since the oscilloscope could not accommodate such a high DC offset. The charging up of the anode required the isolation of the DC power supply with an RL circuit, to prevent parasitic oscillations arising from the analyte signal.[55] The circuit is shown below, with the values of the components used. Note that this circuit imposes a significant bandwidth limit on signal measurement, and could not be used for high resolution analyses.

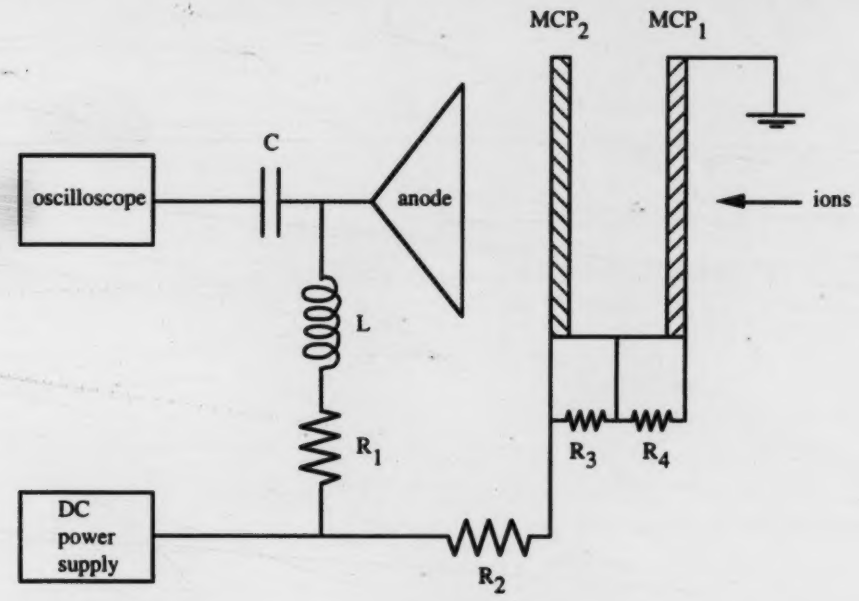

C: 4.3 nF
R_1 = 1 MΩ
R_2 = 0.6 MΩ
R_3 = 4 MΩ
R_4 = 2 MΩ

MCP_1 = 42 MΩ
MCP_2 = 10.2 MΩ
L: 2 6-hole ferrite beads and
2 4-hole ferrite beads

4.6 Literature Cited

(1) Lloyd, P. M.; Suddaby, K. G.; Varney, J. E.; Scrivener, E.; Derrick, P. J.; Haddleton, D. M. *Eur. Mass. Spectrom.* **1995**, *1*, 293.

(2) Danis, P. O.; Karr, D. E. *Macromolecules* **1995**, *28*, 8548.

(3) Danis, P. O.; Karr, D. E.; Xiong, Y.; Owens, K. G. *Rapid Commun. Mass Spectrom.* **1996**, *10*, 862.

(4) Danis, P. O.; Karr, D. E. *Org. Mass Spectrom.* **1993**, *28*, 923.

(5) Montaudo, G.; Montaudo, M. S.; Puglisi, C.; Samperi, F. *Rapid Commun. Mass Spectrom.* **1994**, *8*, 1011.

(6) Cottrell, J. S.; Koerner, M.; Gerhards, R. *Rapid Commun. Mass Spectrom.* **1995**, *9*, 1562.

(7) Montaudo, G.; Montaudo, M. S.; Puglisi, C.; Samperi, F. *Rapid Commun. Mass Spectrom.* **1995**, *9*, 453.

(8) Mowat, I. A.; Donovan, R. J. *Rapid Commun. Mass Spectrom.* **1995**, *9*, 82.

(9) Belu, A. M.; DeSimone, J. M.; Linton, R. W.; Lange, G. W.; Friedman, R. M. *J. Am. Soc. Mass Spectrom.* **1996**, *7*, 11.

(10) Danis, P. O.; Karr, D. E.; Simonsick, W. J.; Wu, D. T. *Macromolecules* **1995**, *28*, 1229.

(11) Dogruel, D.; Nelson, R. W.; Williams, P. *Rapid Commun. Mass Spectrom.* **1996**, *10*, 801.

(12) Yates, H. T.; Scrivens, J.; Jackson, T.; Deery, M. In *Proceedings of the 44th ASMS Conference on Mass Spectrometry and Allied Topics*; May 12-16, Portland, OR, 1996; p 903.

(13) Jackson, A. T.; Yates, H. T.; MacDonald, W. A.; Scrivens, J. H.; Critchley, G.; Brown, J.; Deery, M. J.; Jennings, K. R.; Brookes, C. *J. Am. Soc. Mass Spectrom.* **1997**, *8*, 132.

(14) Lehrle, R. S.; Sarson, D. S. *Rapid Commun. Mass Spectrom.* **1995**, 91.

(15) Cottrell, J. S.; Dwyer, J. L. In *Proceedings of the 44th ASMS Conference on Mass Spectrometry and Allied Topics*; May 12-16, Portland, OR, 1996; p 900.

(16) Kassis, C. M.; Belu, A. M.; DeSimone, J. M.; Linton, R. W.; Lange, G. W.; Friedman, R. M. In *Proceedings of the 44th ASMS Conference on Mass Spectrometry and Allied Topics*; Portland, OR, 1996; p 1096.

(17) Mowat, I. A.; Donovan, R. J.; Monaghan, J. J. In *Proceedings of the 44th ASMS Conference on Mass Spectrometry and Allied Topics*; May 12-16, Portland, OR, 1996; p 897.

(18) Pastor, S.; Wilkins, C. L. *Polym. Prepr.* **1996**, *37*, 284.

(19) Von Helden, G.; Wyttenbach, T.; Bowers, M. T. *Science* **1995**, *267*, 1483.

(20) Montaudo, G.; Scamporrino, E.; Vitalini, D.; Mineo, P. *Rapid Commun. Mass Spectrom.* **1996**, *10*, 1551.

(21) Tang, X.; Dreifuss, P. A.; Vertes, A. *Rapid Commun. Mass Spectrom.* **1995**, *9*, 1141.

(22) Larsen, B. S.; Simonsick, W.J.; McEwen, C. N. *J. Am. Soc. Mass Spectrom.* **1996**, *7*, 287.

(23) Axelsson, J.; Scrivener, E.; Haddleton, D. M.; Derrick, P. J. In *Proceedings of the 44th ASMS Conference on Mass Spectrometry and Allied Topics*; May 12-16, Portland, OR, 1996; p 895.

(24) Martin, K.; Spickermann, J.; Rader, H. J.; Mullen, K. *Rapid Commun. Mass Spectrom.* **1996**, *10*, 1471.

(25) Jackson, C.; Larsen, B.; McEwen, C. *Anal. Chem.* **1996**, *68*, 1303.

(26) McEwen, C.; Jackson, C.; Larsen, B. *Polym. Prepr.* **1996**, *37*, 314.

(27) Guttman, C. M. *Polym. Prepr.* **1996**, *37*, 837.

(28) McEwen, C.; Jackson, C.; Larsen, B. In *Proceedings of the 43rd ASMS Conference on Mass Spectrometry and Allied Topics*; May 21-26, Atlanta, GA, 1995; p 23.

(29) Montaudo, G.; Montaudo, M. S.; Puglisi, C.; Samperi, F. *Rapid Commun. Mass Spectrom.* **1995**, *9*, 1158.

(30) Danis, P. O.; Saucy, D. A.; Huby, F. J. *Polym. Prepr.* **1996**, *37*, 311.

(31) Whittal, R. M.; Li, L. *Anal. Chem.* **1995**, *67*, 1950.

(32) Schriemer, D. C.; Whittal, R. M.; Li, L. In *Proceedings of the 44th ASMS Conference on Mass Spectrometry and Allied Topics*; May 12-16, Portland, OR, 1996; p 896.

(33) Dreisewerd, K.; Schurenberg, M.; Karas, M.; Hillenkamp, F. *Int. J. Mass Spectrom. Ion Processes* **1995**, *141*, 127.

(34) Hillenkamp, F.; Karas, M.; Beavis, R. C.; Chait, B. T. *Anal. Chem.* **1991**, *63*, 1193A.

(35) *Fractionation of Synthetic Polymers: Principles and Practices*; Tung, L. H., Ed.; Marcel Dekker: New York, 1977.

(36) Beavis, R. C.; Chait, B. T. *Chem. Phys. Lett.* **1991**, *181*, 479.

(37) Zhang, W.; Chait, B. T. In *Proceedings of the 44th ASMS Conference on Mass Spectrometry and Allied Topics*; May 12-16, Portland, OR, 1996; p 268.

(38) Juhasz, P.; Vestal, M. L.; Martin, S. A. In *Proceedings of the 44th ASMS Conference on Mass Spectrometry and Allied Topics*; May 12-16, Portland, OR, 1996; p 730.

(39) Russon, L. M.; Whittal, R. M.; Li, L. In *Proceedings of the 44th ASMS Conference on Mass Spectrometry and Allied Topics*; Portland, OR, May 12-16, 1996; p 731.

(40) Szilagyi, M. *Electron and Ion Optics*; Plenum Press: New York, 1988.

(41) Sullivan, P. A.; Axelsson, J.; Sundqvist, B. U. R. *Rapid Commun. Mass Spectrom.* **1995**, *9*, 377.

(42) Westmacott, G.; Ens, W.; Standing, K. G. *Nucl. Instr. and Meth. in Phys. Res. B* **1996**, *108*, 289.

(43) Weinberger, S. R.; Egan, R. W.; Hoppe, T. W.; Gassmann, E.; Schar, M. M.; Bornsen, K. O.; Tarantino, E. R. **1995**, U.S. Patent 5,382,793, 1995.

(44) Weinberger, S. R.; Donlon, E.; Kaplun, Y.; Kornfeld, R.; Li, L.; Whittal, R.; Russon, L. In *Proceedings of the 44th ASMS Conference on Mass Spectrometry and Allied Topics*; May 12-16, Portland, OR, 1996; p 269.

(45) Weinberger, S. R.; Egan, R. W.; Hoppe, T. W.; Gassmann, E.; Schar, M. M.; Bornsen, K. O.; Tarantino, E. R. **1997**, U.S. Patent 5,594,243, 1997.

(46) Laidler, K. J.; Meiser, J. H. *Physical Chemistry*; The Benjamin/Cummings Publishing Company: Don Mills, Ontario, 1982, p 919.

(47) Whittal, R. M.; Russon, L. M.; Weinberger, S. R.; Li, L. Unpublished results (1995), University of Alberta.

(48) Geno, P. W.; Macfarlane, R. D. *Int. J. Mass Spectrom. Ion Processes* **1989**, *92*, 195.

(49) Park, M. A.; Callahan, J. H. *Rapid Commun. Mass Spectrom.* **1994**, *8*, 317.

(50) Imrie, D. C.; Pentney, J. M.; Cottrell, J. S. *Rapid Commun. Mass Spectrom.* **1995**, *9*, 1293.

(51) Bahr, U.; Rohling, C.; Lautz, K.; Strupat, M.; Schurenberg, F. *Int. J. Mass Spectrom. Ion Processes* **1996**, *153*, 9.

(52) Galileo Electro-Optics Corporation, Galileo Park, Sturbridge, MA,

(53) *Determination of Molecular Weight*; Cooper, A. R., Ed.; John Wiley and Sons: New York, 1989; Vol. 103.

(54) Harnett, D. L. *Statistical Methods;* third ed.; Addison-Wesley Publishing: Reading, MA, 1982.

(55) Malmstadt, H.; Enke, C.; Crouch, S. *Electronics and Instrumentation for Scientists*; Benjamin/Cummings Publishing Co., Inc.: Menlo Park, CA, 1981.

Chapter 5

MALDI Analysis of Polymers: Structural Information[a]

5.1 Introduction

Matrix-assisted laser desorption/ionization (MALDI) has proven useful in the structural and compositional analysis of polymeric species. Recent literature has reported repeat unit identification,[1,2] confirmation of end-group chemistry,[3,4] oligomer structural analysis,[5,6] tracking of polymerization kinetics,[7] and a measure of compositional information for pretreated polymers[8-10] and more complex copolymer systems.[11] MALDI is a "soft" ionization technique, generating intact molecular ions almost exclusively. This implies that structural and compositional information can only be gleaned from an accurate mass assignment of well-resolved polymer chains in a distribution.

Until very recently, linear time-of-flight instrumentation for MALDI had a limited capability. Resolution on the order of 200 to 300, and mass measurement accuracies of 0.1% were standard.[12] With the incorporation of time-lag focussing technology,[13-16] the situation has improved. Resolution ranges from the high hundreds to the high thousands, with mass measurement accuracies of 0.01% or better. This chapter discusses the improvements in polymer structural analysis provided by MALDI in a linear time-lag focussing instrument, and addresses limitations for structural determination, in the absence of fragmentation analysis. Simple linear homopolymers are considered, while the following chapter addresses the structural analysis of more complex copolymers.

5.2 Experimental

5.2.1 Instrumentation

Mass spectral data were collected on a linear time-lag focussing MALDI time-of-flight mass spectrometer,[16] modified for operation up to 30 kV. The first extraction plate

---

[a] This chapter represents a summary of two publications. (A) Whittal, R.M.; Schriemer, D.C.; Li, L. "Time-Lag Focusing MALDI Time-of-Flight Mass Spectrometry for Polymer Characterization: Oligomer Resolution, Mass Accuracy, and Average Weight Information" *Anal. Chem.*, **1997**, 69, 2734-2741. (B) (B) Yalcin, T.; Schriemer, D.C.; Li, L. "MALDI Time-of-Flight Mass Spectrometry for the Analysis of Polydienes" *J. Am. Soc. Mass Spectrom.*, **1997**, in press. R.M. Whittal collected the PEG spectra. T. Yalcin collected the spectra for Figures 5.5, 5.6 and 5.7.

was redesigned and a grid was placed on the repeller side. A single DC power supply was used to set the potential on the repeller and first extraction plate and the potential on the second extraction plate through a voltage divider. Under normal operation, the power supply was set to 20 kV DC. In conjunction, a high voltage pulser built in-house and a Hewlett-Packard pulser (Palo Alto, CA) were used to generate the delayed extraction pulse. The extraction pulse and time delay were varied as required to focus the mass range of interest. A nitrogen laser (VSL-337ND, Laser Science, Inc.; Newton, MA) with a 3-ns pulse width was used for desorption at 67.5° to the probe surface normal. A neutral-density filter was used to attenuate the laser energy that reached the sample surface. A mass filter was added to the system. The mass filter prevented saturation of the microchannel plate detector by deflecting matrix ions out of the usual ion trajectory, reducing the ion current from low mass ions.

5.2.2 Data Collection and Mass Calibration

The mass spectra were recorded using a LeCroy 9350M digital oscilloscope at a sampling rate of 500 MHz to 1 GHz in conjunction with Hewlett-Packard MALDI software. In general, mass spectra from 50 to 100 laser shots were summed to produce a final spectrum in this study. Generally, peak centroids were determined with the software, and mass calibration of the instrument was achieved using a two-point linear calibration. Mass calibrations were performed externally, using either peptides or well-characterized polymers. Calibrated spectra were transferred to a PowerMac and processed using Igor Pro data analysis software (WaveMetrics, Inc.; Lake Oswego, OR.). All spectra demonstrating unit mass resolution were interpolated using four-times zero-filling and calibrated in Igor Pro. This was required because the Hewlett-Packard software could not determine accurate centroids of highly resolved peaks. Number average molecular weights (M_n) were calculated in the time domain. The M_n values quoted in this chapter have been corrected for the contribution of the cation. The spectra presented in this chapter were not corrected for the intensity distortions arising from mass calibration.

5.2.3 Sample Preparation

Polymer samples for MALDI analysis were prepared by premixing the analyte, matrix and cationizing agent. All polymer samples were prepared in glass vials. Polystyrene 32 660 and 45 000, as well as all polybutadiene and polyisoprene samples

were dissolved in distilled tetrahydrofuran (THF) to a concentration of 1 mM. The matrix *all-trans*-retinoic acid (tRA) was prepared to 0.15 M in distilled THF. An aliquot of the appropriate polymer solution was added to the matrix solution to give a final polymer concentration of ~200 μM. An aliquot of a saturated ethanolic solution of $AgNO_3$ was added to the polystyrene/tRA solution (at 1% v/v). An aliquot of a copper salt solution (aqueous, 0.1 M) was added to the polybutadiene/tRA and polyisoprene/tRA solutions (at 1% v/v). In all cases, a 1 μl aliquot of the polymer/matrix/cation blend was added to the MALDI sample probe and allowed to dry.

PEG 15 000 was dissolved in 1:1 methanol/water to a concentration of 1 mM. The PEG bis(acetaminophen) and PEG bis(ephedrine) were dissolved in methanol to a concentration of 1 mM. The matrices 2-(4-hydroxyphenylazo)benzoic acid (HABA), 2,5-dihydroxybenzoic acid (DHB) and *trans*-3-indoleacrylic acid (IAA) were used in the analysis of these polymers. HABA was dissolved in 1,4-dioxane to a concentration of 50 mM. DHB was prepared as a 100 mM solution in 1:1 methanol/water, and IAA was prepared as a 200 mM solution in methanol. The polymer and matrix solutions were mixed to give a final polymer concentration of 100 μM. To 100 μL of matrix/polymer solution, 1 μL of 20 mM NaCl (aq) was added. A 1 μL aliquot of the mixture was added to the MALDI sample probe and allowed to dry.

Instrument calibration was achieved with peptides and PEG. Peptide samples were prepared in 0.5 mL Eppendorf microcentrifuge tubes. An aliquot of the sinapinic acid (SA) matrix solution (in acetone, 20 mg/ml) was first applied to the probe and allowed to air-dry, followed by an aliquot of peptide solution premixed 1:1 (v/v) with a saturated sinapinic acid solution (33% acetonitrile/water (v/v)) that was allowed to air-dry as well. Polymer spectra exhibiting masses greater than 4000 u were calibrated using combinations of bovine insulin B chain (oxidized form), bovine ubiquitin, equine cytochrome *c*, bovine carbonic anhydrase II, and bovine serum albumin. The peptide average mass was used in all calibrations. The spectra arising from PEG bis(acetaminophen), PEG bis(ephedrine) and all polybutadiene and polyisoprene samples under 4000 u were calibrated using well characterized PEG samples of the appropriate mass, using the HABA sample preparation method already described, or the tRA method with sodium cationization.

5.2.4 Materials

PEG 15 000 was purchased from Polysciences, Inc. (Warrington, PA). The bovine insulin B chain (oxidized form), bovine ubiquitin, equine cytochrome *c*, bovine

trypsinogen, bovine carbonic anhydrase II, bovine serum albumin, PEG bis(acetaminophen), PEG bis(ephedrine), and PEG 3350, were purchased from Sigma Chemical Company (St. Louis, MO). Polystyrene 32 660 and 45 000 were purchased from Aldrich (Milwaukee, WI). Polyisoprene 3280 and 19 300, as well as polybutadiene 2800 and 22 430 were purchased from Polysciences, Inc. (Warrington, PA). All polymers were analysed without further purification. The matrices HABA, DHB, tRA, IAA, DPB, SA and dithranol were purchased from Aldrich (Milwaukee, WI) and used without purification. The cationizing reagents $AgNO_3$ (Terochem Laboratories Ltd., Edmonton, Canada) and NaCl (BDH Laboratories, Toronto, Canada) were reagent grade. Analytical grade tetrahydrofuran was purchased from VWR Scientific (Toronto, Canada), treated with potassium hydroxide, and then distilled under nitrogen in the presence of sodium metal and benzophenone. HPLC grade methanol was purchased from EM Science (Gibbstown, NJ). Analytical grade 1,4-dioxane was purchased from BDH Laboratories (Toronto, Canada). Water used throughout was from a Milli-Q Plus Ultrapure water system (18.2 MΩ•cm, Millipore, Bedford, MA).

5.3 Results and Discussion

There are certain minimum requirements that must be met before a structural analysis of homopolymers can be attempted. As suggested above, these include sufficient mass resolution and mass accuracy, but also an understanding of cation adduction behaviour arising from the MALDI sample preparation. Each of these points will be addressed in turn.

5.3.1 Mass Resolution

On a very basic level, structural analysis requires the resolution of individual polymer chains (oligomers). In homopolymer analysis by MALDI, the actual value of the upper mass limit where oligomers are resolved is dependent on several factors, including ion extraction conditions, the mass of the repeat unit, the matrix/sample preparation method, and the number of polymeric components present in the sample. Figure 5.1 shows four spectra of PEG 15 000 using a number of matrices, and collected under different experimental conditions for comparison. Figure 5.1 displays two regions; the top of the figure shows the full region between m/z 0 - 20 000, and the bottom the expansion of the m/z 10 000 - 15 000 region. Figure 5.1A was obtained using HABA as matrix and

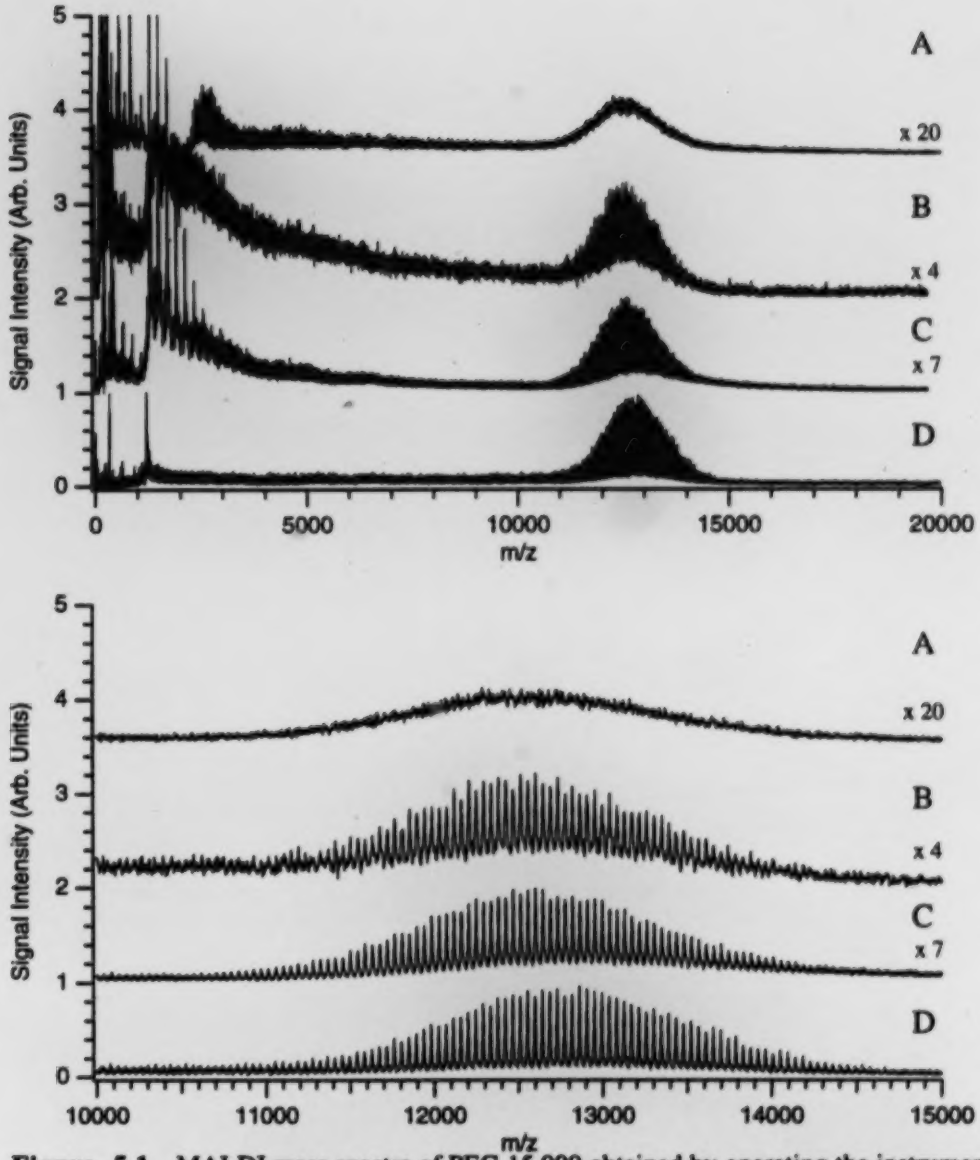

Figure 5.1 MALDI mass spectra of PEG 15 000 obtained by operating the instrument in (A) the continuous extraction mode with HABA as the matrix and sodium cationization; (B), (C), and (D) the time-lag focussing extraction mode with (B) DHB, (C) IAA, and (D) HABA as the matrices and sodium cationization. For (D), M_n = 9380 and PD = 1.20. The supplier certifies M_n = 12 500 and PD = 1.20 by gel permeation chromatography. The lower panel represents an expansion of the upper panel.

continuous extraction; individual oligomers were not resolved above 9000 u. In contrast, the oligomers are well resolved in Figures 5.1B, 5.1C, and 5.1D that were collected using time-lag focussing with DHB, IAA, and HABA as matrices, respectively. Figure 5.1 also shows that the type of matrix used can significantly affect mass resolution in time-lag focussing MALDI. At 12 700 u the resolution is 700, 1060, and 1400 fwhm for Figures 5.1B, 5.1C, and 5.1D, respectively. Lower mass oligomers in the long tail were not resolved with DHB, but were resolved using IAA and HABA. In addition, the overall signal strength was lower for DHB than for HABA or IAA. HABA provided a flat baseline extending to the low mass region while the baselines elevated in the low mass region with DHB and IAA. Intense matrix clusters were produced with IAA, obscuring polymer peaks in the mass range under 3000. The extent of clustering observed with IAA could be reduced with a reduction in laser flux, but resulted in complete loss of polymer signal.

The reason different resolutions for polymer spectra were obtained with different matrices is not immediately obvious. All the matrix preparations gave densely packed micro-crystals on the probe surface. Well-packed microcrystals give improved mass accuracy, resolution, and shot-to-shot reproducibility over preparations that produce large crystals.[17-19] DHB required twice the laser flux used for HABA and IAA, and since the shot-to-shot reproducibility was significantly poorer, lower sensitivity and resolution can be expected. However, the sensitivity and shot-to-shot reproducibility of HABA and IAA are similar. It is speculated that the high abundance of matrix clusters observed with IAA indicates a higher charge density in the desorption plume, leading to increased coulombic repulsion and an unanticipated spatial distribution that could not be compensated for with time-lag focussing. That is, there is no longer a correlation between an ion's position and its initial velocity at the time the extraction pulse is applied and slight peak broadening results.

Polystyrene of narrow polydispersity was examined to illustrate the resolving power of time-lag focussing MALDI for higher molecular weight polymers. Figures 5.2A and 5.2B display mass spectra for polystyrene 32 660 and 45 000. In each case, the pulse voltage was set to optimize the resolution at the centre of the distribution. For both polymers, oligomer peaks were well resolved. The mass resolution observed for polystyrene 32 660 was 870-1065 fwhm, and for poly(styrene) 45000 was 550-670 fwhm. Figure 5.2C is an expansion of Figure 5.2B at the high mass end of the distribution, illustrating that oligomer peaks were resolved at masses beyond 50 000 u. In MALDI time-of-flight (linear or reflectron), there are no other reports of oligomer

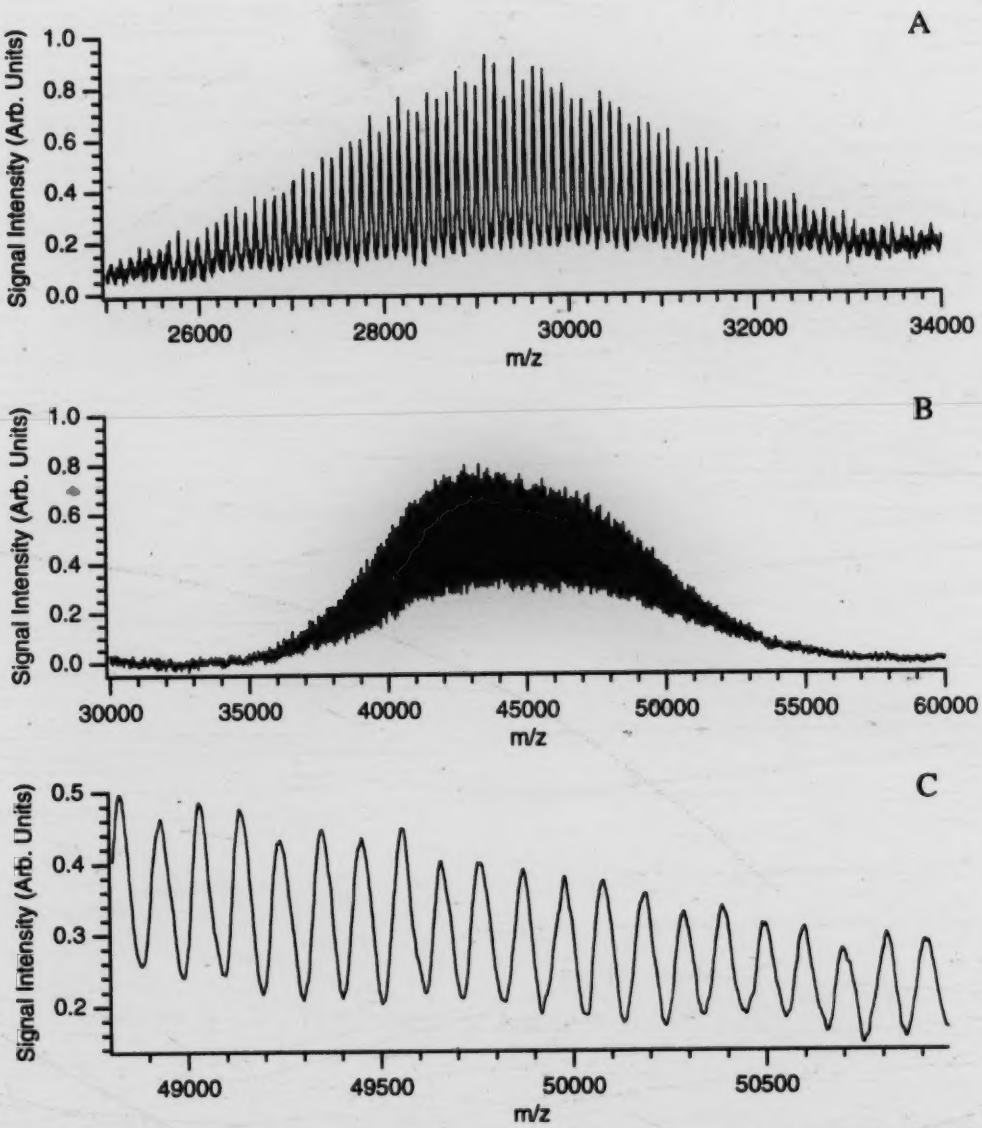

Figure 5.2 MALDI mass spectra of (A) poly(styrene) 32 660 (B) poly(styrene) 45 000, and (C) the expanded spectrum of poly(styrene) 45 000 using retinoic acid as the matrix with silver cationization. For (A) M_n = 29 350 and PD = 1.004. The supplier certifies M_n = 30 000 and PD = 1.025. For (B), M_n = 44 930 and PD = 1.008. The supplier certifies M_n = 45 550 and PD = 1.053. The supplier used gel permeation chromatography for the analyses.

resolution at this high mass for any polymer system. The benefits of current time-lag focussing technology over conventional continuous ion extraction begin to disappear at this point. No improvements in resolution have been demonstrated beyond this mass, by ourselves or others. This is most probably because time-lag focussing does not completely compensate for the initial energy distribution. As the width of these energy distributions increase with mass, compensation becomes less effective. This is analogous to energy compensation in reflectron instruments.[20]

5.3.2 Mass Accuracy

It is important to emphasize that structural information can only be *proposed* from the mass of oligomer peaks, due to the absence of fragmentation. It rests entirely on the mass accuracy of a single oligomer peak. For the instrument used in this study, the average error in mass for externally calibrated spectra is ±70 ppm. This is applicable across a wide mass range (at least up to 45 000 u). Confidence in the assignment of the basic homopolymer type depends, therefore, on the molecular weight of the sample. For example, the repeat unit for polystyrene of mass 2000 u (having a mass of 104.15 u) can be identified with an average error of ±0.2 u. At 45 000 u, the average error is ±4.5 u. At lower mass, the repeat unit can be proposed with confidence, but at the higher masses, this confidence is eroded. These levels of accuracy are often sufficient for confirmation of the basic homopolymer type. If not, pyrolysis/MS, such as described in chapter 2, could provide supporting evidence.

Obtaining high mass accuracy is also important in proposing end-group masses for a polymer. In a MALDI mass spectrum, this is achieved by subtracting the cation mass and the highest integer multiple of the repeat unit from the mass of an oligomer peak. The remaining mass is a fraction of a repeat unit. The proposal of a certain end-group can be supported if the following applies:

$$2(\textit{end-group mass}) = \textit{remaining mass} + n(\textit{repeat unit})$$

where n is an integer. The application of this procedure can be illustrated with two examples. Figure 5.3 shows the mass spectra of PEG bis(ephedrine) (structure **I**) and PEG bis(acetaminophen) (structure **II**).

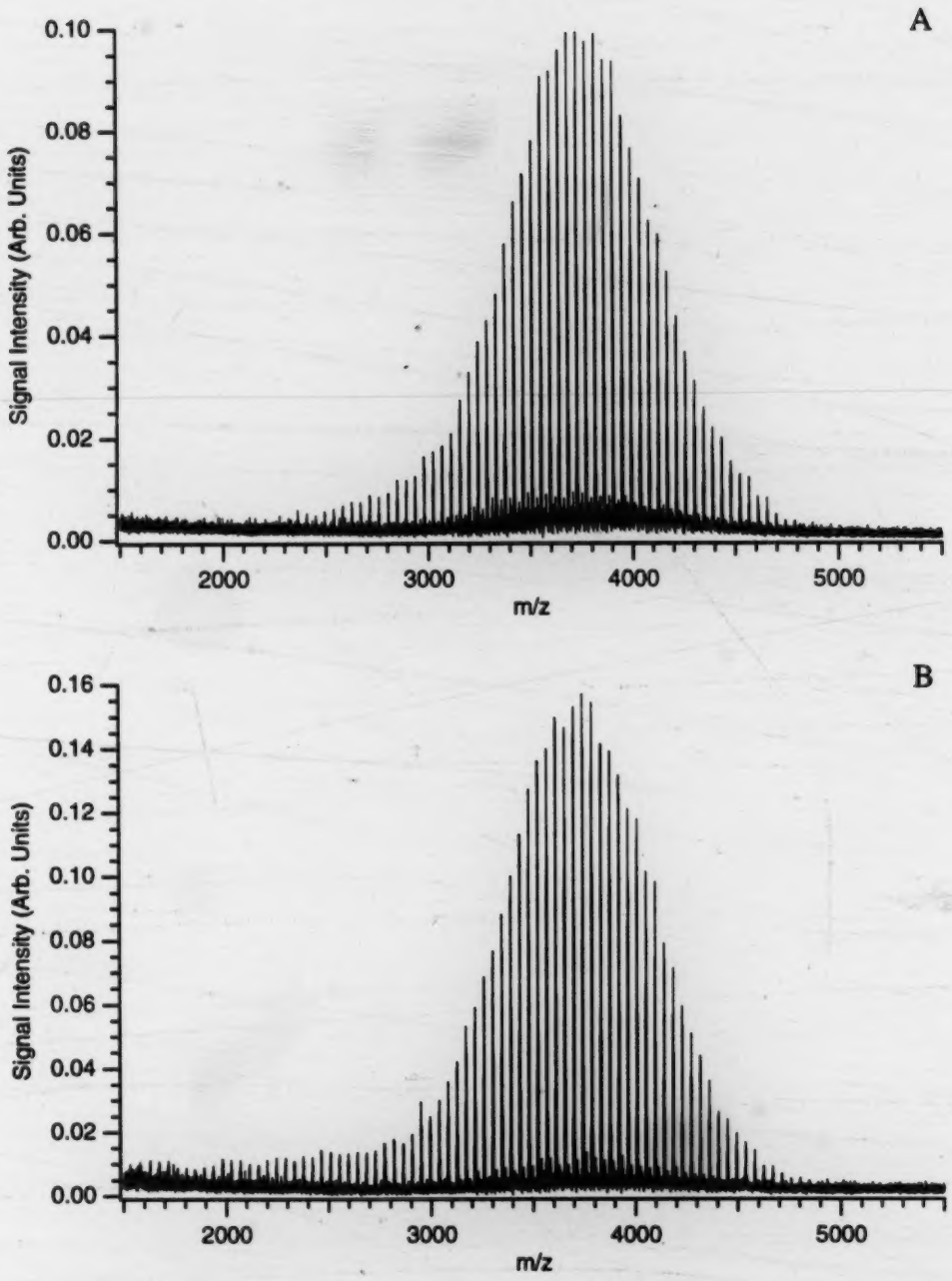

Figure 5.3 MALDI spectra of (A) PEG bis(ephedrine) and (B) PEG bis(acetaminophen) using HABA as matrix and sodium cationization. For (A), M_n = 3670 and PD = 1.007. For (B), M_n = 3520 and PD = 1.014.

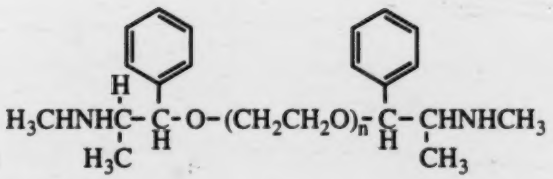

I

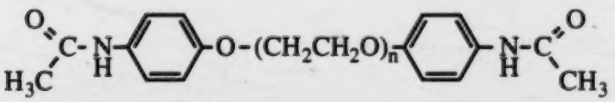

II

The desired product has ephedrine or acetaminophen linked to the polymer at both ends. Dosage determination is partly dependent upon the success of derivatization of the polymer, and on the M_n value. As shown in Table 5.1, the mass difference between a singly-labelled polymer with n repeat units and a doubly-labelled polymer with n-3 repeat units is +15.06 u.

Table 5.1 Mass Measurement Accuracy of Selected Oligomer Peaks of PEG bis(ephedrine) in Figure 5A[a]

Mass $(M + Na)^+$ (u)					
Calculated Mass					Mass Error (ppm)
n[b]	1 label[c]	n	2 labels	Observed Mass	2 labels
63	2963.59	60	2978.66	2978.66	0
73	3404.13	70	3419.19	3419.03	-47
83	3844.66	80	3859.72	3859.70	-5
93	4285.20	90	4300.26	4299.99	-63

a Externally calibrated with PEG 3350

b n is the number of repeat units in the polymer

c Label refers to the ephedrine moiety as the end group of the polymer

The data shown in Table 5.1 support the supposition that the sample has ephedrine linked to both ends of the polymer. In a similar fashion it could be shown that unlabelled polymer with *n+3* repeat units would generate a mass difference with a singly-labelled product of -15.06 u. Neither the unlabelled or singly labelled distributions are evident in the spectrum of Figure 5.3A.

However, when PEG bis(acetaminophen) was analysed, the demand on the mass accuracy of the instrument increased. Table 5.2 shows that the mass difference between the singly-labelled PEG with *n* repeat units and the doubly labelled PEG with *n-3* repeat units is only -0.99 u. In the mass range of interest, continuous extraction MALDI could not provide sufficient mass accuracy to distinguish between the two possibilities. With time-lag focussing MALDI, there is strong support for suggesting that PEG bis(acetaminophen) is the main product. For example, the peak with an observed m/z of 3699.24 could represent a sodium cationized oligomer with 80 repeat units and one acetaminophen end group. The expected mass would be 3698.43 u. However, if this peak represents a sodium cationized oligomer with two acetaminophen end groups and 77 repeat units then the expected mass is 3699.42 u. If there were two acetaminophen end groups, the mass error would be -49 ppm; if there were one acetaminophen end group, the mass error would be +219 ppm. Since the average error in analysis by time-lag focussing MALDI for externally calibrated spectra is usually less than 70 ppm, this supports the attachment of two acetaminophen groups. This type of analysis is not possible in a conventional continuous extraction instrument where external mass accuracy in this mass range is ~1000 ppm. Note that unlabelled polymer with *n+3* repeat units would generate a peak with a mass 0.99 u lower than the singly-labelled product (1.98 u less than the nearest doubly labelled product). In a MALDI spectrum of the PEG bis(acetaminophen) the singly-labelled and unlabelled products, if present, would cause peak fronting and decreased resolution, in addition to a peak centroid shift. This is was not observed, suggesting that these species were not present in significant abundance. Their presence in lower abundance, however, could not be ruled out.

The above examples illustrate a limitation of the MALDI method, in that some prior knowledge of the chemistry of the polymeric system under investigation is required. It should be cautioned that using the M_n value of the polymer distribution to deduce information on labelling chemistry is limited. During chemical modification, PEG can undergo hydrolysis or other decomposition processes that can result in a less than expected shift in the average molecular weight distribution.[4]

Table 5.2 Mass Measurement Accuracy of Selected Oligomer Peaks of PEG bis(acetaminophen) in Figure 5B[a]

Mass $(M + Na)^+$ (u)						
Calculated Mass					Mass Error (ppm)	
n[b]	1 label[c]	n	2 labels	Observed Mass	1 label	2 labels
40	1936.29	37	1937.28	1937.32	+532	+21
50	2376.83	47	2377.82	2377.89	+446	+29
60	2817.36	57	2818.35	2818.13	+273	-78
70	3257.90	67	3258.89	3258.65	+230	-74
80	3698.43	77	3699.42	3699.24	+219	-49
90	4138.97	87	4139.96	4140.07	+266	+27
100	4579.50	97	4580.49	4580.69	+260	+44

a Externally calibrated with PEG 3350

b n is the number of repeat units in the polymer

c Label refers to the acetaminophen moiety as the end group of the polymer

5.3.3 Adduction Behaviour

The manner in which polymer chains retain a charge during the MALDI process can affect the amount of information recoverable from a spectrum. This will be illustrated with a discussion on the analysis of polybutadiene (**III**) and polyisoprene (**IV**), using tRA and copper cationization.

$$CH_3CH_2CH(CH_3)[CH_2CR{=}CHCH_2]_nH$$

III R = H **IV** R = CH_3

The divalent copper salt $Cu(NO_3)_2$ was used as the cationization reagent, and represents a new method for the analysis of these polymers. This matrix/cation combination has allowed for the highest reported mass analysis of polybutadiene and

polyisoprene (see Chapter 3). Copper salts have been used previously for a number of mass spectral investigations, including amino acid analysis by fast-atom bombardment[21] and polymer analysis by laser desorption.[22,23] One recent report details the use of $CuCl_2$ with dithranol in the MALDI analysis of a low molecular weight polystyrene.[24]

Figure 5.4 shows the spectrum of polyisoprene 3280 collected from a tRA/$Cu(NO_3)_2$ preparation. The determination of individual oligomer masses suggested that the principal distribution was generated from Cu^+ ion attachment. It is speculated that the generation of [polymer+Cu]$^+$ species was induced upon desorption into the gas phase. Many matrices have been noted to generate radical species upon irradiation.[25] Laser irradiation of the solid sample likely generated a gas plume containing free electrons and radical forms of the matrix capable of reducing Cu^{2+} to Cu^+. Solution chemistry has many examples of the formation of alkene-Cu^+ complexes, while Cu^{2+} complexes are rare or unknown.[26] Thus, it is reasonable to propose a coupled desorption/reduction step for the generation of Cu^+, which is capable of interacting with alkenes. If appreciable Cu^+ were generated in the solution phase during sample handling, one might expect precipitation of the CuCl salt, when $CuCl_2$ is used as the cationization reagent (since attempting to solubilize CuCl in THF was not successful). This was not observed; in fact a solution of polymer, matrix and $CuCl_2$ was stable for many days.

The spectrum in Figures 5.4 reveals a common occurrence in the analysis of polymers by MALDI, namely, the appearance of secondary distributions of lower intensity than the principal distribution. Such secondary distributions could be due to adduction with different ionic species and/or the presence of other polymeric species with different end-group masses. For example, potassium adducts arise in addition to the predominant sodium adducts in the analysis of PEGs.[4] This gives rise to two distributions, shifted by 16 u. Measures are usually taken to suppress the additional distribution. In the case of PEG analyses, this can involve purification for potassium removal or the addition of excess sodium cation. However, inaccurate structural assignments could be made if the full adduction behaviour for a polymer/matrix/cation blend is not well characterized.

Investigation of the spectra corresponding to copper ionization of polyisoprene (Figure 5.4) reveals an apparent mass shift of 22.4 u between distributions. The shift was measured as a positive deviation from the nearest oligomer of lower mass in the principal distribution. This is consistent with the generation of salt cluster complexes, similar to what has been observed in the electrospray ionization of polystyrene.[24] For polyisoprene, it takes the form of [polyisoprene+Cu(copper retinoate)]$^+$. This amounts to an actual shift

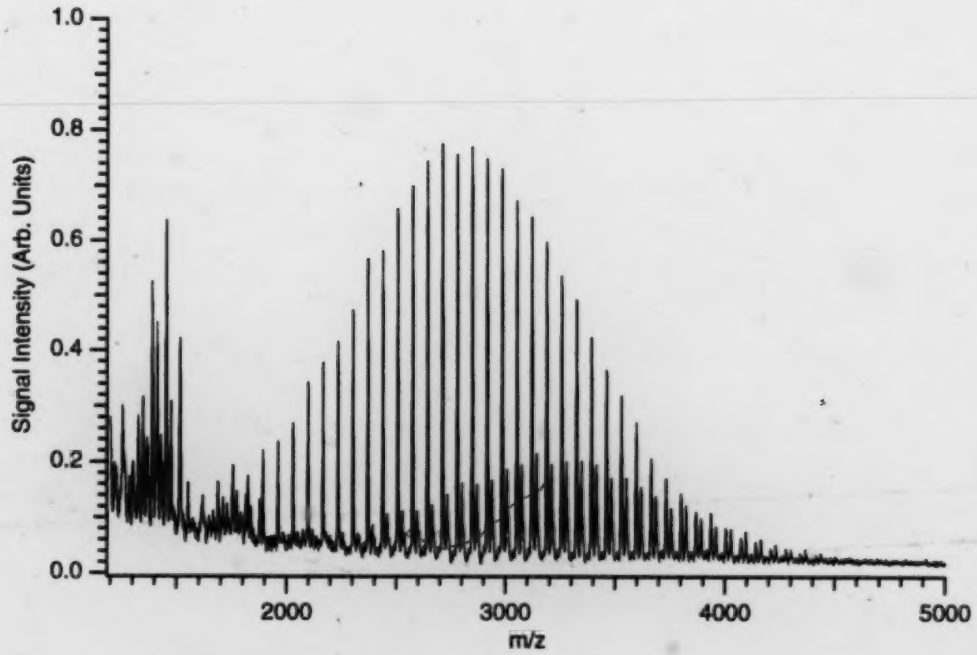

Figure 5.4 MALDI mass spectra of polyisoprene 3280 obtained using tRA with $Cu(NO_3)_2$ as cationization reagent.

of 363.0 u with respect to the principal distribution of [polymer+Cu]$^+$, or the observed mass shift of 22.4 u plus five repeat units of 68.12 u. Similar behaviour was also observed for polybutadiene with copper cationization, and for both polymers with silver cationization.

Using $CuCl_2$ as the cationization reagent and tRA as the matrix, a secondary distribution in the MALDI analysis of polyisoprene 3280 is observed, in addition to the principal [polymer+Cu]$^+$ distribution (Figure 5.5A). With an apparent mass shift of 30.9 u, this is consistent with a structural assignment of [polyisoprene+Cu(CuCl)]$^+$, in which the actual mass shift generated from such adduction behaviour is 99.0 u. An analysis of polybutadiene 2800 using the same cationization reagent leads to a secondary distribution conforming to a similar structural assignment (Figure 5.5B). In this case, the secondary distribution exhibits an apparent mass shift of 45 u. Due to its low intensity and presence as a shoulder on the principal distribution, the mass shift of this distribution could only be assigned with unit mass accuracy.

The structural assignments discussed above are lent validity by the experimental results displayed in Figure 5.6. This figure compares the adduction behaviour of polyisoprene 3280 arising from different cationization reagents. Figure 5.6A shows four peaks in the secondary distribution that arose from cationization with $Cu(NO_3)_2$, with an apparent mass shift of 22.4 u from the principal distribution. Doping molar equivalents of KCl and $Cu(NO_3)_2$ into the polymer/matrix solution gave rise to a spectrum showing two secondary distributions (Figure 5.6B). One distribution is isobaric with the secondary distribution of Figure 5.6A. The other, with an apparent mass shift of 30.9 u, is isobaric with the secondary distribution of Figure 5.6C. The latter spectrum was obtained using $CuCl_2$ as the cationization reagent. Figure 5.6B then strongly suggests that both [polyisoprene+Cu(copper retinoate)]$^+$ and [polyisoprene+Cu(CuCl)]$^+$ are present. One further implication of this series of spectra is that chloride ion competes effectively with the retinoate anion in the adduction process.

When additional adduction is observed, spectral congestion increases and it becomes difficult to assess whether polymers with different structures are present or not. Furthermore, the accuracy of an average molecular weight determination could be compromised by the presence of secondary distributions. If a spectrum cannot be collected with sufficient resolution, then an average molecular weight determination would necessarily include all ion forms within the polymer distribution. If the secondary distributions are significantly intense relative to the principal distribution, the molecular weight determination would be erroneous. This can be illustrated with the spectrum in

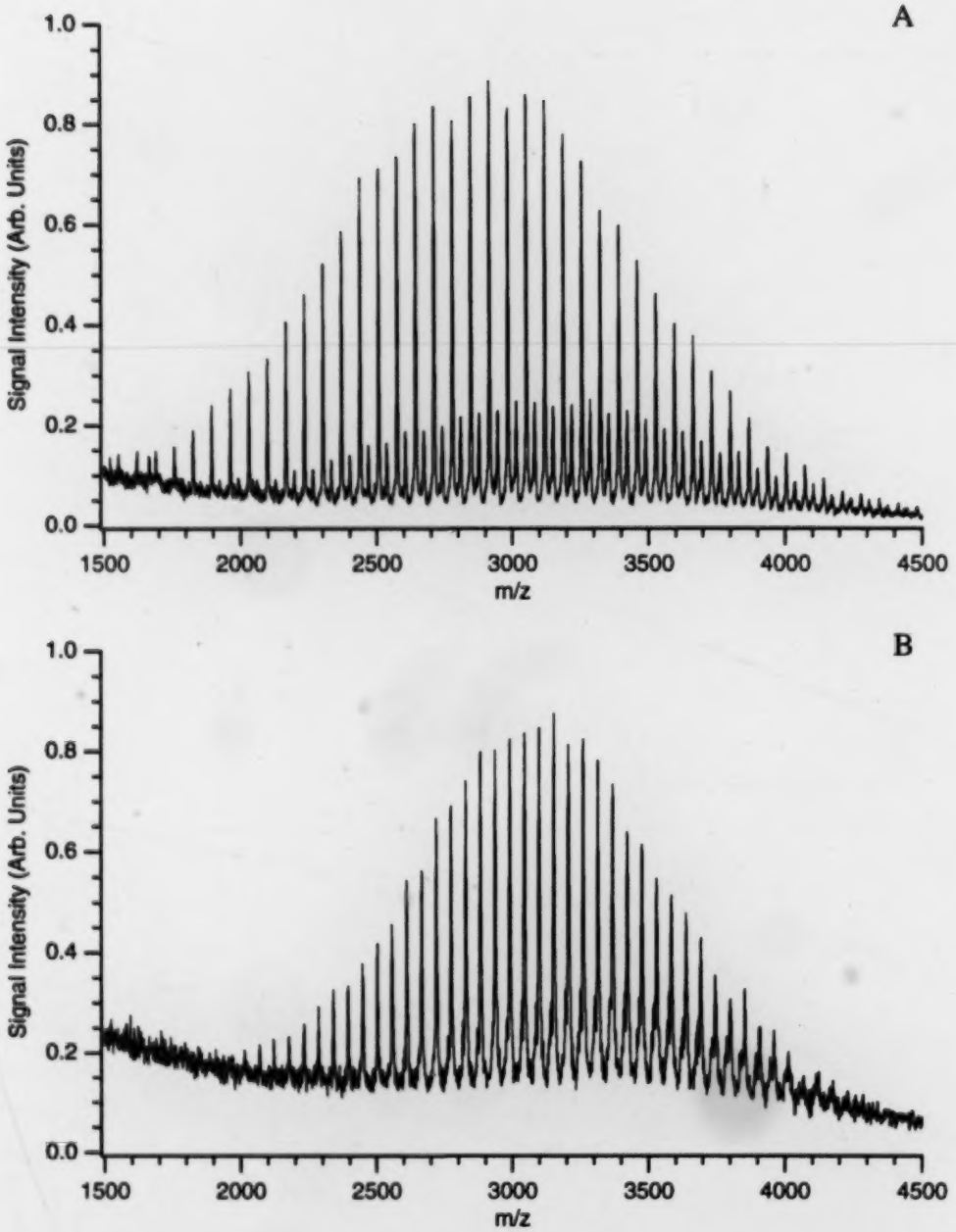

Figure 5.5 The effect of the addition of $CuCl_2$ on the observed secondary distribution arising from the MALDI analysis of (A) polyisoprene 3280 and (B) polybutadiene 2800.

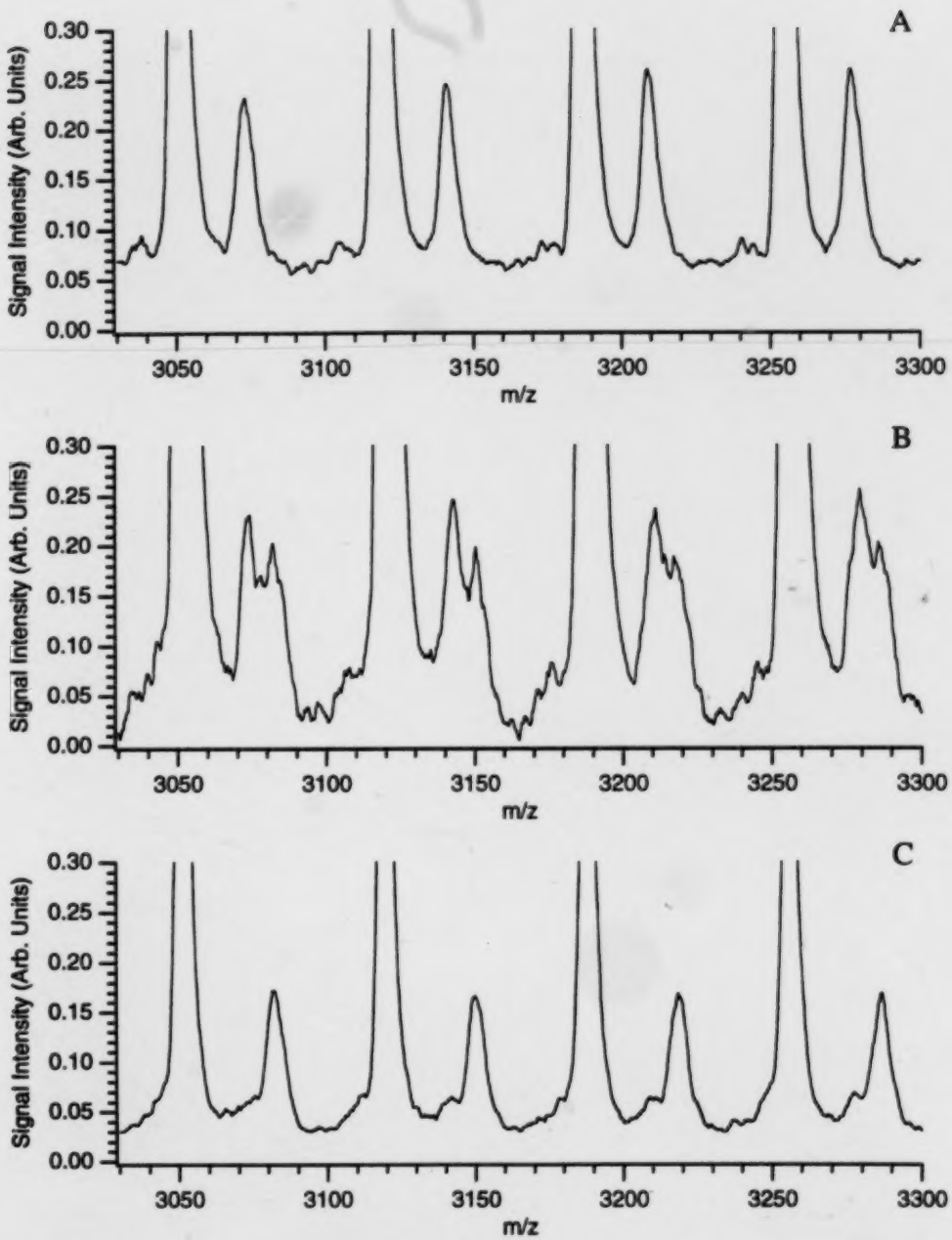

Figure 5.6 The effect of cationization reagent on the appearance of the secondary distribution in polyisoprene 3280, using tRA with (A) $Cu(NO_3)_2$, (B) $Cu(NO_3)_2$ with KCl and (C) $CuCl_2$.

Figure 5.4, in which all oligomer forms are resolved. The M_n value of the principal distribution was measured at 2780, while that of the secondary distribution was measured at 3137. The precision of both measurements were 0.3% RSD and 0.6% RSD, respectively (based on five sample analyses). When both distributions were included, the M_n value was measured at 2861 (0.5% RSD). The difference between this value and the M_n value of the principal distribution is statistically significant at 81 u, where "significance" is determined by the t-test for the comparison of two means (at the 99% confidence limit). This suggests that inclusion of the secondary distribution would introduce a slight error to the M_n determination. Nevertheless, it is only in the low mass, narrow polydispersity region where this difficulty could arise. If the polymer molecular weight increases, the increment in M_n due to different adduction behaviour would remain the same. This translates into a decrease in the percent difference between the M_n of principal and secondary distributions. When the polydispersity increases, the precision of the M_n determination becomes worse, such that the error introduced by the secondary distribution would be insignificant.

Ideally, if the cationization efficiency bears the same mass dependency for both distributions, the M_n of the secondary distribution would be 363.0 u greater than that of the principal distribution, due to the additional attachment of copper retinoate. The observed difference between the measured M_n values is 357 u. In other words, there is a difference of only 6 u between the expected and observed values for the secondary distribution. Based on the t-test for the comparison of means, this is statistically insignificant even at the 50% confidence limit. This supports the conclusion that the cationization efficiency represented in the secondary distribution is similar to that of the principal distribution.

Another complication arising from this adduction behaviour between copper ions and tRA is pertinent to the upper mass limit of oligomer resolution. Polymers of higher molecular weights are not as well resolved as they would be in the absence of secondary distributions. Nevertheless, with time-lag focussing MALDI, oligomer resolution can still be obtained for polydienes with masses up to 25 000. For example, Figure 5.7 displays the spectra of polyisoprene 19 300 and polybutadiene 22 430. In both spectra, individual oligomers are sufficiently resolved so as to substantiate the basic polymer type (repeat unit and end-groups). The additional adduct formation experienced with the use of $Cu(NO_3)_2$ prohibits baseline resolution.

Dithranol was found to provide strong signals for low molecular weight polydienes (M_n < 20 000), although it failed to generate signals for higher molecular weight polydienes. Figure 5.8 shows a spectrum of polyisoprene 3280 analysed from dithranol

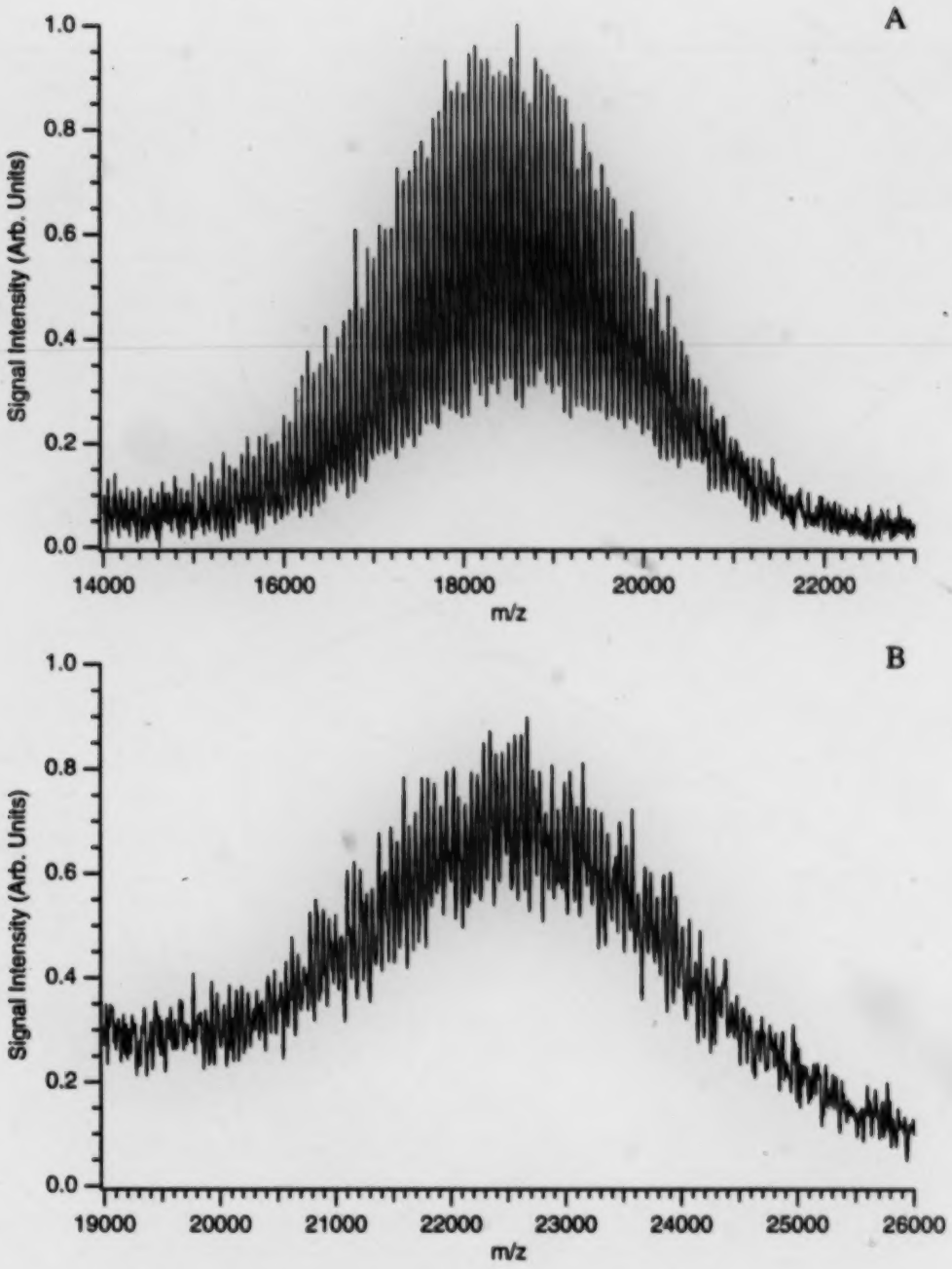

Figure 5.7 MALDI mass spectra of (A) polyisoprene 19 300 and (B) polybutadiene 22 430 demonstrating optimum resolution.

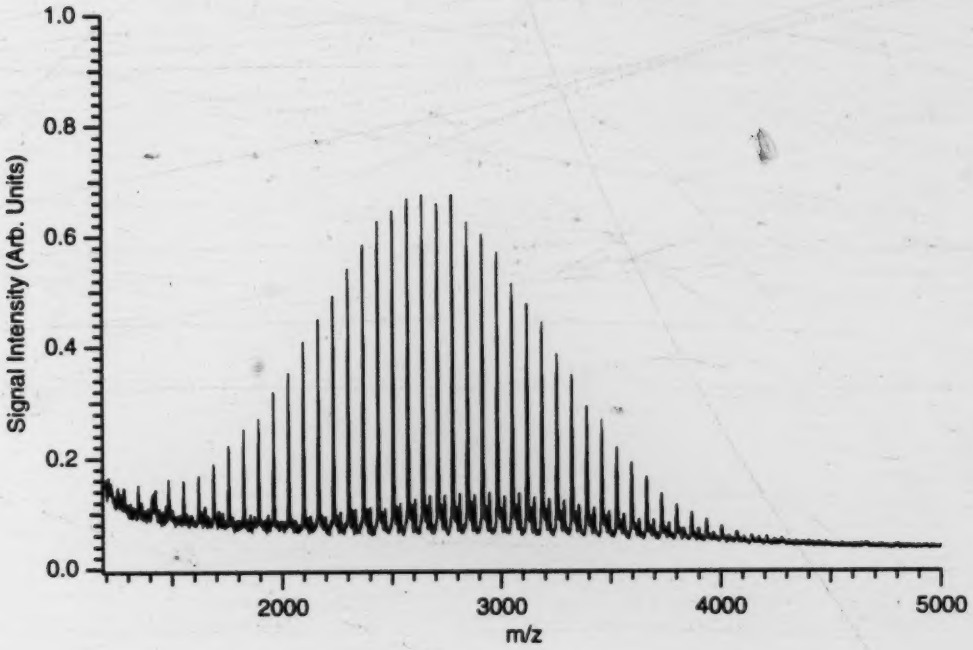

Figure 5.8 MALDI spectrum of polyisoprene 3280, using dithranol as matrix with $Cu(NO_3)_2$. Spectrum collected from a THF solution containing 0.15 M dithranol, 200 µM polymer and 1% (v/v) of a 0.1 M $Cu(NO_3)_2$ aqueous solution. A 1 µl aliquot was allowed to dry on the probe tip.

doped with $Cu(NO_3)_2$. The M_n value from the principal distribution was measured to be 2649 (1.0% RSD). This spectrum reveals a small distribution with an apparent mass shift of 30.9 u, consistent with the formation of [polyisoprene+Cu(CuCl)]$^+$, generating an actual shift of 99.0 u. A third, even weaker distribution is in evidence, with an apparent mass shift of 16.3 u. Analogous to tRA, this is consistent with the formation of [polyisoprene+Cu(copper-dithranol)]$^+$, generating an actual mass shift of 288.8 u. This adduction behaviour, therefore, is not unique to tRA. Considering all ion forms in the measurement of M_n results in a value of 2669 (1.0% RSD). These secondary distributions are sufficiently weak such that they do not interfere with the measurement of an accurate average molecular weight.

Note the discrepancy between the M_n values of the principal distributions as determined by tRA (2780, RSD = 0.3%, Figure 5.4) and dithranol (2649, RSD = 1.0%). A small but contributing factor to this discrepancy arose from the increased chemical noise in the low mass tail of the tRA analysis. More lower mass oligomers were distinguishable in the analysis based upon dithranol. However, determining M_n for both principal distributions using a common starting point of ~1820 u resulted in values that still differ by 98 u, with the tRA analysis giving the higher value. The most probable peak (M_p) values also indicate a shift of approximately 100 u. These shifts are significant by the t-test (at the 99% confidence limit), and could have arisen from differences in polymer desorption and/or ionization efficiencies of the matrices. Average molecular weights obtained using dithranol would seem less reliable than those obtained by tRA. This conclusion is reached from an assessment of the upper mass limits of each preparation. For dithranol, no signals for polyisoprene could be obtained above 20 000 u. For tRA, this limit was approximately 150 000 u. Desorption/ionization efficiency is expected to diminish in both preparations, as the oligomers in the polymer distribution approach the upper mass limit. As the mass limit for dithranol is much lower than tRA, the reduction in efficiency would be more severe, and lead to a greater discrimination against higher mass oligomers than with tRA. Dithranol would be more applicable for structural analysis of low mass polymers, particularly if the chloride contamination could be removed. Lower spectral congestion arising from reduced adduct formation would allow for a better opportunity to identify peaks among the principal distribution.

In summary, time-lag focussing time-of-flight mass spectrometry has led to improvements in both resolution and mass accuracy that have extended the analytical utility of MALDI for polymer structural analysis. Confirmation of expected structures is straightforward. Complexity in adduction behaviour reduces the information content of a

spectrum. Careful selection of sample preparation procedures and an understanding of the possible adduction behaviour are required for the mass analysis of minor polymeric components in the spectrum.

5.4 Literature Cited

(1) Bahr, U.; Deppe, A.; Karas, M.; Hillenkamp, F. *Anal. Chem.* **1992**, *64*, 2866.

(2) Juhasz, P.; Costello, C. E. *Rapid Commun. Mass Spectrom.* **1993**, *7*, 343.

(3) Whittal, R. M.; Li, L.; Lee, S.; Winnik, M. A. *Macromol. Rapid Commun.* **1996**, *17*, 59.

(4) Lee, S.; Winnik, M. A.; Whittal, R. M.; Li, L. *Macromolecules* **1996**, *29*, 3060.

(5) Jackson, A. T.; Yates, H. T.; Scrivens, J. H.; Critchley, G.; Brown, J.; Green, M. R.; Bateman, R. H. *Rapid Commun. Mass Spectrom.* **1996**, *10*, 1668.

(6) Weidner, S.; Kuhn, G.; Just, U. *Rapid Commun. Mass Spectrom.* **1995**, *9*, 697.

(7) Danis, P. O.; Karr, D. E.; Westmoreland, D. G.; Piton, M. C.; Christie, D. I.; Clay, P. A.; Kable, S. H.; Gilbert, R. G. *Macromolecules* **1993**, *26*, 6684.

(8) Burger, H. M.; Muller, H.-M.; Seebach, D.; Bornsen, K. O.; Schar, M.; Widmer, M. *Macromolecules* **1993**, *26*, 4783.

(9) Weidner, S.; Kuhn, G.; Friedrich, J.; Schroder, H. *Rapid Commun. Mass Spectrom.* **1996**, *10*, 40.

(10) Weidner, S.; Kuhn, G.; Friedrich, J.; Unger, W.; Lippitz, A. *Rapid Commun. Mass Spectrom.* **1996**, *10*, 727.

(11) Wilczek-Vera, G.; Danis, P. O.; Eisenberg, A. *Macromolecules* **1996**, *29*, 4036.

(12) Hillenkamp, F.; Karas, M.; Beavis, R. C.; Chait, B. T. *Anal. Chem.* **1991**, *63*, 1193A.

(13) Colby, S. M.; King, T. B.; Reilly, J. P. *Rapid. Commun. Mass Spectrom.* **1994**, *8*, 865.

(14) Brown, R. S.; Lennon, J. J. *Anal. Chem.* **1995**, *67*, 1998.

(15) Vestal, M. L.; Juhasz, P.; Martin, S. A. *Rapid Commun. Mass Spectrom.* **1995**, *9*, 1044.

(16) Whittal, R. M.; Li, L. *Anal. Chem.* **1995**, *67*, 1950.

(17) Vorm, O.; Roepstorff, P.; Mann, M. *Anal. Chem.* **1994**, *66*, 3281.

(18) Dai, Y.; Whittal, R. M.; Li, L. *Anal. Chem.* **1996**, *68*, 2494.

(19) Edmondson, R. D.; Russell, D. H. *J. Am. Soc. Mass Spectrom.* **1996**, *7*, 995.

(20) Cotter, R. J. *Time-of-Flight Mass Spectrometry: Instrumentation and Applications in Biological Research*; American Chemical Society: Washington, DC, 1997.

(21) Wen, D.; Yalcin, T.; Harrison, A. G. *Rapid Commun. Mass Spectrom.* **1995**, *9*, 1155.

(22) Dean, P. A.; O'Malley, R. M. *Rapid Commun. Mass Spectrom.* **1993**, *7*, 53.

(23) Mowat, I. A.; Donovan, R. J. *Rapid Commun. Mass Spectrom.* **1995**, *9*, 82.

(24) Deery, M. J.; Jennings, K. R.; Jasieczek, C. B.; Haddleton, D. M.; Jackson, A. T.; Yates, H. T.; Scrivens, J. H. *Rapid Commun. Mass Spectrom.* **1997**, *11*, 57.

(25) Ehring, H.; Karas, M.; Hillenkamp, F. *Org. Mass Spectrom.* **1992**, *27*, 472.

(26) Cotton, F. A.; Wilkinson, G. *Advanced Inorganic Chemistry;* fifth ed.; John Wiley & Sons: Toronto, 1988, p 757.

Chapter 6

MALDI Analysis of Polymers: Compositional Analysis[a]

6.1 Introduction

Advances in polymer chemistry have generated polymeric systems of very diverse composition and chemistry. Many of these new materials contain two or more monomeric components, and can be classified as block, graft, alternating, gradient or random copolymers.[1] Aside from their polydispersity and average molecular weight, the physical properties of these materials are dependent on the ratio of the monomers, as well as the monomer sequence.[1-3] Determining overall chemical composition and structure is important in the development of structure-property relationships, and understanding the mechanisms of copolymerization as well as the effects of reaction conditions on polymer structure.[2,4,5]

A number of techniques provide compositional information for those situations where the monomeric units display different analytical characteristics. These include elemental analysis, functional group determination by chemical methods (e.g.: titration), refractive index determination, gel permeation chromatography, pyrolysis mass spectrometry, as well as spectroscopic methods such as IR, UV-visible spectroscopy, and NMR.[1,6-10] If the monomeric units are chemically similar, then a cloud point titration procedure could be used to determine overall composition.[1] These methods cannot be universally applied as their success is dependent on the chemistry of the polymer analysed and its composition. For example, discrimination between polymer blends and true copolymers could be difficult, as most of the above techniques provide only bulk sample information. Therefore, it is desirable to develop analytical techniques that would provide information on the structural composition of complex polymer systems, ideally on an oligomer-by-oligomer basis.

Chapters 3 and 4 have shown that the absence of mass discrimination is required for an accurate measurement of polymer average molecular weight. Chapter 5 has demonstrated that high resolution and mass accuracy for oligomer peaks are required for a structural analysis of homopolymers. For such polymers, structural information can be

[a] A form of this chapter has been published: Schriemer, D.C.; Whittal, R.M.; Li, L. "Analysis of Structurally Complex Polymers by High Resolution Matrix-Assisted Laser Desorption Ionization Time-of-Flight Mass Spectrometry" Macromolecules, **1997**, 30, 1955-1963. R.M. Whittal collected the spectra for the Dow polyols.

obtained even in the presence of mass discrimination. This is because structural information is based solely upon the mass determination of the individual oligomer peaks, and not their intensity. There are no restrictions in applying MALDI to structurally complex polymers aside from the usual concerns of finding a suitable matrix, solvent and cationizing reagent. However, determining the composition of heterogeneous polymer systems requires high resolution, high mass accuracy *and* uniformity in the detection of all polymer forms (i.e.: no discrimination based on mass or chemical type). This is because a compositional analysis of copolymers requires the measurement of oligomer peak intensity. In the present chapter, this will be illustrated through the MALDI analysis of several alternating and block copolymers, using time-lag focussing in a linear time-of-flight instrument.

6.2 Experimental

6.2.1 Instrumentation

Mass spectral data were collected on a linear time-lag focussing MALDI TOF mass spectrometer,[11] modified for operation up to 30 kV. The first extraction plate was redesigned and a grid was placed on the repeller side. A single DC power supply was used to set the potential on the repeller and first extraction plate and the potential on the second extraction plate through a voltage divider. Under normal operation, the power supply was set to 20 kV DC. In conjunction, a high voltage pulser built in-house and a Hewlett-Packard pulser (Palo Alto, CA) were used to generate the delayed extraction pulse. The extraction pulse and time lag were varied as required to focus the mass range of interest. A nitrogen laser (VSL-337ND, Laser Science, Inc.; Newton, MA) with a 3-ns pulse width was used for desorption at 67.5° to the probe surface normal. A neutral-density filter was used to attenuate the laser energy that reached the sample surface. A mass filter was added to the system. The mass filter prevented saturation of the microchannel plate detector by deflecting matrix ions out of the usual ion trajectory, reducing the ion current from low mass ions. Proton NMR spectra for the samples of poly(bisphenol A-co-epichlorohydrin) were recorded on a Bruker 400AM instrument, using 35 second relaxation delays.

6.2.2 Data Collection and Mass Calibration

The mass spectra were recorded using a LeCroy 9350M digital oscilloscope at a sampling rate of 500 MHz or 1 GHz, in conjunction with Hewlett-Packard MALDI software. In general, mass spectra from 50 to 100 laser shots were summed to produce a final spectrum in this study. Peak centroids were determined with the software, and mass calibration of the instrument was achieved using a two-point linear calibration. Mass calibrations were performed externally, using well-characterized polymers. Calibrated spectra were transferred to a PowerMac and processed using Igor Pro data analysis software (WaveMetrics, Inc.; Lake Oswego, OR.). All spectra demonstrating unit mass resolution were interpolated using four-times zero-filling and calibrated in Igor Pro. This was required because the Hewlett-Packard software could not determine accurate centroids for highly resolved peaks. Number average molecular weights (M_n) were calculated according to the procedure outlined in Chapter 4. The spectra displayed in this chapter were not corrected for the intensity distortions arising from calibration. Note that the peak areas discussed in this chapter refer to the peak areas calculated in the time domain.

6.2.3 Sample Preparation

Polymer samples for MALDI analysis were prepared by premixing the analyte, matrix and cationizing agent. All polymer samples were prepared in glass vials. The polymers poly(propylene glycol-b-ethylene glycol-b-propylene glycol)bis(2-aminopropyl ether) (PPEP), glycidyl end-capped poly(bisphenol A-co-epichlorohydrin) (PBAE) and Dow polyols A and B were dissolved in 1,4-dioxane to a concentration of 1 mM. The matrix 2-(4-hydroxyphenylazo)benzoic acid (HABA) was used in the analysis of these polymers. HABA was dissolved in 1,4-dioxane to a concentration of 50 mM. The polymer solution and matrix solution were mixed to give a final polymer concentration of 100 μM, and matrix concentration of 45 mM. To 100 μL of PPEP/matrix solution, 1 μL of 10 mM NaCl (aq) was added. No NaCl was added to the PBAE/matrix solution. A 1 μl aliquot of the appropriate mixture was added to the MALDI sample probe and allowed to dry.

Acetone was used to dissolve poly[(o-cresyl glycidyl ether)-co-formaldehyde] (PGF) to a concentration of 1 mM. The matrix 1,4-diphenylbutadiene (DPB) was prepared to a concentration of 0.17 M in acetone, and the polymer stock solution diluted ten-fold with the matrix solution to give a final polymer concentration of 100 μM. To this mixture

was added 1% (v/v) of a saturated ethanolic solution of $AgNO_3$. For MALDI analysis, 1 µl of the mixture was added to the MALDI probe tip and allowed to dry.

The spectra arising from PPEP, PBAE, PGF and Dow polyols A and B were calibrated with well-characterized poly(ethylene glycol) samples of the appropriate mass, using the HABA sample preparation method already described.

6.2.4 Materials

PPEP, PBAE 1750, PBAE 4000, PBAE 6100 and PGF were purchased from Aldrich (Milwaukee, WI). Polyols A and B were provided by the Dow Chemical Company. These were copolymers containing an unspecified ratio of ethylene oxide and propylene oxide repeat units. All polymers were analysed without further purification. The matrices HABA and DPB were purchased from Aldrich and used without purification. The cationizing reagents $AgNO_3$ (Terochem Laboratories Ltd., Edmonton, Canada) and NaCl (BDH Laboratories, Toronto, Canada) were reagent grade. Analytical grade 1,4-dioxane was purchased from BDH Laboratories (Toronto, Canada). Water used throughout was from a Milli-Q Plus Ultrapure water system (18.2 MΩ•cm, Millipore, Bedford, MA).

6.3 Results and Discussion

6.3.1 Alternating Copolymers

Figure 6.1 displays the MALDI mass spectrum for poly[(o-cresyl glycidyl ether)-co-formaldehyde] (PGF, polymer **I**). The polymer was analysed as its silver adduct, using the DPB as the matrix.

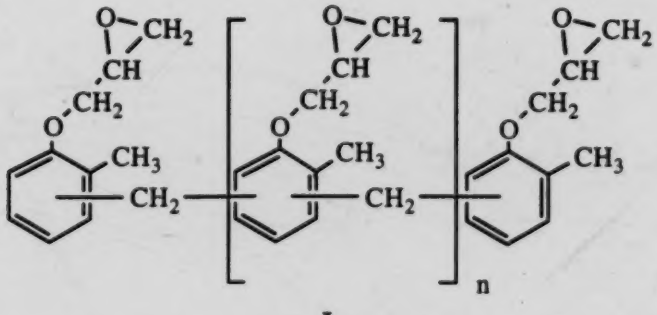

I

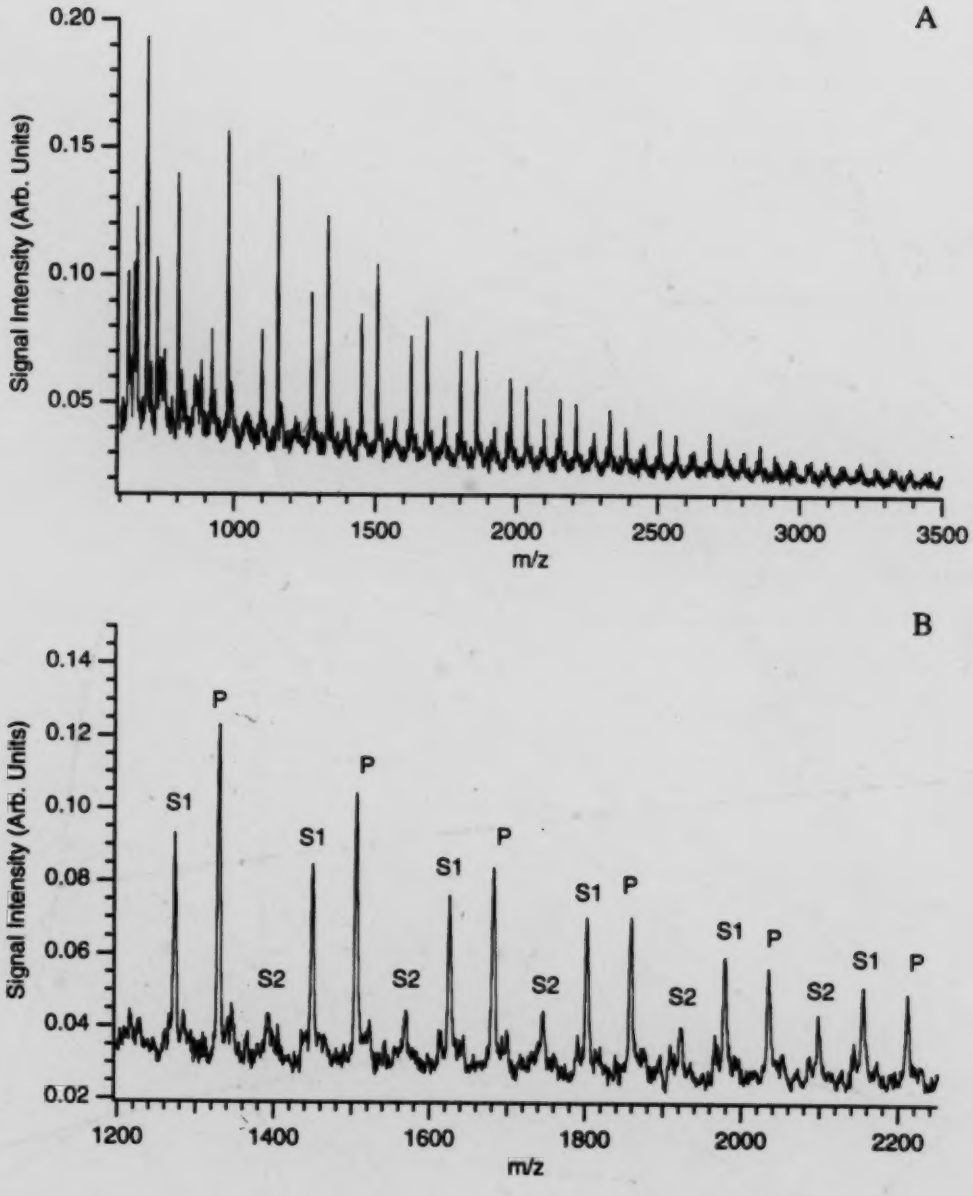

Figure 6.1 MALDI mass spectrum of an alternating copolymer (A) poly[(o-cresyl glycidyl ether)-co-formaldehyde] with (B) an expansion.

Such a formulation was successful in preserving the epoxide functionality, as similar spectra were obtained from aged solutions of matrix and polymer. The expanded spectrum in Figure 1B reveals a number of features. This sample contains at least two other polymeric components that appear to become more dominant with increasing molecular weight. There are three major series of peaks, labelled as P, S1, and S2, each bearing a repeat unit of 176.2 u. The P series arises from the intact PGF. The S1 series, being 56 u lower than the P series, is likely due to the absence of one glycidyl ether group. The less intense peaks of the S2 series have masses corresponding to PGF minus two glycidyl ether groups (-112 u). This example demonstrates that the MALDI method can provide qualitative compositional information on an oligomer-by-oligomer basis that is otherwise difficult to obtain.

Ideally, a complete mass spectral analysis would involve the quantitation of the various polymeric forms in the sample. This would allow for the determination of the overall epoxide content, and also its mass dependency. In this context, "quantitation" requires measuring the peak areas of all oligomers in all distributions, and assuming that these areas accurately reflect the polymer composition. It is instructive to consider some of the literature regarding quantitation by MALDI. Most of the work in this area has considered the quantitation of proteins and peptides, using internal standards and the method of standard addition. One study investigated the quantitation of insulin, cytochrome c and lactoferrin and reported RSDs (for the analyte/internal standard ratio) ranging from 9 to 18%, over an order of magnitude of concentration.[12] One of the impediments to quantitation concerns the matrix crystallization step. Variability in this step leads to poor shot-to-shot reproducibility as well as sample-to-sample reproducibility.[13] Improved sample preparation methods have allowed for RSDs (for the analyte/internal standard ratio) of 6 to 12% in the quantitation of bovine insulin, with a linear dynamic range over three orders of magnitude.[14] The proper choice of internal standard was shown to be crucial. Generally, a proper standard is one which is chemically similar to the analyte, close in mass to the analyte yet completely resolved from it and chemically stable during the analysis.[13,15] One of the remaining difficulties that has been identified concerns the suppression of the signal arising from the less concentrated component by the more concentrated component.[13] In other words, the relative peak areas can be sensitive to the concentration of the analyte in the matrix. This has been demonstrated for polymers as well, in the concentration study of Chapter 4. Overall, the accuracy of quantitation is rarely better than 10%.[13]

Average molecular weight and compositional analysis of polymers by MALDI requires quantitation in the absence of internal standards. Considering the above-noted difficulties in quantitation, MALDI has been quite successful in generating useful data from polymer analyses. For homopolymers, individual oligomers are chemically similar so that quantitation for average molecular weight determination is feasible. This is at least true for narrow polydispersity materials where the masses of the oligomers do not span a large mass range.[16-19] However, for more heterogeneous polymer systems, the relative detection efficiencies of the various oligomers cannot be assumed. In MALDI analysis, the term "detection efficiency" can be used to express a combination of various factors, including efficiencies of analyte entrapment in the matrix, sample vaporization, ionization, ion transmission and detection. As an example, the addition of a pyrene end-group to poly(ethylene glycol) has been shown to lower the detection efficiency of the altered polymer with respect to the unaltered polymer.[20] Presumably, the large non-polar pyrene affects the extent of polymer inclusion into the polar matrix, giving rise to a reduced desorption efficiency. Therefore, even for copolymers of narrow polydispersity, chemical diversity among the oligomers could be sufficiently great (from a MALDI point of view) to falsify the assumption of uniform detection efficiency.

The case involving PGF represents only mild structural differences between the distributions, suggesting that quantitation might be possible. The supplier has indicated an overall epoxide content of 0.9 for this polymer, defined as the ratio of epoxide groups to the sum of the repeat units and end-groups in the polymer. This is a quantity determined from the bulk sample, and therefore represents an average, weighted according to the abundance of the various oligomers. The epoxide content could be determined for each oligomer in the MALDI mass spectrum, and weighted according to its intensity, to determine the overall epoxide content. With this method, an average value of 0.94 was obtained. This would seem to indicate that the differences in the overall detection efficiency between distributions were minor, as a good agreement with the supplier's data was obtained. The M_n of this polymer, considering all components, was determined to be 1417 with a polydispersity of 1.25. The supplier indicated a value of 1270. Note that the MALDI determination of M_n is based on area calculations of peaks having masses above 600 u. While the matrix material did not generate peaks overlapping expected oligomer peaks, none were observed below this mass.

If the goal of a polymer analysis by MALDI is to compare a product with a standard or reference material, then some of the difficulties regarding non-uniform detection efficiency can be avoided. This could be demonstrated with the analysis of an alternating

copolymer, poly(bisphenol A-co-epichlorohydrin) (PBAE, polymer **II**). Figures 6.2A-C show the spectra of three samples of PBAE with nominal molecular weights of 1750, 4000 and 6100, respectively. These samples were terminated with epichlorohydrin to obtain a glycidyl end-capped product. All samples were analysed using HABA as matrix, resulting in oligomers cationized with endogenous sodium cation.

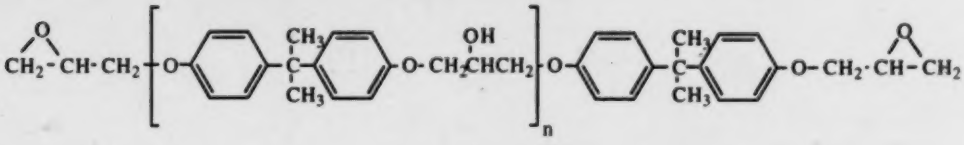

II

The MALDI spectra shown in Figure 6.2 indicate that the chemical compositions of the three samples are significantly different. Consider two of the samples, i.e. PBAE 1750 and PBAE 6100. Expanded sections of the spectra of PBAE 1750 and PBAE 6100 are displayed in Figures 6.3A and 6.3B, respectively. The principal distribution labelled as P in Figure 6.3 has an expected repeat unit of 284.4 u with oligomer masses that conform to the expected structure. Several other features are common to both spectra. The principal peaks in the spectra exhibit a small peak 18 u higher (P+18). A peak 36 u higher than the principal peak (P+36) is also observed. These two series of peaks likely correspond to products from the hydrolysis of one and two epoxide end-groups. This hydrolysis was not due to the sample preparation, as incubation of the sample in the matrix solution for variable periods of time (5 minutes to 2 hours) did not lead to any change in the relative intensity of these peaks.

In both spectra of Figure 6.3, there are satellite peaks about the principal distribution with mass shifts equivalent to the mass of one glycidyl unit (56 u, labelled P+56 in Figure 6.3A). In the spectrum of PBAE 6100, a feature with a mass shift of 60 u (labelled P+60 in Figure 6.3B) partially overlaps the feature with a mass shift of 56 u. It should be noted that the P+60 peak begins to appear in the high mass end of the spectrum of PBAE 1750 as well. While the identity of the peak with a mass shift of 60 u is unknown, those with a shift of 56 u seem to indicate the addition of a third glycidyl unit in addition to the two end caps, possibly on a secondary OH group in one of the repeat units. Furthermore, this feature suggesting tri-capping becomes more dominant with an increase in oligomer molecular weight or chain length. Hydrolysis products are also observed, as

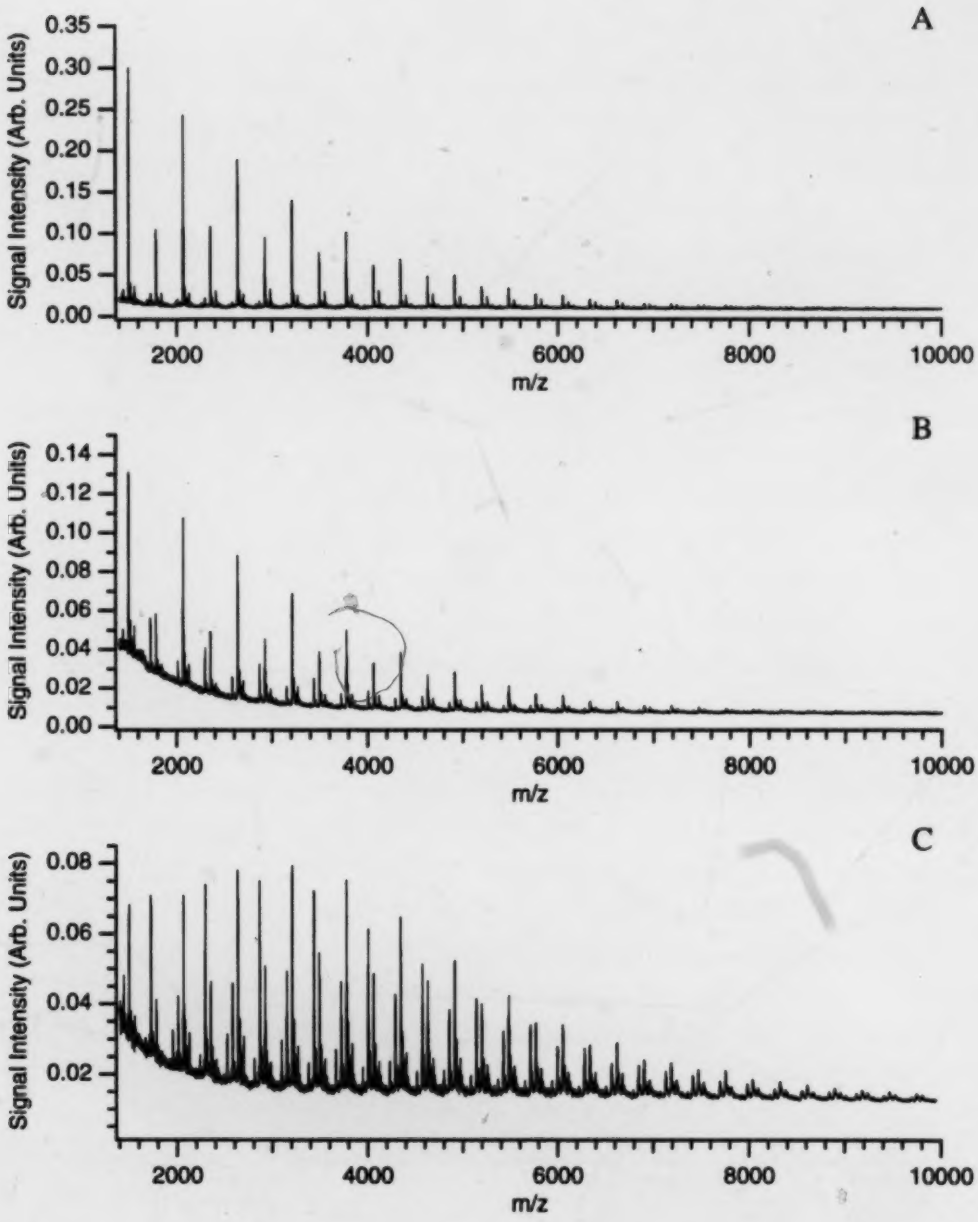

Figure 6.2 MALDI mass spectra of glycidyl end-capped poly(bisphenol A-co-epichlorohydrin) with nominal molecular weights of (A) 1750, (B) 4000 and (C) 6100.

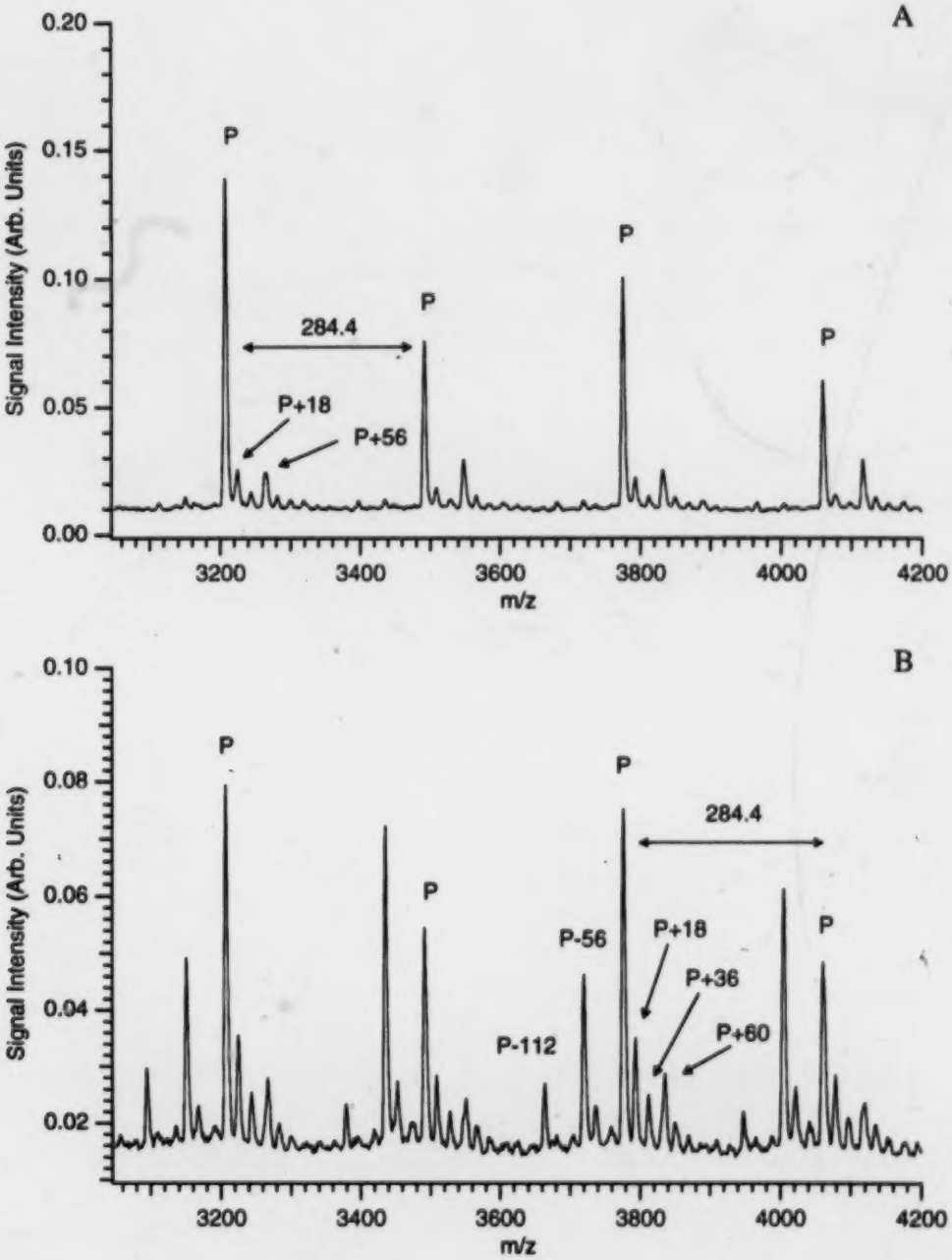

Figure 6.3 Expansions of the MALDI mass spectra of (A) PBAE 1750 and (B) PBAE 6100.

indicated by peaks +18 u and +36 u from the P+56 series. A peak corresponding to the complete hydrolysis (+54 u) could not be determined with confidence due to very low signal strengths. In the PBAE 1750 sample, the end-capping seemed to be complete. That is, there appears to be only negligible amounts of oligomers that were not terminated with two glycidyl units. The situation is different for the PBAE 6100 sample (Figure 6.3B). Here, end-capping appears more distributed and incomplete. A significant portion of the sample seems to contain either one or no glycidyl end caps as indicated by the -56 and -112 u shifts from the principal distribution (i.e., P-56 and P-112 peaks in Figure 6.3B), in addition to the fraction that is tri-capped.

An interesting feature in the spectra of Figure 6.3 concerns the obvious intensity patterns. For example, in the principal distribution of the spectrum for PBAE 1750 (Figure 6.3A), peaks from *even* numbers of repeat units appear more intense than peaks with an *odd* number of repeat units. Examining the oligomer compositions of both PBAE 1750 and 6100 more closely shows that all distributions containing an even number of glycidyl units reveal this pattern. This intensity pattern is reversed for the distributions containing an odd number of glycidyl units, i.e., the oligomer peaks representing even numbers of repeat units are less intense than those representing odd number of repeat units. The variation in end-capping for both PBAE 1750 and PBAE 6100 can be illustrated graphically (Figure 6.4A and 6.4B, respectively). For PBAE 1750, Figure 6.4A represents the ratio of the peak areas for the di-glycidyl and tri-glycidyl forms of a given oligomer, showing the dependence on the number of repeat units. For PBAE 6100, Figure 6.4B displays a similar ratio for the di-glycidyl and mono-glycidyl forms of a given oligomer. The alternating patterns are clearly evident in both figures. Also note that the alternation tends to even out with higher molecular weight, approaching a common value.

As was expressed in the above analysis of the spectrum for PGF, one cannot tacitly assume a constant detection efficiency for all forms of the polymeric species in the absence of supporting information. In other words, although the trends and patterns of Figures 6.4A and 6.4B are valid, there is uncertainty as to how accurately the above ratios reflect the true oligomer content. This necessarily leads to uncertainty in the M_n values obtained from these spectra, calculated to be 3530 (PD=1.21) for PBAE 1750 and 4300 (PD=1.19) for PBAE 6100, as these calculations consider all forms of the oligomers. Perhaps a more useful approach for the comparison between samples would be to determine the M_n of corresponding series in the spectra. For example, the M_n of the P series for PBAE 1750 is 2490 (PD=1.30), and for PBAE 6100 is 4030 (PD=1.19).

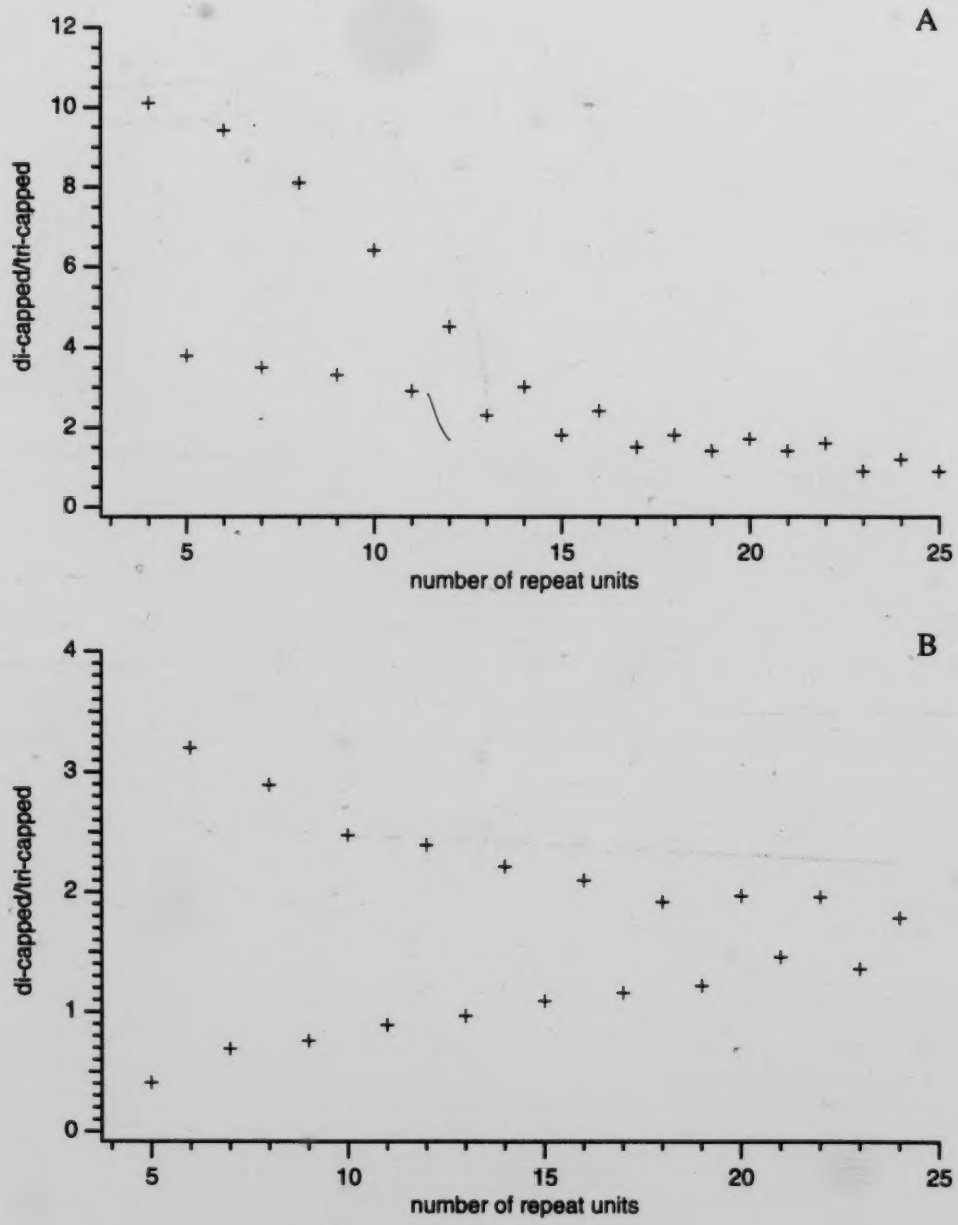

Figure 6.4 End-group compositional analysis of (A) PBAE 1750 and (B) PBAE 6100, for the indicated oligomeric forms. Ratios are calculated from the areas of corresponding peaks.

If the goal of the analysis is to compare the spectrum of one product with the spectrum of a standard or reference material, then another option exists. Considering the PBAE samples, the product might possess oligomers with a certain ratio of mono-glycidyl capping to di-glycidyl capping chemistry. In absolute terms, this can be expressed as follows:

$$\frac{N_{x(2)}}{N_{x(1)}} \tag{1}$$

where $N_{x(1)}$ represents the number of molecules of oligomer x with a single glycidyl unit and $N_{x(2)}$ represents the number of molecules of oligomer x with two glycidyl units. The relative areas can be obtained from the spectrum, which relates to the above ratio in the following way:

$$\frac{A_{x(2)}}{A_{x(1)}} = \frac{\sigma_{x(2)} N_{x(2)}}{\sigma_{x(1)} N_{x(1)}} \tag{2}$$

where A denotes the area of the indicated oligomer type and σ denotes the detection efficiency of the indicated oligomer type. This area ratio allows the comparison of oligomers in a spectrum as was done in Figure 6.4. Since the detection efficiencies of the various forms of the oligomers are not known, the area ratio does not necessarily reflect the absolute ratio as expressed in (1). However, if a given oligomer is being compared between the spectra of two samples, the following expression applies:

$$Q = \left(\frac{A_{x(2)}}{A_{x(1)}}\right)_p \Big/ \left(\frac{A_{x(2)}}{A_{x(1)}}\right)_s = \left(\frac{\sigma_{x(2)} N_{x(2)}}{\sigma_{x(1)} N_{x(1)}}\right)_p \Big/ \left(\frac{\sigma_{x(2)} N_{x(2)}}{\sigma_{x(1)} N_{x(1)}}\right)_s \tag{3}$$

where p refers to the product in question and s to the standard material. This can be reduced to the following expression:

$$\left(\frac{N_{x(2)}}{N_{x(1)}}\right)_p = Q\left(\frac{N_{x(2)}}{N_{x(1)}}\right)_s \tag{4}$$

where Q is obtained solely from the areas of the peaks in question. This expression removes the need for determining the detection efficiency of each oligomer, for the purpose of comparison with a standard product. The only assumption in this case is that the detection efficiency for a given oligomer type is constant between samples. Equation (4)

can be applied to every oligomer in the spectra, resulting in Q values that can be plotted as a function of the number of repeat units. For illustration, such a procedure was applied to the comparison of the mono-glycidyl and diglycidyl species in PBAE 4000 and PBAE 6100, where Q represents the ratio of the diglycidyl to mono-glycidyl area fraction, between PBAE 6100 and PBAE 4000. A plot of Q versus the number of repeat units is shown in Figure 6.5. From the equation of the linear fit, some observations can be made. The trend in capping chemistry is virtually the same between the two samples, as indicated by a line slope close to zero and a low scatter of the points about this line. In this situation, the Q value is constant at ~0.34. Therefore, PBAE 4000 contains $1/Q$ or 3 times the amount of diglycidyl species contained in PBAE 6100, relative to the amount of mono-glycidyl species.

Note that certain molecular weight determination methods rely on end-groups. For example, NMR and end-group titration methods can be accurate techniques for the molecular weight determination of polymers, if the number and structure of end groups per oligomer are known with certainty.[1] In certain cases, the MALDI method could be used to assess the validity of these techniques. As an example, a proton NMR spectrum of PBAE 1750 was obtained, from which a molecular weight of 1760 was calculated, assuming all oligomers were present in the diglycidyl form. The MALDI spectrum for this polymer indicates a certain percentage of tri-glycidyl species, implying that the NMR-determined molecular weight is too low. How much it is in error cannot be ascertained in the absence of σ values for the various oligomer forms in the MALDI spectrum. The loss of low mass oligomer data in the MALDI spectrum due to matrix interference could be one reason why the MALDI-determined M_n is substantially higher. As was done for the analysis of PGF, a mass cutoff was established for the purpose of M_n calculation, and in the analysis of PBAE this neglected some of the signal for the low mass oligomers. A cutoff of 930 u was set for PBAE 1750 and 1450 u for PBAE 4000 and 6100.

Some concluding remarks can be made regarding the PBAE samples based on a MALDI analysis. Clearly all three samples contain more than the intended products. The presence of hydrolysis products formed during synthesis, and a distribution in the number of glycidyl groups seems likely. The interesting patterns evident in the spectra raise some questions regarding the nature of the polymerization process. Furthermore, since the use of these resins as prepolymers depends on the extent of glycidyl end-capping, heterogeneity in capping (particularly when there is less than two glycidyl groups per oligomer) could affect the overall structure of a crosslinked polymer.[2] Providing fast access to such information is a strength of the MALDI time-of-flight technique, allowing

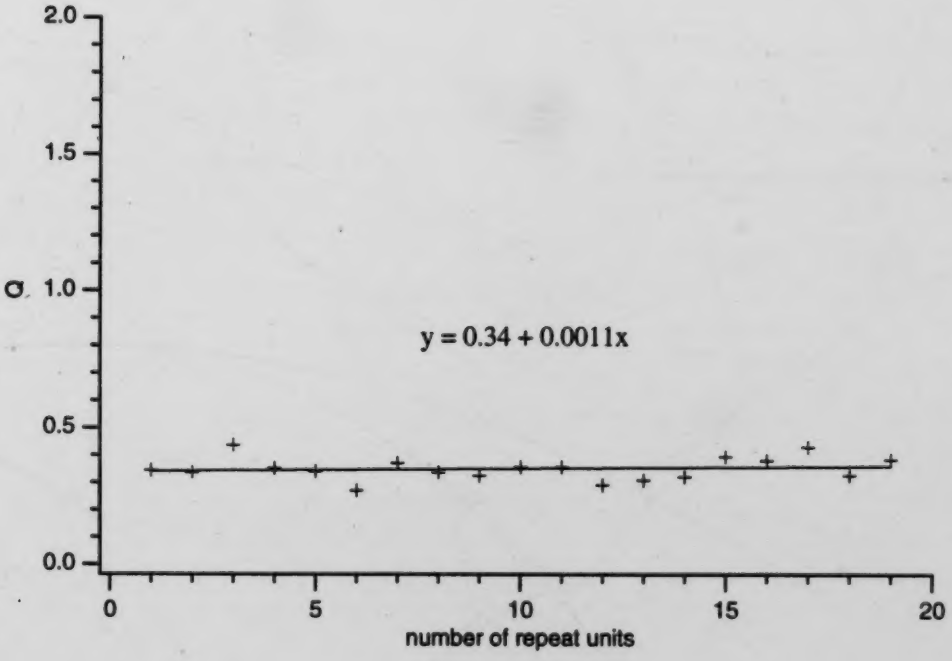

Figure 6.5 Comparison of PBAE 4000 and PBAE 6100 through Q, the ratio of the fraction of diglycidyl species to mono-glycidyl species, over a certain mass range.

for rapid quality control and the ability to "fine-tune" the polymerization procedure to arrive at a more precisely engineered product.

6.3.2 Block/Random Copolymers

The MALDI spectra of alternating copolymers (and homopolymers) are relatively easy to interpret by inspection, due to the existence of a well-defined repeat unit. The spectra of block or random copolymers can be much more complex. For these polymers, there exists no definite repeat unit, i.e., they contain a much higher degree of compositional heterogeneity than do alternating copolymers. This heterogeneity arises from the molecular weight as well as sequence differences from oligomer to oligomer, and translates into a greater demand on instrumental resolution and mass accuracy to extract structural and compositional information. In the spectra of homopolymers, the mass of the monomer is generally self-evident, therefore a probable end-group mass can be determined. These two pieces of information are often sufficient for establishing the overall polymeric structure. However, in the analysis of block and random copolymers, the specification of monomer and end-group masses will not always be obvious. Two examples are described below to illustrate the extent of compositional information that can be obtained from a MALDI analysis of block copolymers.

Figure 6.6 shows the MALDI mass spectra of a low molecular weight block copolymer poly(propylene glycol-b-ethylene glycol-b-propylene glycol)bis(aminopropyl ether) (PPEP, polymer **III**). Our MALDI time-lag focussing instrument provides unit mass resolution across most of the displayed mass range for this polymer. It is clear from the expansion in Figure 6.6B that there is a pattern of three isotope clusters repeating every 44.03 u, from which one might postulate the presence of ethylene oxide. However, the identity of the other monomer and the end-group is not directly obvious from the spectrum. To elicit compositional information from a well resolved spectrum such as this, one ***requires*** the masses of the end-groups and the copolymerized monomers.

$$CH_3CH(NH_2)CH_2[OCH(CH_3)CH_2]_x[OCH_2CH_2]_y[OCH_2CH(CH_3)]_zNH_3$$

III

Furthermore, if the mass accuracy is poor, there will exist more possible monomer combinations for a given mass than if the accuracy is high. With the current instrument

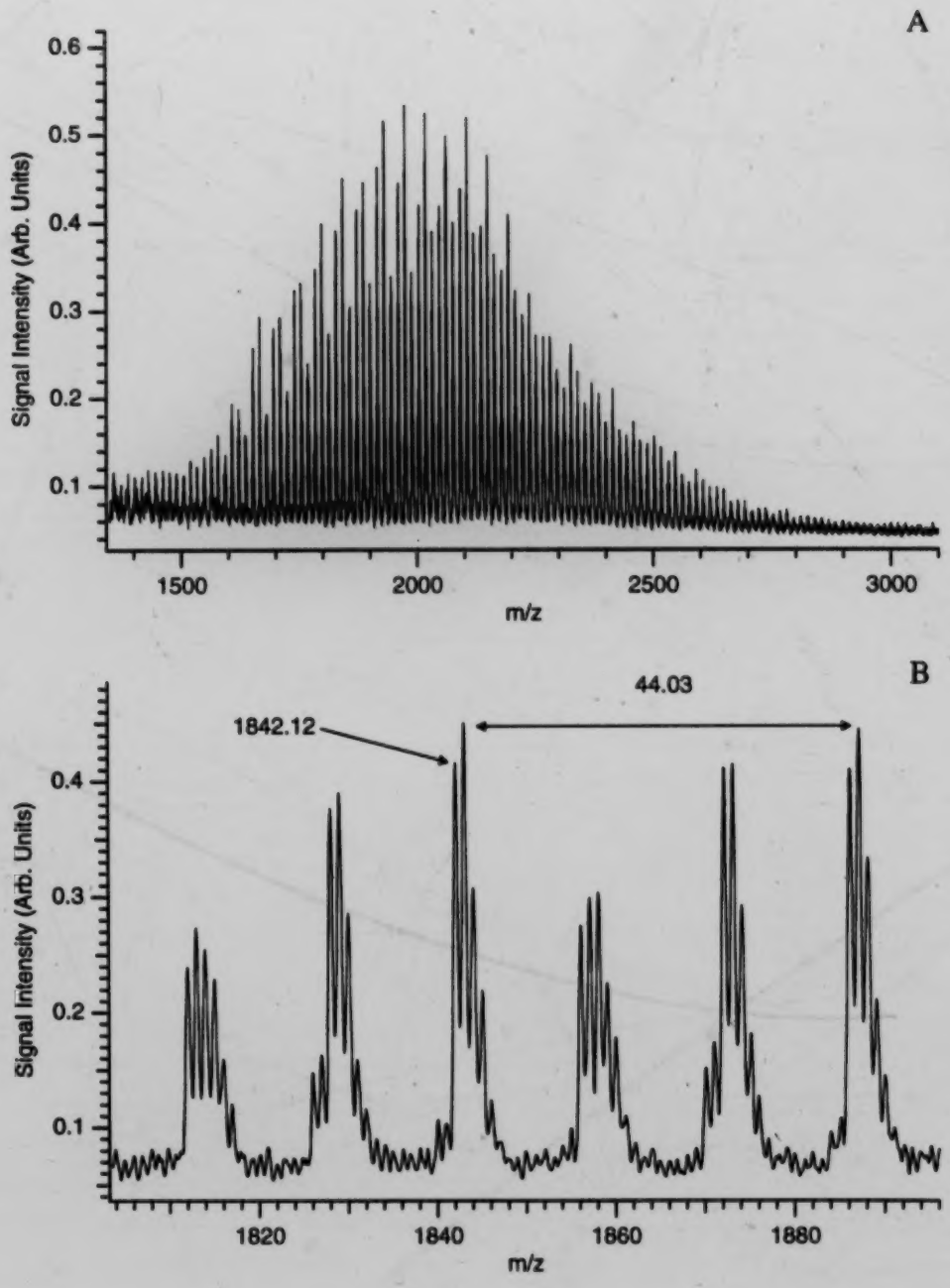

Figure 6.6 MALDI mass spectrum of (A) poly(propylene glycol-b-ethylene glycol-b-propylene glycol)bis(2-aminopropyl ether) with (B) an expansion.

design, an average mass accuracy of 70 ppm externally calibrated can be expected for this polymer. With this accuracy, a single peak representing a monoisotopic mass can be selected from one of the isotope clusters, and assigned a possible monomer composition. For example, the peak with a m/z of 1842.12 has two possible compositions that fall within the accuracy of the mass determination, namely 37 ethylene oxide and 2 propylene oxide monomers (calculated $M+Na^+$ of 1842.13 u), or 8 ethylene oxide and 24 propylene oxide monomers (calculated $M+Na^+$ of 1842.29 u). A more extensive mass range can be considered, as Table 6.1 demonstrates. This table shows that for a series of peaks with a mass difference corresponding to one ethylene oxide monomeric unit, one composition is favored over the other for the above-stated peak, that of 37 ethylene oxide and 2 propylene oxide monomers. The spectrum can be checked for self-consistency as a test for the validity of this assignment. The (37 ethylene oxide)/(2 propylene oxide) composition is confirmed through inspection of the rest of the distribution, as each peak in the spectrum could be assigned using this composition as a starting point. This is not true of the (8 ethylene oxide)/(24 propylene oxide) formulation, as there are peaks that could not be assigned using this composition as the starting point.

Table 6.1 Comparison of experimental mass data and calculated values for several peaks shown in Figure 6.6.

Measured Mass	Proposed (EO/PO)*	Calculated Mass	Mass Acc. (%)	Proposed (EO/PO)*	Calculated Mass	Mass Acc. (%)
1798.03	(36/2)	1798.10	0.004	(7/24)	1798.26	0.013
1842.12	(37/2)	1842.13	0.001	(8/24)	1842.29	0.005
1886.12	(38/2)	1886.15	0.002	(9/24)	1886.31	0.010
1930.18	(39/2)	1930.18	0.000	(10/24)	1930.34	0.008
1974.16	(40/2)	1974.21	0.002	(11/24)	1974.37	0.010
2018.11	(41/2)	2018.23	0.006	(12/24)	2018.39	0.014
2062.11	(42/2)	2062.26	0.008	(13/24)	2062.42	0.015
2106.10	(43/2)	2106.29	0.009	(14/24)	2106.45	0.016

*The ratio between the number of ethylene oxide repeat unit and the number of propylene oxide repeat unit.

All peaks in the spectrum were then assigned relying on the combination of mass accuracy and self-consistency tests. A complete analysis of the resulting data reveals that each oligomer contains 28-61 ethylene oxide monomers, and 0-6 propylene oxide oligomers. The distribution of propylene oxide monomers appears to be independent of the ethylene oxide content.

Table 6.2 contains the peak assignments for a typical repeat pattern as is found in the spectrum of Figure 6.6B. These assignments identify the monoisotopic form of the indicated oligomers, and provide an appreciation for the problem of block or random copolymer analysis by MALDI. Within a 30 u mass window, five oligomers are represented. This spectral congestion would only worsen with increased compositional heterogeneity. Note that sequence information is beyond the capability of current one dimensional MS techniques. Therefore, while it is possible to conclude that this sample is not a blend of homopolymers, it is not possible to determine if this sample is a random copolymer or a block copolymer. The assistance of NMR-based techniques, for example, would be required to obtain this information.[8,9]

Table 6.2 Assignment of peaks detected for a typical repeat unit shown in Figure 6.6.

Measured Mass	EO*	PO*
1856.14	36	3
1858.11	40	0
1870.13	35	4
1872.15	39	1
1886.15	38	2

*EO represents the number of ethylene oxide repeat unit and PO represents the number of propylene oxide repeat unit contained in the oligomer.

A report on the MALDI analysis of a block copolymer consisting of styrene and methylstyrene monomers has been published, whereby the average molar composition

could be determined, as well as the compositional distribution of two monomer types.[4] A resolution (m/Δm) of approximately 275 was achieved for the separation of all the oligomers. However, mass accuracy was not sufficient to allow a unique assignment of the peaks, requiring the aid of an NMR study. In the above analysis of PPEP, a resolution of approximately 2600 allowed isotope separation across the entire distribution, and mass accuracy sufficient for unique peak identifications. This comparison underscores the importance of achieving the best possible resolution and mass accuracy.

A computer-assisted approach would be useful here, where spectral simulations could be performed and fit to the experimental spectrum to obtain the relative intensities of assigned peaks. Various compositional iterations could be assessed, to arrive at the best fit to the data. Such an approach becomes essential for the extraction of relative oligomer compositions and overall average polymer composition where overlapping isotopic distributions from oligomers occur. Although the isotope pattern overlap for different oligomers is identifiable (Figure 6.6B), the relative contributions of the different oligomers to the pattern cannot be determined directly by inspection. Of course, the determination of polymer composition by MALDI analysis relies on the validity of extracting quantitative data across the range of composition expressed by the sample. For structurally very similar polymeric systems such as poly(ethylene glycol) and poly(propylene glycol) or polystyrene and polymethylstyrene, the assumption of uniform detection efficiency may be valid. In light of the preceding discussion on quantitation in MALDI, it is necessary to have supporting evidence of uniform detection efficiency.

The situation becomes more complex with an increase in polymer molecular weight and compositional heterogeneity. This is demonstrated in Figure 6.7 for the analysis of ethylene oxide/propylene oxide copolymers from Dow Chemical. The expansion of the spectrum for one of the samples, Dow Polyol B, is shown in Figure 6.8. At low mass, sufficient resolution exists to allow an analysis similar to that performed on PPEP. This permits a probable oligomer composition to be assigned for a well resolved peak. However, at higher mass a number of difficulties arise to thwart an analysis by inspection. Where there is still unit mass resolution, the opportunity for determining monomer composition exists but the isotopic envelopes begin to include two *or more* possible oligomer compositions. It becomes unclear which peaks in the envelope correspond to the monoisotopic masses of the oligomers. Obviously, the left-most isotope peak in an isotope distribution corresponds to the monoisotopic peak of one (or more) oligomers in this mass range, but when *partial* oligomer overlap occurs, all the contributing monoisotopic peaks cannot be readily identified. This prevents a visual inspection of the spectrum for the

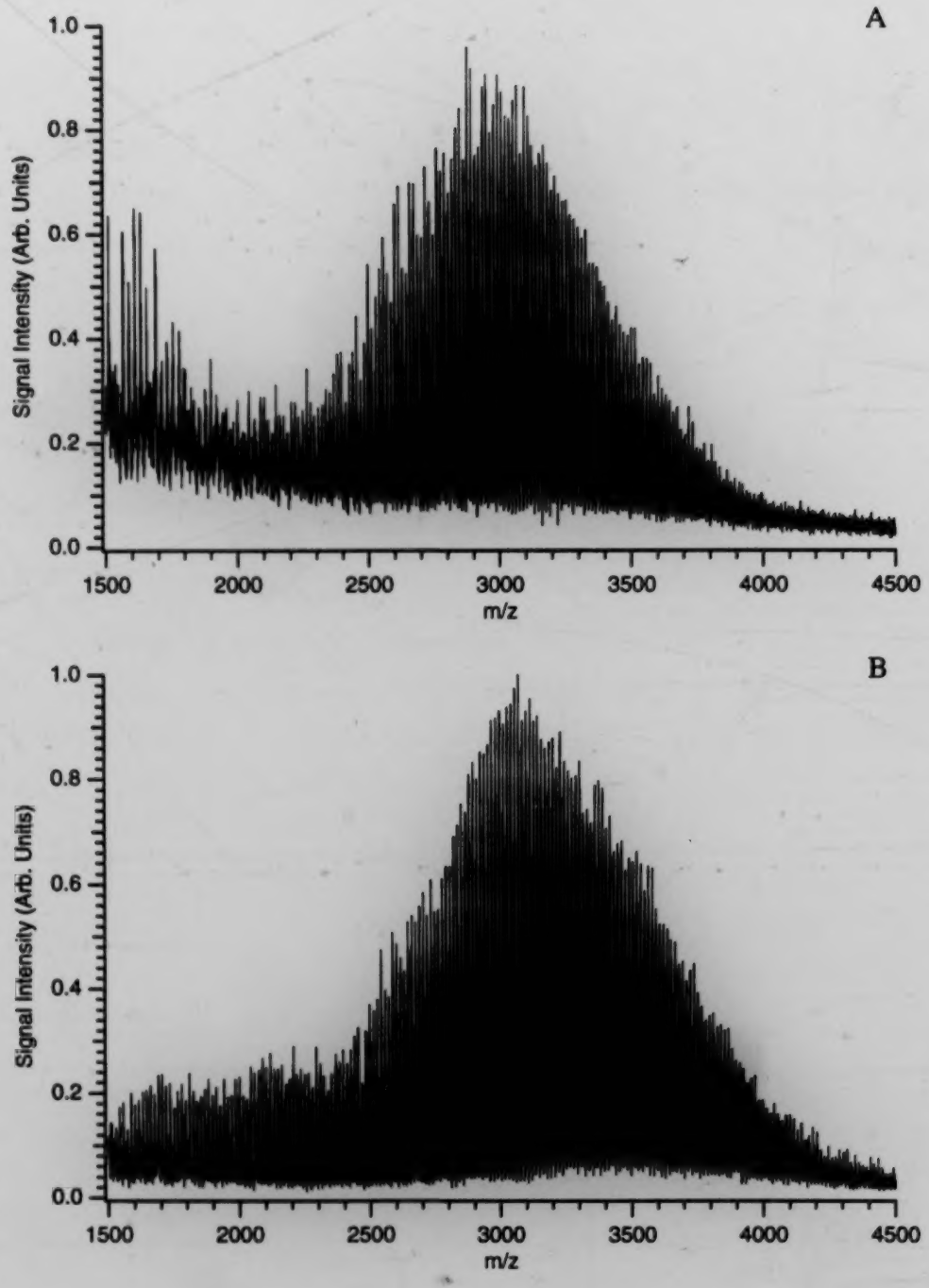

Figure 6.7 MALDI mass spectra of (A) Dow Polyol A and (B) Dow Polyol B.

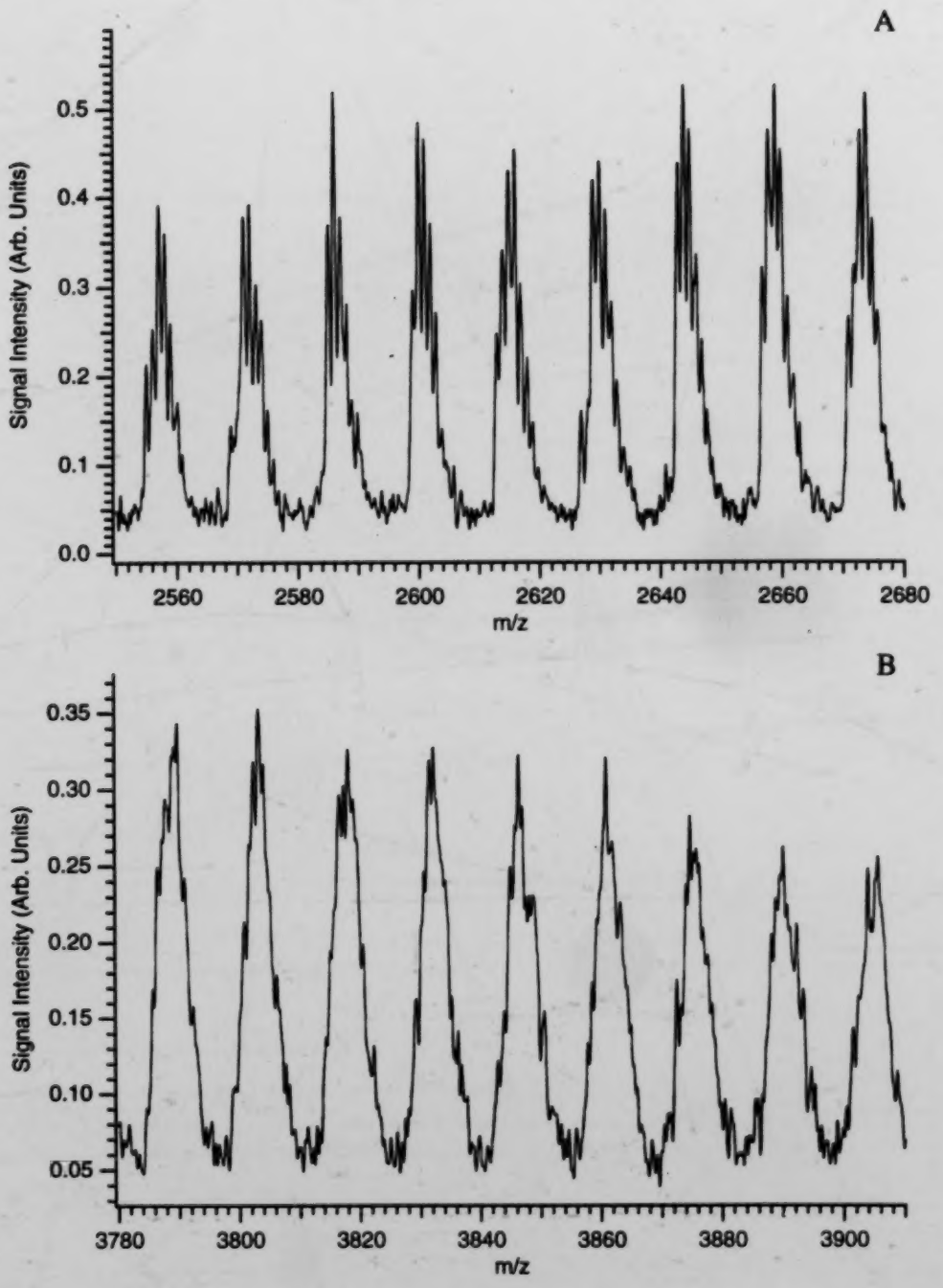

Figure 6.8 Expansions of the MALDI mass spectrum of Dow Polyol B showing (A) the low mass region and (B) the high mass region.

determination of the monomer distribution for each oligomer, as was done for PPEP in Table 6.2. With still higher mass, loss of unit mass resolution, combined with the greater number of possible oligomer compositions prevents the determination of oligomer composition.

In conclusion, the benefits of high resolution and mass accuracy as provided by time-lag focussing time-of-flight mass spectrometry have been extended to the determination of compositional information. Experimental demands are greater than for simple structural validation, as uniformity in the detection of all species in the sample is required. When independent confirmation of uniformity can be determined, then substantial compositional information can be obtained. If independent confirmation cannot be determined, then a conformational analysis based on peak area determinations is cast into doubt. However, for the purpose of quality control or validation against a reference material, detailed information on an oligomer-by-oligomer basis can be recovered. Generally, random and block copolymer analysis by time-of-flight is limited to lower masses than alternating copolymers. This is due to the increased demands on resolution and mass accuracy imposed by increased spectral congestion and compositional heterogeneity.

6.4 Literature Cited

(1) Elias, H.-G. *Macromolecules;* 2 ed.; Plenum Press: New York, 1984; Vol. 1.

(2) Allcock, H. R.; Lampe, F. W. *Contemporary Polymer Chemistry;* 2 ed.; Prentice-Hall: New Jersey, 1990.

(3) Elias, H.-G. *Macromolecules*; Plenum Press: New York, 1984; Vol. 2.

(4) Wilczek-Vera, G.; Danis, P. O.; Eisenberg, A. *Macromolecules* **1996**, *29*, 4036.

(5) Danis, P. O.; Karr, D. E.; Westmoreland, D. G.; Piton, M. C.; Christie, D. I.; Clay, P. A.; Kable, S. H.; Gilbert, R. G. *Macromolecules* **1993**, *26*, 6684.

(6) *Modern Methods of Polymer Characterization*; Barth, H. G.; Mays, J. W., Ed.; John Wiley and Sons: New York, 1991; Vol. 113.

(7) *Determination of Molecular Weight*; Cooper, A. R., Ed.; John Wiley and Sons: New York, 1989; Vol. 103.

(8) *Hyphenated Techniques in Polymer Characterization*; Provder, T.; Urban, M. W.; Barth, H. G., Ed.; American Chemical Society: Washington D.C., 1994; Vol. 581.

(9) *Multidimensional Spectroscopy of Polymers*; Urban, M. W.; Provder, T., Ed.; American Chemical Society: Washington, D.C., 1995; Vol. 598.

(10) *Analysis of Polymer Systems*; Bark, L. S.; Allen, N. S., Ed.; Applied Science Publishers: London, 1982.

(11) Whittal, R. M.; Li, L. *Anal. Chem.* **1995**, *67*, 1950.

(12) Nelson, R. W.; McLean, M. A.; Hutchens, T. W. *Anal. Chem.* **1994**, *66*, 1408.

(13) Gusev, A. I.; Wilkinson, W. R.; Proctor, A.; Hercules, D. M. *Fresenius J. Anal. Chem.* **1996**, *354*, 455.

(14) Gusev, A. I.; Wilkinson, W. R.; Proctor, A.; Hercules, D. M. *Anal. Chem.* **1995**, *67*, 1034.

(15) Boyd, R. K. *Rapid Commun. Mass Spectrom.* **1993**, *7*, 257.

(16) Larsen, B. S.; Simonsick, J., W.J.; McEwen, C. N. *J. Am. Soc. Mass Spectrom.* **1996**, *7*, 287.

(17) Burger, H. M.; Muller, H.-M.; Seebach, D.; Bornsen, K. O.; Schar, M.; Widmer, M. *Macromolecules* **1993**, *26*, 4783.

(18) Schriemer, D. C.; Li, L. *Anal. Chem.* **1997**, in press.

(19) Schriemer, D. C.; Li, L. *Anal. Chem.* **1997**, in press.

(20) Whittal, R. M.; Li, L.; Lee, S.; Winnik, M. A. *Macromol. Rapid Commun.* **1996**, *17*, 59.

Chapter 7

Combining Avidin-Biotin Chemistry with Matrix-Assisted Laser Desorption/Ionization[a]

7.1 Introduction

A MALDI procedure adapted to biochemical analysis usually requires the inclusion of a purification procedure, or a means of recognizing only the analyte of interest. Samples extracted from biological systems are complex, and can contain high salt concentrations, lipids and extraneous proteinaceous material that affect the success of the mass analysis. On one level, impurities could prohibit the formation of an effective matrix/analyte sample.[1,2] On another level, the presence of protein contaminants could reduce the information content of the mass spectrum. For example, not all the components of a peptide mixture will necessarily be represented in a MALDI spectrum due to discrimination effects arising in the crystallization, desorption and/or ionization steps.[3]

Several non-covalent affinity interactions for the purification of biochemicals have been incorporated into MALDI. For example, Hutchens has demonstrated a surface-enhanced affinity capture (SEAC) procedure in which lactoferrin could be captured from solution by a single-stranded DNA immobilized to agarose gel particles.[4] These particles containing the bound complexes could then be analysed directly by MALDI time-of-flight mass spectrometry. Selective capture and identification of peptides containing the linear epitope of a protein have also been achieved by immunoprecipitation with monoclonal antibodies.[5] This technique relied on the MALDI mass spectral detection of peptides directly from agarose beads. Recently, Tomer and coworkers extensively investigated the direct analysis of species bound to affinity chromatography supports in a MALDI format.[6] Good sensitivity could be obtained, however the presence of the particulate supports in the matrix material had deleterious effects on resolution and mass accuracy. To overcome these disadvantages resulting from the presence of particles on the probe tip, Williams and coworkers developed a method for elution of the analyte from small volumes of chromatographic supports.[7] The supernatant could then be directly analysed by MALDI. An alternative approach for improving MALDI performance has involved the chemical

---

[a] A form of this chapter has been published: Schriemer, D.C.; Li, L. "Combining Avidin-Biotin Chemistry with Matrix-Assisted Laser Desorption/Ionization Mass Spectrometry" *Anal. Chem.*, **1996**, 68, 3382-3387.

derivatization of the probe tip to generate a flat surface containing the affinity product.[8] The matrix would then be deposited directly on this surface.

The avidin-biotin interaction is an attractive candidate for incorporation into the MALDI technique. This interaction is being used extensively in molecular biology, biochemistry, analytical biochemistry, histochemistry, and cytochemistry.[9-11] Its appeal lies in the extremely strong affinity of avidin for biotin, having an association constant on the order of 10^{15} M^{-1}. Some of the more common uses of the avidin-biotin interaction include non-radioactive enzyme immunoassays, glycoconjugate analyses and DNA detection.[11] Probe molecules can be biotinylated, usually without loss of activity, and can be used with an avidin-based detection system for the identification of proteins[9] and nucleic acids.[12] It has also found use in cell separation[13] and cytochemical staining.[14] The interaction can also be used for the direct purification of avidin or biotin-containing systems, and forms the basis of avidin-biotin affinity chromatography.[15,16] As an example, single stranded DNA can interact with its complementary biotinylated oligonucleotide. The resulting complex can be isolated with the appropriate immobilized avidin product.[17] Due to the versatility of this interaction, many immobilizing and tagging procedures have been developed. This has generated a large body of products incorporating either biotin or avidin.

In this chapter, a method is described that allows for the direct incorporation of commercial chromatographic supports containing avidin/biotin species into MALDI. It is shown that the avidin-biotin interaction, though strong in solution, can be overcome under relatively mild conditions, causing elution of the biotinylated species onto the probe tip. A matrix formulation was designed in which the beads could be removed prior to analysis. This retains good resolution and mass accuracy. In this work, several avidin-biotin systems were studied to determine the most appropriate chromatographic products for the direct purification and identification of biotin-peptides.

7.2 Experimental

7.2.1 Biotinylation and Isolation of Peptides and Proteins

The bradykinin and bovine insulin used as test compounds in this study were both purchased from Sigma (St. Louis, MO). The biotinylated species were synthesized, with the exception of biotin-insulin (Sigma). The structures for the biotin derivatives used in this study are provided in Chart 1.

Chart 1

Name	Structure	Spacer Arm Length (Angstroms)
NHS-biotin	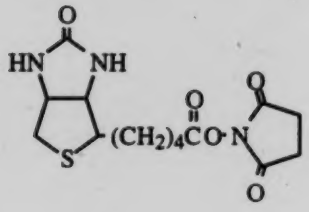	13.5
NHS-LC-biotin	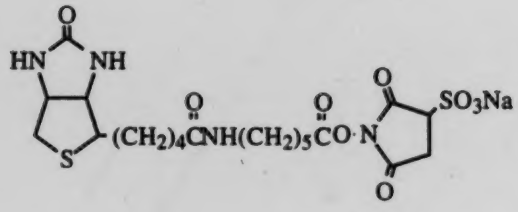	22.4
NHS-SS-biotin	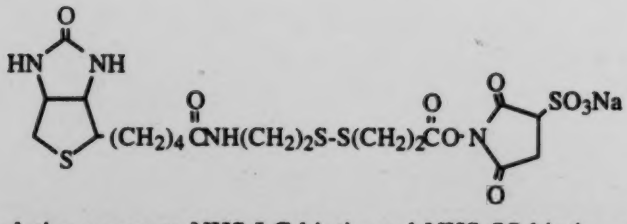	24.3

The biotinylation reagents NHS-LC-biotin and NHS-SS-biotin were purchased from Pierce (Rockford, IL). NHS-Biotin was purchased from Calbiochem (La Jolla, CA). To achieve amine-specific biotinylation, the peptide was dissolved in 0.1 M sodium bicarbonate buffer (pH 8.5), to which was added an excess of the relevant biotinylation reagent in solution form.[18] The NHS (N-hydroxysuccinimide) esters of biotin are reactive towards amines. Reactions were carried out at room temperature for under six hours, whereupon the excess reagent was quenched by addition of excess ethanolamine. NHS-biotin was dissolved in N,N-dimethylformamide prior to addition to the peptide solution, while NHS-LC-biotin and NHS-LC-biotin reagents were dissolved in water.

Biotinylated species were isolated from solution using various immobilized avidin products. Tetrameric avidin directly immobilized on crosslinked, beaded agarose (Pierce, catalog number 20219) was used, as well as a proprietary immobilized monomeric avidin product, also on beaded agarose (Pierce, catalog number 20228). Streptavidin immobilized

on beaded agarose (Sigma, catalog number S-1638) was also used. The beads were added to the solution containing the biotinylated species, buffered with phosphate-buffered saline (PBS: 0.1 M sodium phosphate, 0.15 M NaCl, pH 7.2), and incubated with agitation for approximately 10 minutes. The resulting slurry was then centrifuged to settle the beads, and the supernatant drawn off. Several washing cycles were carried out, with PBS followed by deionized water. One µl or more of settled gel could be handled in this fashion. The beads were then resuspended in a minimum amount of water to produce a 50 % (v/v) slurry (2-10 µl). This slurry was then sampled for MALDI analysis.

7.2.2 Instrumentation

All MALDI experiments were conducted on a model G2025A MALDI time-of-flight system (Hewlett Packard, Palo Alto, CA), equipped with a pulsed nitrogen laser (337 nm radiation). This instrument was operated in positive mode at high voltage (28 kV). In general, 100 laser shots were averaged to produce a mass spectrum. Spectra were acquired and processed with Hewlett Packard supporting software, and reprocessed with the Igor Pro software package (WaveMetrics, Inc., Lake Oswego, Oregon) for presentation. For the mass range examined in this chapter, the average error in mass determination for this instrument was ~0.05% based on external calibration.

7.2.3 MALDI Sample Preparation

The matrices used in this work were α-cyano-4-hydroxycinnamic acid (HCCA) and sinapinic acid (SA). Both matrices were purchased from Aldrich (Milwaukee, WI). A schematic of the sample preparation procedure is shown in Figure 7.1. A layer of matrix (dissolved in acetone, 25 mg/ml) was first applied to the MALDI probe tip, forming a dense layer of small crystals.[19] One µl of the bead slurry (in water) was then added and allowed to dry partially. An aliquot of a second matrix solution could then be applied. The composition of this second matrix solution varied, with the proviso that it be saturated with the matrix to prevent dissolution of the bottom layer. The application of this second solution and the dehydration of the beads resulted in the elution of the bound species, and the incorporation of these species into the matrix crystals. Upon complete drying, the beads were blown off with a stream of dry nitrogen. All solution samples were analysed in a similar fashion; the analyte was diluted with the second matrix solution and deposited on the first matrix layer.

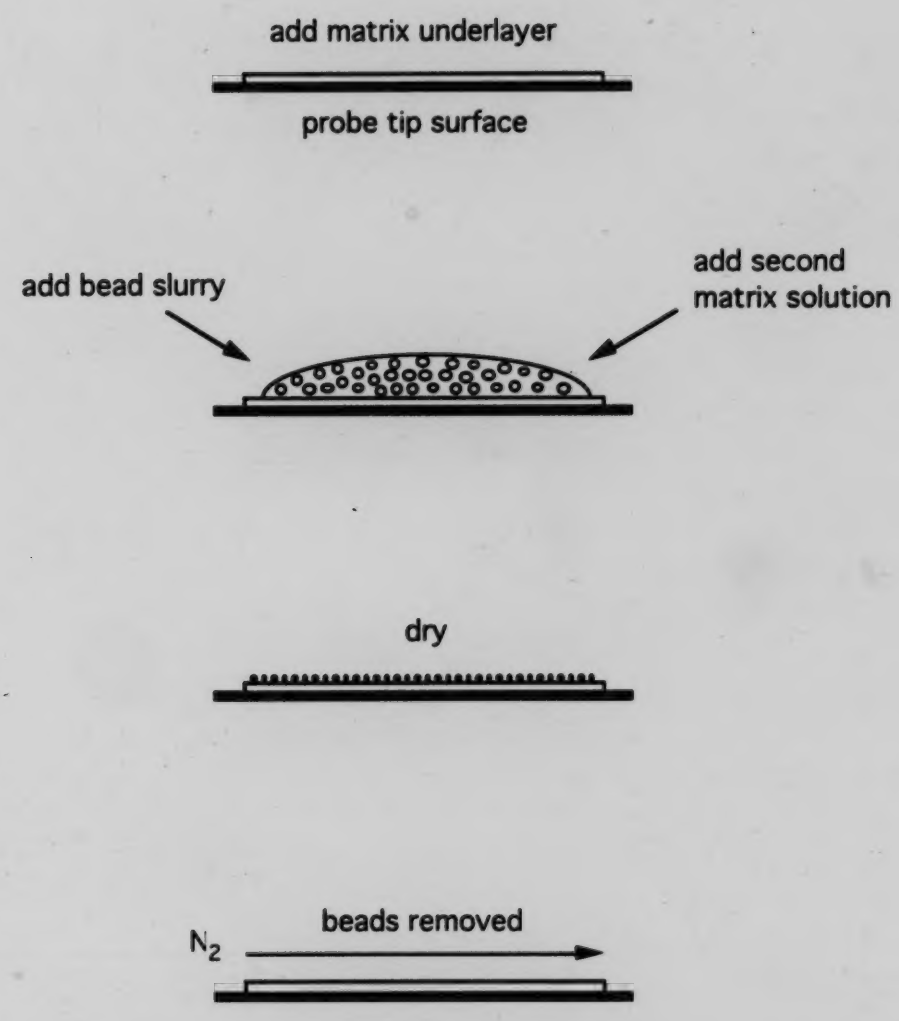

Figure 7.1 Schematic of the MALDI procedure for the analysis of biotinylated species complexed to avidin, immobilized on agarose beads.

7.3 Results and Discussion

Rather than designing specialized surfaces for affinity trapping, it was decided that a technique based on preexisting avidin-biotin technology would be the easiest to incorporate into the biochemical mass spectrometric laboratory. Preliminary work has demonstrated the feasibility of directly analysing immobilized avidin chromatography products.[20,21] Various commonly used biotinylation reagents as well as a number of commercially available avidin products immobilized on chromatographic supports were investigated for their ability to allow for rapid purification and mass analysis of mixtures containing biotinylated peptides.

7.3.1 Biotinylation Reagents

An array of biotinylation products exist that differ primarily according to their reactivity and length of the spacer arm between the reactive site and the biotin moiety. Reagents reactive towards amines, carbohydrates, carboxyls and sulfhydryls can be purchased, with varying spacer-arm lengths geared to adjust the strength of the interaction with avidin.[11] Products are also available that allow for chemical cleavage of the biotin tag from the biotinylated species. Three products were initially chosen for investigation, all of which are reactive towards primary amines (see Chart 1).

The neuropeptide bradykinin was chosen as a test compound. While this peptide does not contain any lysines, the NHS esters of biotin can react with the free amine of the N-terminus. Figures 7.2A-C shows the spectra obtained after the biotinylation of bradykinin with the three reagents in Chart 1. Each spectrum represents the analysis of ~0.5 pmol of total peptide. The mixtures were then incubated with immobilized tetrameric avidin in PBS. After washing with PBS and water to remove the unreacted bradykinin, the beads were applied to the probe tip as described in the experimental section, and blown off the probe tip after drying. This was possible as the beads did not aggregate with the matrix on the probe tip. The second matrix solution in all three cases consisted of a 1:2:3 solution of formic acid:2-propanol:water (FA/2P/H_2O) saturated with HCCA.[3] Figures 7.2D-F displays the spectra of the purified biotin-bradykinin samples. Each of these spectra represents approximately 0.5 pmol total peptide before application of the beads (peptide concentration of 15 nM before purification). Excellent purification and S/N were obtained for biotin-LC-bradykinin and biotin-SS-bradykinin, while relatively poor results were obtained for biotin-bradykinin.

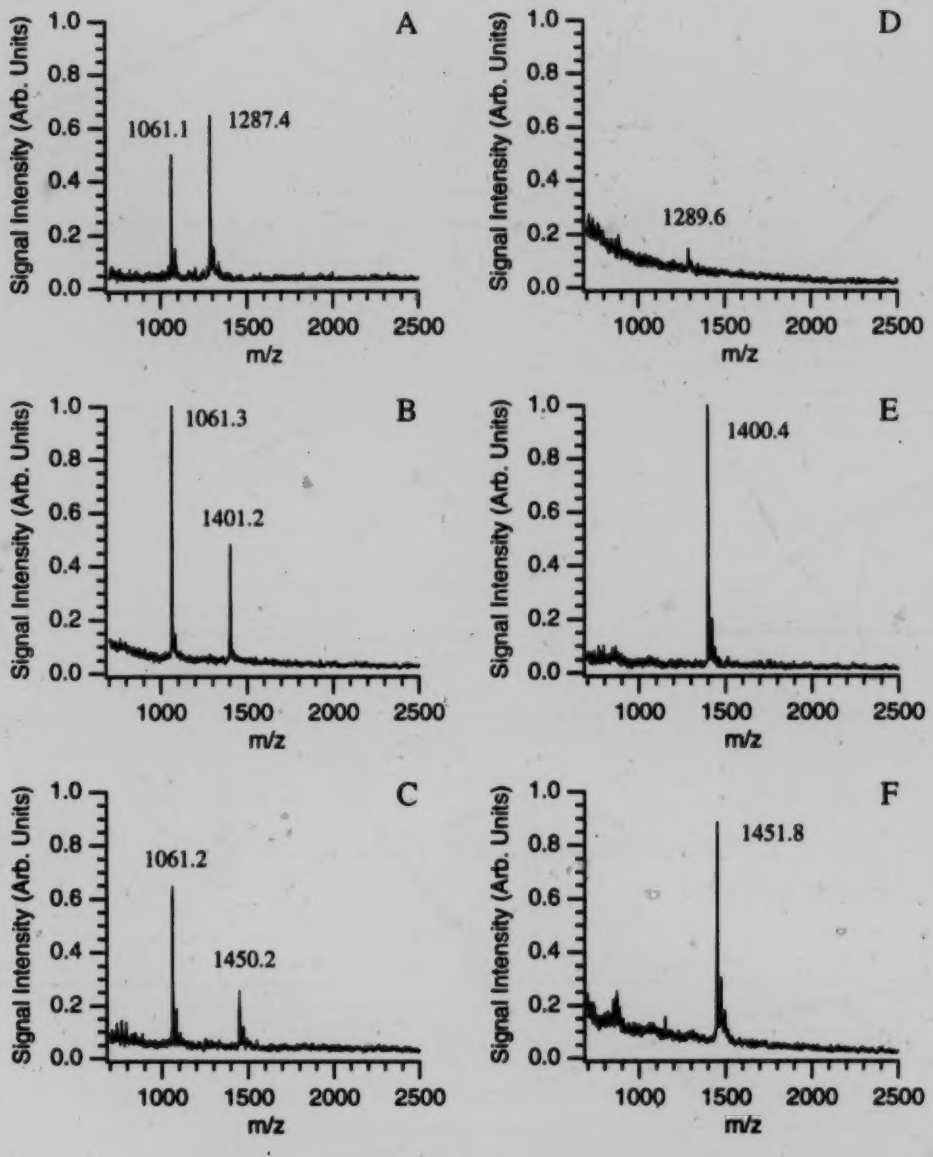

Figure 7.2 MALDI mass spectra of bradykinin (expected MH^+ = 1061.2 u) and (A) biotin-bradykinin (expected MH^+ = 1287.5 u), (B) biotin-LC-bradykinin (expected MH^+ = 1400.7 u) and (C) biotin-SS-bradykinin (expected MH^+ = 1450.8 u) reaction mixtures from HCCA. MALDI mass spectra of (D) biotin-bradykinin, (E) biotin-LC-bradykinin and (F) biotin-SS-bradykinin from HCCA, after purification with immobilized tetrameric avidin.

The poor result shown for biotin-bradykinin was likely due to the weak interaction between the short chain biotin-bradykinin and the immobilized avidin, resulting in elution of the analyte during washing. It is known that steric hindrance can attenuate the strength of the avidin-biotin interaction. Long chain spacers are added in biochemical applications in order to increase the strength of this interaction by overcoming steric hindrance to binding.[11] This is particularly important for the analysis of larger proteins where the site of biotinylation could be somewhat buried. The site of biotinylation in this peptide is the amino terminus (biotin NHS esters do not react with the guanidino group of arginine). Arginine is the amino acid on the N-terminal. Consequently, the binding to the avidin through the biotin tag could be somewhat hindered by the presence of the fairly long side chain on this amino acid. An alternative explanation is that the short chain biotin-bradykinin was bound so tightly that the matrix formulation did not lead to elution. Monomeric avidin, immobilized on beaded agarose, exhibits a lower biotin association constant than tetrameric avidin (approximately $2 \times 10^7\ M^{-1}$).[22] When applied to bradykinin biotinylated in the above ways, it was found that good spectra representing biotin-LC-bradykinin and biotin-SS-bradykinin could be obtained after purification, but not for biotin-bradykinin. This provides confirmation of the hypothesis that biotin-bradykinin binds less strongly than the species with the longer chain spacers.

Biotinylation reagents with cleavable side chains have been developed to allow for the recovery of the tagged species after forming the strong avidin-biotin interaction. These reagents provide an attractive feature in the MALDI analysis, namely the confirmation of biotinylation. One such reagent is NHS-SS-biotin (Chart 1), which contains a cleavable disulphide group. Applying one µl of 50 mM dithiothreitol (DTT) to the beads on the probe tip, prior to the addition of the second matrix solution, results in significant disulphide reduction. Bradykinin was derivatized with this reagent, and analysed in the above fashion, with the inclusion of the on-probe reduction. The spectrum is shown in Figure 7.3. The peak at m/z 1451.1 indicates protonated biotin-SS-bradykinin (expected MH^+ = 1450.8 u), while the peak at m/z 1150.2 results from the protonated reduced product (expected MH^+ = 1149.4 u). Note that application of DTT did not appear to reduce the quality of the matrix formulation, provided that the sample spot was washed with cold water before analysis.

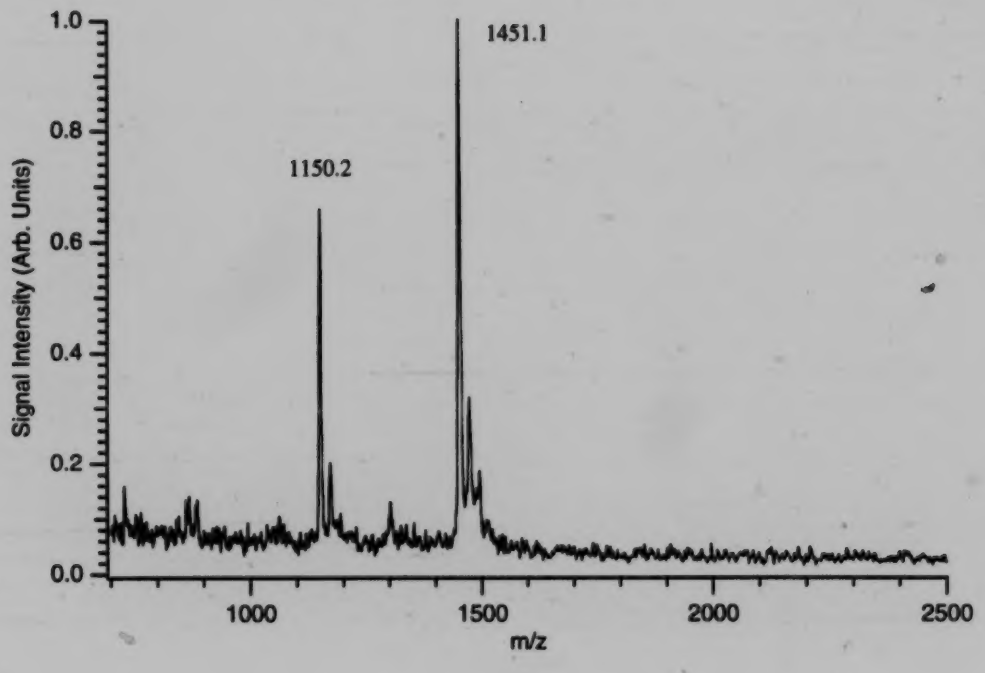

Figure 7.3 An on-probe reduction of the disulphide spacer between biotin and bradykinin. The mass spectrum was obtained from the same solution as used for Figure 7.2F.

7.3.2 Immobilized Avidin/Biotin

Biotinylated bovine insulin was used as the analyte in the assessment of various immobilized avidin/biotin products. This species binds strongly to avidin, even with a short chain spacer arm. Insulin is a challenging species for this work since it proved to be a very "sticky" compound; vigorous washing was necessary to overcome non-specific binding to the chromatographic support. Figure 7.4A shows the spectrum of biotinylated insulin, revealing that the sample contains non-biotinylated insulin (expected MH^+ = 5734.6 u) as well as the mono-, di- and tri-biotinylated analogues, as indicated by the progressive 226 u mass shifts. In this protein, there are only three likely sites for biotinylation via primary amines (two alpha amino groups and the side chain of lysine). It should be noted that the mass increment from the biotinylation unit in this case (226.3 u) roughly corresponds to the common adduct ions from sinapinic acid (206, 224 u). The weaker peaks corresponding to insulin-$biotin_3$ observed at an m/z of ~6414 in Figure 7.4 have a higher degree of error due to overlap with the sinapinic acid adducts of insulin-$biotin_2$.

The following four immobilized species have been incorporated into this work:

1. Tetrameric avidin immobilized on beaded agarose. Avidin, being a protein consisting of four identical subunits, binds biotin very strongly ($K_a \sim 10^{15} M^{-1}$).

2. Monomeric avidin immobilized on beaded agarose. The isolated subunits or monomers of avidin bind biotin with a K_a of $\sim 10^7 M^{-1}$. This immobilized monomeric avidin has been marketed as a platform for the reversible coupling of biotinylated species. This product still contains an unknown amount of tetrameric avidin which must first be blocked by biotin before application of analyte.

3. Streptavidin immobilized on beaded agarose. Avidin is a glycoprotein, with a very high pI value (approximately 10). As such, it is prone to contamination by non-specific binding. Streptavidin, also a biotin-binding protein of similar size, has a more neutral pI (5-6) and does not possess any carbohydrate, therefore it is postulated to be less prone to non-specific binding.[11] The biotin-binding site appears to be buried more deeply,[23] necessitating long chain spacer arms between the biotin and analyte.

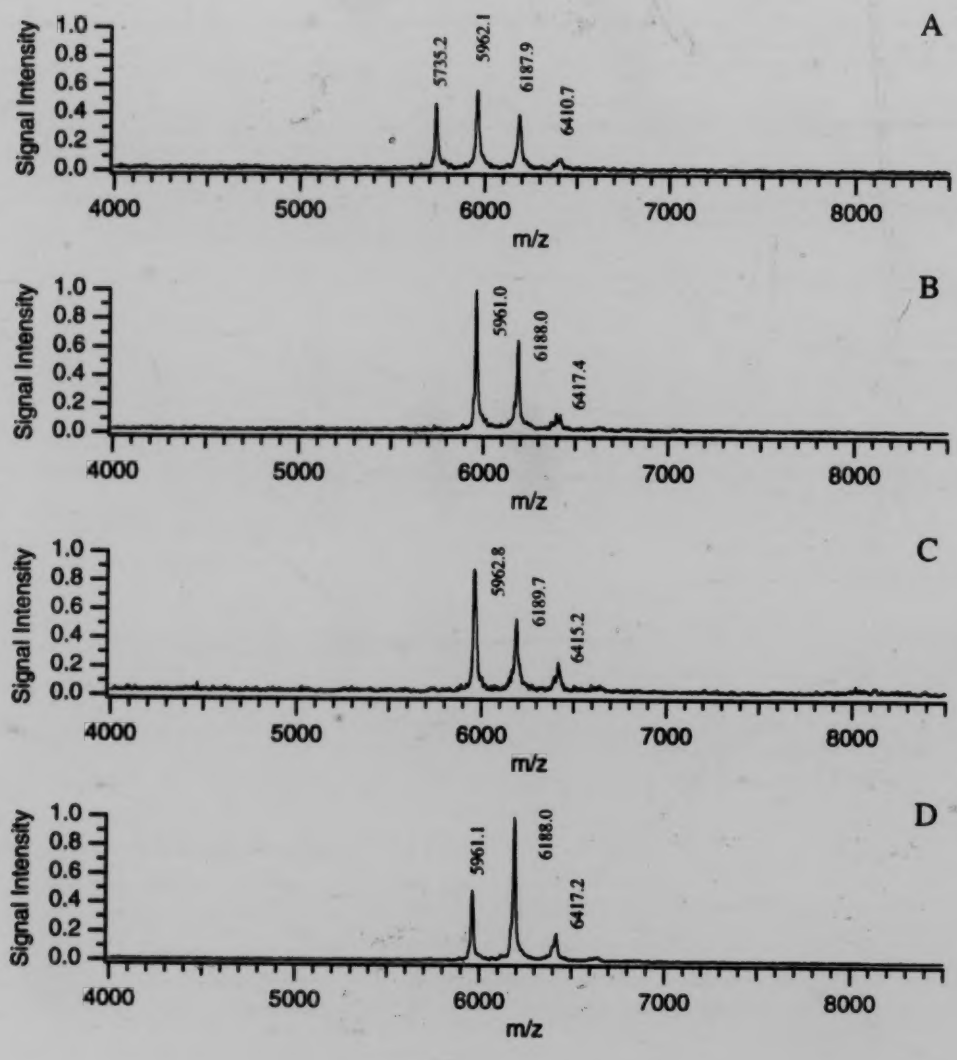

Figure 7.4 (A) Mass spectrum of biotin-insulin from SA with approximately 0.5 pmol total protein loaded. Expected MH^+ values are 5734.6 u (insulin), 5960.9 u (insulin-biotin), 6187.2 u (insulin-biotin$_2$), and 6413.5 u (insulin-biotin$_3$). Mass spectra demonstrating the purification of biotin-insulin using (B) immobilized tetrameric avidin, (C) immobilized biotin, where the biotin-insulin was complexed with avidin in solution prior to purification with the beads, and (D) immobilized monomeric avidin.

4. Biotin immobilized on beaded agarose. Avidin-biotin technology has been applied in conjugated or hyperextended fashion (e.g., enzyme-linked immunosorbent assay (ELISA) techniques). There are situations where it may be advantageous to start with immobilized biotin, and have it bind with other biotinylated species through avidin.[9]

Figures 7.4B to 7.4D show the mass spectra of the purified biotinylated insulin samples obtained using three of the above purification schemes: immobilized tetrameric avidin, immobilized biotin with avidin, and immobilized monomeric avidin, respectively. All the analyses of purified biotinylated insulin used sinapinic acid (SA) as the matrix. A saturated solution of this matrix (in 1:2 acetonitrile: 0.1% trifluoroacetic acid(TFA)) was used for the second matrix application. There was essentially no difference in the results obtained for the tetrameric avidin and the conjugated (biotin-avidin-biotin-insulin) approach, as illustrated in Figures 7.4B and 7.4C, respectively. Immobilized monomeric avidin demonstrated higher non-specific binding characteristics (likely due to increased exposure of the agarose gel), and a greater sensitivity to washing conditions. For example, in purifying the sample of biotinylated insulin, complete removal of insulin required a washing that removed some of the biotin-insulin (singly tagged). This can be seen in Figure 7.4D, where the relative intensities of the biotinylated species as observed in Figure 7.4A was not maintained. This suggests that multiply tagged species bear a stronger affinity for avidin on this chromatographic support.[8] There are two ways this could occur. The overall increase in the strength of binding could be due to a multi-site interaction. Although insulin is a small protein, the flexibility of the agarose support might allow for more than one avidin molecule to interact with a multiply-biotinylated insulin.[11] Conversely, it is possible that the three distinct binding sites on insulin differ in their relative binding strengths with avidin, due largely to steric considerations. The multiply biotinylated insulin analogues would have a greater percentage of these higher-strength binding sites.

The biotinylated insulin sample could not be successfully purified using the streptavidin-agarose product. This is likely because the binding site is deeper in streptavidin than in avidin. Biotinylation of insulin with a biotin reagent containing a long chain spacer (biotin-LC-insulin) allowed for its purification by streptavidin. However, it was found that the non-biotinylated insulin required more extensive washing to remove it from the immobilized streptavidin beads, compared with the immobilized avidin system.

7.3.3 Method of Analyte Elution

While avidin itself can be difficult to denature, the avidin-biotin complex is even more resistant to dissociation. For example, the complex can withstand brief exposure to temperatures as high as 132 °C, although avidin itself is inactivated at 85 °C.[24] The dissociation of biotinylated species from tetrameric avidin usually involves extremes of pH and high chaotropic salt concentrations. Guanidinium chloride at a concentration of 8M and a pH of 1.5 is required for efficient dissociation of the complex.[11] Outside of the 2-13 pH range, the complex dissociates due to the denaturation of the avidin into its subunits.[11] It is desirable to avoid harsh conditions and the introduction of high salt concentrations in the MALDI format. The elution procedures described in the Experimental Section (see Figure 7.1) were found to be very effective, resulting in a sample/matrix preparation that was suitable for the MALDI experiments.

Interestingly, the efficacy of the elution step in the MALDI format did not require low pH or high organic solvent content. Various solvent systems were tested for the second matrix solution. These included FA/2P/H_2O systems in which the acid content was varied from 0 to 17%, and the alcohol content from 0 to 33%. Solutions containing various ratios of CH_3CN/0.1% TFA were also investigated. Both HCCA and SA were investigated. Based on the application of these solutions to the analysis of complexed biotin-LC-bradykinin and biotin-LC-insulin on tetrameric avidin agarose, it was concluded that the composition of the second matrix solution was not critical to the success of the elution step. In fact, elution occurred even when no second matrix solution was added. For example, in the purification of biotin-LC-bradykinin with immobilized tetrameric avidin, allowing the agarose beads to dry from a water slurry on the initial HCCA matrix layer generated a preparation that was as sensitive as when a second, harsh matrix solution was added (HCCA in FA/2P/H_2O).

A similar analysis was performed on purified biotin-LC-insulin, using SA as the matrix. Elution of this species could also be obtained from a water slurry, although the signal strength was somewhat lower than when a second matrix solution was used (SA in CH_3CH/0.1% TFA). Essentially, allowing the beads to dry from a water slurry is analogous to the fast evaporation sample/matrix preparation of Vorm et al.[19] This preparation is not an effective formulation for the analysis of insulin. Therefore, it is possible that the reduced sensitivity observed in the analysis of purified biotin-LC-insulin from a water slurry was due to a poor matrix preparation rather than a poor elution procedure. It should be noted that the second matrix solution itself is insufficient for

eluting the biotin-analyte from immobilized tetrameric avidin. A sample of biotin-LC-insulin was purified with immobilized tetrameric avidin, and then slurried in a harsh second matrix solution (HCCA in FA/2P/H_2O). The supernatant was removed and analysed, but no signal for biotin-LC-insulin was obtained. The importance of these observations is as follows: since the avidin-biotin complex appears to dissociate easily under MALDI sample preparation conditions, the researcher can choose a formulation that is suitable for the species being studied, rather than remaining bound to a formulation necessary for dissociating the complex.

Although this sample deposition technique was developed for the avidin-biotin work, it has proven to be an excellent approach for standard MALDI analyses.[25,26] In conventional MALDI experiments, mixing the analyte with a second matrix solution, followed by deposition on an initial matrix layer produced excellent preparations in terms of sensitivity, tolerance to impurities and ease of washing. This method is somewhat analogous to the crushed crystal method of Beavis,[1] however in our hands appears to be more reproducible as the crushing step is avoided. Both HCCA and sinapinic acid were used successfully in this manner. Various solvent systems could be used for the second matrix solution, including CH_3CN/H_2O and CH_3CN/TFA combinations, as well as FA/2P/H_2O combinations. The best results were obtained with saturated solutions having a concentration no greater than 30 mM (to prevent matrix aggregates from forming). This method was found to be useful for a wide mass range, from small peptides (MW 600) to high mass proteins (>MW 100 000).

7.3.4 Avidin Signal Suppression and the Mechanism of Analyte Elution

Insulin was reacted with NHS-LC-biotin in a 1:1 molar ratio to produce only minor biotinylation of the protein. The spectrum of the final product is shown in Figure 7.5A, which indicates only a single biotinylation in addition to a large fraction of unlabelled insulin. Figure 7.5B shows a mass spectrum resulting from the isolation of biotin-LC-insulin from this mixture, using tetrameric avidin immobilized on agarose beads. It was obtained from beads containing a maximum of 50 fmol biotin-LC-insulin. For ease of handling, 250 fmol of biotin-insulin was extracted with one µl of settled beads, which could be sampled five times. In this analysis, the avidin subunits on the beads were present in excess of the analyte at a molar ratio of ~200:1. The actual analyte concentration in the slurry was 5 nM. A signal-to-baseline noise ratio of 30 was obtained, indicating the good sensitivity of the technique. In this case, the FA/2P/H_2O solution was used. Figure

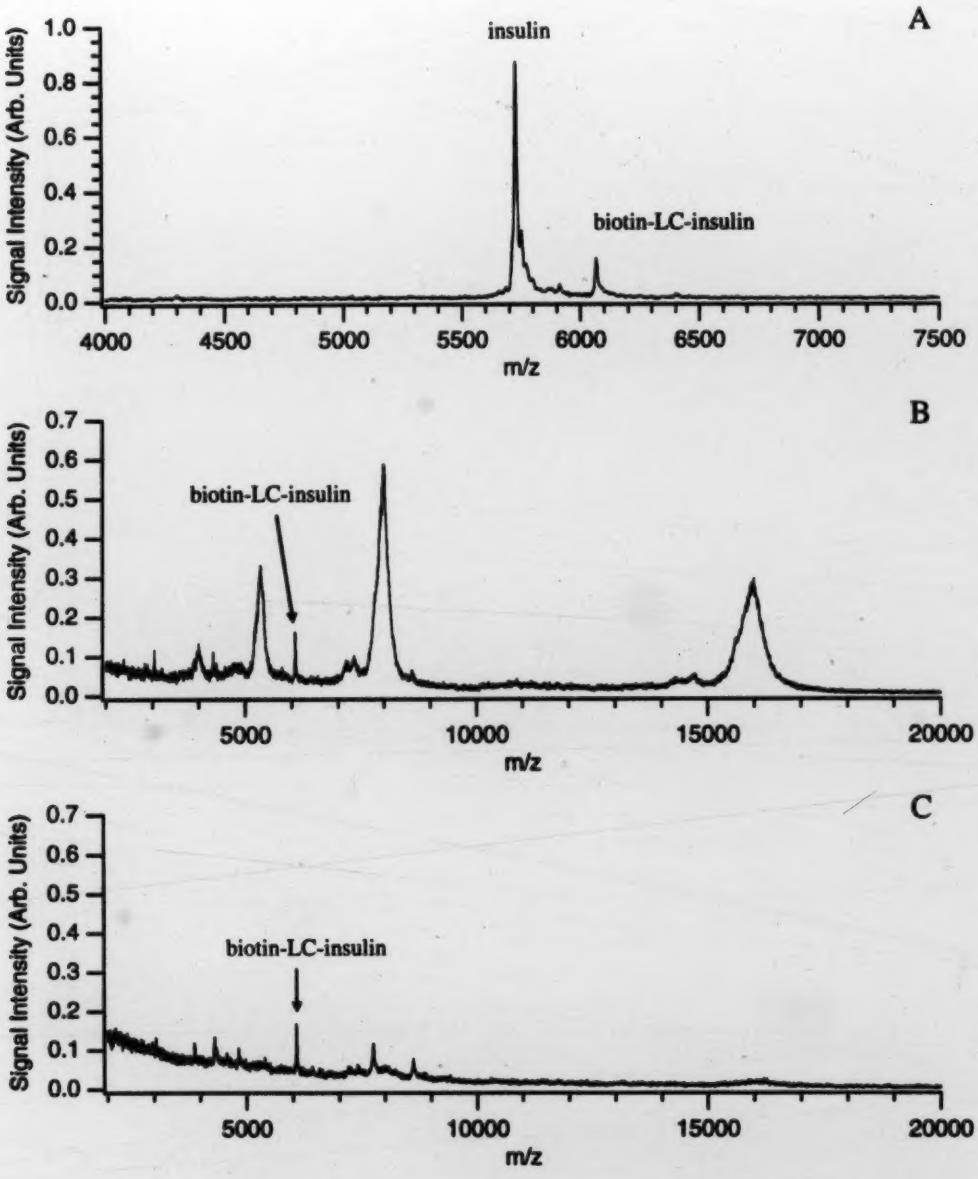

Figure 7.5 Mass spectra showing the sensitivity of the immobilized tetrameric avidin-based procedure: (A) spectrum of the reaction mixture, (B) spectrum from the analysis of 50 fmol of biotin-LC-insulin revealing the strong avidin subunit interference and (C) suppression of the avidin subunit peaks with the addition of an aliquot of a biotin solution.

7.5A also shows several broad peaks arising from the avidin subunits. This is the case for all preparations with a significant acid component. These peaks are broad due to the heterogeneity of avidin imparted by glycosylation. The presence of broad avidin signals causes a serious interference, as they obscure a significant portion of the mass range.

By adding a 1 µl aliquot of an aqueous biotin solution (approximately 8 mM) to the beads on the probe tip prior to the application of the second matrix solution, the avidin signal could be completely suppressed without affecting analyte sensitivity. This is demonstrated in Figure 7.5C, representing the analysis of 50 fmol of biotin-LC-insulin after the application of the biotin solution. When avidin complexes biotin, it is even more resistant to denaturation at low pH than in the uncomplexed form.[11,24] The added biotin effectively binds all the remaining avidin active sites, and prevents its dissociation. As the addition of biotin can suppress the avidin subunit signal, while not affecting the analyte signal, it would seem that denaturing of the avidin is not a prerequisite for obtaining a signal. The observance of avidin signal under the more acidic conditions must arise from the denaturing of *non-complexed* avidin. Therefore, under the MALDI preparation conditions, a denaturation of the avidin-biotin complex appears to be the general mechanism by which the biotinylated species find their way to the probe, which does not require the predissociation of avidin into its subunits.

As indicated earlier, this denaturation does not rely on strongly acidic conditions. It seems that the simple action of dehydration of the beads and complex on the MALDI probe tip provides the necessary energy for biotin release. This could be due to a slight conformational change in and around the active site, causing an decrease in the association constant. Admittedly, the addition of acid to the second matrix application might facilitate the dissociation. No mechanistic information could be derived from the observation of poorer signals when using immobilized streptavidin. This is because streptavidin is both more resistant to denaturation by acid, and conformationally different than avidin.[11]

It was possible to conduct these experiments with the beads retained on the probe tip, in a fashion similar to that used by Papac et al.[6] Removing the matrix underlayer, and simply adding one matrix solution to the beads ensured retention of the beads on the probe tip. There is no benefit to be derived from such a procedure, as shot-to-shot reproducibility was poor due to a poor crystallization environment (matrix aggregates on beads), as was resolution and mass accuracy.

7.3.5 Assessment

The selection of the appropriate protocol will remain somewhat dependent upon the application, but a number of observations can be made on the suitability of the various schemes for MALDI. It is clear from the above that long spacer arms between the biotin and analyte provide the most favorable conditions for analysis by this technique. Where possible, it is also advantageous to incorporate a cleavable spacer arm, to provide confirmation of purification by generating a characteristic mass shift when the spacer arm is cleaved on the probe tip. Regarding the selection of the affinity chromatography product, immobilized tetrameric avidin seems the most attractive. It provides spectra which appear representative of solution composition, allows robust washing and is the least costly product. Furthermore, "subunit suppression" is possible, allowing for high sensitivity across the whole mass range. The immobilized monomeric avidin product contains non-covalently bound avidin subunits that almost always appear in the spectra. These subunits cannot be suppressed with the addition of excess biotin, and therefore limits the usefulness of this product. Using the conjugated approach where the avidin is complexed to the beads by way of immobilized biotin provides a performance very similar to the immobilized tetrameric product, with a minimum of avidin subunits appearing in the spectra. The immobilized streptavidin product could be used in place of tetrameric avidin. It appears to be more resistant to denaturing than avidin in this experimental approach, and provides strong binding to biotin in solution. In certain cases, however, the depth of the binding site may be prohibitive as was demonstrated with biotinylated insulin.

In summary, a highly versatile affinity interaction has been coupled to MALDI time-of-flight mass spectrometry in an analytical technique that allows for rapid purification and mass analysis. Elution of the tightly bound biotinylated species was easily achieved using broadly applicable matrices and matrix preparations. A new matrix preparation was designed that allowed for the beads to be removed from the probe tip, thus avoiding the resolution and mass accuracy problems associated with an uneven matrix surface. An assessment of commonly used avidin/biotin products was undertaken, and for the compounds studied in this work, tetrameric avidin/agarose was deemed most successful.

7.4 Literature Cited

(1) Xiang, F.; Beavis, R. C. *Rapid Commun. Mass Spectrom.* **1994**, *8*, 199.

(2) Billeci, T. M.; Stults, J. T. *Anal. Chem.* **1993**, *65*, 1709.

(3) Cohen, S. L.; Chait, B. T. *Anal. Chem.* **1996**, *68*, 31.

(4) Hutchens, T. W.; Yip, T.-T. *Rapid Commun. Mass Spectrom.* **1993**, *7*, 576.

(5) Zhao, Y.; Chait, B. T. *Anal. Chem.* **1994**, *66*, 3723.

(6) Papac, D. I.; Hoyes, J.; Tomer, K. B. *Anal. Chem.* **1994**, *66*, 2609.

(7) Nelson, R. W.; Krone, J. R.; Bieber, A. L.; Williams, P. *Anal. Chem.* **1995**, *67*, 1153.

(8) Brockman, A. H.; Orlando, R. *Anal. Chem.* **1995**, *67*, 4581.

(9) Wilchek, M.; Bayer, E. A. *Anal. Biochem.* **1988**, *171*, 1.

(10) *Methods in Enzymology: Avidin-Biotin Technology*; Wilchek, M.; Bayer, E. A., Ed.; Academic Press, Inc.: Toronto, 1990; Vol. 184.

(11) Savage, M. D.; Mattson, G.; Desai, S.; Mielander, G. W.; Morgensen, S.; Conklin, E. J. *Avidin-Biotin Chemistry: A Handbook*; Pierce Chemical Company: Rockford, IL, 1994.

(12) French, B. T.; Maul, H. M.; Maul, G. G. *Anal. Biochem.* **1986**, *156*, 417.

(13) Wilchek, M.; Bayer, E. A.; Skutelsky, E. In *Methods in Enzymology: Avidin-Biotin Technology*; M. Wilchek and E. A. Bayer, Ed.; Academic Press, Inc.: Toronto, 1990; Vol. 184; p 340.

(14) Wormmeester, J.; Stiekema, F.; De Groot, C. In *Methods in Enzymology: Avidin-Biotin Technology*; M. Wilchek and E. A. Bayer, Ed.; Academic Press, Inc.: Toronto, 1990; Vol. 184; p 314.

(15) Henrikson, K. P.; Allen, S. H. G.; Maloy, W. L. *Anal. Biochem.* **1979**, *94*, 366.

(16) Wilchek, M.; Bayer, E. A. In *Protein Recognition of Immobilized Ligands*; T. W. Hutchens, Ed.; Alan R. Liss Inc., 1989; p 83.

(17) Wahlberg, J.; Lundeberg, J.; Hultman, T.; Uhlen, M. *Proc. Natl. Acad. Sci. U.S.A.* **1990**, *87*, 6569.

(18) Parmley, S. F.; Smith, G. P. *Gene* **1988**, *73*, 305.

(19) Vorm, O.; Roepstorff, P.; Mann, M. *Anal. Chem.* **1994**, *66*, 3281.

(20) Maleknia, S. D.; Yao, X.-W.; Fuchs, M.; McGuinness, B. F.; Afeyan, N. In *Proceedings of the 42nd ASMS Conference on Mass Spectrometry and Allied Topics*; Chicago, IL, 1994; p 928.

(21) Schriemer, D. C.; Li, L. In *Proceedings of the 43rd ASMS Conference on Mass Spectrometry and Allied Topics*; Atlanta, GA, 1995; p 923.

(22) Green, N. M.; Toms, E. J. *Biochem. J.* **1973**, *133*, 687.

(23) Gitlin, G.; Khait, I.; Bayer, E. A.; Wilchek, M.; Muszkat, K. A. *Biochem. J.* **1989**, *259*, 493.

(24) Donovan, J. W.; Ross, K. D. *Biochem.* **1973**, *12*, 512.

(25) Edmondson, R. D.; Russell, D. H. *J. Am. Soc. Mass Spectrom.* **1996**, *7*, 995.

(26) Dai, Y.; Whittal, R. M.; Li, L. *Anal. Chem.* **1996**, *68*, 2494.

Chapter 8

Applications of Avidin-Biotin/MALDI for Rapid Sample Purification and Identification[a]

8.1 Introduction

This chapter presents two separate applications of the avidin-biotin/MALDI technique. The first involved the off-line purification and analysis of complex solutions containing trace amounts of biotinylated peptides. The second investigated the usefulness of the procedure for the extraction of biotinylated antibody:antigen complexes.

The first study involved a model system designed to mimic an investigation of protein modification. Such an investigation must answer a basic question: where in the primary sequence does the modification occur? This needs to be determined in order to understand the functional manifestation of protein modification. The general strategy developed for protein primary structure determination by mass spectrometry involves a series of steps. The protein is first digested either enzymatically or chemically into a set of smaller peptides. For a simple amino acid substitution, a mass spectral map can be obtained from the unfractionated mixture to roughly locate the site of modification. The peptide map can be compared with the map arising from the unmodified protein, for identification of the altered peptides. More extensive modifications such as glycosylation often require purification and further enzymatic processing prior to mass spectral analysis and identification of the altered peptide.[1,2]

An exact identification of the modification site requires the sequencing of the identified peptide. Sequencing could be performed in the conventional fashion by Edman degradation or with exoproteases , although modifications can prohibit sequencing and the sample requirements can be excessive (>100 pmol).[3,4] These methods require the isolation of the peptide to be sequenced. More recently, tandem mass spectrometry has allowed for peptide sequencing on unfractionated peptide mixtures.[5-7] Little sample handling is involved, and sample requirements are low. The appropriate peptide ion is mass selected and dissociated, followed by mass analysis of the resulting fragments. The fragmentation patterns generated by the dissociation step are rich in information. However, determining the primary sequence from the pattern can be quite difficult due to the complexity of

[a] A section of this chapter is being prepared for publication. T. Yalcin assisted in the collection and interpretation of the MS/MS data.

fragmentation processes.[8] As a result, complete sequencing is not always realized. In practise, both tandem mass spectrometry and the conventional sequencing approaches are used to provide complementary information.[9-12] A detailed structural analysis usually arises from such an approach, yet the conventional sequencing approach remains the limiting step in terms of sample requirements.

As an alternative approach, the incorporation of a biotin tag allows for rapid isolation and identification of a modified peptide. In this study, enzymatic sequencing and tandem mass spectrometry protocols, in conjunction with the avidin-biotin/MALDI technique, were developed to sequence a biotinylated peptide. A failed attempt to apply this methodology to the identification of an active site in an enzyme allowed for refinement of the procedure, and the identification of its limitations.

A variant of the avidin-biotin/MALDI technique is also considered in this chapter. A biotinylated antibody was used to recognize an antigen in a mixture, and immobilized tetrameric avidin used in the extraction of the resulting complex.

8.2 Experimental

8.2.1 Biotinylation of Troponin C

The reagent N-[6-(biotinamido)hexyl]-3'-(2'-pyridyldithio)propionamide (biotin-HPDP, structure **I**) was purchased from Pierce (Rockford, IL), and used to achieve sulfhydryl-specific biotinylation.

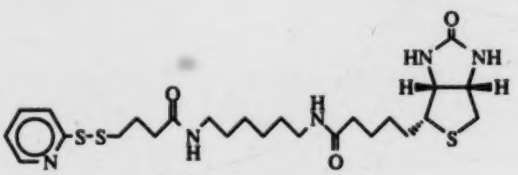

I

A 4 mM solution of biotin-HPDP was prepared in N,N-dimethylformamide (DMF). Avian skeletal muscle troponin C (TnC) was dissolved in phosphate buffer (PBS: 50 mM phosphate, 0.5 M NaCl, 1 mM EDTA and pH 7.4) to a concentration of 1 mM. The TnC was provided by Drs. M. Li, L. Smillie and B. Sykes of the Department of Biochemistry (University of Alberta). The biotinylation reagent and the protein were combined in

equimolar amounts and diluted with water such that the final solution contained 5% (v/v) DMF. The final protein concentration was 200 μM. The reaction was carried out at room temperature for two hours and then stored at -20 °C.

8.2.2 Inhibition of PAM

The enzyme peptidylglycine α-amidating mono-oxygenase (PAM) was inhibited with biotin-derivatized phenylbutenoic acids. The cDNA for this enzyme was cloned from RNA originating from rat medullary thyroid carcinoma cells, and expressed in mouse C127 cells.[13] Phenylbutenoic acids are mechanism-based inhibitors for the hydroxylating segment of this bifunctional enzyme.[14] Two biotin-derivatized phenylbutenoic acids were prepared in the laboratory of Dr. J. Vederas (Chemistry Department, University of Alberta), in which the biotin was attached to phenylbutenoic acid through an amide moiety. Structure **II** represents a compound with a cleavable disulphide group, while structure **III** represents a similar inhibitor without a readily cleavable spacer arm.

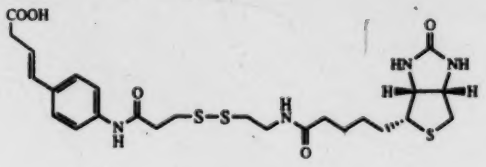

II

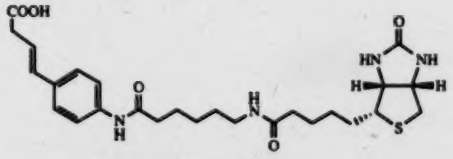

III

These species were confirmed as inhibitors of PAM in Dr. Vederas' laboratory, by a spectrophotometric assay.[15]

The inhibition of PAM with compound **II** was achieved by combining:

N,N-dimethyl-1,4-phenylenediamine (DMPD, 2.5 mM)
copper sulphate (4 μM)
catalase (6 μM)
PAM (0.8 μM)
inhibitor (0.4 mM)

in 4 ml of phosphate buffer (50 mM, 0.2 M NaCl, pH 6.8). The mixture was incubated for 30 minutes at 37 °C and then desalted and concentrated by repeated filtration, using a Centricon filter with a molecular weight cutoff of 10 000. This procedure removed all but the catalase and the PAM (final PAM concentration of 2.7 μM). In a separate incubation, the catalase was removed.

The inhibition of PAM with compound **III** was achieved in the same fashion, by combining all of the above in 4 ml of phosphate buffer. Incubation and sample clean-up was performed in the same fashion. Incubations with and without catalase were also performed.

8.2.3 Enzymatic Digestions

Enzymatic digests using bovine trypsin (TPCK-treated), yeast carboxypeptidase Y (Sigma, St. Louis MO) and porcine leucine aminopeptidase M (1 mg/ml slurry in 3.8 M ammonium sulphate, Fluka BioChemika, Buchs, Switzerland) were undertaken in the analysis of the model system. Digestions were carried out on various combinations of TnC, biotinylated TnC, bovine serum albumin (BSA) and equine cytochrome c. Tryptic digests were carried out at room temperature in PBS or water for three hours. Approximately equimolar amounts of trypsin were used to digest a protein sample. Soybean trypsin inhibitor (Sigma) was added to terminate the digestion after the specified time. To obtain sequencing information, leucine aminopeptidase M (LAP) or carboxypeptidase Y (CPY) digests of the tryptic digests were undertaken.[16-18] For N-terminal sequencing, LAP and trypsin-digested protein (in PBS) were combined. Ratios are cited in section 8.3. After a 75 minute digestion at room temperature, tetrameric avidin immobilized on beaded agarose was added to extract the biotinylated peptides for analysis by MALDI, according to the procedure in Chapter 7. For C-terminal sequencing, ~30 pmol CPY was combined with ~1 nmol of trypsin-digested protein (in water), and digested for variable periods of time (see section 8.3). After digestion, the biotinylated peptides were isolated with the appropriate immobilized avidin product and analysed by MALDI.

Tryptic digests of PAM inhibited with compound **II** were carried out at 37 °C from 3 to 24 hours in PBS, using equimolar amounts of trypsin and PAM. A 0.9 ml aliquot of the solution of PAM inhibited with compound **III** was treated with 10 μl of 45 mM dithiothreitol (DTT) for 15 minutes at 50 °C. The solution was cooled to room temperature, and then 10 μl of 100 mM iodoacetamide was added. After 15 minutes, the

solution was combined with trypsin in a 10:1 molar ratio (PAM:trypsin). Tryptic digests were carried out in PBS, for 3 to 24 hours.

8.2.4 Oligosaccharide Analysis

A biotinylated antibody with a known specificity for the chemical repeating unit of the *Salmonella* serogroup B *O*-polysaccharide was obtained from the laboratory of Dr. D. Bundle (Chemistry Department, University of Alberta). This antibody is a single-chain Fv product, expressed in E. coli. It has been shown that the antibody has an affinity for an abequose-mannose branching point in this repeat unit.[19] A simple mixture of two synthetic oligosaccharides (from the laboratory of Dr. O. Hindsgaul) was prepared, where one contained this branching point (structure **IV**, CCL-402) while the other did not (structure **V**, H-type 2).

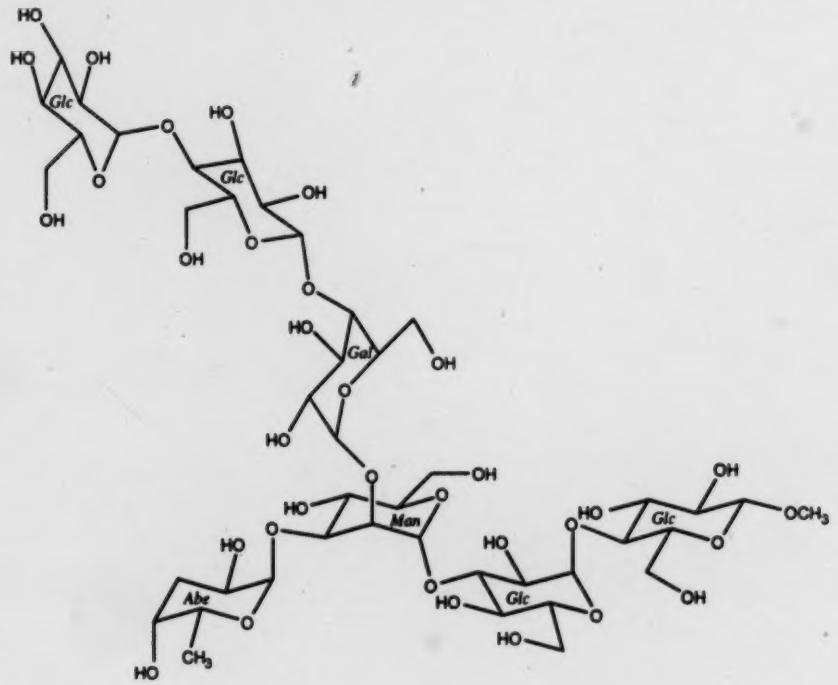

IV

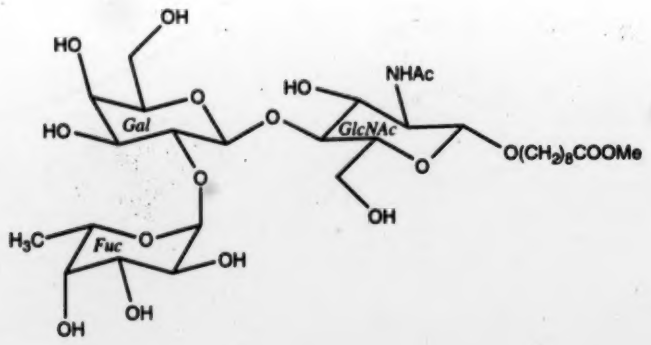

V

The K_a value for the CCL-402/antibody complex is 1.14 x 10^6 M^{-1}.[20] The mixture was incubated for 30 minutes with the biotinylated antibody, in the presence of tetrameric avidin immobilized on beaded agarose. The mixture contained the following:

0.5 nmol CCL-402
0.5 nmol H-type 2
~0.4 nmol biotinylated antibody
immobilized tetrameric avidin with a biotin-binding capacity of
0.3 nmol (~5 µl of settled agarose beads)
50 µl Tris buffer (25 mM Tris, 75 mM NaCl, pH 8)

After incubation, the beads were settled and the supernatant drawn off. The beads were then washed with two 25 µl portions of water. A 4 µl portion of 2-propanol/water (2:1) was added to the beads, and then agitated. It is estimated that the solution composition at this point was 1:2 (2-propanol/water). After the beads settled, the supernatant was sampled for MALDI analysis.

8.2.5 Instrumentation

Mass spectra were collected on a linear time-lag focussing MALDI TOF mass spectrometer similar to the one described in Chapter 5, but with a slightly longer flight tube (1.15 m). MALDI collisionally-induced dissociation (CID) spectra were collected on a hybrid sector/time-of-flight instrument, the ZabSpec orthogonal acceleration (oa) time-of-flight (TOF) instrument from Micromass (Manchester, UK). A nitrogen laser (337 nm)

was operated at 10 Hz in the ion source region. The precursor ions were accelerated by a voltage of 8 kV and mass selected with the EBE mass spectrometer. The ions were introduced into the collision cell floated to 7200 kV, imparting 800 eV to the precursor ions. Xenon was used as the collision gas, and on average, the intensity of the precursor ion pulses were attenuated by ~30%. The ions exiting the collision cell were guided into the oa-time-of-flight spectrometer, and pulsed into the flight tube for mass separation. Ions were detected with a microchannel plate detector.

8.2.6 MALDI Sample Preparation

The matrices used in this work were α-cyano-4-hydroxycinnamic acid (HCCA) and sinapinic acid (SA). Both matrices were purchased from Aldrich (Milwaukee, WI). Purification and analysis of the biotinylated peptides resulting from digestion were analysed as described in Chapter 7. The direct analysis of tryptic digest solutions employed the two layer method, using HCCA in FA/2P/H_2O as the matrix preparation (Chapter 7). The analysis of intact TnC and PAM involved the two layer method using SA as the matrix.

For the analysis of the oligosaccharide samples dissolved in 1:2 2P/H_2O, HCCA was used. A thin layer of microcrystals was formed from the application of 1 µl of a 20 mg/ml solution of the matrix in acetone. After evaporation of the acetone, 0.75 µl of the oligosaccharide solution was applied, and then *immediately* vacuum-dried using a Hewlett-Packard model G2024A vacuum drying station.

8.3 Results and Discussion

8.3.1 Isolation of Biotinylated Peptides

This section presents the investigation of two separate systems. The first system was used to develop the methodology. This methodology was then applied to a second system for the study of enzyme inhibition.

8.3.1.1 Identifying the Location of a Protein Tag. Biotinylated TnC

TnC is a 162 amino acid muscle protein, having a molecular weight of 18 256.4 u. It contains only one cysteine.[21] A spectrum was obtained from the pure protein, and is displayed in Figure 8.1A. The measured $[M+H]^+$ value of 18 256.6 u agrees with the

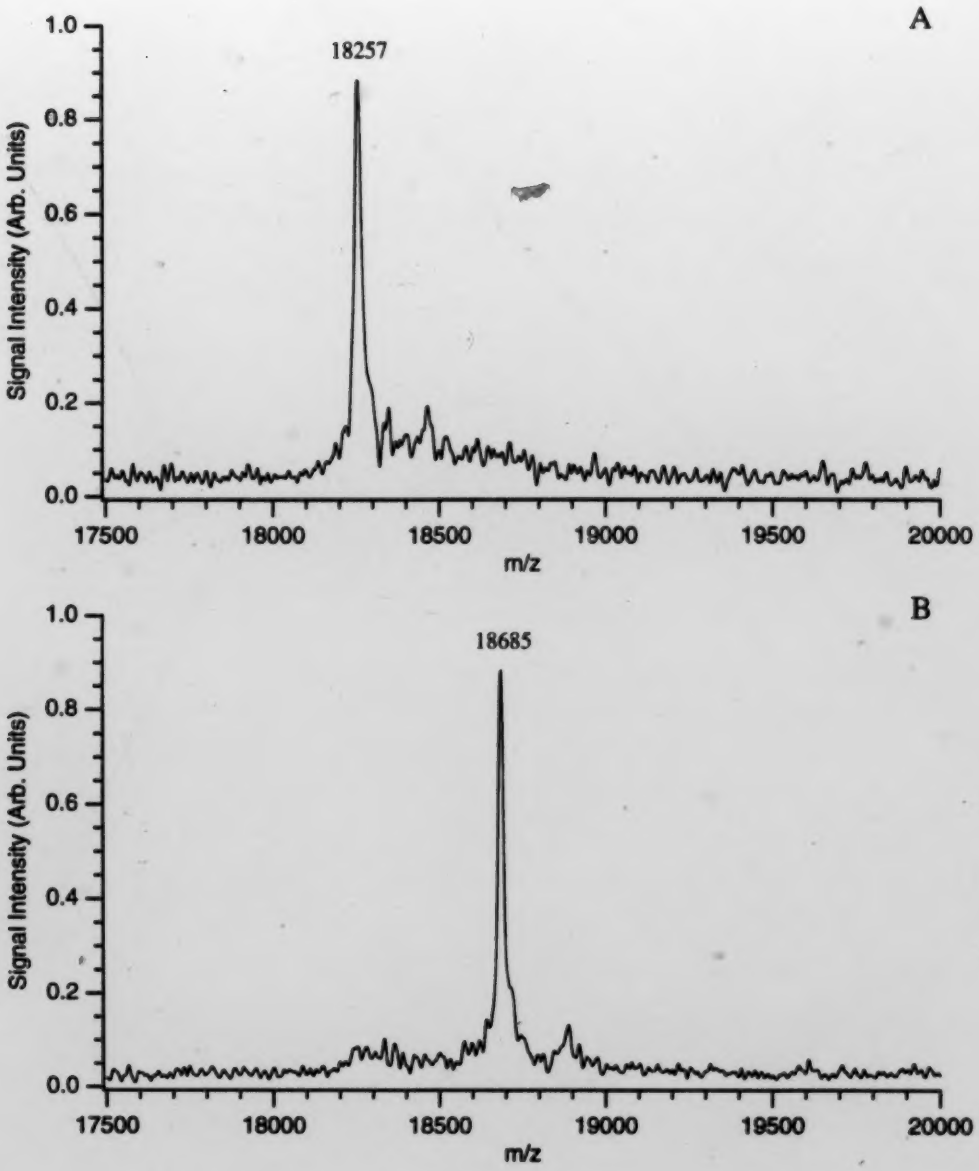

Figure 8.1 MALDI mass spectra of (A) unlabelled TnC (expected $[M+H]^+$ = 18 257.4 u) and (B) biotinylated TnC (expected $[M+H]^+$ = 18 685.0 u).

expected value, within acceptable error. A sulfhydryl-specific biotin reagent (biotin-HPDP, **I**) was chosen to react with the cysteine residue in the protein, resulting in tagged protein and loss of pyridine-2-thione, as shown in the schematic below.

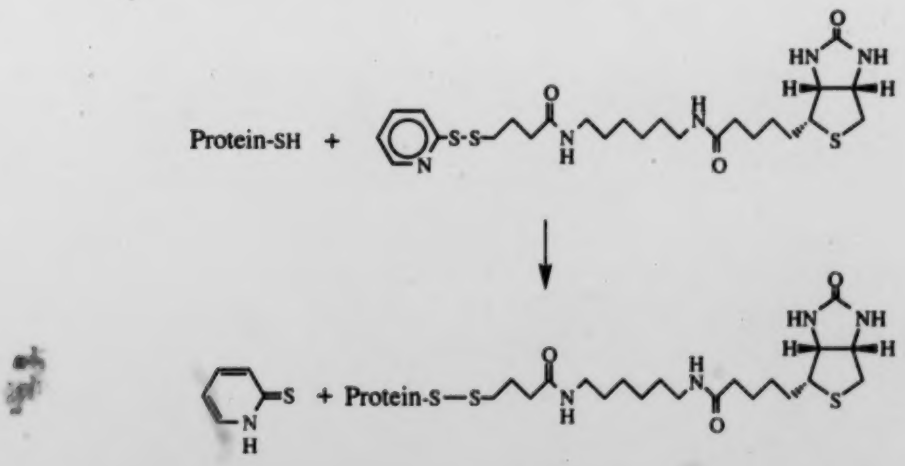

A spectrum was collected from the reaction mixture (Figure 8.1B). The measured $[M+H]^+$ value of 18 685 u indicates a mass shift of 428 u, which agrees with the expected mass shift from biotinylation (428.6 u). The absence of a peak at 18 257 suggests that the reaction was complete.

A mixture containing one nmol of TnC and 10 pmol of biotin-TnC was prepared and digested in PBS for three hours. The digest was then sampled for MALDI analysis, generating the mass spectrum displayed in Figure 8.2A. Approximately 80% sequence coverage was observed from complete cleavage products. Peaks arising from incomplete cleavage were also observed at higher masses, as well as trypsin autolysis products. Note that some measure of methionine oxidation must have occurred during digestion, as some tryptic fragments were represented in the spectrum at a mass 16 u higher than expected.

One tenth of this crude mixture was purified and analysed using the avidin-biotin/MALDI procedure. Approximately one fifth of the settled beads were sampled for mass analysis. The spectrum arising from this procedure is shown in Figure 8.2B, indicating mono-isotopic peaks at m/z 1625.9 and 1197.7. This mass difference of 428.2 u agrees with the expected mass difference arising from biotinylation. The peak at m/z 1625.9 would therefore seem to indicate a biotinylated peptide, with the peak at m/z 1197.7 representing the loss of the biotin tag. The lower mass peak likely arose from the partial reduction of the disulphide in the spacer arm of the tag, due to the high acid content of the

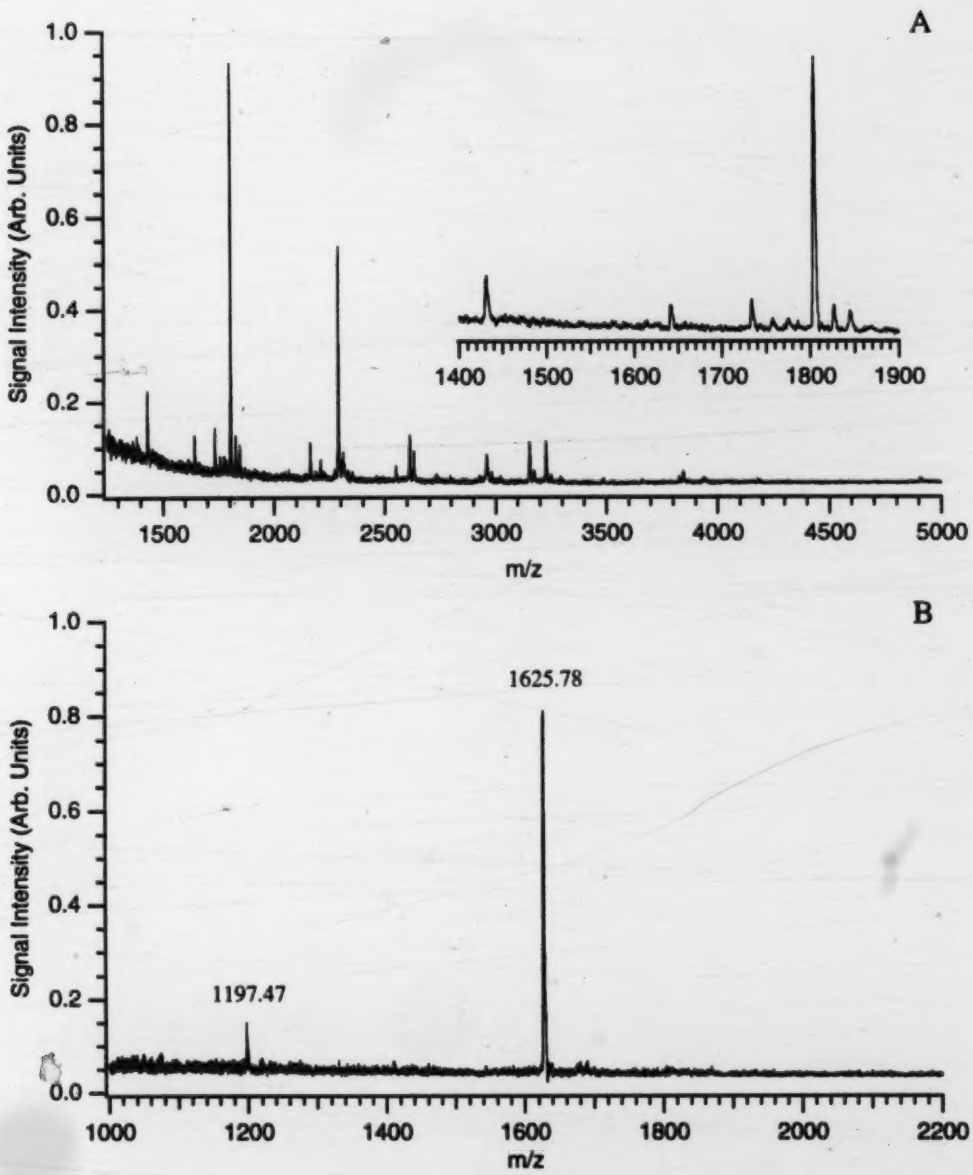

Figure 8.2 (A) Mass spectrum from a sample of the tryptic digest of a 100:1 blend of TnC and biotinylated TnC. Inset shows an expansion of the region from m/z 1400 to 1900; (B) purification and analysis of the tryptic digest using the avidin-biotin/MALDI procedure, representing at most 200 fmol of peptide applied to the probe tip.

matrix preparation. A search of the possible protonated tryptic fragments of TnC identified a candidate with a mono-isotopic mass of 1197.52 u. This would correspond to a mass error of 150 ppm. Note that this spectrum was obtained on a second, recently constructed, time-lag focussing time-of-flight mass spectrometer. The mass measurement accuracy is expected to be similar to the instrument used in the work of Chapters 4,5 and 6, although it has not yet been optimized in this regard. The next candidate at 1198.48 u would involve an unreasonably high error of 650 ppm. The sequence of the candidate peptide is SEEELANCFR. The presence of the only cysteine in this sequence supports the labelling of the peak at m/z 1625.9 as the biotinylated SEEELANCFR (expected $[M+H]^+$ of 1625.7 u), and the peak at m/z 1197.7 as its reduced analogue. Note that the one-letter code for amino acids is used throughout this chapter.

From the inset of Figure 8.2A, note that the spectrum does not show a peak at m/z 1625.7. The concentration of the corresponding peptide in solution was simply too low to be observed. A more complex digest solution was then prepared and analysed, to further demonstrate the purifying power of the avidin-biotin affinity interaction. Figure 8.3 represents the spectrum arising from the purification of a tryptic digest that contained 10 nmol BSA, 10 nmol cytochrome c, 10 nmol trypsin, one nmol TnC and 100 fmol of biotinylated TnC in 1 ml of PBS. Approximately one fourth of the settled beads were sampled for mass analysis in this spectrum. A peak at m/z 1197.5 representing the reduced peptide was not observed, either due to the acidified matrix or in a separate experiment by the addition of DTT. At this point, an accurate peak mass is the only information available for confirmation of biotinylation.

Identification of the modification site based solely on the mass of a single peptide becomes virtually impossible when the parent protein is large. This is because so many possibilities can exist for a certain mass, given the accuracy of MALDI time-of-flight mass determinations. At this point, partial or even full sequencing of the identified peptide is necessary. Sequencing based on Edman degradation or exoproteases require that the peptide be purified to a high degree. However, simplification of the purification results if the tagged peptide can be complexed to a protein through a high affinity interaction. To illustrate, both N-terminal and C-terminal enzymatic sequencing of the biotinylated peptide represented at m/z 1625.9 were undertaken. Ideally, partial and successive cleavage of amino acids would generate a series of peptides all containing the biotin tag.

A solution consisting of 1 nmol TnC and 10 pmol biotinylated TnC in 100 µl PBS was digested with trypsin, and the presence of the biotinylated peptide confirmed. For N-

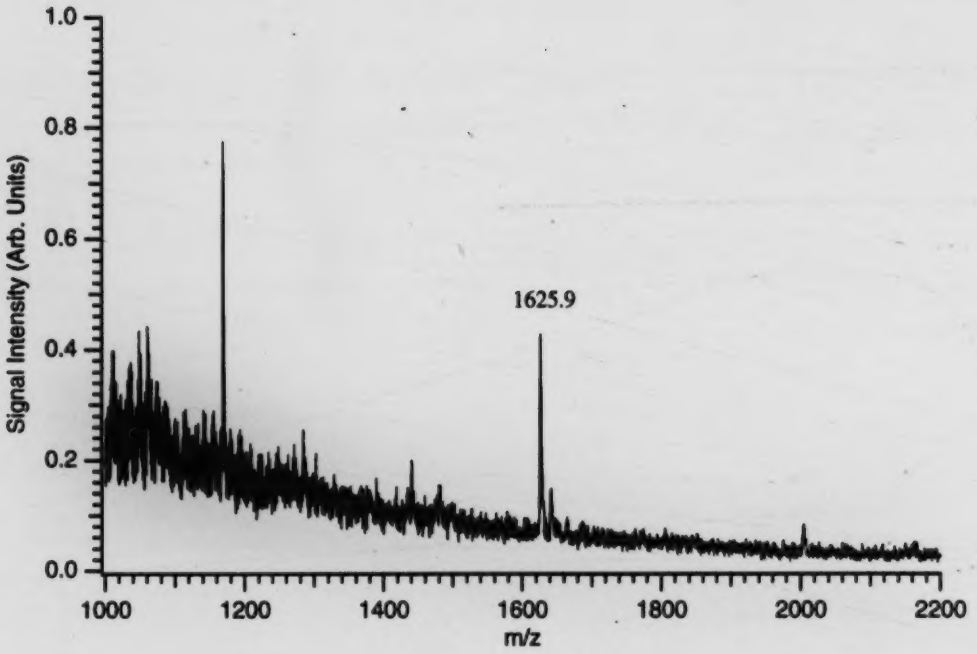

Figure 8.3 Mass spectrum obtained from a tryptic digest of a solution containing BSA, cytochrome c, TnC and a trace amount of biotinylated TnC. Purification and analysis was achieved using the avidin-biotin/MALDI procedure. Spectrum represents at most 20 fmol of peptide applied to the probe tip.

terminal sequencing, the solution was split into two equal portions (~45 µl each). Approximately 400 pmol of LAP slurry was added to one portion, and 1.2 nmol to the other. After equivalent digestion times, one fourth of each sample was purified and analysed using the avidin-biotin/MALDI procedure. Figure 8.4A shows the spectrum from the digestion using 400 pmol of LAP. Note the two smaller peaks in this spectrum, in addition to the expected peaks at m/z 1625.7 and 1197.5. These smaller peaks reflect the cleavage of amino acids from the N-terminal of the biotinylated peptide. Mass accuracy is sufficient to identify the loss of 87.0 u as arising from serine, and the loss of 129.1 arising from the loss of glutamic acid. Incubating the rest of the digest for longer periods of time gave no further sequence information. However, the digestion solution that contained 1.2 nmol of LAP demonstrated more extensive cleavage (Figure 8.4B). The peaks at 1625.8 and 1197.7 were less intense, and two new peaks arose at lower mass. A large gap of 371.0 u was observed between the peak at m/z 1038.7 and 1409.7. This would correspond to at least 3 amino acids, and is indicative of the different cleavage rates for exoproteolysis.[16-18] Clearly, the enzyme processes this part of the sequence very quickly and efficiently. The two new, lower mass peaks differ by 71.1 u, indicating the presence of alanine at least five amino acids removed from the N-terminal. Again, incubation for a longer period of time gave no further sequence information. Note that all these tests, including confirmation of biotinylation, were performed on 10 pmol of biotinylated TnC in the presence of substantial contamination.

A similar approach was followed for C-terminal sequencing using CPY as the exoprotease. A tryptic digest of 1 nmol TnC and 10 pmol biotinylated TnC in 100 µl of water was prepared, and the presence of the biotinylated peptide confirmed. CPY was added to the mixture, and the digestion monitored with time. One tenth of the sample was removed in each case. Figures 8.5A-C show the spectra obtained at 10, 40 and 120 minutes, respectively. Rapid cleavage of the first amino acid was indicated by the intense peak in Figure 8.5A. The difference of 156.3 u between the two peaks of this spectrum indicate that arginine is the C-terminal amino acid. At 40 minutes, the parent peptide of 1625.9 u was completely digested, however no new sequence information was available (Figure 8.5B). After 120 minutes, a small peak corresponding to the loss of phenylalanine (147.1 u) was observed.

Partial, successive cleavage of amino acids from a peptide such as described above has been dubbed "ladder sequencing", and has been demonstrated as useful for the identification of protein/peptide modifications.[22] If high-affinity tagging is possible, Figures 8.4 and 8.5 show that such sequencing can also be performed quickly on crude

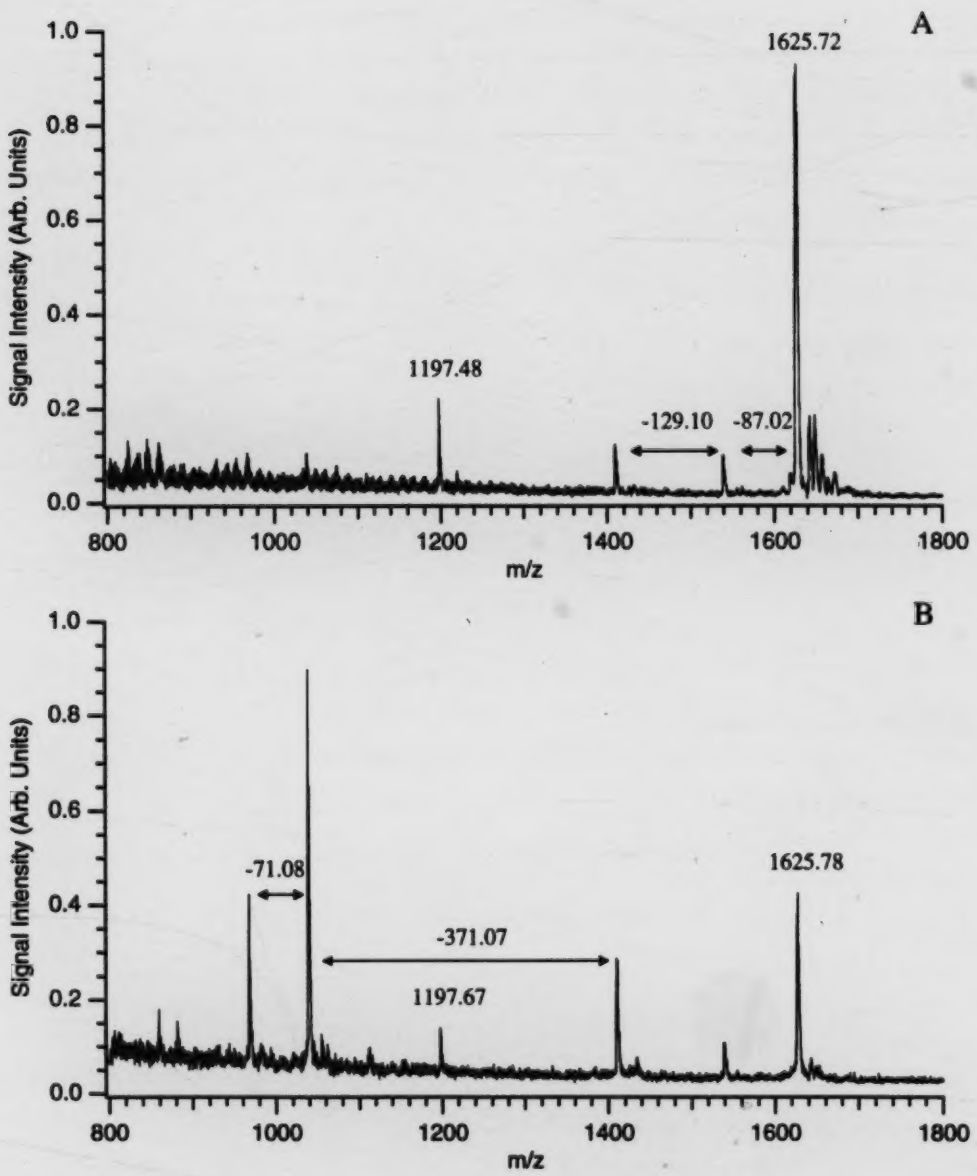

Figure 8.4 Mass spectra obtained from 75 minute LAP digestions of an unpurified tryptic digest containing trace amounts of a biotinylated peptide, using (A) 400 pmol and (B) 1.2 nmol of LAP. Biotinylated species were isolated and analysed using the avidin-biotin/MALDI procedure.

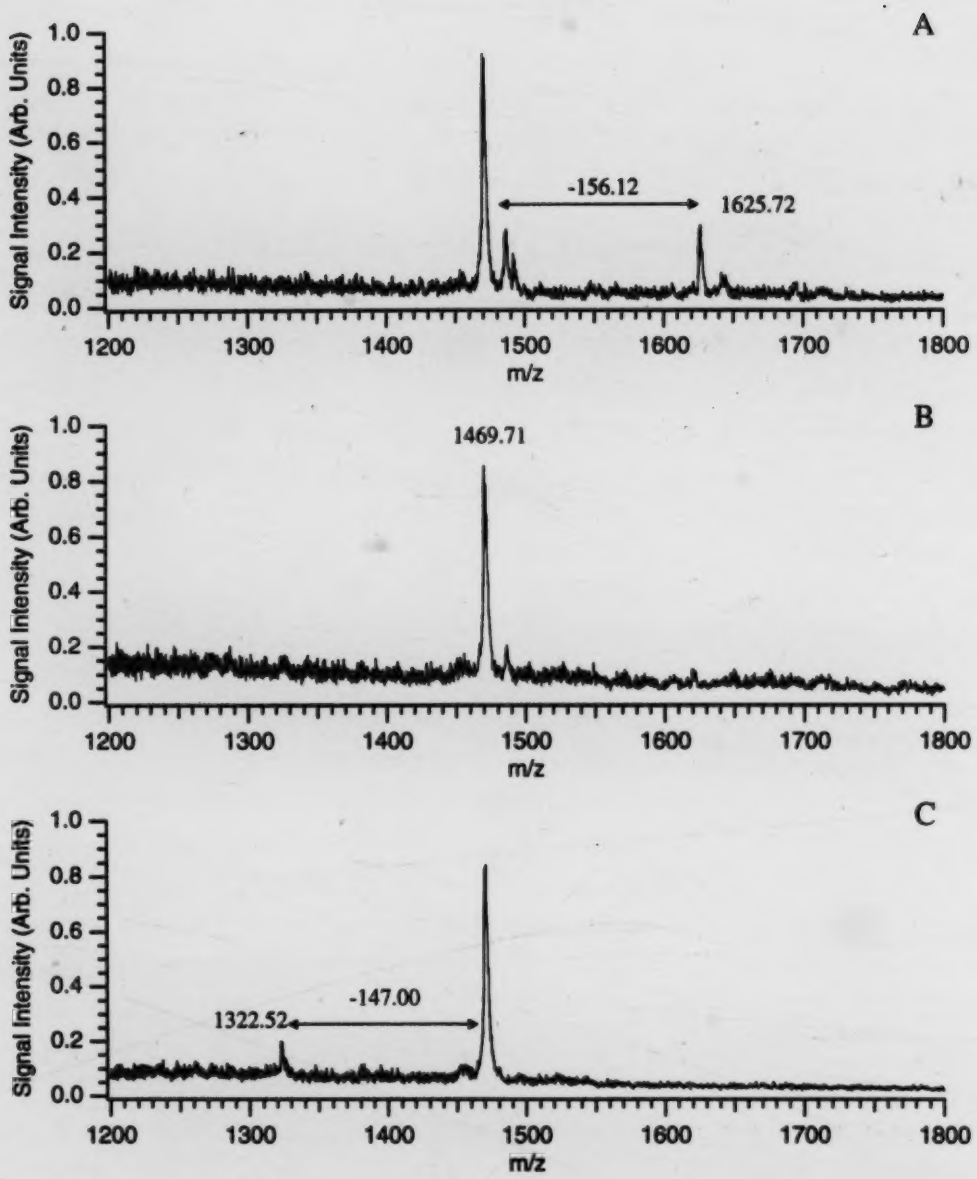

Figure 8.5 Mass spectra obtained from a CPY digestion of an unpurified tryptic digest containing trace amounts of a biotinylated peptide. The digestion was sampled at (A) 10 minutes, (B) 40 minutes and (C) 120 minutes. Biotinylated species were isolated and analysed using the avidin-biotin/MALDI procedure.

mixtures. A current shortcoming with this technique relates to the difficulty in achieving efficient, successive enzymatic digestions. As no purification was imposed on the sample from the initial tryptic digests onward, only one buffer system for all digestions could be used. CPY digests do not tolerate phosphate buffers, therefore the initial tryptic digest was carried out in pure water in this case (CPY digests work well in pure water[17]). Such a compromise will not always be tolerable. An unsuccessful attempt was made to enzymatically sequence the bound biotinylated tryptic fragment. The tight complexation with avidin would allow for buffer exchange by washing. No ladder sequencing was obtained in this case, presumably because the enzymes had restricted access to the bound peptide. A further drawback with the current procedure is that an amount of digestion enzyme must be chosen that is sufficient to cleave all components in the mixture, including impurities. This can lead to a high consumption of expensive digestion enzymes.

Based on accurate mass determination, enzymatic sequencing, and foreknowledge of the tagging chemistry, a definite confirmation of peptide identity and tag location can be made. However, if the tagging chemistry is not known, complete sequencing is needed to determine where the modification has occurred. In anticipation of a following example (section 8.3.1.2), this situation could arise in the investigation of new suicide inhibitor, where the chemistry and site of inhibition is to be determined.

In an attempt to independently determine the binding site in the model study, MS/MS spectra from the biotinylated peptide were collected, using a tandem sector/time-of-flight instrument. The ZabSpec oa-TOF used in this work was outfitted with a MALDI source, to allow for a sample preparation that was identical to that used in the linear time-of-flight analysis. Sample requirements were somewhat higher for the ZabSpec oa-TOF. Usually a loading of ~10pmol of peptide on the probe tip was necessary to obtain strong signals. The fragmentation patterns observed in tandem mass spectrometry are complex and highly conditional upon both the structure of the peptide and the instrumental configuration used in the spectral collection. Certain key points pertinent to the interpretation of fragmentation patterns will be considered, as summarized from reviews by Biemann,[23] Papayannopoulos,[8] and Gross.[24]

Collisions between a precursor ion and a simple gaseous species such as He, Ar or Xe can be classified as a low energy CID event, or a high energy CID event. Low energy CID occurs from precursor ions with energies typically below 100 eV, while high energy CID occurs from precursor ion energies in excess of 1 keV. These are simply crude benchmarks; it is common to identify CID in a triple quadrupole mass spectrometer as low energy, and CID in a sector instrument as high energy. In the present study, the CID

process can be considered high energy. In either CID process, fragmentation along the peptide backbone is common, often accompanied by the transfer of one or two hydrogens for ion stability. Fragments with charge retention on the N-terminal are denoted as **a**, **b** or **c** ions, whereas fragments with charge retention on the C-terminal are denoted as **x**, **y** or **z** ions (see Figure 8.6). High energy CID is capable of generating all the ion types, while low energy CID mainly produces **b** and **y** ion types.

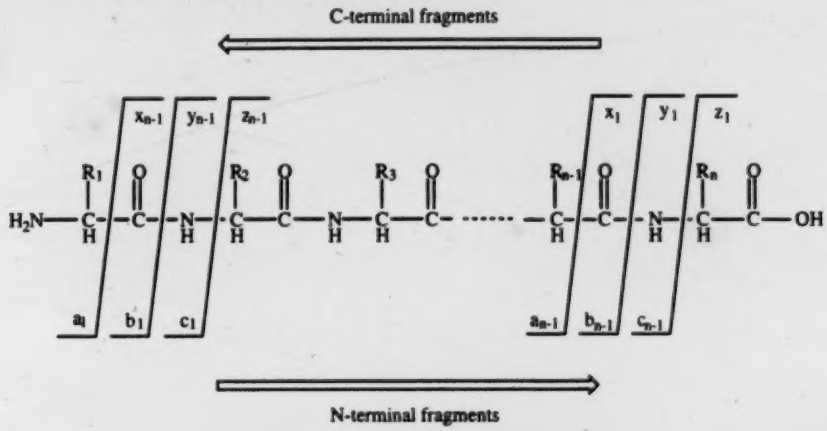

Figure 8.6 Nomenclature for the backbone fragmentation of peptide ions. Subscripts refer to the amino acid position in the sequence, determined from the N-terminal (for **a**, **b**, **c** ions) or C-terminal (for **x**, **y**, **z** ions). R refers to the amino acid side-chain.

High energy CID generates more intense low mass species than low energy CID. These low mass species are dominated by immonium ions, produced from the individual amino acids in the peptide. They have the form $[H_2N{=}CH\text{-}R]^+$. Most amino acids generate unique immonium ions.

High energy CID can also lead to side-chain fragmentation. These ions are indicated with a **d** if the charge is retained on the N-terminal, or with a **w** if the charge is retained on the C-terminal. When the entire side-chain is lost, the resulting ion is indicated with a **v**. This has only been observed for C-terminal fragments. Other fragmentations include the loss of water and ammonia (more common in low energy CID). Internal fragment ions can also be formed, which require multiple collisions with the gas to generate two backbone cleavages.

A high energy CID spectrum of the peptide corresponding to m/z 1625.7 was collected on the AzbSpec oa-TOF, under conditions favoring single collisions.[24] The full spectrum is shown in Figure 8.7A, with expansions shown in Figures 8.7B, 8.8A and 8.8B. In the ensuing discussion, it will be assumed that the sequence of the isolated peptide is known, but not the modification site or chemistry.

The spectrum generally indicates a high degree of fragmentation, and little useful sequence information between m/z 500 and the precursor ion peak. Figure 8.7B is an expansion of the immonium ion region of the spectrum, and the positively identified amino acids are represented by their one-letter code. Note that the peak at m/z 86.0 could correspond to leucine or isoleucine; one cannot distinguish between these amino acids on the basis of immonium ions. The peak at 87.0 is indicative of both arginine *and* asparagine. Peaks due to arginine also arise at m/z 70.2, 100.1 and 112.0. The $\mathbf{y_1}$ peak at 175.1 (Figure 8.8A) confirms that arginine resides at the C-terminal. The presence of arginine in the spectrum casts doubt upon the assignment of m/z 87 as being at least partially due to asparagine. However, since its presence in the sequence is known, this assignment is reasonable. Note that no immonium ion corresponding to cysteine was observed (expected at m/z 76). All of the other amino acids appear to be represented, supporting an initial hypothesis that the tag was bound to the cysteine.

This hypothesis should receive reinforcement from the sequence information present in the spectrum. Figures 8.8A and 8.8B show expansions of higher m/z portions of the spectrum. A series of **b** ions were observed, up to $\mathbf{b_4}$. This identifies a portion of the N-terminal sequence as SEEE. Recall from the LAP enzymatic sequencing (Figure 8.4) that a sequence jump of 371 u was observed. The **b** ion information from the high CID spectrum reveals that EE accounts for part of the jump. This leaves a mass of 112.9, which must indicate leucine or isoleucine. A $\mathbf{y_2}$ ion was identified in Figure 8.8A, corresponding to FR. Other **y** ions could not be positively identified.

At this point, a combination of enzymatic sequencing and tandem mass spectrometry have identified that the tag does *not* reside on the following amino acids in the peptide (indicated by underscoring):

SEEELANCFR

Figure 8.8B provides additional insight. A strong cluster of peaks is visible in the spectrum. Note that the peak at m/z 429.1 coincides with the protonated biotinylation reagent, minus the pyridine-2-thione leaving group. The strong peak at m/z 431.1 could

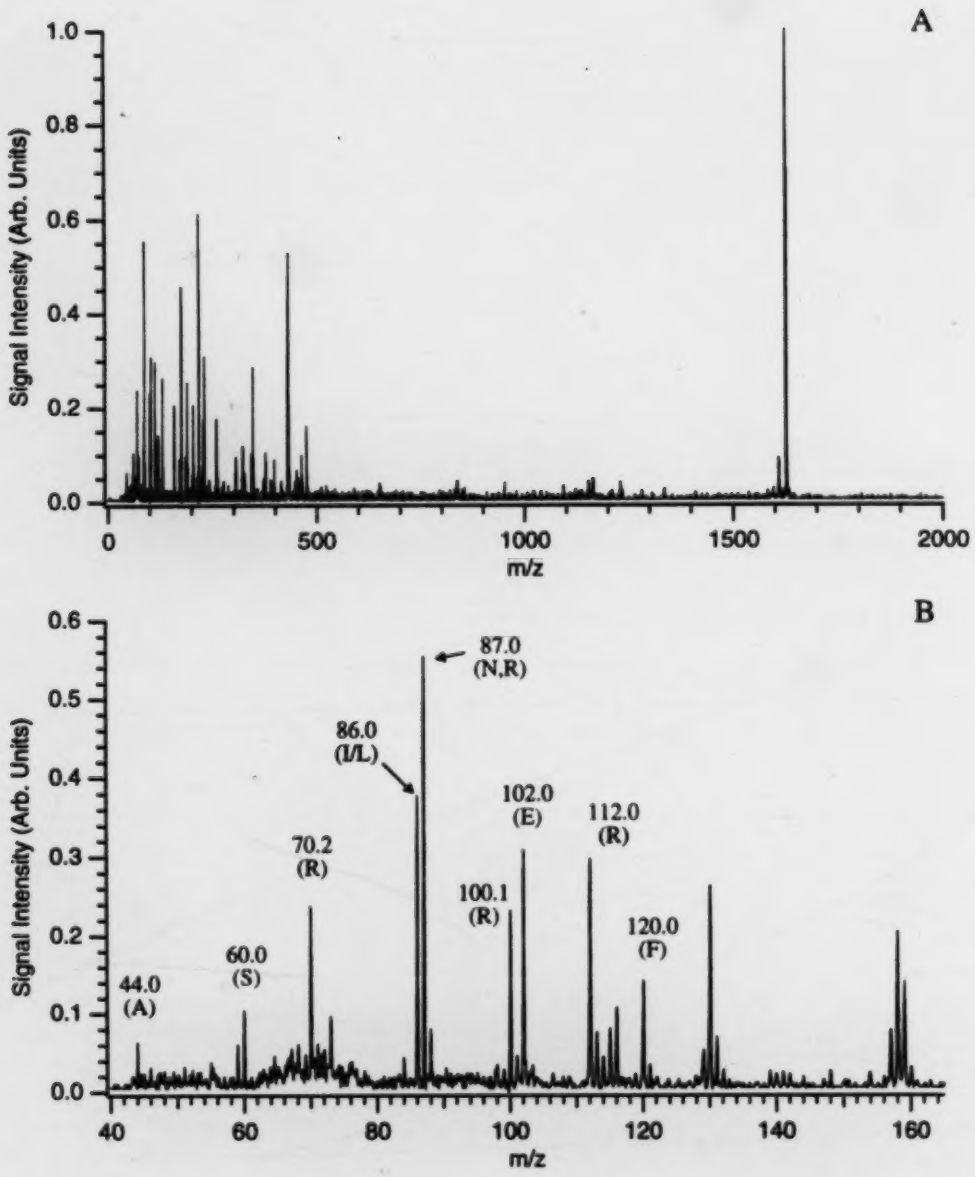

Figure 8.7 MS/MS spectrum of m/z 1625.7 biotinylated peptide, obtained with high energy CID on the ZabSpec oa-TOF. (A) Full spectrum, (B) expansion of the immonium ion region. The biotinylated peptide was isolated and analysed from a tryptic digest using the avidin-biotin/MALDI procedure.

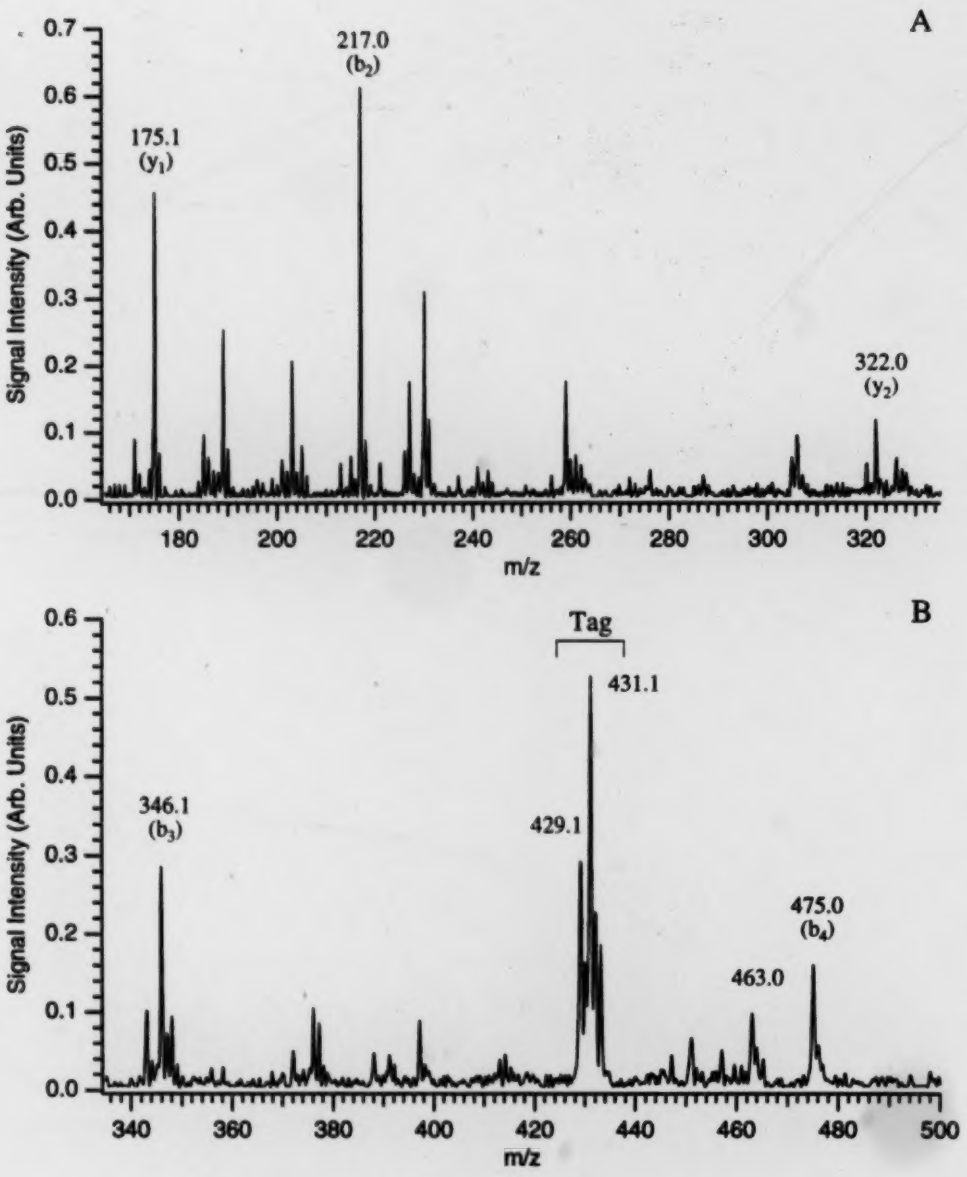

Figure 8.8 Expansions of the MS/MS spectrum of Figure 8.7, showing the (A) m/z 165 to 335 region and (B) the m/z 335 to 500 region.

indicate the acquisition of two hydrogens for ion stabilization.[8] None of the peaks in this cluster seem to correspond to a rational cleavage of the peptide itself. Also note that a smaller cluster 32 u higher suggests that the tag is bound to a sulphur in the peptide. These peaks as well do not correspond to a rational cleavage of the peptide. Unfortunately, no immonium ion for the tagged amino acid is evident in the spectrum at higher m/z.

In summary, with the aid of a high energy CID spectrum and enzymatic sequencing, cysteine can be identified as the strongest candidate for tagging. While the tagging chemistry was assumed to be unknown, the *suspected* reactivity of the tag correlates well with the identification of cysteine as the modification site. This model study emphasizes that complementary information can be obtained by a combination of sequencing techniques. When based on a high affinity separation, such information can be obtained from low pmol quantities of protein in contaminated solutions.

8.3.1.2 Identifying the Location of a Protein Tag. Inhibition of PAM

The bifunctional enzyme PAM catalyzes the conversion of glycine-extended peptide hormone precursors into C-terminal amides[25,26] Approximately half of the bioactive peptides in the nervous and endocrine system possess a C-terminal amide;[25] therefore determining the biosynthetic pathway to such peptides (and how to regulate it) is an important area of research. By the late 1980's, the bifunctionality of this enzyme had been ascertained,[26] with amidation arising from an hydroxylating step, and a lysing step:

Hydroxylation:

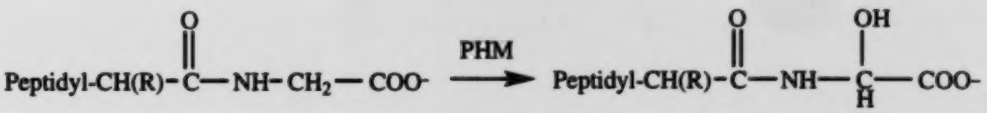

Lysis:

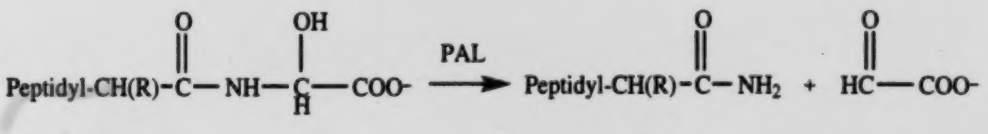

Discrete domains of the enzyme correlate with these functions, and are referred to as peptidyl α-hydroxylating mono-oxygenase (PHM) and peptidyl-α-hydroxyglycine α-amidating lyase (PAL). PHM requires copper, molecular oxygen and a suitable electron donor for activity, while PAL has no cofactor requirements. For the bifunctional enzyme, hydroxylation is the rate-determining step.[27] The PHM domain serves as the most promising target for enzyme regulation, partly because lysis can occur by other mechanisms as well.[27]

Mechanism-based, or suicide, inhibitors are being developed for PHM. This type of inhibitor is characterized by a highly specific and irreversible deactivation of an enzyme, through covalent binding. An inhibitor such as this is chemically unreactive in the absence of the enzyme, but becomes activated by the catalytic machinery of the targeted enzyme (hence the term "suicide").[28] Peptide substrate analogues,[29] 4-phenyl-3-butenoic acid[30] and unsaturated thioacetic acids[31] have been identified as suicide inhibitors of PHM.

In this study, phenylbutenoic acids were derivatized with biotin, as indicated in section 8.2.2. These derivatized phenylbutenoic acids were confirmed as inhibitors of a PAM enzyme, by the DMPD spectrophotometric assay.[15] Figure 8.9A represents the spectrum of the PAM isolated from cell culture. Figure 8.9B represents the spectrum of the PAM after inhibition with compound **III** and filtration (for salt removal). In keeping with an initial characterization of the enzyme,[13] structural heterogeneity is indicated by the broad peak in Figure 8.9A. It was determined that at least part of this heterogeneity was due to inefficient glycosylation during expression.[13] The molecular weights of the pure PAM (76 400) and the inhibited PAM (76 500) are indistinguishable given the precision of their measurements (standard deviation ~150 u). It would seem that complete inhibition of the enzyme with inhibitor **III** did not occur, as covalent binding of the tag would generate a mass shift of ~500 u. Based on the measurement precision, one cannot say if partial inhibition had occurred. Similar results were obtained for the inhibition with compound **II** (containing the disulphide group).

The solutions of PAM inhibited with compound **II** were digested following the protocols cited in section 8.2.3. Upon purification and analysis by the avidin-biotin/MALDI method, the spectrum from inhibition with compound **II** (with catalase) showed two peaks consistent with a biotinylated peptide (Figure 8.10). The confirmation was based upon the observation of the corresponding reduced forms of the tagged peptides, following treatment with DTT on the probe tip. The tagging chemistry was to be determined from the overall analysis, therefore the true mass of the tag on the peptide was not known. Nevertheless, it is expected that the tagging behaviour would be the same for

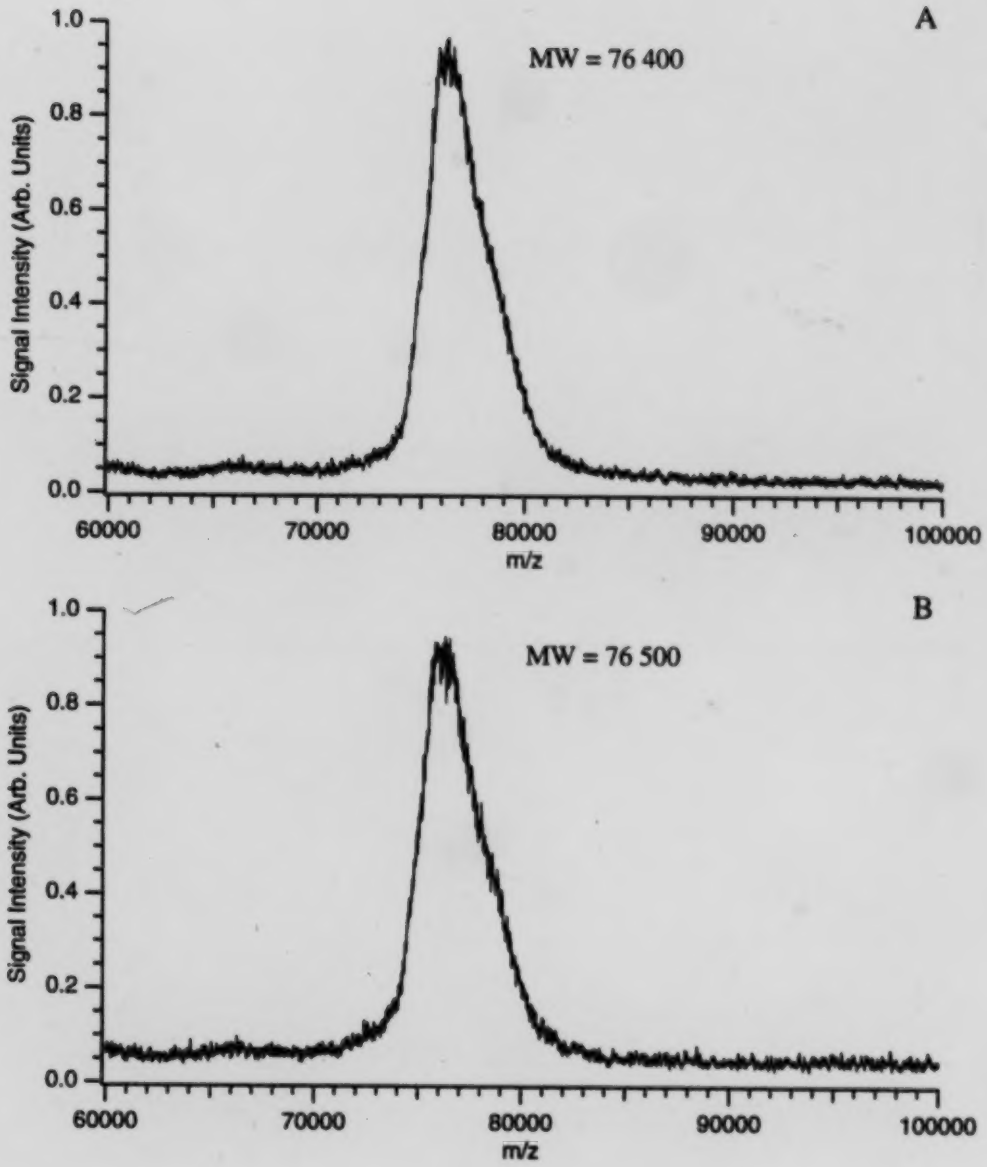

Figure 8.9 MALDI spectra of the (A) pure and (B) inhibited PAM (using compound **III**).

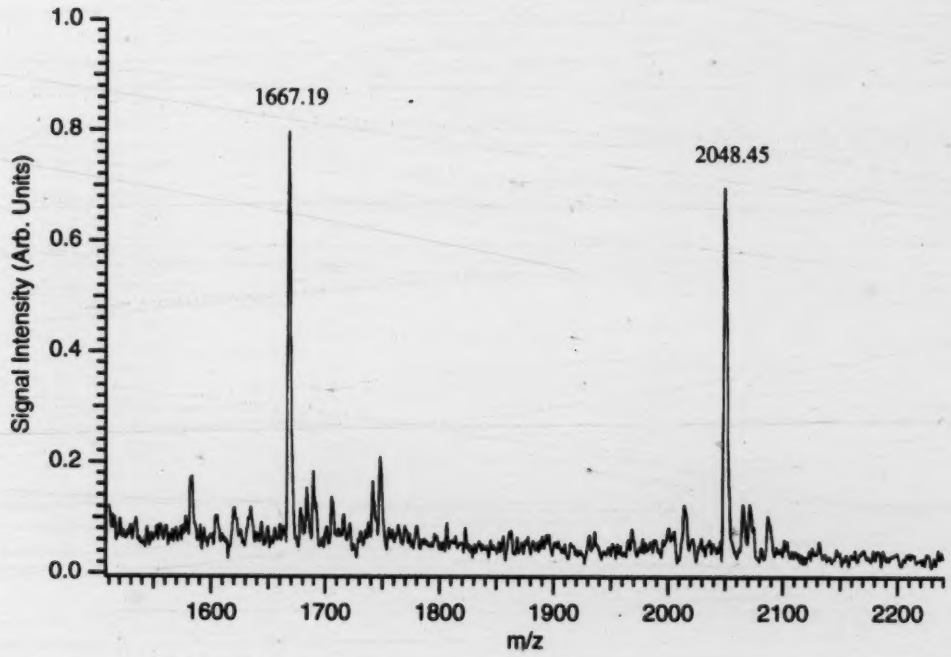

Figure 8.10 Spectrum arising from the avidin-biotin/MALDI analysis of PAM inhibited with compound **II**. The m/z values indicated represent the mono-isotopic peaks.

both peptides. Based on this expection, there were no fragments that matched the observed mass difference between the peaks. A similar analysis of the enzyme inhibited with compound **II** (and no catalase) yielded no peaks consistent with biotinylation.

An investigation of the possible tryptic fragments of catalase (a protein with a molecular weight of ~58 000) revealed two peptides having molecular weights matching the mass difference identified in Figure 8.10. Their sequences are:

LGPNYLQIPVNCPYR

and

YLQIPVNCPYR.

The first peptide corresponds to a tryptic fragment, while the second represents a partial, non-specific hydrolysis of this fragment. Note that these peptides contain a cysteine. It appears that the disuphide in the tag cleaved during inhibition and formed a disuphide with at least one cysteine in catalase. Such a process would give a tag with a mass of 301.4 u, and expected $[M+H]^+$ values of 1667.10 and 2048.30 for the two peaks. These values agree with the measured values. This seems to be a reasonable hypothesis, given that the inhibition was carried out in an oxidizing environment. Catalase serves an equivocal role in the inhibition, as some researchers have incorporated it,[27,30] while others have not.[15]

Unfortunately, no identification of the active site has been determined at this point. The incorporation of a non-cleavable spacer arm (compound **III**, with or without catalase) gave no positive results. There is an indication that the tag does not bind to the enzyme, at least with the retention of the biotin tag. This conclusion is reached because an analysis of the intact, inhibited PAM using the avidin-biotin/MALDI procedure produced no peak corresponding to the inhibited enzyme. If the inhibitor did bind, its efficiency under the cited experimental conditions must have been very low. It is interesting to note that other researchers searching for the active site of this enzyme by an HPLC-ESI/MS/MS approach have not been successful either.[32] It is their speculation as well that phenylbutenoic acids do not form a stable covalent bond with the enzyme.[33]

This study has provided some useful information from a methodological point of view. It was observed that minor peaks could always be found in the spectra from the digestion solutions. These were of a variable nature, in terms of intensity and m/z value, and represent non-specific binding between the immobilized avidin/agarose beads. In situations where only trace amounts of tagged peptide are generated, it is necessary to develop a clear means for confirming whether or not the peptide reflected in the spectrum is

tagged or not. One method involves saturating the avidin active sites with biotin prior to incubation with the digest. If the candidate peak in the spectrum disappears consistently (i.e., over many trials), then proof of tagging is strong. An ideal method incorporates two tagged inhibitors that do not differ in reactivity with the enzyme, but do exhibit a mass difference. This could be easily tracked in the mass analysis. For example, a ^{13}C-labelled form of biotin would be sufficient for an investigation based on tryptic digestion.

Finally, the stability of the tag during inhibition and digestion must be known. As indicated above, the incorporation of a disulphide was a poor choice given the incubation conditions. Efficient endoproteolysis of PAM by trypsin required the prior cleavage of disulphides and carboxyamidomethylation of all cysteines, rendering this tagging approach ineffective.

8.3.2 Screening for Antigens

While there are many uses for a MALDI method incorporating strong affinity interactions, it is attractive to be able to incorporate weaker interactions as well. To this end, a preliminary investigation of an antibody:antigen interaction was undertaken. The spectrum of a biotinylated antibody directed against *Salmonella* is shown in Figure 8.11. Note the distribution of biotinylation, and that a short-chain spacer arm was used (indicated by the progressive 226 u peak shifts). A solution of the two oligosaccharides (compounds **IV** and **V**) was prepared in Tris buffer. Compound **IV** represents an antigen for this antibody, having a K_a value of 1.14×10^6 M^{-1}.[20] Figure 8.12A displays the MALDI spectrum of this mixture. The peak at m/z 722.30 represents the non-antigenic compound **V**, while the peak at m/z 1157.35 represents the antigen compound **V**. Note that these oligosaccharides were ionized by alkali cation attachment. The indicated peaks represent the sodium adducts. Therefore, their expected masses are 722.32 u for compound **IV** and 1157.40 u for compound **V**. Satellite peaks for both compounds are present 16.0 u higher in mass, indicating potassium adducts. These cations were present as impurities in the matrix/analyte preparation.

The oligosaccharide mixture was then incubated with immobilized avidin/agarose and the biotinylated antibody. After incubation and washing, a small volume of a 2-propanol solution was applied to the beads, for extraction of the bound antigen. A MALDI analysis of the supernatant generated the spectrum in Figure 8.12B. Note the disappearance of the peak for the non-antigen, indicating purification. This level of purification demanded a high amount of sample. The spectrum of Figure 8.12B was

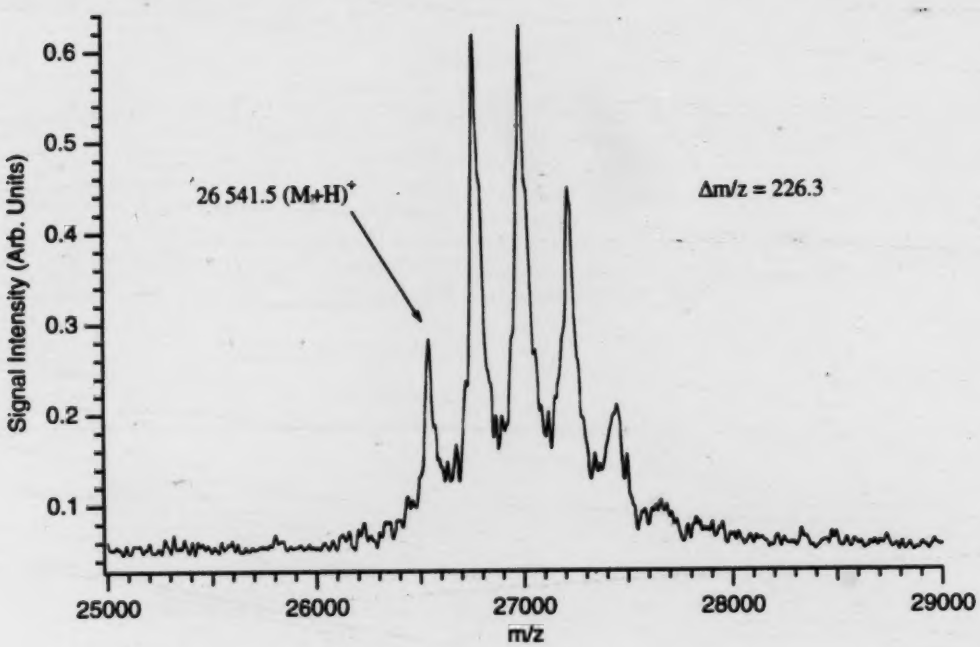

Figure 8.11 Spectrum of the biotinylated control antibody, using SA as the matrix. Note multiple biotinylation, indicated by the spacing of peaks by 226 u.

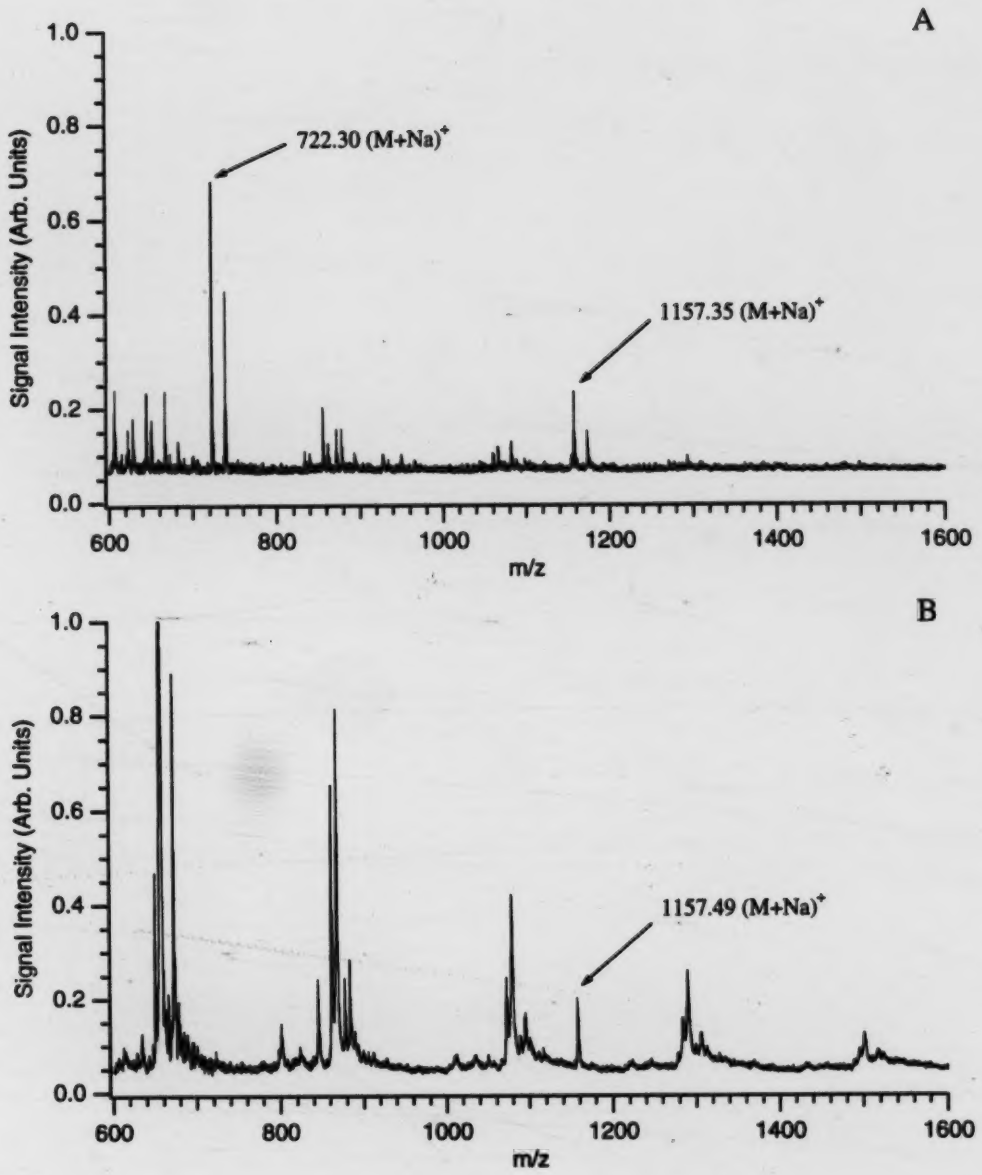

Figure 8.12 Spectra of the oligosaccharide mixture (A) before and (B) after purification.

obtained from a 0.75 µl sample of the total 8 µl volume. The high matrix background in relation to the analyte peak height suggests a loading in the mid to high fmol range. The incubation was carried out with 0.5 nmol of antigen present. Even allowing for the small sample used to obtain the MALDI spectrum, this represents significant sample loss. With the current handling procedures, there is room to miniaturize the scale of the procedure by a factor of 10. In the present case, this would allow for a more reasonable amount of 50 pmol of antigen. The interaction selected for this particular study represents a strong association constant for an antibody:carbohydrate complex,[19] however within the broader scope of macromolecular interactions the association constant is fairly typical, if not weak.[28]

This work indicates that affinity chromatographic techniques can be successfully incorporated into a MALDI procedure, and may have a place in the screening of potential antigens or enzyme inhibitors. Nevertheless, it portrays the boundaries of the "solid phase extraction" method. When the affinity interaction is too weak, a batch-style washing procedure removes excessively high amounts of complexed material from the agarose beads. A limit of sorts was reached in this study, as the amount of washing required to remove the non-antigen was just sufficient to reduce the inorganic salt concentration to levels amenable for MALDI analysis. Also, repetitive handling of small volumes makes it difficult to achieve reproducibility in these experiments. The beads themselves do not need to be applied to the probe tip in the case of these weaker interactions, as they do in the direct purification of biotinylated species. Therefore, it is more appropriate to develop an off-line affinity column method. The column eluant could be sampled at regular intervals for MALDI mass analysis. The high sensitivity of MALDI should allow for column miniaturization and more efficient use of enzyme, substrate, etc.

8.4 Literature Cited

(1) McComb, M. E.; Perreault, H. In *Proceedings of the 44th ASMS Conference on Mass Spectrometry and Allied Topics*; Portland, OR, 1996; p 1070.

(2) Yang, Y.; Levin, T.; Austin, T.; Orlando, R. In *Proceedings of the 44th ASMS Conference on Mass Spectrometry and Allied Topics*; Portland, OR, 1996; p 1071.

(3) Mathews, C. K.; van Holde, K. E. *Biochemistry*; The Benjamin/Cummings Publishing Co.: Redwood City, CA, 1990.

(4) Smillie, L. B.; Carpenter, M. R. In *HPLC of Peptides and Proteins: Separation, Analysis, and Conformation*; C. T. Mant and R. S. Hodges, Ed.; CRC Press, Inc.: Boca Raton, FL, 1991; p 875.

(5) Yates, J. R.; McCormack, A. L.; Link, A. J.; Schieltz, D.; Eng, J.; Hays, L. *Analyst* **1996**, *121*, R65.

(6) Wilm, M.; Mann, M. *Anal. Chem.* **1996**, *68*, 1.

(7) James, P. *Biochem. Biophys. Res. Commun.* **1997**, *231*, 1.

(8) Papayannopoulos, I. A. *Mass Spectrom. Rev.* **1995**, *14*, 49.

(9) Roberts, G. D.; Johnson, W. P.; Burman, S.; Anumula, K. R.; Carr, S. A. *Anal. Chem.* **1995**, *67*, 3613.

(10) Burgisser, D. M.; Siegenthaler, G.; Kuster, T.; Hellman, U.; Hunziker, P.; Birchler, N.; Heizmann, C. W. *Biochem. Biophys. Res. Commun.* **1995**, *217*, 257.

(11) Berger, B.; Hunziker, P. E.; Hauer, C. R.; Birchler, N.; Dallinger, R. *Biochem. J.* **1995**, *311 Part 3*, 951.

(12) Taylor, J. A.; Johnson, R. S. *Rapid Commun. Mass Spectrom.* **1997**, *11*, 1067.

(13) Beaudry, G. A.; Mehta, N. M.; Ray, M. L.; Bertelsen, A. H. *J. Biol. Chem.* **1990**, *265*, 17694.

(14) Zabriskie, T. M.; Klinge, M.; Szymanski, C. M.; Cheng, H.; Vederas, J. C. *Arch. Insect Biochem. Phys.* **1994**, *26*, 27.

(15) Li, C.; Oldham, C. D.; May, S. W. *Biochem. J.* **1994**, *300*, 31.

(16) Thiede, B.; Liebold-Wittman, B.; Bienert, M.; Krause, E. *FEBS Letters* **1995**, *357*, 65.

(17) Patterson, D. H.; Tarr, G. E.; Regnier, F. E.; Martin, S. A. *Anal. Chem.* **1995**, *67*, 3971.

(18) Woods, A. S.; Huang, A. Y. C.; Cotter, R. J.; Pasternack, G. R.; Pardoll, D. M.; Jaffee, E. M. *Anal. Biochem.* **1995**, *226*, 15.

(19) Bundle, D. R.; Eichler, E.; Gidney, M. A. J.; Meldal, M.; Ragauskas, A.; Sigurskjold, B. W.; Sinnot, B.; Watson, D. C.; Yaguchi, M.; Young, N. M. *Biochem.* **1994**, *33*, 5172.

(20) Bundle, D. personal communication.

(21) Gagne, S. M.; Tsuda, S.; M.X., L.; Smilie, L. B.; Sykes, B. D. *Nature Struct. Biol.* **1995**, *2*, 784.

(22) Chait, B. T.; Wang, R.; Beavis, R. C.; Kent, S. B. H. *Science* **1993**, *262*, 89.

(23) Johnson, R. S.; Martin, S. A.; Biemann, K. *Int. J. Mass Spectrom. Ion Processes* **1988**, *86*, 137.

(24) Hayes, R. N.; Gross, M. L. In *Methods in Enzymology: Mass Spectrometry*; J. A. MaCloskey, Ed.; Academic Press: San Diego, CA, 1990; Vol. 193; p 237.

(25) Eipper, B. A.; Mains, R. E. *Ann. Rev. Physiol.* **1998**, *50*, 333.

(26) Eipper, B. A.; Stoffers, D. A.; Mains, R. E. *Annu. Rev. Neurosci.* **1992**, *15*, 57.

(27) Merkler, D. J.; Young, S. D. *Arch. Biochem. Biophys.* **1991**, *289*, 192.

(28) Fersht, A. *Enzyme Structure and Mechanism;* 2nd ed.; W.H. Freeman and Company: New York, 1985.

(29) Zabriskie, T. M.; Cheng, H.; Vederas, J. C. *J. Am. Chem. Soc.* **1992**, *115*, 2270.

(30) Bradbury, A. F.; Mistry, J.; Roos, B. A.; Smyth, D. G. *Eur. J. Biochem.* **1990**, *189*, 363.

(31) Casara, P.; Ganzhorn, A.; Philippo, C.; Chanal, M.-C.; Danzin, C. *Bioorg. Med. Chem. Lett.* **1996**, *6*, 393.

(32) Marquez, C. D.; Treston, A. M. In *Proceedings of the ASMS Conference on Mass Spectrometry and Allied Topics*; Portland, OR, 1996; p 302.

(33) Marquez, C. D. personal communication.

Chapter 9

Conclusions and Future Work

The incorporation of the laser for sample volatilization and ionization has revolutionized and revitalized time-of-flight mass spectrometry. The work presented in this thesis reflects the many ways in which lasers can be used to great effect. Chapter 2 shows that a very simple design can allow for both electron impact and multiphoton ionization using lasers, in conjuction with a laser-based volatilization method. The remaining chapters have attempted to investigate and expand the versatility of the MALDI method in both polymer and biopolymer analysis.

The photoelectron impact ionization (PEI) method discussed in Chapter 2 was shown to have advantages over those methods using conventional electron beams or other approached to photoelectron generation. It is recognized that very well developed technology for electron impact ionization already exists, in the form of magnetic sector, quadrupole and ion trap systems. Nevertheless, the design presented in this chapter represents one of the best ways of coupling electron impact ionization with a *pulsed* sample introduction interface such as laser volatilization. The examples presented in this chapter have illustrated the advantages of being able to readily switch between different ionization modes. Furthermore, the potential exists for its application to fast gas chromatography/time-of-flight mass spectrometry designs. This is limited by the repetition rates of currently available (and reasonably priced) pulsed lasers.

A large portion of this thesis (Chapters 3 through 6) deals with the development and assessment of the MALDI technique for the analysis of industrial polymers. MALDI is a rapid analytical technique with the potential to supplant or supplement gel permeation chromatography (and other slower analytical methods) in an industrial setting. This industrial application has provided the impetus for the current investigation. The work discussed in this thesis has demonstrated the qualified success of the method for routine average molecular weight analysis (Chapters 3 and 4). Sample preparations exist for a wide assortment of polymer types, however there are glaring omissions that should be pursued (e.g., polyethylene, polypropylene). Methods for certain non-polar homopolymers such as polystyrene, polybutadiene and polyisoprene have been developed, with polystyrene detectable up to 1.5 million u. The accuracy of the average molecular weight determination for polymers of narrow polydispersity appears acceptable, however a similar analysis for polymers of wide polydispersity is plagued with difficulties. It would

appear that sample fractionation is required in this case, with the individual fractions then analysed by MALDI. However, some improvement in the situation may be possible. An empirical response curve might be generated that compensates for many of the instrumental factors giving rise to mass discrimination. Further work should also be done to expand (and explain) the troubling observation of mass discrimination in the desorption/ionization step.

The MALDI method is not restricted to providing molecular weight information. Chapters 5 and 6 indicate that, with sufficient resolution and mass accuracy, a wealth of structural and compositional information can be obtained. Of course, this is fundamentally limited by the absence of fragmentation analysis since the method generates molecular ions almost exclusively. Nevertheless, a certain amount of information is usually known about the polymer to be analysed, so MALDI is an excellent tool for structural confirmation and quality control. Caution must be exercised in the extraction of compositional information, since this depends on the absence of a quantitative bias. This was illustrated with the analysis of copolymers in Chapter 6.

An ideal mass spectrometric method would provide mass measurement accuracy across an unlimited mass range, structural information that would identify endgroups, monomers and impurities, and compositional information for complex polymer systems. A tall order. Within the limitations discussed in this work, there is room for MALDI as a useful addition to the analytical tools used by polymer chemists. The problem areas addressed herein leave room for further refinement of the technique. In particular, the coupling of MALDI and tandem mass spectrometry for fragmentation analysis of individual oligomer ions should provide a higher degree of structural and compositional information.

The MALDI analysis of biopolymers has undergone a rich development in the 10 years since its inception. It is now being used routinely in biochemistry and medicinal chemistry to accelerate research programs. This acceleration is possible partly because only small amounts of sample are required for a mass analysis. New methods of sample handling have also contributed to this acceleration. The work in Chapters 7 and 8 represent the coupling of a widely used affinity interaction with MALDI, for the rapid and sensitive interrogation of a biotinylated analyte present in complex solutions. When coupled with additional procedures such as enzymatic digestion and tandem mass spectrometry, peptide sequence determination can be achieved on trace amounts of an appropriately tagged peptide in the presence of a vast excess of contaminating peptides.

Unfortunately, the application of the avidin:biotin/MALDI method to the investigation of the binding site in PAM was unsuccessful, but this does not detract from

the usefulness of the methodology. At the very least, this technique suggests that the inhibition of PAM may not be as straightforward as was first expected. This section of Chaper 8 indicates the validity of the approach, and it is hoped that its merits will be incorporated into other enzyme-inhibitor studies.

The investigation of the antigen:antibody example in Chapter 8 suggests that the benefits of the avidin:biotin system as a probe for other interactions can also be incorporated into the MALDI method. For weak interactions, however, it is felt that either an off-line affinity chromatography/MALDI, or an on-line affinity chromatography/ESI method would be more effective. A more automated approach needs to be developed in order to allow for a high-throughput screening of combinatorial libraries.

From a methodological point of view, the mechanism of biotin-peptide release to the probe tip needs to be investigated further. Often, biochemists are interested in recovering a macromolecule bound to avidin through a biotin linker. As was indicated in Chapter 7, standard denaturing conditions are harsh and can often lead to the denaturing of the macromolecule itself. If the method described in the chapter truly represents a mild method of elution, then it would be of interest to the biochemical community to develop this procedure as an alternative means of sample recovery. This should include a determination of the efficiency of biotin-peptide recovery.

Finally, incorporating small amounts of chromatographic materials into a MALDI procedure represents an effective means of reducing the complexity of a spectrum. It is well known in the MALDI analysis of peptide mixtures that discrimination can arise in the crystallization step. Incorporating even a crude, single step enrichment using a small amount of chromatographic material might "clean up" the sample sufficiently to allow for the analysis of the targeted analytes.